Università degli Studi di Firenze
Facoltà di Scienze Matematiche, Fisiche e Naturali
Dipartimento di Chimica "Ugo Schiff"

Dottorato di Ricerca in Scienze Chimiche
XXIII ciclo

SSD CHIM/06

Synthesis of new molecular structures designed for targeting tumor cells

Alessandro Pratesi

Tutor
Prof. Mauro Ginanneschi

Ph.D. Supervisor
Prof. Andrea Goti

Co-tutor
Prof. Luigi Messori

Tornano in alto ad ardere le favole.

Cadranno colle foglie al primo vento.

Ma venga un altro soffio,
Ritornerà scintillamento nuovo.

Giuseppe Ungaretti – Stelle, 1927

Chapter 1

INTRODUCTION

For centuries, physicians have pursued effective and selective methods for treating diseases. Over just the past two centuries, it was discovered that there are substances in the blood that could fight infection, and by the turn of the last century, "magic bullets" were envisioned as a new frontier in medicine, particularly microbiology. However, it was not until the late 1940s that was provided the first evidence that antibodies developed against rodent tumors, and tagged with a radionuclide, could localize specifically to these targets.[1,2,3,4] Today, we continue to face many of the same challenges that these early investigators encountered for radioconjugate targeting, such as antibody specificity, radiolabeling, and pharmacokinetics.

Specificity is the *Holy Grail* for all targeted compounds. While specificity conjures visions of uniqueness between the target and its environment, more often specificity is derived from quantitative differences between the target and other host tissues. Architectural separation that isolates presentation in the environment from the more accessible presentation in the target can also produce a level of specificity. The lack of suitably specific antibodies for targeting human tumors was the most prominent factor contributing to the waning interest in radioantibody targeting in the 1960s. However, a key realization that a human colonic tumor xenografted in a hamster cheek pouch continued to express a newly defined human oncofetal antigen, CEA (carcinoembryonic antigen), paved the way for resurgence of radioantibody targeting in the 1970s that led to the first successful demonstration of tumor localization in patients by external scintigraphy.[5,6] Affinity-purified (monospecific) polyclonal antibodies used in these early clinical studies

[1] Korngold, L.; Pressman, D. *Cancer Res.* **1954**, *14*, 96–99.
[2] Pressman, D. *Cancer* **1949**, *2*, 697–700.
[3] Pressman, D.; Eisen, H.N.; Fitzgerald, P.J. *J. Immunol.* **1950**, *64*, 281–287.
[4] Bale, W.F.; Spar, I.L.; Goodland, R.L. *Cancer Res.* **1960**, *20*, 1488–1494.
[5] Goldenberg, D.M.; Hansen, H.J. *Science* **1972**, *175*, 1117–1118.
[6] Goldenberg, D.M.; Preston, D.F.; Primus, F.J.; Hansen, H.J.; *Cancer Res.* **1974**, *34*, 1–9.

were quickly replaced with murine monoclonal antibodies, and more recently with less immunogenic humanized or fully human antibodies and recombinant proteins. Monoclonal antibodies enhanced selectivity to a unique conformational determinant within a molecule, and recombinant antibodies have greatly amplified the repertoire of targeting structures with altered affinity/avidity and pharmacokinetic properties, but all base their binding on the guiding principles of antibodies and their specificity.

Of course, tumor detection and therapy with radiolabeled antibodies could never have advanced without the contributions of the radiochemists and chemists, who expanded our choices from the staple radionuclide used for many years, ^{131}I, which has poor imaging properties, to a host of new radionuclides with diverse imaging and therapeutic properties.[7,8,9,10]

While specificity has a major role in defining the targeting utility of a given compound, its pharmacokinetic and biodistribution properties often have a more profound impact on tissue uptake than an agent's specificity. This is because targeting is a passive process, where a molecule injected into the bloodstream wanders in the vascular or extravascular fluid, being carried along by the natural flow of body fluids, until it encounters a cell bearing a target molecule it can bind to. Once bound, the antibody has the potential to be held there until the radionuclide decays, it may be released from the cell and return to extracellular fluid volume, it can be catabolized by local peptidases or internalized by the tumor cells and catabolized by lysosomal enzymes. From this process, the radionuclide is freed from the antibody, where it may be released back into the circulation or retained locally by the cells. Many free radionuclides have an affinity for certain body tissues, such as radiometals for bone or radioiodine for the thyroid, or they can bind to serum proteins and then can be redirected to other tissues. Only a small portion of the injected antibody is deposited within a tumor, while the rest of the antibody eventually extravasates from the blood, like all other proteins, and is catabolized by the body's tissues, mainly the liver, spleen, and other reticuloendothelial-rich organs. The delayed clearance from the tumor creates a differential uptake, where there is a higher

[7] Scheinberg, D.A.; Strand, M.; Gansow, O.A. *Science* **1982**, *215*, 1511–1513.
[8] Meares, C.F.; Moi, M.K.; Diril, H. *et al. Br. J. Cancer Suppl*. **1990**, *10*, 21–26.
[9] Deshpande, S.V.; DeNardo, S.J.; Meares, C.F. *et al. J. Nucl. Med.* **1988**, *29*, 217–225.
[10] Griffiths, G.L.; Goldenberg, D.M.; Jones, A.L.; Hansen, H.J. *Bioconj. Chem.* **1992**, *3*, 91–99.

concentration in the target than surrounding tissues, enabling visualization or potentially providing a therapeutic window of opportunity.

The body's blood vessels lead to well-defined regions of the body, but there are many tributaries that divert and dilute the radioimmunoconjugate within the total fluid volume of the body. This is where an agent's properties, such as its size and composition, determine its fate. A molecule's size/shape chiefly determines whether it will pass easily through the openings in the vascular channels and percolate into the extravascular space, where most diseases (targets) reside. Size also defines how quickly it will be sequestered from the blood by the reticuloendothelial system, primarily in the liver, spleen, and lymph nodes, where the larger sinusoidal openings between the endothelial cells enable more rapid extravasation, or if small enough (e.g., <60 kDa), to be removed via glomerular filtration.[11] The composition of a molecule defines its charge and hydrophilicity, which can result in nonspecific binding to various tissues or even serum components. Composition naturally endows the conformational shape of the molecule that is key to binding to a target of interest, but other regions within the molecule's structure might bind unintentionally to other tissues that could diminish specificity. Glycosylation also impacts tissue uptake and blood clearance.[12,13] The high degree of homology in the basic core structure of an IgG reduces the potential for variable tissue binding and clearance that otherwise might be encountered with *de novo* targeting agents. Of course, agents can be administered in a defined compartment, such as the peritoneal cavity, by hepatic artery perfusion into the liver, or by the intrathecal route, or surgically resected cavity within the brain, to reduce the impact that a molecule's pharmacokinetic properties might have on targeting.[14] Compartmental administration for tumors that are anatomically confined allows the antibody to be exposed first to the antigen, but often, a sizable portion of the agent escapes into the blood or lymphatic channels, free to travel throughout the body.

Some innovative methods for circumventing many of the pharmacokinetic challenges posed by a directly radiolabeled antibody, are based on the technique called *pretargeting*.

---

[11] Trejtnar, F.; Laznicek, M. *J. Nucl. Med.* **2002**, *46*, 181–194.
[12] Leung, S.O.; Qu, Z.; Hansen, H.J. *et al. Clin. Cancer Res.* **1999**, *5*, 3106s–3117s.
[13] Govindan, S.V.; Griffiths, G.L.; Michel, R.B.; Andrews, P.M.; Goldenberg, D.M.; Mattes, M.J. *Cancer Biother. Radiopharm.* **2002,** *17*, 307–316.
[14] Sharkey, R.M.; Goldenberg, D.M. *Adv. Drug. Deliv. Rev.* **2008**, *60*, 1407–1420.

Perhaps, surprisingly, the biggest problem with most radionuclide–antibody conjugates is that they are highly stable in the blood, and thus, generally wherever the antibody is distributed, the radionuclide follows. A radionuclide that dissociates from the antibody would have very unfavourable properties. For example, cyclic DTPA (diethylene triamine pentaacetic acid) anhydride was one of the first chelate derivatives used to complex a radiometal (^{111}In or ^{90}Y) to an antibody,[7,15] but the radiometals, particularly ^{90}Y, would slowly dissociate from the chelate, allowing the unbound metal to be taken up by other tissues, such as the cortical bone. When other chelates that bound the radiometal more tightly were developed (e.g., DOTA), they quickly replaced cyclic DTPA anhydride.[16] Other chemistries have been developed that allow selective cleavage of the chelate–radiometal complex from the antibody when it is catabolized in the liver.[17] This cleavable linkage improved tumor/liver ratios, but it did not address the high concentration of radioantibody remaining in the blood, and thus this method was unable to increase the radiation-absorbed dose delivered to the tumor. Molecular engineering has made great strides in crafting constructs that try to strike a balance between optimal blood and tissue clearance with reasonable tumor uptake and retention,[18] but another approach had already achieved rapid blood clearance with high tumor uptake/good retention in the mid-1980s. This method is pretargeting, a technique that has evolved over the past 20 years to include three different approaches based on bispecific monoclonal antibodies (bsMAb) with radiolabeled haptens, avidin or streptavidin used for targeting radiolabeled biotin (Figure 1.1), and antibody–oligonucleotide conjugates for targeting radiolabeled complementary oligonucleotides. In this thesis will be discussed only the Avidin/Biotin pretargeting system.

[15] Hnatowich, D.J.; Layne, W.W.; Childs, R.L. *et al. Science* **1983**, *220*, 613–615.
[16] Camera, L.; Kinuya, S.; Garmestani, K. *et al. Eur. J. Nucl. Med.* **1994**, *21*, 640–646.
[17] Peterson, J.J.; Meares, C.F. *Bioconj. Chem.* **1999,** *10*, 553–557.
[18] Seitz, K.; Zhou, H. *J. Clin. Pharmacol.* **2007**, *47*, 1104–1118.

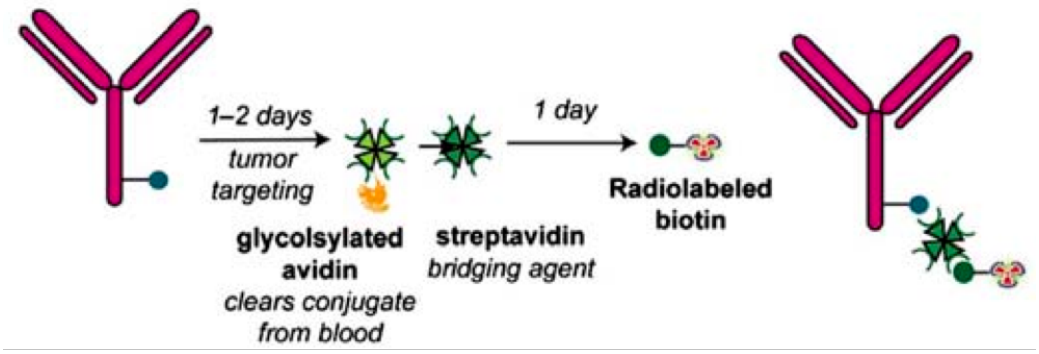

Figure 1.1 Schematic representation of the Pretargeting System

The most significant advance in pretargeting occurred when Hnatowich *et al.* introduced a new method to bridge the antibody and radionuclide targeting steps based on the ultrahigh affinity of biotin for avidin/streptavidin.[19] Such avidin/biotin binding methods were already in use for *in vitro* immunoassays and immunohistochemistry. These and other investigators explored several configurations, using an antibody conjugated with avidin paired with radiolabeled biotin, or biotin-conjugated antibodies used to capture radiolabeled avidin.[20,21,22] This avidin–biotin affinity was nearly 6 logs higher than most antibody–antigen interactions ($K_d = 10^{-15}$ M), which essentially ensured an irreversible bond between biotin and avidin. Glycosylated avidin and its non-glycosylated counterpart, streptavidin, have four binding sites for biotin, which offers the potential that multiple radiolabeled biotins could be captured by a single pretargeted antibody–avidin conjugate. Importantly, the radiolabeled biotin had very rapid clearance from the body (biological half-life = 30 min), indicating that it had rapid extravasation and minimal binding to tissues as well as efficient renal excretion. The initial animal studies showed great potential of this method, and 2 years later, the first clinical studies were performed using the human milk fat globule-1 (HMFG1) IgG (anti-MUC1) coupled to streptavidin followed 2–3 days later with ^{111}In-biotin.[23] In addition to establishing important safety data, this study also showed that endogenous biotin, which is present in the serum and tissues, did not block the streptavidin–IgG conjugate's ability to bind the subsequently administered ^{111}In-biotin.

[19] Hnatowich, D.J.; Virzi, F.; Rusckowski, M. *J. Nucl. Med.* **1987**, *28*, 1294–1302.
[20] Paganelli, G.; Belloni, C.; Magnani, P. *et al. Eur. J. Nucl. Med.* **1992**, *19*, 322–329.
[21] Paganelli, G.; Magnani, P.; Zito, F. *et al. Cancer Res.* **1991**, *51*, 5960–5966.
[22] Paganelli, G.; Ferrari, M.; Ravasi, L. *et al. Clin. Cancer Res.* **2007**, *13*, 5646s–5651s.
[23] Kalofonos, H.P.; Rusckowski, M.; Siebecker, D.A. *et al. J. Nucl. Med.* **1990**, *31*, 1791–1796.

This was not the case in mice, where the concentration of endogenous biotin is much higher than in humans and requires animals to be fed a biotin-deficient diet for several days before initiating pretargeting studies.[24,25] Tumor targeting was observed in 8/10 patients but, disappointingly, similar uptake was seen in at least 5 of these patients given ^{111}In-biotin alone. This most likely represented blood pool radioactivity with slower washout from tumors due to their abnormal physiology. They also found that the streptavidin conjugate was immunogenic, with antibodies formed to both the murine IgG and the streptavidin. However, the more important finding from this study was the very low normal tissue and blood pool radioactivity (i.e., ^{111}In-biotin cleared with an alpha- and beta-phase half-life of 2.4 min and 4.2 h, respectively), suggesting that this method, when properly optimized, could greatly reduce blood and tissue background radioactivity.

This particular approach was perfected by the contributions of investigators at NeoRx Corp. (Seattle, WA). They focused their efforts on the development of a streptavidin conjugate prepared with the murine monoclonal antibody, NR-LU-10, as the pretargeting agent with ^{111}In/^{90}Y-DOTA (1,4,7,10-tetraazacyclododecane-*N,N',N'',N'''*-tetraacetic acid)-biotin. They also introduced the use of a clearing agent, galactose-conjugated and biotinylated human serum albumin, to remove excess streptavidin–IgG from the blood before the radiolabeled biotin was injected. Hepatocytes have galactose receptors that effectively remove galactosylated antibody immune complexes from the blood,[26,27] and biotin not only serves as a specific binding ligand for the streptavidin conjugate but also, in sufficient excess, it would prevent the binding of the subsequently administered radiolabeled biotin, allowing it to flow relatively unabated through the body until it reaches the tumor. In their procedure, the streptavidin–IgG conjugate was allowed 2–3 days to achieve maximum tumor uptake, and then the clearing agent was given. One day later, the radiolabeled biotin was administered. Using this technique, Axworthy et al.[28] were the first to present provocative animal data indicating not only that a pretargeting approach could improve tumor/blood and tumor/tissue ratios, but also that the tumor uptake could be similar to that of a directly radiolabeled IgG. In some respects, this finding

[24] Hnatowich, D.J. *Nucl. Med. Commun*. **1994**, *15*, 575–577.
[25] Sharkey, R.M.; Karacay, H.; Griffiths, G.L. *et al. Bioconj. Chem.* **1997**, *8*, 595–604.
[26] Mattes, M.J. *J. Natl. Cancer Inst.* **1987**, *79*, 855–863.
[27] Ong, G.L.; Ettenson, D.; Sharkey, R.M. *et al. Cancer Res.* **1991**, *51*, 1619–1626.
[28] Axworthy, D.B.; Fritzberg, A.R.; Hylarides, M.D. *et al*. *J. Immunother.* **1994**, *16*, 158.

was puzzling since the pharmacokinetic behaviour of directly labelled IgG and antibody fragments predicted that the more rapidly an agent cleared from the blood, the lower would be its tumor accumulation. The radiolabeled biotin cleared more rapidly from the blood than any other previously reported directly conjugated antibody fragment, but despite this, it was able to achieve IgG-like tumor uptake. So how did this pretargeting procedure accomplish this targeting panacea? A comparison of a typical directly radiolabeled antibody targeting procedure with pretargeting procedures reveals some very important differences.

With a directly radiolabeled antibody, the main goal should be to administer the smallest possible radioantibody protein dose prepared at the highest possible specific activity, which increases the probability that each molecule reaching the target would deliver a radioactive payload. Unfortunately, pharmacokinetic, biodistribution, and even specificity issues often dictate that additional unlabelled antibody be added (coadministered or preadministered) with the radiolabeled antibody to improve the antibody's biodistribution or targeting. Any competition for radioantibody with an unlabelled antibody runs the risk of reducing the total amount of radioactivity delivered to the tumor, with a preinfusion having a greater risk of blocking some of the more accessible antigen-rich regions within the tumor before the radioantibody is given. Since uptake and tumor/blood ratios for an IgG are already low, it is not surprising that RIT (Radioimmunotherapy) with directly radiolabeled antibodies has had limited therapeutic impact, except for lymphomas, which have an inherently high radiosensitivity. As mentioned, smaller antibody fragments bearing radiometals have exceptionally high renal uptake and retention that greatly exceeds that delivered to the tumor. There have been animal studies reporting improved therapeutic activity for antibody fragments versus IgG, and there even have been methods that reduce renal uptake of radiometals.[29,30,31] While each of these has been clinically evaluated, neither provided a sufficient therapeutic boost to spur further clinical evaluation.

Pretargeting procedures often start with the injection of relatively high doses of the immunoconjugate (e.g., IgG-streptavidin or biotin conjugate) or bsMAb (Recombinant

[29] Behr, T.M.; Behe, M.; Stabin, M.G. *et al*. *Cancer Res*. **1999**, *59*, 2635–2643.
[30] Behr, T.M.; Blumenthal, R.D.; Memtsoudis, S. *et al. Clin. Cancer Res.* **2000**, *6*, 4900–4907.
[31] Behr, T.M.; Memtsoudis, S.; Sharkey, R.M. *et al. Int. J. Cancer.* **1998**, *77*, 787–795.

bispecific antibodies). This maximizes the conjugate loading in the tumor, which increases the number of binding sites available for the radiolabeled biotin or hapten (i.e., effector). Because the pretargeting immunoconjugate/bsMAb is not radiolabeled, there are no inherent radiotoxicity limitations to the amount administered. However, optimal pretargeting conditions do not demand administration of excessively high protein doses at levels that might saturate antigen binding sites in the tumor. Instead, optimal conditions will occur as long as the amount of conjugate or bsMAb prelocalized to the tumor is sufficient to capture the highest fraction of the effector that will ultimately reach the tumor. If an effector is radiolabeled at 2 mCi (74 MBq)/nmole, then often only 100 nmoles would be given. With such rapid elimination, only a small fraction of the effector will every pass through the tumor. Therefore, the administered amount of pretargeting agent needs only to be sufficient to optimize the capture of this small quantity of effector. In our experience, the optimal bsMAb dose can be reasonably approximated from the amount of hapten administered (which in our case is conjugated to a peptide) and is expressed as the mole ratio of the bsMAb to peptide-hapten.

Pagel *et al*.[32] provided additional insight into this point by showing in a human lymphoma xenograft model that the uptake of radiolabeled biotin (effector) could not be improved by pretargeting with immunoconjugates directed against multiple antigens, as compared to the best single antigen (e.g., CD20, CD22, or HLA-DR). By combining one immunoconjugate that had the highest uptake in the tumor with others that had lower uptake, they effectively reduced the number of moles of individual immunoconjugates in the tumor, thereby reducing the effector-capturing efficiency.

In order to give the radiolabeled effector the best chance of binding to the prelocalized immunoconjugate in the tumor, the residual immunoconjugates in the body need to be blocked/cleared. The blood is the primary concern since any radiolabeled effector introduced by intravenous injection will encounter circulating immunoconjugates there first. However, other tissues also need to be considered, such as the liver that is the primary organ for removing IgG from the blood. Since most bsMAb studied to date have been $F(ab')_2$ fragments, investigators simply waited for the concentration of the bsMAb in the blood to be reduced to a level where interaction with the radiolabeled hapten-peptide

[32] Pagel, J.M.; Hedin, N.; Subbiah, K. *et al. Blood.* **2003**, *101*, 2340–2348.

was minimized. The molar ratios of immunoconjugate to hapten and degree of blood clearance required to minimize hapten-bsMAb interaction will vary depending on the binding affinity of the antihapten portion of bsMAb. Avidin–biotin approaches have relied on clearing agents that block and clear the immunoconjugates from the blood following a 1–3 day period during which the immunoconjugate has an opportunity to reach peak levels in the tumor. This is particularly important for these procedures, because the ultrahigh affinity of biotin for avidin will ensure stable binding, even if very small amounts of the immunoconjugates remain in the blood and tissues.

The timing requirements for a pretargeting procedure impose a restriction on the types of antigens that can be targeted; they must remain accessible (i.e., not internalized or catabolized) in sufficient quantity to bind the radiolabeled effector.

However, the real strength of a pretargeting system is its ability to very efficiently trap the radiolabeled effector in the tumor. As with any injected agent, only a small fraction will percolate the vasculature of the tumor, so it is important to have the pretargeted immunoconjugates accumulate and be retained in the tumor in sufficient amounts to maximize the capture of the effector molecules. At least for the radiolabeled effectors commonly used in pretargeting, those leaving the vascular space will quickly encounter the pretargeted immunoconjugates bound to the surface of tumor cells. Binding to the effector-capturing agent, whether it is streptavidin or a bsMAb, will retain the effector in the tumor, while within minutes, the unbound effector molecules are rapidly eliminated from the body, creating almost immediate and exceptionally high tumor/blood ratios. The radiolabeled effector will persist in the tumor as long as it remains bound to the bsMAb's antieffector arm or to streptavidin, and as long as the immunoconjugate remains fixed to the tumor antigen. Unlike the initial bsMAb pretargeting configuration, where the effector was a single chelate–radiometal complex (i.e., a hapten), LeDoussal *et al.* found that tethering two haptens together with a small peptide linker enhanced uptake and retention of the effector; this was referred to as an *affinity enhancement system* (AES).[33]

An antibody or even a fragment, whose larger size impedes its transvascular movement into tumors, and rather than being easily eliminated, it continues to circulate in the body, awaiting catabolism for excretion of the radioactivity. While this might provide

[33] LeDoussal, J.M.; Martin, M.; Gautherot, E.; Delaage, M.; Barbet J. *J. Nucl. Med.* **1989**, *30*, 1358–1366.

the potential for multiple tumor passes, the concentration of the antibody in the blood eventually decreases over time, being sequestered by other tissues in the body, thereby making it less available for tumor uptake. In addition, the longer the tumor uptake is delayed, the more of the radionuclide will be released by catabolism and be redistributed to other parts of the body, contributing to toxicity. Thus, pretargeting procedures are more highly adept at achieving exceptionally rapid tumor uptake and blood clearance than direct targeting of radioimmunoconjugates. The end result is that tumor radionuclide delivery is maximized, with possible higher radiation dose rates and often increased radiation-absorbed doses, while most normal tissues are spared prolonged radiation exposure[34,35] (Figure 1.2). As a consequence, significantly improved antitumor responses have been observed in a variety of animal models with pretargeting procedures compared to direct RIT.[36]

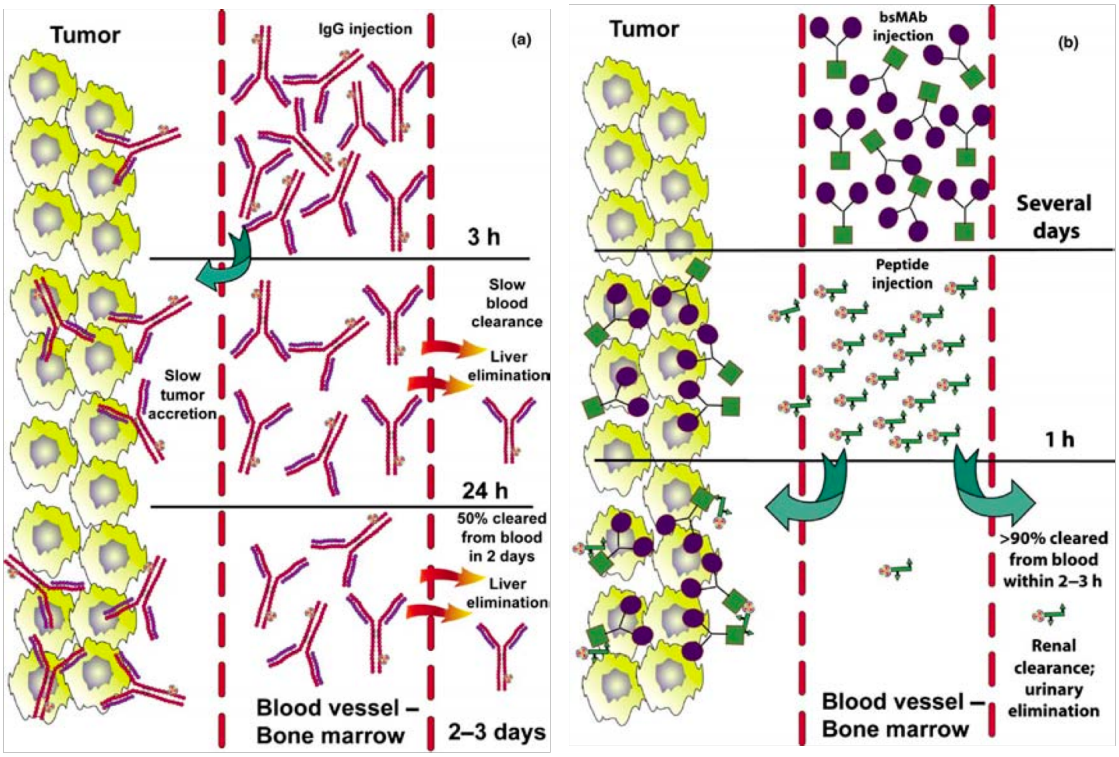

Figure 1.2 Radiolabeled antibodies (a) vs. radiolabeled biotin (b).

[34] Axworthy, D.B.; Reno, J.M.; Hylarides, M.D. *et al. Proc. Natl. Acad. Sci. USA* **2000**, *97*, 1802–1807.
[35] Sharkey, R.M.; Karacay, H.; Cardillo, T.M. *et al. Clin. Cancer Res.* **2005**, *11*, 7109s–7121s.
[36] Pagel, J.M.; Pantelias, A.; Hedin, N. *et al. Cancer Res.* **2007**, *67*, 5921–5928.

A different pretargeting procedure based on streptavidin-biotin was first proposed by Paganelli *et al.*,[37] who compared a two-step and a three-step method for delivering either ^{131}I-streptavidin or ^{111}In-biotin, respectively, to athymic mice bearing peritoneal implants of a human colon cancer cell line (LoVo) pretargeted with a biotinylated antibody (AUA1). Radiolabeled streptavidin was localized to tumors pretargeted 1 day earlier with the biotinylated antibody. In the second case, instead of using a streptavidin–IgG conjugate to localize the radiolabeled biotin, the same antibody conjugated instead to biotin was administered. One day later, animals were injected with a 10-fold molar excess of unlabeled avidin, and then 2 h later with ^{111}In-biotin. ^{111}In-biotin was used to evaluate the procedure, but it is not a therapeutic analogue of biotin (^{90}Y-biotin would be required for treatment). All injections were given intraperitoneally. Tumors isolated from the peritoneal cavity 4 h after the radiopharmaceutical injection had an uptake of approximately 24% ID/g with the pretargeted approach and using ^{131}I-streptavidin; this was four times higher than with a directly radiolabeled IgG (MAb AUAI), and with improved tumor/blood ratios (~3.5:1 versus <1:1). However, ^{131}I-streptavidin uptake in the liver was elevated, because streptavidin formed complexes with circulating biotinylated antibody in the blood, which were then deposited in the liver. They found that an intraperitoneal injection of unlabelled avidin could reduce the concentration of the biotinylated antibody in the blood, and so they decided in the second approach to administer an excess of unlabelled avidin 2 h before administering ^{111}In-biotin. In this procedure, the unlabelled avidin would bind first to the biotinylated antibody prelocalized to the peritoneal tumors, and as the excess avidin enters the bloodstream from the peritoneal cavity, it would bind to the circulating biotin IgG that would then be removed quickly by the liver (avidin is glycosylated, which accelerates its clearance by hepatic asialoglycoprotein receptors). When ^{111}In-biotin was subsequently injected i.p. 2 h later, tumor/blood and tumor/liver ratios were improved to approximately 50:1 and 35:1 just 2 h after radiopharmaceutical administration. However, tumor/kidney ratios were decreased to <1:1, reflecting the higher retention of ^{111}In-biotion in the kidneys compared to ^{125}I-streptavidin in the former approach.

This method was quickly examined in patients, but with all injections given intravenously (i.v.). In this first clinical study, patients with a variety of CEA-producing

[37] Paganelli, G.; Pervez, S.; Siccardi, A.G. *et al. Int. J. Cancer* **1990**, *45*, 1184–1189.

tumors received 1mg of a biotinylated anti-CEA IgG (murine MAb FO23C5), followed 3 days later by 4–6 mg of avidin, and finally 2 days later by ^{111}In-biotin. Tumor visualization was apparent on gamma camera scans with tumor/blood and tumor/liver ratios exceeding 5:1 within 20 min (tumor/kidney ratios were ~1:1). Two patients were imaged 1 month later without the benefit of pretargeting with the biotinylated antibody; one was administered ^{111}In-biotin alone, the other given the same dose of avidin followed by ^{111}In-biotin. In these follow-up studies, there was no obvious tumor targeting, whereas the pretargeting procedure localized their lesions. Imaging of one patient with ^{111}In-FO23C5 anti-CEA F(ab')$_2$ 2 weeks prior to the pretargeting study failed to disclose metastatic deposits in the liver because of elevated normal liver uptake, but with the pretargeting approach, these lesions were seen subsequently. These studies established the proof-of-principle for this new alternative cross-linking method based on streptavidin–biotin binding, and set the stage for future therapeutic use.

The first radiotherapeutic trial with the avidin–biotin pretargeting system was subsequently reported using this method but with a slight modification.[38,39] The trial, performed in patients with high-grade gliomas, involved the intravenous injection of an antitenascin IgG-biotin immunoconjugate (35 mg/m^2). The clearing step was modified to include first an injection with avidin (30 mg) that was followed 30 min later by streptavidin (50 mg). This modification first allowed avidin to clear the biotin conjugate from the blood by forming complexes that would be removed by the liver (avidin's glycosylation aids in hepatic removal of the complexes). By administering streptavidin later, when most of the circulating biotinylated antibody conjugate was already complexed with avidin and shuttled to the liver, it would circulate somewhat longer in the blood, allowing it enough time to bind to the pretargeted biotin immunoconjugate in the tumor. The next day, patients received ^{111}In or ^{90}Y-labeled biotin for binding to the streptavidin now prelocalized to the tumor and bound to the biotinylated antibody. Given the potential for limited transport across the blood-brain barrier, it was interesting to note that the investigators chose to administer all these agents intravenously. However, imaging studies clearly showed the tumors were localized. Even 12 months after treatment, 17% of the

[38] Paganelli, G.; Grana, C.; Chinol, M. *et al. Eur. J. Nucl. Med.* **1999**, *26*, 348–357.
[39] Cremonesi, M.; Ferrari, M.; Chinol, M. *et al. Eur. J. Nucl. Med.* **1999**, *26*, 110–120.

patients still showed tumor reduction, and one patient was alive and without evidence of disease after a 10-year follow-up.

These promising results led to a follow-up pretargeted RIT trial in grade III/IV glioma patients using the same protocol as above immediately after primary surgery and radiotherapy, to determine time to relapse and overall survival.

Chapter 2

BIOTIN DERIVATIVES

2.1 The radioimmunotherapy

In the recent years, large experience has been accrued through the clinical applications of radiolabeled monoclonal antibodies in diagnosis and therapy of malignant diseases. Currently, the cancer treatments involve surgery often followed by chemotherapy and radiation therapy. The therapy depends on the differences in sensitivity from the normal tissue compared to the tumor. Radiation and chemotherapy have the disadvantage that they destroy both healthy and malignant cells thus causing severe side-effects. A new type of radiation therapy, called radioimmunotherapy (RIT), uses monoclonal antibodies (MoAbs) to address the radiation on the tumor. The radioimmunotherapy can be used to treat metastases otherwise difficult to detect and to treat by other diagnostic means because in RIT method the radiation comes from inside of the tumor differently from the conventional external radiation therapy. The RIT, in fact, is a clinical technique allowing, through radiopharmaceuticals, the radionuclide to bind a tumor-associated antigen on the membrane of tumor cells.

2.2 Radiopharmaceuticals

A radiopharmaceutical is a radioactive compound used for diagnosis and/or therapeutic treatment of human diseases. Usually radiopharmaceuticals have not pharmacologic effects, because in most cases they are used in traces.

A radiopharmaceutical is made up of two parts: 1) **the vector**, i.e. the drug, which localises itself in the target area, and 2) **the radioisotope**, i.e. ^{99}Tc, ^{111}In, ^{131}I. Radiopharmaceuticals are administered by intravenous or intra-peritoneal way. For this reason they must be sterile, pyrogen free, not toxic and are made according to the GMP of conventional drugs. ^{133}Xe itself, for example, can be considered as a radiopharmaceutical;

on the other side, radiolabeled compounds are considered radiopharmaceuticals, i.e. proteins labelled with ^{131}I. Radiopharmaceuticals must have some preset characteristics:

- *Easy availability*: the synthesis must be cheap and easy.
- *Short effective half-life*: the physical half-life (T_p) is the time necessary the activity of a radiopharmaceutical to be halved. T_p is characteristic for each radionuclide and independent from the chemical and physical features. The constant decay is correlated with T_p by the formula $\lambda_p = 0.693/T_p$. The biologic half-life (T_b) is the time necessary to eliminate from the body the moiety of the administered dose. Radiopharmaceuticals can be excreted in several ways, for example through excrements or urine. The elimination of a radiopharmaceutical from an alive organism depends both on the physical decay of the radionuclide and on the biological clearance. The effective half-life (T_e), for this reason, is lower than T_p and T_b and it must be lower as possible.
- *Particle emission*: the choice of radioisotope is important. For diagnosis, a γ-emitting radioisotope with a short half-life will give the clearest images and the lowest radiation dose to the patient. In a therapeutic radiolabeled drug, ideal radioisotopes are characterised by an abundance of non-penetrating radiations (i.e., β or α particle emitters).
- *High target-to nontarget activity ratio*: the main aim is to obtain the high concentration of the radiopharmaceutical, in the target organ, both for therapeutic and diagnostic applications. The surrounding tissues might have a lower concentration of radiopharmaceutical. In this case the instrumentation can measure the radioactivity distribution with high accuracy. The organ involved in the pathology is so detected.
- *Metabolic stability*: obviously a radiopharmaceutical must be stable *in vivo*. In the most cases the organism metabolizes the drug during the diagnostic text; in other circumstances the metabolism can give important information after accumulation in the organ.

2.3 Radionuclides

Radionuclides are defined by several physical parameters: type of particles emitted, energy and physical half-life (Table 2.1). Chemical parameters are also important, as the chemistry involved in radiolabeling largely imparts on *in vivo* stability of the conjugates. Finally, the radiochemical purity and the specific activity that may be achieved in clinical practice are also important.

Table 2.1 Radionuclides physical half-life, decay and maximum penetration.

Radionuclide	Physical half-life	Particle energy (MeV)	Maximum tissue range
^{32}P	14.3 d	β (1.71)	8.7 mm
^{67}Cu	2.58 d	β (0.54), γ (0.185)	1.8 mm
^{90}Y	2.67 d	β (2.28)	12.0 mm
^{105}Rh	1.48 d	β (0.57), γ (0.320)	1.9 mm
^{109}Pd	13.6 h	β (1.0)	4.6 mm
^{111}Ag	7.47 d	β (1.05), γ (0.34)	4.8 mm
^{125}I	60.0 d	γ (0.027)	10 nm
^{131}I	8.04 d	β (0.6), γ (0.364)	2.0 mm
^{177}Lu	6.7 d	β (0.497), γ (0.208)	1.5 mm
^{186}Re	3.77 d	β (1.08), γ (0.131)	5.0 mm
^{188}Re	16.95 h	β (2.13), γ (0.155)	11.0 mm
^{198}Au	2.7 d	β (0.97), γ (0.411)	4.4 mm
^{211}At	7.2 h	α (6.8)	65 μm
^{212}Bi	1 h	α (7.8), γ (0.72)	70 μm
^{99m}Tc	6 h	γ (0.143)	6.7 mm
^{64}Cu	12.7 h	β (0.573), γ (1.34)	10 μm

The kind of particles emitted by the radionuclide is the most important parameter. Depending on their decay, radionuclides can be divided into two primary classes: diagnostics and therapeutics. Diagnostic radiopharmaceuticals (radioimmunoscintigraphy) are molecules labelled with γ-emitting isotopes. Gamma rays (high energy photons) can be detected by appropriate instruments (Gamma cameras); they are electromagnetic radiations and provide a non-invasive method of assessing the disease showing ill tissues and

monitoring the effect of treatment. β-emitters and α-emitters are used mainly for radioimmunotherapy. α particles, because of its very large mass and its charge, have a very short range. They are not suitable for radiation therapy for their great destructive power within a short range. In contact with fast-growing membranes and living cells, they cause maximum damage. The β-emitters have a greater radius penetration than α-particles, but still much less than gamma rays (Figure 2.1). They show ideal characteristics for treatment of solid tumours.

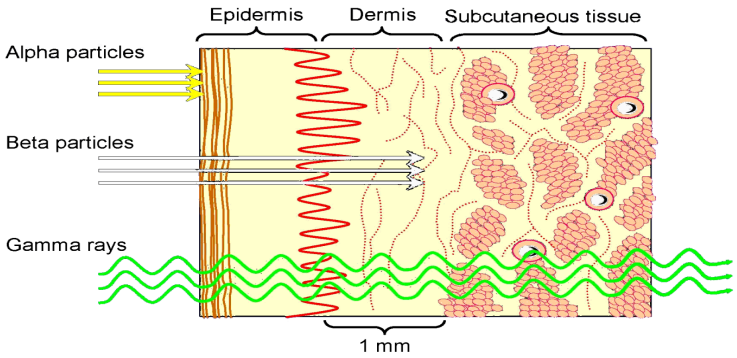

Figure 2.1 Penetration range.

The path lengths of β-particles are significantly greater than the diameter of cancer cells. The radiation effect of beta particles from the site of antibody binding on the neighbouring cells is the so-called 'crossfire effect' (Figure 2.2). This effect allows a therapeutic radiation doses to cells in bulky, poorly vascularised tumors, or even in tumors with heterogeneous antigen expression. This phenomenon reduces the requirement to target every single tumour cell, thereby bypassing tumour antigen heterogeneity and inadequate tumour vascularisation.

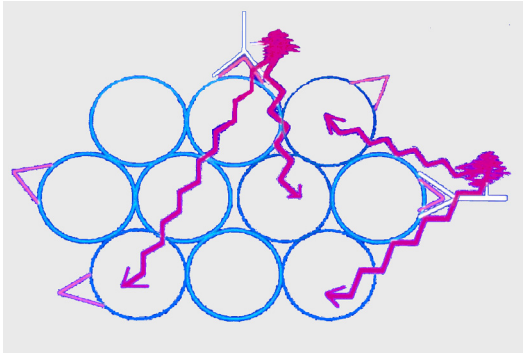

Figure 2.2 Crossfire effect.

While the range of radioisotope for diagnostic application is broad enough (In, I, Te, etc.), for therapeutic application is limited as only two radionuclides are used, Yttrium-90 and Renium-186. In particular Yttrium-90 (^{90}Y) has been applied with success to the treatment of several malignancies, it is easily obtained by a generator ^{90}Sr/^{90}Y; ^{90}Y has an half-life of 2.7 days and it is a pure β-emitter.

2.3.1 Radionuclides and chelating agents

In the past, biological macromolecules like enzymes, antibodies or other kinds of peptides, were radiolabeled binding the radioactive metal directly on the molecule. In particular the most frequently used radioisotope has been iodine (^{125}I and ^{131}I), due to its abundance and to its easy introduction into aminoacidic residues of proteins.

Currently it is preferred to proceed through indirect method. This involves the use of a chelator (specific to the particular metal) and a linker to covalently attach the chelator to the biomolecule. It is necessary to pay attention so that the label does not modify the zones appointed for the binding to the receptor and does not negatively influence therefore the affinity of the biological system. For example the chelating agent generally links to some part of the antibodies through a modified group of lysine. This random interaction risks to modify the receptor site of the antibody and consequently to alter its affinity for the antigen. In order to obviate to the problem, the chelator is attached to sulphur residues, far from the zone of tie with the antigen.[40]

The peraza-crown macrocycles constitute the greatest group among multidentate macrocyclic compounds.[41] These ligands are involved in numerous applications as selective complexing agents of transition and heavy metals and other metallic ions like alkaline earths.[42,43] The peraza-crown generally forms strong complexes when they have at least three nitrogen atoms on the ring. Two cyclic tetraamines have played a key role in

[40] Aftab, E.; Stoldt, H.S.; Testori, A.; lmperatori, A.; Chinol, M.; Paganelli, G.; Geraghty, J. *Eur. J. Surg. Oncol.* **1996**, *22*, 381-396.
[41] Bradshow, J.S.; Krakowiak, K.E.; Izatt, R.H. "Aza-crown macrocycles" in "*The chemistry of heterocyclic compounds*" Edward, C., Taylor, Ed., Wiley, J. & Sons Inc., New York, **1993.**
[42] Bianchi, A.; Micheloni, M.; Paoletti, P. *Coord. Chem. Rev.* **1991**, *110*, 17.
[43] Tsukube, H.; Yamashita, K.; Iwachido, T.; Zenki, M. *Tetrahedron Lett.* **1989**, *39*, 3983.

this field: the 12-membered 1,4,7,10-tetraazacyclododecane (cyclen) and the 14-membered 1,4,8,11-tetraazacyclotetradecane (cyclam)[44] (Figure 2.3).

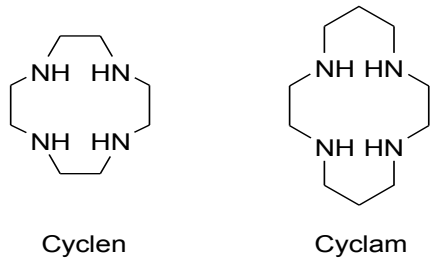

Figure 2.3 Cyclen and Cyclam structures.

These macrocycles have the advantage being N- and C-functionalized with side chains carrying ligating groups.[45,46] In particular, the respective tetraacetic acids: 1,4,7,10,-tetraazacyclododecane-*N,N',N'',N'''*-tetraacetic (H_4-DOTA or DOTA) and 1,4,8,11-tetraazacyclotetradecane-*N,N',N'',N'''*-tetraacetic (H_4-TETA or TETA) (Figure 2.4) were prepared from the previously mentioned macrocycles.

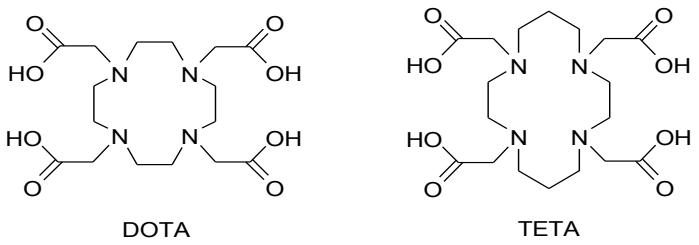

Figure 2.4 DOTA and TETA structures.

The first publication about the synthesis of these ligands has been described by Stetter *et al*.; their use have led to some improvements in stability *in vivo* compared to EDTA.[47,48]

Desreux *et al.* also conducted ^{1}H and ^{13}C-NMR studies on complexes of DOTA with lanthanides[49] and potentiometric measurements on this and other chelates.[50] Other studies

[44] Richmann, J.E.; Atkins, T.J. *J. Am. Chem. Soc*. **1974**, *96*, 2268.
[45] Di Vaira, M.; Mani, F.; Stoppioni, P. *J. Chem. Soc. Dalton Trans* **1998**, 1879-1884.
[46] Bu, X.H.; Cao, X.C.; Zhang, W.Q.; Zhang, R.H.; Clifford, T. *Transition Met. Chem*. **1997**, *22*, 513-515.
[47] Stetter, H.; Frank, W. *Angew. Chem.* **1976**, *88*, 760.
[48] Stetter, H.; Frank, W.; Mertens, R. *Tetrahedron* **1981**, *37*, 767.
[49] Desreux, J.F. *Inorg. Chem*. **1980**, *19*, 1319-1324.

on tetraaza-cyclams and their derivatives, as DOTA and TETA, investigated the connection between cavity size and ability to complex calcium[51] and trivalent lanthanides as La(III), Eu(III), Pr(III), Yb(III).[52]

The research work on the complexing ability of DOTA and TETA towards In(III) and Y(III) salts was particularly important. In fact ^{111}In (γ-emitter) and ^{90}Y (β-emitter) isotopes were already used for medical applications such as tracers.[53] In particular the stability of ^{90}Y-DOTA complex in physiological conditions appears very high.

In order to understand the importance of these results, it is appropriate to remember that since '70 Meares and his group tried to introduce binding sites for metal ions into the protein using modified chelating agents.[54]

The successful attempt in this field opened the possibility to use radioactive ions as tracers. In the following years monoclonal antibodies, labeled with macrocyclic chelates bind to radioactive metal ions as ^{111}In, ^{90}Y, ^{67}Cu, were introduced in the organism for tumors therapy and diagnosis.[55]

In order to favour the coupling with the specific immunoglobulin, one of the carboxylic groups of the *N*-tetraazamacrocycles was activated in the following way[56] (Figure 2.5).

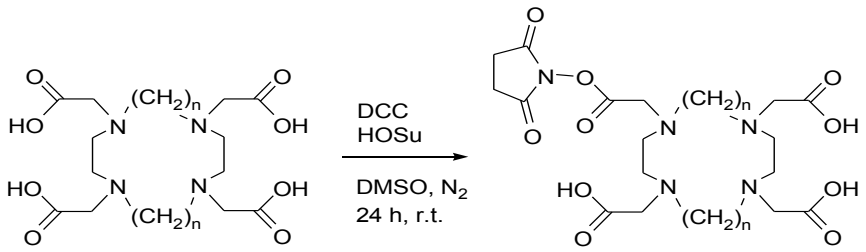

Figure 2.5 Activation of a chelating tetraazamacrocycle.

[50] Desreux, J.F.; Merciny, E.; Loncin, M.F. *Inorg. Chem.* **1981**, *20*, 987-991.
[51] Stetter, H.; Frank, W. *Angew. Chem. Int. Ed. Engl*. **1976**, *15*, 686.
[52] Desreux, J.F.; Barthelemy, P.P. *Nucl. Med. Biol*. **1988**, *15*, 9.
[53] Wu, C.; Virzi, F.; Hnotovich, D.J. *Nucl. Med. Biol.* **1992**, *19*, 239.
[54] Meares, F.; Goodwin, D.A.; Lenny, C.S.H.; Girgis, A.Y.; Silvester, D.J.; Nunn, A.D.; Lovender, P.J. *Proc. Natl. Acad. Sci. USA* **1976**, *73*, 3803.
[55] Hnatowich, J.; Layne, R.L.; Lanteigne, D.; Davis, M.A. *Science* **1982**, *220*, 613; Hnatowich, D.J.; Virzi, F.; Doherty, P.W. *J. Nucl. Med.* **1985**, *26*, 503; Cox, P.L.; Jankowski, K.J.; Kataki, R. *J. Chem. Soc. Chem. Comm.* **1989**, *12*, 797; Hnatowich, D.J. *Nucl. Med. Biol*. **1990**, *17*, 49; Deshpende, S.V.; De Nardo, S.J.; Kukis, D.L.; Mori, M.K; McCall, M.J.; De Nardo, C.L.; Meares, C.F. *J. Nucl. Med*. **1990**, *31*, 473.
[56] Buckeley, R.C.; Searle, F. *FEBS* **1984**, *166*, 202.

The carboxylic group, so activated, was reacted with the suitable monoclonal antibody of the class IgG and the compound obtained was labelled with halogen metal. Subsequent development of these chelating agents was the synthesis of bifunctional molecules. This type of molecules carried on one side strong chelate groups and on the other a pendant arm with a reactive functional group.[57] Among these, 2-(*p*-nitrobenzyil)-1,4,7,10-tetraazacyclododecane-*N,N',N'',N'''*-tetraacetic acid (*p*-nitrobenzyl-DOTA) (Figure 2.6) was particularly important.

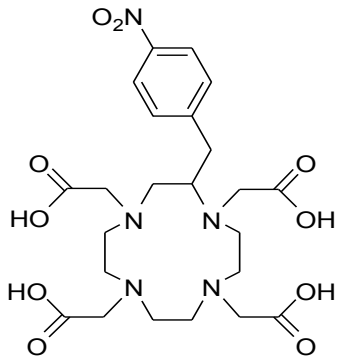

Figure 2.6 Structure of *p*-nitrobenzyl-DOTA.

This molecule is able to coordinate ^{90}Y strongly also in presence of biological ligands[58] and can binds G immunoglobulin (IgG) directly.

More recently, somatostatin analogues were used for carrying radioactive metals complexed with macrocyclic ligands on the human cancer cells[59,60] exploiting the fact that some classes of tumors were known to over-express certain receptors for the somatostatin. Among these compounds there is the eight amino acid somatostatin analogue octreotide (Figure 2.7).

[57] Meares, F.; Wensel, T.G. *Acc. Chem. Res*. **1984**, *17*, 202.
[58] Mori, M.K.; Meares, C.F.; De Nardo, S.J. *J. Am. Chem. Soc*. **1988**, *110*, 6266; Renn, O.; Meares, C.F. *Bioconjugate Chem*. **1992**, *3*, 563.
[59] Albert, R.; Smith-Jones, P.; Stolz, B.; Simeon, C.; Knecht, H.; Bruns, C.; Pless, J. *Bioorg. Med. Chem. Lett*. **1998**, *8*, 1207-1210.
[60] Heppeler, A.; Froidevaux, S.; Mäcke, H.R.; Jermann, E.; Béhé, M.; Powell, P.; Hennig, M. *Chem. Eur*. **1999**, *5*, 1974-1981.

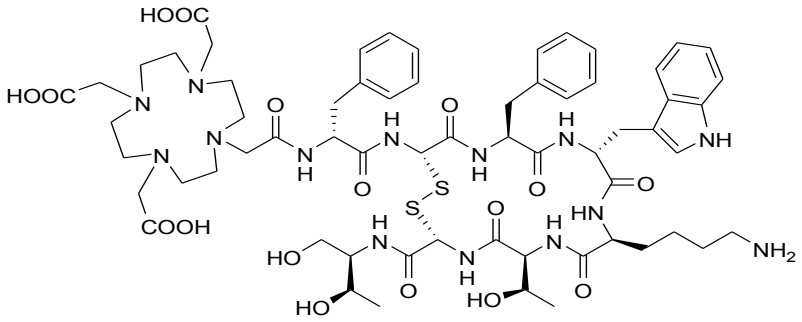

Figure 2.7 DOTA-Octreotide.

This compound was linked to DOTA to obtain the [DOTA°] adducts octreotide which were successful in for tumors individuation (if complexed with ^{111}In γ-emitter) but also in therapeutic applications with β-emitters such as ^{90}Y complexes.[61,62]

2.4 Radiolabeled monoclonal antibodies

The antibodies are glycoproteins produced by B-lymphocytes in the bone marrow; they help fight against foreign substances called antigens. When an antigen enters the body, it stimulates the immune system to produce antibodies. They can be divided into five classes (IgG, IgM, IgA, IgD and IgE) based on physical characteristics including the structure of the heavy chain, size, valency, and amino acid sequence.

The antibody consists of four polypeptide chains connected by disulfide and noncovalent bonds: two identical light (low molecular weight) chains and two identical heavy (high molecular weight) chains. At the end of these chains there is the amino terminal variable domain that is the binding site of antigens (Figure 2.8).

[61] De Jong, M.; Bakker, W.H.; Breeman, W.A.P.; Bernard, B.F.; Hofland, L.J.; Visser, T.J.; Srinivasan, A.; Schmidt, M.; Béhé, M.; Mäcke, H.R.; Krenning, E.P. *Int. J. Cancer* **1998**, *75*, 406-411.

[62] De Jong, M.; Breeman, W.A.P.; Bakker, W.H.; Kooij, P.P.M.; Bernard, B.F.; Hofland, L.J.; Visser, T.J.; Srinivasan, A.; Schmidt, M.; Erion ,J.L.; Bugaj, J.E.; Mäcke, H.R.; Krenning, E.P. *Cancer Research*, **1998**, *58*, 437-441.

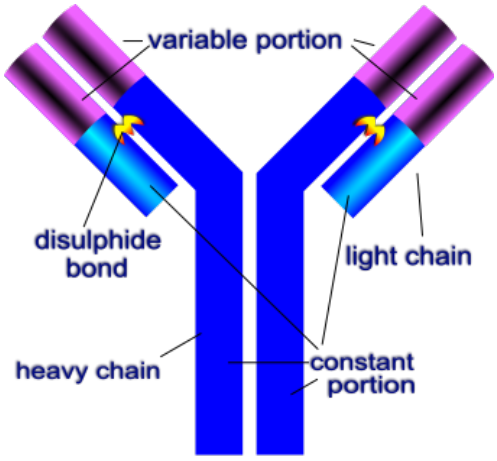

Figure 2.8 Antibody structure.

The production of monoclonal antibodies (MoAbs) (Figure 2.9) requires the use of animals, usually mice. The immunization of a mouse with an antigen is the first step in the production of MoAbs. When the mouse begins to produce antibodies against the antigen, its spleen is removed. Antibody-producing cells of the spleen are then fused with a myeloma tumor cells. That kind of cells can grow indefinitely in culture (myeloma is a B-cell cancer). They have lost the ability to produce antibodies. The fused hybrid cells (called hybridomas), are cancer cells and they will multiply rapidly and indefinitely. In this way it is possible to produce a large amounts of antibodies. The desired fusions are between healthy B-cells, producing antibodies against the antigen of interest, and myeloma cells. The production of the right hybridoma is not a simple process. The major problem is that some hybridomas produce wrong antibodies, constituted by two different antibodies: the first deriving from B-lymphocytes, the other one from unspecific antibody of tumoral cell. To solve this problem are used only myeloma cells that have lost a specific enzyme (hypoxanthine-guanine phosphoribosyltransferase, HGPRT). This enzyme enables cells to synthesize purines, using an extracellular source of hypoxanthine as a precursor. Ordinarily, the absence of HGPRT is not a problem for the cell because cells have an alternative pathway that they can use to synthesize purines. When cells are exposed to aminopterin (a acid folic analogue), they are unable to use this other pathway and are now fully dependent on HGPRT for survival. Therefore cannot grow under certain conditions (namely in the presence of HAT medium). Unfused myeloma cells cannot grow because they lack HGPRT. Unfused normal spleen cells cannot grow indefinitely because of their

limited life span. Hybridoma cells (produced by successful fusions) are able to grow indefinitely because the spleen cell partner supplies HGPRT and the myeloma partner is immortal. Hybridoma cultures can be maintained indefinitely: *in vitro* (culture vessels) or in mice.

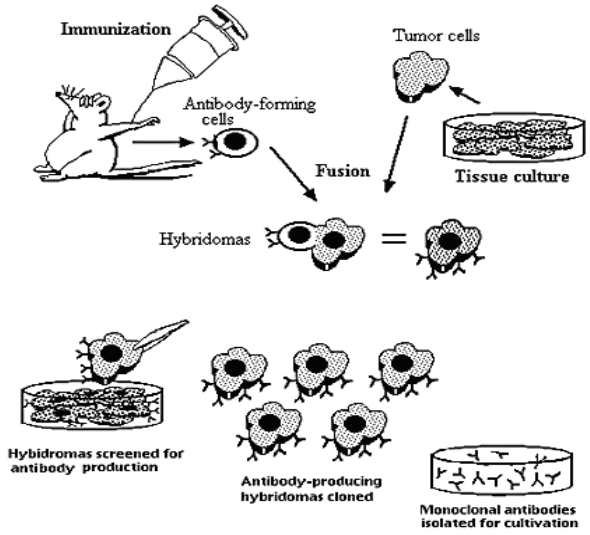

Figure 2.9 Production of monoclonal antibodies.

Monoclonal antibodies are important agents used in biomedical research, in diagnosis of diseases and in treatment of such diseases as infections and cancer.[63]

When they are used in therapy, monoclonal antibodies can react against specific antigens on cancer cells and may enhance the patient's immune response. They can be conjugated or linked to anticancer drugs, radioisotopes, biologic response modifiers, or toxins. Antibodies are used in several diagnostic tests to detect small amounts of drugs, toxins or hormones and for AIDS diagnosis. They can be used to treat viral diseases, to classify strains of a single pathogen, to identify and to trace specific cells or molecules in an organism. Furthermore they are used in the radioimmunodetection and radioimmunotherapy of cancer.[64,65,66,67] Radiopharmaceuticals based on monoclonal

[63] Zalutsky, M.R. *C.R.C. Press*, Boca Raton, Florida **1989**.
[64] Mach, J.P.; Buchegger, F.; Forni, M. *Immunol. Today* **1981**, *2,* 239.
[65] Epenotos, A.A.; Britton, K.E.; Mather, S. *Lancet* **1982**, *2*, 999.
[66] Larson, S.M. *J. Nucl. Med.* **1985**, *26,* 538.
[67] Buraggi, G.L.; Callegaro, L.; Mariani, G.; Turrin, A.; Cascinelli, N.; Attili, A.; Bombardieri, E.; Terno, G.; Plassio, G.; Dovis, M. *Cancer Res.* **1985**, *45*, 3378.

antibodies require validation and quality control. The tests are performed on compounds radiolabeled before their administration. In several studies, some authors showed that a big amount of radioactivity recovered in blood and normal tissues was caused by radiolabeled monoclonal antibodies denatured or with any immunogenic property.

Radiochemical purity is defined as the total radioactivity percentage bounded to antibody and it is measured by simple chromatographic techniques.

There are many limitations when using radiolabeled monoclonal antibodies for treating solid tumors in humans.[68] One of the most limitation using MoAbs in RIT is an abnormal high interstitial pressure of the tumor. This characteristic belongs overall to the center of tumor where, moreover, the vascularization is reduced or absent. In particular the diffusion of the smallest MoAbs (150 kDa) from blood-vessels to interstitial matrix is decelerate by high interstitial pressure. In addition, directly labelled MoAbs circulate for days with maximum tumor concentration occurring at 1-2 days with continuing high blood concentration for several more days. Therefore, even when properly selected MoAbs are employed, only a small percentage (usually not more than 1%) actually localizes on the tumor. The remaining 99% continues to circulate in the blood stream and diffuses to different parts of the organism, accumulating radioactivity in healthy tissues particularly in the kidneys, liver and bone marrow, causing possible damage. The accumulation of radioactive dose in tumor models obtained from mice is about 20-30% of the administered dose per gram of tumor, while 0,1% is obtained in human models.[69,70]

This low tumor-background ratio remains the main problem of the Radioimmunotherapy strategy. In attempt to overcome the low uptake of label by the tumor and improve the tumor-to-blood ratio, at the end of ’80 years many pretargeting systems were studied.[33,71,72,73] The concept of tumor pretargeting is based on the separate administration of MoAbs and radiolabel. Such systems need a modified monoclonal antibody (first conjugates) that permits a second component (second conjugates) to bind specifically to it. Pretargeting protocols, based on the Av/biotin system, are currently used

[68] Epenetos, A.A.; Snook, D.; Durbin, H. *Cancer Res* **1986**, *46*, 3183-3191.
[69] Strand, S.E.; Zanzonico, P.; Johnson, T.K. *Med. Physics* **1993**, *20*, 515.
[70] Mann, D.B.; Cohen, M.B.; Saxton, R.E.; Morton, D.L.; Benedict, W.F.; Korn, E.L.; Spolter, L.; Graham, L.S.; Chang, C.C.; Burk, M.W. *Cancer* **1984**, *54*, 1318.
[71] Paganelli, G.; Malcovati, M.; Fazio, F. *Nucl. Med. Commun*. **1991**, *12*, 211.
[72] Goodwin, D.A.; Meares, C.F.; McCall, M.J.; McTigue, M.; *J. Nucl. Med*. **1988**, *29*, 226-234.
[73] Goodwin, D.A. *J. Nucl. Med*. **1995**, *36*, 876-879.

for applications in clinical oncology because the specific MoAbs are easily biotinilated and can bind the avidin with high affinity.

2.5 Pretargeting approaches: rationale for Pretargeting

Pretargeting techniques have been first proposed by Goodwin *et al*.[74,75] to improve the performances of radioimmunodetection (immunoscintigraphy) and RAIT. Instead of chemically coupling the radioactive isotope to the antibody itself, or to a fragment of the antibody, a tumor- seeking agent (an immunoconjugate) bearing a binding site for a small molecule is used to target tumor cells. This immunoconjugate, which is not labeled, is injected first. It diffuses and tags the target cells with specific binding sites for the small molecule that carries the active payload. After partial excretion of the immunoconjugate, the labelled molecule is injected in a second step and binds to the tumor bound immunoconjugate (Figure 2.10). In pretargeting techniques, the slow antibody plasma clearance, which favours tumor uptake, is not associated with increased radiation dose to normal tissues since the antibody is not labelled. The small labelled molecule has a fast diffusion in body tissues and a rapid plasma clearance which should result in fast tumor uptake and low circulating activity. Obviously, antigen shedding and antibody internalization are potential limitations to pretargeting approaches. Antibodies or antibody fragments usually constitute the tumor-specific ligands, but any substance capable of binding specifically to tumor cells *in vivo* could be used. Many different systems have been proposed to ensure the recognition between the antibody and the tracer: another antibody (usually an anti-hapten antibody), the avidin-biotin system[23,76] or complementary nucleotides.

[74] Goodwin, D.A.; Mears, C.F.; McTigue, M.; David, G.S. *Nucl. Med. Commun.* **1986**, *7*, 569.
[75] Goodwin, D.A.; Meares, C.F.; David, G.F.; McTigue, M.; McCall, M.J.; Frincke, J.M.; Stone, M.R.; Bartholomew, R.M.; Leung, J.P. *Int. J. Rad. Appl. Instrum. B.* **1986**, *13*, 383.
[76] Paganelli, G.; Magnani, P.; Zito, F.; Villa, E.; Sudati, F.; Lopalco, L.; Rossetti, C.; Malcovati, M.; Chiolerio, F.; Seccamani, E. *Cancer Res.* **1991**, *51*, 5960-5966.

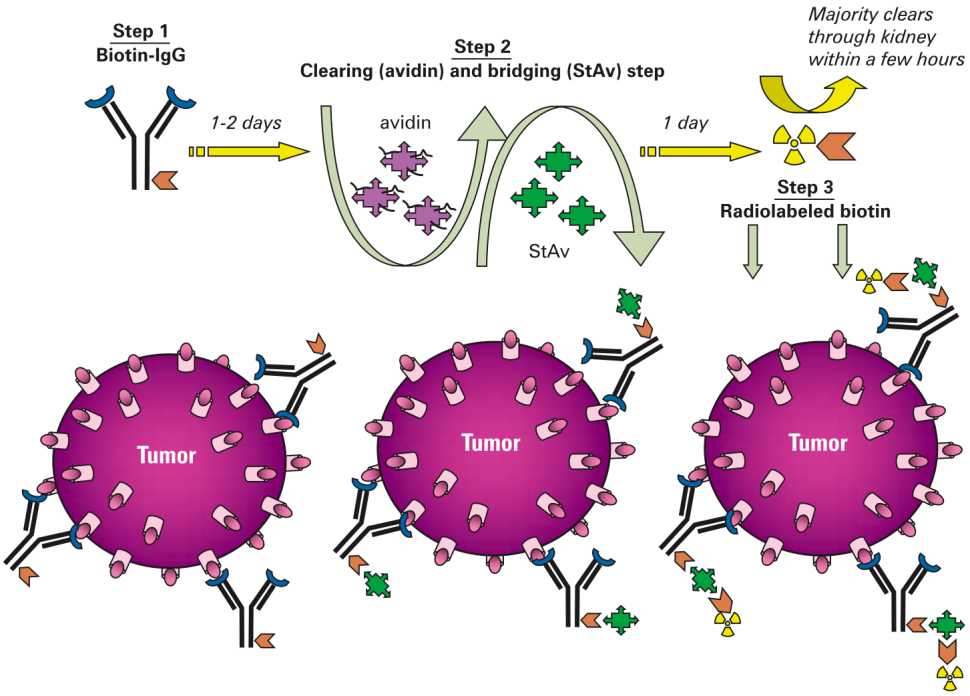

Figure 2.10 Schematic of a three-step procedure.

If pretargeting was used just as described above, it would not achieve much higher targeting efficacy than directly-radiolabeled antibodies. Indeed, excess immunoconjugate present in the circulation binds the labelled molecule and reduces its clearance. With high-affinity systems, large immunoconjugate doses or short time intervals between immunoconjugate and labelled molecule injections, high irradiation doses are delivered to normal tissues because of extended whole-body retention of the activity. Conversely, if the labelled molecule is injected only when most antibody conjugate has cleared or if its affinity for the antibody conjugate is weak, it disappears rapidly from the circulation, usually through the kidneys and only a small fraction of the injected activity binds the tumor. High tumor-to-non-tumor contrast ratios can be obtained, but tumor uptake and radiation exposure are low.[77,78] Using sophisticated pharmacokinetic computer models, Jain *et al.*[79] and Weinstein *et al.*[80] concluded that simple pretargeting techniques afford

[77] Kranenborg, M.H.; Boerman, O.C.; Oosterwijk-Wakka, J.C.; de Weijert, M.C.; Corstens, F.H.; Oosterwijk, E. *Int. J. Cancer* **1998**, *75*, 74.
[78] Klivenyi, G.; Schuhmacher, J.; Patzelt, E.; Hauser, H.; Matys, R.; Moock, M.; Regiert, T.; Maier-Borst, W. *J. Nucl. Med.* **1998**, *39*, 1769.
[79] Zhu, H.; Jain, R.K.; Baxter, L.T. *J. Nucl. Med.* **1998**, *39*, 65.
[80] Sung, C.; van Osdol, W.W.; Saga, T.; Neumann, R.D.; Dedrick, R.L.; Weinstein, J.N. *Cancer Res.* **1994**, *54*, 2166.

only limited improvement over directly-labelled antibodies. For these reasons, the basic concept of pretargeting has been further improved as described below.

2.5 Avidin-biotin system

This biological system has long been widely used for in vitro applications, in ELISA (Enzyme-Linked Immunosorbent Assay) tests and in molecular biology. The system takes advantage from the extremely high affinity between avidin and biotin in order to form macromolecular complexes on target molecules, which are thus made detectable by physical or chemical means.[81,82]

The avidins are functionally defined by their ability to bind biotin with high affinity and specificity, without recognising or binding any other physiological compound with any strength. Avidins are small oligomeric proteins made up of four identical subunits, each bearing a single binding site for biotin.

Avidin (Table 2.2) is a 66 KDa glycosylated protein, commonly isolated from hem egg white, and positively charged with an isoelectric point of approximately 10.5.

Streptavidin, a non glycosilated analogue, isolated from *Streptomyces avidinii*, is nearly neutral at physiological pH, in contrast to avidin, with an isoeletric point approximately 6.

Table 2.2 Avian Avidin and Streptavidin characteristics.

Characteristics	Avian Avidin	Streptavidin
Molecular weight	66.000	65.000
Number of subunits	4	4
Subunit M.W.	16.000	16.000
Biotin binding sites/mole	4	4
Kd of biotin complex	10^{-15}	10^{-15}
Oligosaccharide subunit	1	0
Mannose subunit	4.5	-
Glucosamine subunit	3	-
Isoelectric point	10.5	6

[81] Wilchek, M.; Bayer, E.A. *Anal. Biochem.* **1988**, *171*, 1.
[82] Wilchek, M.; Bayer, E.A. *Immunol. Today* **1984**, *5*, 39.

Biotin (vitamin H) (Figure 2.11) is a 244 Da molecule, constituted by a functional "head" region (bicyclic ring) which binds avidin and a functionally irrelevant carboxyl "tail" end (valeric acid), which can be chemically altered with little or no effect on the molecule.

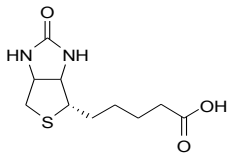

Figure 2.11 Biotin (vitamin H).

The latter can be differently functionalized. Biotin is the coenzyme for four carboxylases. Through its carboxyl group, biotin is linked covalently to epsilon-amino group of lysine in four carboxylases that play critical roles in intermediary metabolism. The avidin can inhibit these reactions because "seizes" the biotin. A large series of biotin derivatives, obtained by modifying the carboxyl group, are commercially available and can be used to covalently bind to a variety of molecules containing primary amines, thiol groups aldehydes and so on. The biotinylation of MoAbs does not usually alter the biodistribution of antibodies and in general many properties of the molecules.[76] The avidin-biotin binding is noncovalent but for the dissociation is required a value of pH superior to 13 or inferior to 2, very improbably in physiological conditions. The studies of crystal structures of the biotin-avidin (A) and biotin-streptavidin (B) complexes (Figure 2.12) showed many hydrogen-bond networks of the respective proteins with the native ligand.[83] In particular the biotin ring system shows a similar network of interactions in both proteins, whereas the respective biotin carboxylates show distinct differences.

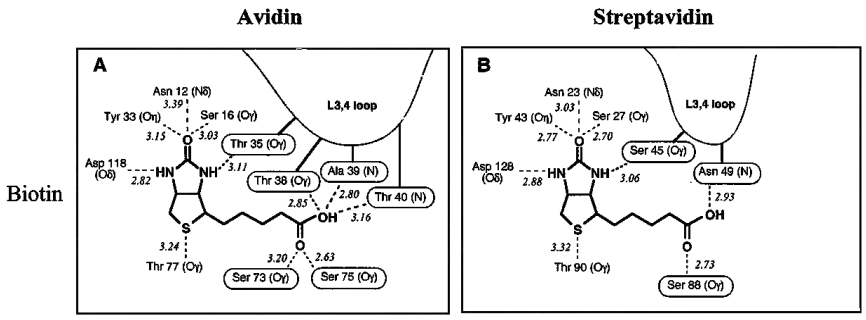

Figure 2.12 Biotin-avidin and biotin-streptavidin complexes.

[83] Pazy, Y.; Kulik, T.; Bayer, E.A.; Wilchek, M.; Livnah, O. *J. Biol. Chem.* **2002**, *277*, 30892-30900.

The external part of the binding site is covered essentially from non-polar aminoacids, as moreover the head of the biotin is non-polar. The advantages of the biotin-avidin system are:

- Avidin binding to biotin is specific enough to ensure the binding is directed only to the target of interest.
- The affinity of avidin for biotin is extremely high, with a dissociation constant of the avidin-biotin complex of 10^{-15} M. For practical purposes, their binding can be regarded as irreversible.[84,85]
- The avidin is not toxic for the animals.

However the avidins, xenomolecules, can give an immune response. A study about this problem showed that 20% of the patients treated with avidin develops an antibody response.

2.5.1 Strategies of pretargeting

Two major methods, 2 steps and 3 steps, are presently used in the clinical settings with the aim to improve the delivery of radionuclides to tumors.[71,72,86]

The 2 Step Pretargeting System (Figure 2.13) has been used mainly to target intraperitoneal tumors. In a typical protocol, biotinylated MoAbs are injected intraperitoneally (first step). In this way MoAbs recognize rapidly the target tissue: the immunoglobulines not bound to the tumor leave the intraperitoneal cavity trough the lymphatic system and than trough the blood stream. To obtain diagnostic images with high resolution, it is necessary that the metabolic systems discharge free MoAbs from the organism. 3-5 days later a solution of radiolabeled streptavidin is injected intraperitoneally (second step). After 3 hours from the second administration, SPECT (Single Photon Emission Computed Tomography) exam is performed. This approach originated very high radioactivity distribution tumor to normal tissue (9:1) and tumor to blood ratios (14:1) suggesting that this two-step strategy might be superior to conventional radiolabeled MoAbs for intraperitoneal targeting of tumors.

[84] Green, N.M. *Biochem. J*. **1963**, *89*, 585.
[85] Green, N.M. *Adv. Protein Chem.* **1975**, *29*, 85-133.
[86] Paganelli, G.; Riva, P.; Deleide, G.; Clivio, A.; Chioleiro, F.; Scasselati, G.A.; Malcovati, M.; Siccardi, A. *Int. J. Cancer*. **1988**, *2*, 121.

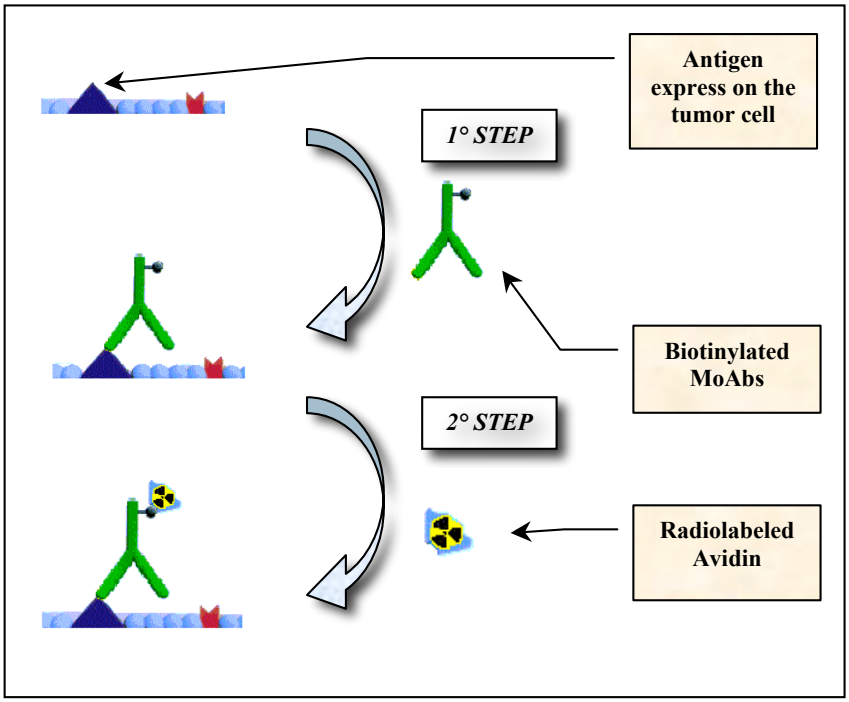

Figure 2.13 2-Step Pretargeting System.

The locoregional approach is useful when tumor is confined into the peritoneal cavity or in other locoregional approaches. In the presence of widespread disease, a systemic injection of the tracer is nonetheless required. A three-step approach has been designed for these cases, where conjugates need to be cleared not only from a well-defined body cavity, but also from the entire blood pool.

A typical three protocol (Figure 2.14) involves the systemic injection of biotinylated MoAbs (first step). These antibodies will reach their target (the tumor) in 24 to 48 hours. 1-2 days after the first injection, the patient receives an endovenous injection of avidin. Due to the high affinity between these two molecules, avidin will bind to the biotin, which is already on the tumor. The excess circulating biotinylated antibodies in the form of cold complexes via avidin will be metabolised by the liver. On the third day, when dispersed antibodies have been eliminated, the patient receives the last injection: a dose of biotin, which has been previously labelled with a radioactive isotope. In this way, the radioactive biotin is strongly attracted by the avidin on the tumor and reaches its specific target in few minutes, destroying it. Radioactive biotin not bound to the tumor is rapidly excreted through the kidneys thus it is a very small molecules.

The rapid blood clearance of the radiolabeled biotin allows imaging to be performed short time (90-120 minutes) after injection and with very low background activity.

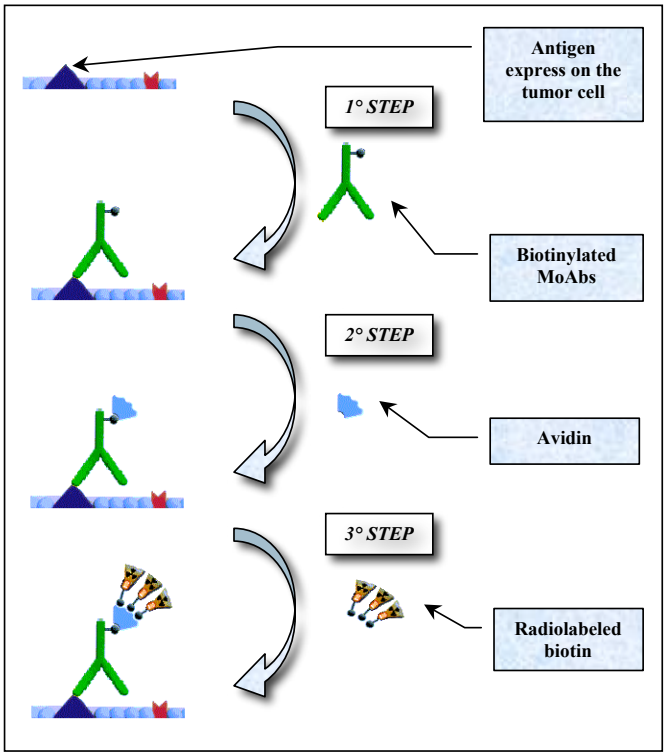

Figure 2.14 3-Step Pretargeting System.

In both Pretargeting Systems (2 and 3 step), the label does not alter any avidins properties and their affinity is maintained (approximately 90%).

The new strategies based on pretargeting techniques have shown many advantages compare to the use of directly labelled antibodies:[87]

- Fast clearance of the labelled molecule. With small radiopharmaceuticals the background radioactivity levels are very low and this allows to perform imaging in a few minutes after injection.
- The removal of circulating antibodies. In the 3-step the excess of circulating biotinylated MoAbs are removed as cold complexes, which are taken up and metabolized by the liver. This is the major factor in background reduction and it is obtained prior to label injection.

[87] Magnani, P.; Paganelli, G.; Modorati, G. *J. Nucl. Med*. **1995**, *37*, 967-971.

- Retention of immunoreactivity of MoAbs. The biotinylation does not usually alter many properties of the antibodies.
- Signal amplification. In this strategy, because of each avidin has four small pockets where biotin molecules can be bound, the signal is triplicate.

The disadvantages are mainly two:

- The request of reiterated injections with particular attention to doses and times of administration.
- The immunogenicity of the avidin: an immune response is observed in 20% of patients.

At the first time the 3-step pretargeting system was tested in 20 patients with CEA-expressing tumors, using antibodies anti-CEA (anticarcinoembryonic).

Presently, this system has been used for melanomas, gliomas, carcinomas and other types of tumors but, in theory, it can be applied to all types of tumor for which specific antibodies are available. It requires, however, a specially equipped area for the manipulation of radioisotopes.

2.6 Previous results in the production of radiolabelled biotin derivatives

The conjugation of the biotin with a chelating agent is obtained trough the reactivity of the carboxyl group tail end. The –COOH group can react with almost all types of compounds. At first the carboxylic chains of DOTA or of 1,4,7,10-tetraazacyclo-tridecane-*N*,*N'*,*N''*,*N'''*-tetraacetic acid (TRITA) were used to link the macrocycle to biotin.

Than, structures with different spacer arms were studied. Among the compounds synthesized on a large scale, the 2-(*p*-nitrobenzyil)-1,4,7,10-tetraazacyclododecane-*N,N',N'',N'''*-tetraacetic acid (*p*-nitrobenzyl-DOTA) gives the respective derivative *p*-aminobenzylic (Figure 2.15) by hydrogenation in the presence of a catalytic amount of Pd/C. This derivative, trough its amino group, can be linked to biotin molecule, directly or trough a spacer arm.[88]

[88] Renn, O.; Soodwin, D.A.; Studer, M.; Moran, J.K.; Jacques, V.; Meares, C.F. *J. Control. Release* **1996**, *39*, 239.

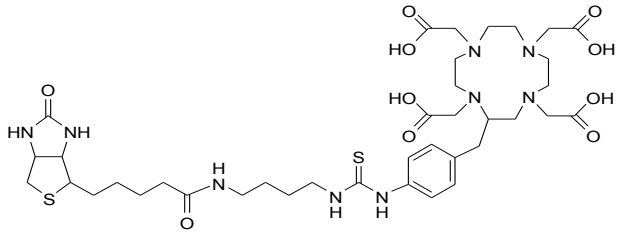

Figure 2.15 Structure of a biotinyl derivative conjugated with *p*-aminobenzyl-DOTA.

The spacer arm between the carboxyl group and the chelating agent has the function to maintain the 'head' of biotin at the right distance from the azamacrocycle. This is a suitable distance for binding the biotin moiety to the Av pocket and for using the best activity of the labelled part.

A biotin derivative containing an azamacrocycle as chelating agent has been recently prepared in our laboratory:[89] 10-[2-[[6-[[5-[(3a*S*,4*S*,6a*R*)-Hexahydro-2-oxo-1*H*-thieno[3,4-*d*]imidazol-4-yl]pentyl]amino]hexyl]amino]-2-oxoethyl]-1,4,7,10-tetraazacyclododecane-1,4,7-triacetic Acid (MonoDOTA) (Figure 2.16), conjugated trough one of the four N-carboxymethyl chains of DOTA to a six carbon atoms alkylamino spacer. The –COOH groups of the macrocycle are involved in the radionuclide coordination. But literature dates demonstrated which the metallic ion is coordinated via carboxylic oxygen atoms of only two of the four functionalized chains; so the amide bond with the spacer arm does not have important effect on the coordination capacity of the DOTA for radioisotopes.

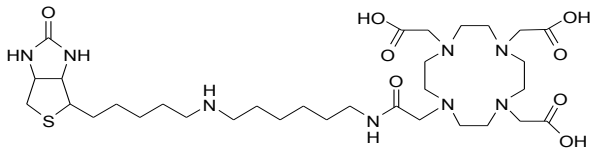

1

Figure 2.16 MonoDOTA.

This biotinyl derivative, compared to compounds synthesized in the past, can also overcome the limitations due to instability in physiologic environment. The amide bond between the sidearm of biotin and the spacer carrying the chelating moiety, are *per se*

[89] Sabatino, G.; Chinol, M.; Paganelli, G.; Papi, S.; Chelli, M.; Leone, G.; Papini, A.M.; De Luca, A.; Ginanneschi, M. *J. Med. Chem.* **2003**, *46*, 3170-3173.

easily hydrolysable by the serum biotinidase,[90] an enzyme that is also able to break biotinyl peptides. At the same time, molecular changes of the biotin side arm, carrying the radionuclide chelating unity, can affect the binding to Av or Sav, diminishing the affinity and causing loss of the radiating power on cancer cells. The pivotal work of Wilbur's group[91] and of other researchers[92] has highlighted some structural characteristics of the biotin conjugates, which hamper the action of biotinidase and allow to retain high affinity for Av and Sav pockets. Pazy *et al*. showed that the avidin pocket is much more sensible than Sav to structural changes on the biotin side chain, which caused the disordered conformation of a critical loop.[83] On the basis of these findings, these authors suggested an explanation of the fundamental role of streptavidin when administered in the three-step procedure.

The new biotin conjugate, obtained in a few steps synthesis, already described in the original work by Sabatino *et al.*, was prepared for reaction of the original carboxyl group of the biotin with diamino hexane. Subsequently, the amide CO was reduced to CH_2 group in order to prevent the recognition at the site of the enzymatic attack and, finally, the *N*-hexylamine was coupled to one of the four carboxymethyl chains of DOTA chelator. The reduction is an excellent way to prevent the enzimatical degradation but the synthetic step is not so simply and occur with very low yield.

The binding and stability studies in vitro on the new molecule labelled with ^{90}Y and ^{111}In (labelling yield greater than 97%) with avidin, confirmed its clinic applicability.

In particular the binding studies of the new ^{90}Y-labeled biotin derivative **1**, in the presence of a 1:2 Av/**1** molar ratio (which is two times the natural 1:4 molar ratio), showed that about 85% of ^{90}Y-labeled compound **1** was bound to Av, whereas at the natural 1:4 molar ratio only about 50% was bound. Data at 2 and 24 hours at 37 °C were similar, indicating that the binding occurs rapidly and is almost irreversible despite the linkage with the bulky DOTA molecule. Stability studies showed that in both saline and diluted human serum the activity was almost completely associated to the labelled **1** molecule up to 48

[90] Wilbur, D.S.; Hamlin, D.K.; Chyan, M.K.; Kegley, B.B.; Pathare, P.M. *Bioconjugate Chem.* **2001**, *12*, 616-623.
[91] Wilbur, D.S.; Hamlin, D.K.; Chyan, M.K.; Kegley, B.B.; Quinn, J.; Vessella, R.L. *Bioconjugate Chem.* **2004**, *15*, 601-616, and references therein.
[92] Axworthy, D.B.; Theodore, L.J.; Gustavson, L.M.; Reno, J.M. *United States Patent* **1997**, *5*, 608-660.

hours. Consequently, we can affirm that biotinidase are not able to break the **1** conjugate in a significant extent.

Due to the good results obtained in vitro experiments, in particular the high affinity to avidin, the ^{111}In-labeled compound **1** (a radionuclide γ-emitter) was used in a clinical study in order to verify the bio distribution into health and ill tissues.

A therapy trial based on the 3-step pretargeting has been conduced in a patient with histologically confirmed grade III or IV glioma and documented residual disease or recurrence after conventional treatment. The first step of the protocol consisted of biotinylated anti-tenascin monoclonal antibodies, injected i.v., at a dose of 2 mg. Avidin (10 mg) were then administered i.v. 24 hours after the antibody. At the third day 5 mg of HAS (Human Serum Albumin) biotinylated were administered, followed, after 15 minutes, by 3 mCi of ^{111}In-DOTA-biotin.

Experimental conditions and procedures will be discussed adequately in Chapter 5.0.

2.7 BisDOTA derivatives

2.7.1 Solid phase synthesis of BisDOTA

In this PhD thesis it is described for first the synthesis on solid phase of new mono-biotin derivatives containing azamacrociclic chelating agents and it is shown the preliminary study of their biological activity such as potential radiopharmaceuticals for a future application in clinical oncology in according to the pretargeting system.[93] In the second part of this section will be described the synthesis and preliminary tests *in vitro* of BisBiotin derivatives.

In the three-step pretargeting technique, the radioactivity is carried on the tumor by the radiolabeled biotin, which is functionalized with the DOTA chelator. Since only a small percentage really localizes on the tumoral lesion, it is important that the DOTA-biotin conjugate is labelled at high specific activity. The maximum allowed stoichiometry of a DOTA conjugated molecule is one metallic radionuclide per molecule, and this may limit the dose effectively delivered to the tumor. Further developments are now being

[93] Pratesi, A.; Bucelli, F.; Mori, I.; Chinol, M.; Verdoliva, A.; Paganelli, G.; Riveccio, V.; Gariboldi, L.; Ginanneschi, M. *J. Med. Chem*. **2010**, *53*, 432–440.

explored and are here presented: new biotin derivatives, carrying two DOTA groups per molecule (BisDOTA), have been synthesized and tested. BisDOTA is substantially a modified biotin, conjugated with two molecules of DOTA through bi-functional spacers.

The rationale is to label the BisDOTA-biotin at higher specific activity if compared to the MonoDOTA analogue. In fact, each biotin can theoretically bind up to two metallic radionuclides. In this way, BisDOTA-Biotin radiolabeled at high specific activity could deliver a higher radiation dose to the tumour and then improve the efficacy of targeted radionuclide therapy, provided the high affinity for Av is retained.

We report the synthesis of new biotin derivatives carrying two DOTA groups, featured by spacers chosen to have a good compromise between the necessity of a correct distance of the bulky DOTA chelating groups from each other and from the biotin head.

In the solid phase synthesis, activation of carboxylic acids is a key step for the formation of amide or ester bonds.

The coupling reactions, carried out with carbodiimides, (Figure 2.17) proceed by conversion to an *O*-isoacylurea, which is very reactive and can undergo a rearrangement to give unreactive species (*N*-acylurea) or cause loss of chiral integrity. Active species can be captured using a hydroxylamine derivative to give the corresponding active ester. In this regard, HOBt is less reactive than the *O*-isoacylurea but is more stable and less prone to racemization. HOAt is an additive more expensive compared to HOBt, but gives best results.

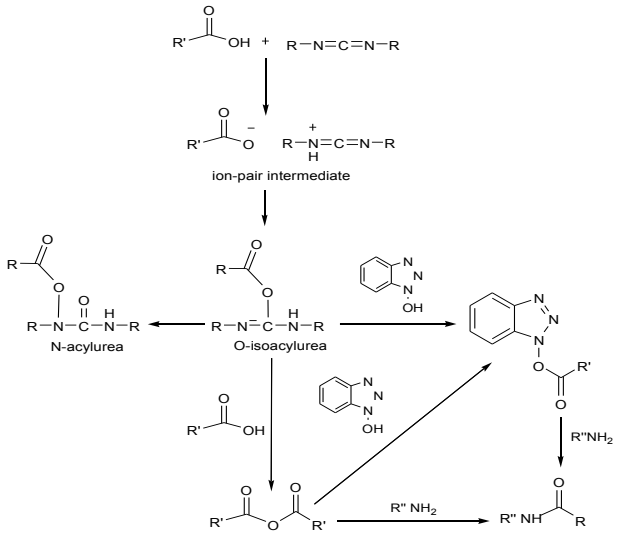

Figure 2.17 Carbodiimide mechanism.

Following the growing interest in peptides, numerous coupling reagents have been developed and became commercially available, including carbodiimmides,[94] alone or plus additives (HOBt, HOAt),[95] phosphonium salts,[96] and uronium (aminium) salts[97] (Figure 2.18).

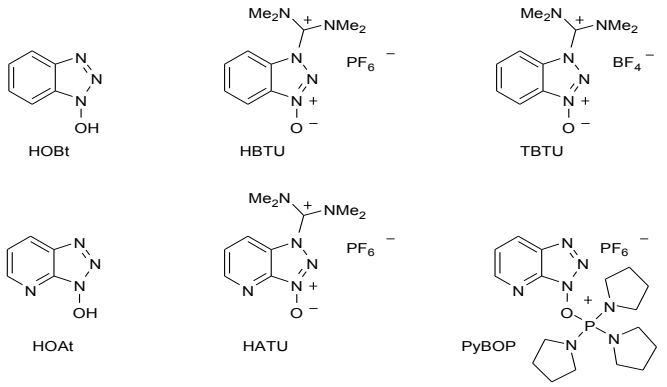

Figure 2.18 Comercially available HOBt-based coupling reagents.

The most valuable approach involves the use of *in situ* coupling reagents. Most of them engaged the benzotriazole,[98] or azabenzotriazole[99] ring system as crucial chemical structures, subsequently transformed into a good leaving group.

When described for the first time, HBTU was assigned the structure of uronium salt, presumably by analogy with the previously described phosphonium salts. Following studies showed that the true structures, in both the crystalline state and in solution, were the aminium isomers and not the uronium isomers (Figure 2.19).

[94] Sheehan, J.C.; Hess, G.P. *J. Am. Chem. Soc*. **1955**, *77*, 1067.
[95] König, W.; Geiger, R. *Chem. Ber*. **1970**, *103*, 788; Carpino, L.A. *J. Am. Chem. Soc.* **1993**, *115*, 4397.
[96] Castro, B.; Dormoy, J.R.; Evin, G.; Selve, C. *Tetrahedron Lett*. **1975**, *16*, 1219-1222; Coste, J.; Le-Nguyen, B.; Castro, B. *Tetrahedron Lett*. **1990**, *31*, 205-208.
[97] Carpino, L.A.; Imazumi, H.; El-Faham, A.; Ferrer, F.J.; Zhang, C.; Lee, Y.; Foxman, B.M.; Henklein, P.; Hanay, C.; Mugge, C.; Wenschuh, H.; Klose, J.; Beyermann, M.; Bienert, M. *Angew. Chem. Int. Ed*. **2002**, *41*, 441-445; Li, P.; Xu, J.C. *J. Chem. Soc. Perkin 2*, **2001**, 113-120.
[98] Carpino, L.A.; Henklein, P.; Foxman, B.M.; Abdelmoty, I.; Costisella, B.; Wray, V.; Domke, T.; El-Faham, A.; Muegge, C. *J. Org. Chem*. **2001**, *66*, 5245-5247.
[99] Carpino, L.A.; Xia, J.; Zhang, C.; El-Faham, A. *J. Org. Chem*. **2004**, *69*, 62-71; Carpino, L.A.; Ferrer, F.J; Albericio, F. *J. Org. Lett*. **2001**, *3*, 2793-2795.

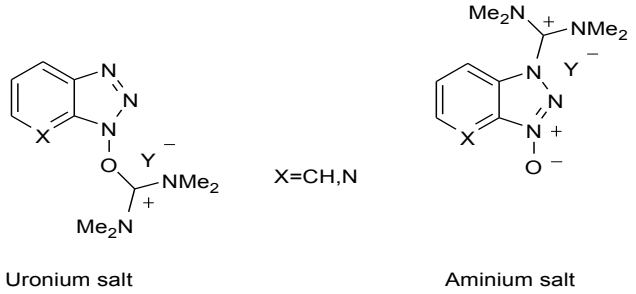

Figure 2.19 HOBt-based coupling reagents (uronium and aminium isomers).

The carbodiimide reagents, used in the presence of HOBt or HOAt for the inhibition of side reactions such as racemization, are mostly replaced by phosphonium and aminium salts of HOBt or HOAt.[100]

The same active esters formed by the system DCC/HOBt can be prepared with onium (aminium/uronium and phosphonium) salts in the presence of a base. Couplings with aminium/uronium salts in the presence of base have proven to be more effective than those carried out with phosphonium reagents or carbodiimide in the presence of hydroxylamine derivatives. On the other hand, reagents based on phosphonium salts are preferred to their aminium/uronium counterparts for cyclization, because the latter compounds can give guanidilation reactions on the amino group. The tetrafluoroborate or the hexafluorophosphate anions, generally used as non-nucleophilic counterions in the aminium salts, had no significant influence on the coupling rate or racemization, but only in the solubility of the coupling reagents. BOP was one of the first phosphonium salts developed for SPPS. However, this reagent generates a poisonous by-product (HMPA, hexamethylphosphoramide) (Figure 2.20).

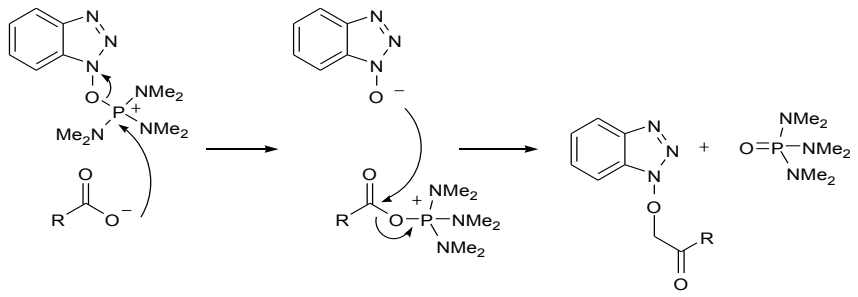

Figure 2.20 Mechanism of the BOP.

[100] Carpino, L.A.; El-Faham, A.; Minor, C.A.; Albericio, F. *J. Chem. Soc. Chem Commun*. **1994**, 201.

For this reason, halogeno-phosphonium salts and phosphonium-HOBt reagents, were then developed. The progenitor of the aminium salts was HBTU (the mechanism, up to now not well defined, is described below in Figure 2.21).

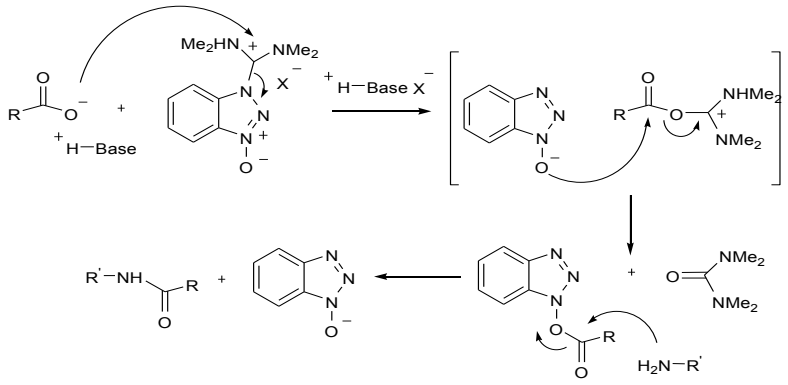

Figure 2.21 Mechanism of the aminium salts.

The most common side reactions in peptide coupling reactions are the formation of *N*-carboxyanhydrides, diketopiperazines and guanidines (Figure 2.22).

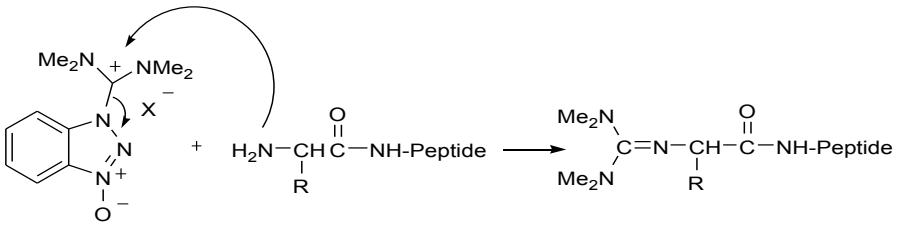

Figure 2.22 Guanidine derivative formation with aminium salts.

The amino group block can happen if the reagent is added directly to amino component. For this reason the carboxylic group have to be activated with the uronium salt before the addition of the amino component. Anyway the activating reagents have not to be in excess compared with the carboxylic function.

A critical point of synthetic pathways of MonoDOTA and BisDOTA, prepared in solution, reduction of the amidic group to an aminic by a suspension of the starting amide in THF with $BH_3 \cdot THF$ reagent. This reaction required a tedious work-up of the crude product even if the yield was quite satisfactory. Recently, Wilbur and co-workers claimed that biotin amide derivatives which have a carboxylate function α to the biotinamide bond

block biotinidase activity.[92] These considerations prompted us to prepare α-biotinamido lysine derivatives by direct coupling of biotin with L-lysine suitably protected on the ε-amino group. Then, the introduction of the bi-functional spacer and of two DOTA molecules should have to complete the synthesis. Aiming to ensure a fast synthetic approach, we decided to exploit the solid phase peptide synthesis (SPPS), routinely used in our laboratory of peptide chemistry. This technique can rapidly afford the products in the range from μM to mM scale. In the SPPS technique the compound is bound to an insoluble support: thus at the end of any synthetic step, each unreacted reagent can be removed by a simple washing procedure, greatly decreasing the time required for synthesis. A key step in that synthetic strategy is the activation of carboxylic acids, as previously. Moreover it is necessary to protect the side-chains by using protecting group, like in this case Fmoc, *t*-Bu and MTT groups (Table 2.3).

Table 2.3 Main protecting groups.

Protecting groups	Deprotection conditions	Stability conditions
Fmoc	Piperidine 20% in DMF	TFA, Pd
MTT	1% TFA in DCM 1-5% TIS	Pd(0), hydrazine, piperidine
t-Bu	95% TFA	TFA<60%, Pd(0), Pd, hydrazine, piperidine

These groups are orthogonal each other, i.e. they are removed in different conditions (Figure 2.23), in this way we can deprotect selectively only an amine group.

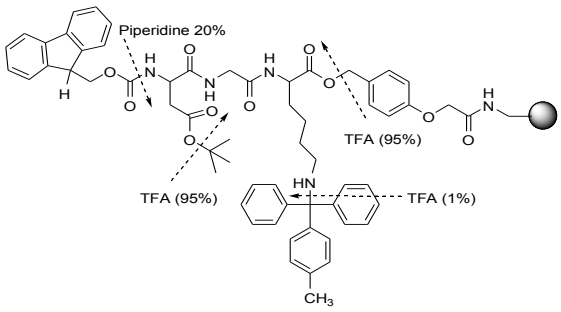

Figure 2.23 Fmoc/MTT/*t*-Bu strategy.

The resin used for the synthesis, commercially available, is a Wang resin, *p*-benzyloxybenzyl alcohol, (100-200 mesh) (Figure 2.24) functionalized by a lysine protected in α with Fmoc and in ε with MTT.

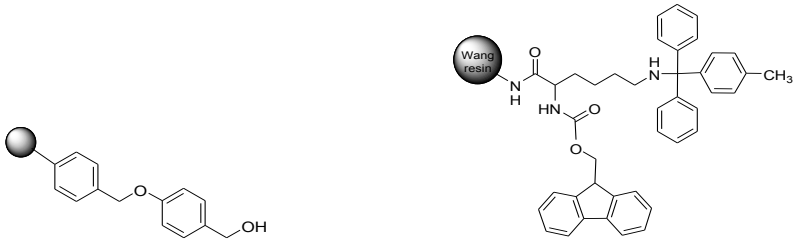

Figure 2.24 Wang resin and Fmoc-Lys-(MTT)-Wang resin.

For the determination of the effective resin loading, it is necessary to weigh exactly the dried Fmoc-amino acid resin (about 1 μmol, related to Fmoc) into a 10 mL volumetric flask and to add piperidine (0.4 mL) and DCM (0.4 mL) (Scheme 2.1).

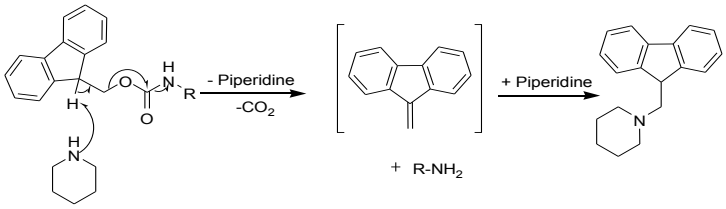

Scheme 2.1

After 30 min the mixture is diluted with MeOH (1.6 mL) and DCM to 10 mL. Absorbance of the solution is measured at 301 nm against a blank reagent (0.4 mL of piperidine and 1.6 mL of MeOH diluted to 10 mL with DCM). The substitution ratio is calculated from the formula:

$$\frac{mmol}{g} = \frac{A_{301}}{7800} \times \frac{10\ ml}{g\ of\ resin}$$

The procedure should be carried out in duplicate, taking an average from the two values obtained.

Uncertain coupling results were checked by the ninhydrin test as described by Kaiser.[101]

Peptide cleavage from the resin and deprotection of the amino-acids side chains were carried for the Wang resin with a solution of TFA/TIS/H_2O (95:2.5:2.5). TIS is a nucleophilic reagent (known as scavenger) which is added to the cleavage mixture in order to prevent the generation of reactive cationic species. These obtained from the protecting groups and the handles on the resin, can, unless trapped, react with residues which contain nucleophilic functional groups: Trp, Met, Tyr and Cys. In addition to TIS, the most commonly used scavengers are EDT, thioanisole and phenol. EDT is not only an extremely good scavenger for *t*-butyl cations, but it assists in the removal of the trityl protecting group from cysteine and is particularly effective in preventing acid catalyzed oxidation of tryptophan residues. Thioanisole is known to accelerate Arg removal in TFA. Phenol is thought to offer some protection to Tyr and Trp residues.

2.7.2 Synthesis of BisDOTALys-C_3

The orthogonally protected Fmoc-L-lysine-(MTT) was purchased already bonded to Wang resin (Scheme 2.2). After deprotection of the α-amino group by piperidine, the coupling with the activated biotin (HOBt/TBTU/NMM in DMF) was performed only one time. The MTT group was removed with a solution of TFA/TIS/DCM (1:2.5:96.5). Initially the solution became a fluorescent yellow colour, indicating the presence of MTT in solution. Washing was continued until the wash solution became colourless again.

The Fmoc-protected spacer **5** (Figure 2.25), readily available for SPPS, was activated as above and then added to the resin affording the Fmoc-protected diamine. Three couplings are necessary to obtain a negative Kaiser test.

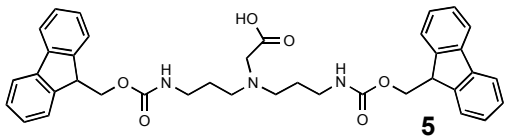

5

Figure 2.25 *N,N*-Bis[3-(Fmoc-amino)propyl]glycin

[101] Kaiser, E.; Colescott, R.L; Bossinger, C.D.; Cook, P.I. *Anal. Biochem*. **1970**, *34*, 595.

In the case of the SPPS technique, the solid support does not allow the use of aqueous solutions and DMF or DCM are the commonly used solvents, ensuring a good resin swelling. Therefore, tris(*t*-butyl) ester of DOTA,[102,103] well soluble in DMF, was exploited as the coupling agent in the preparation of these bioconjugates.

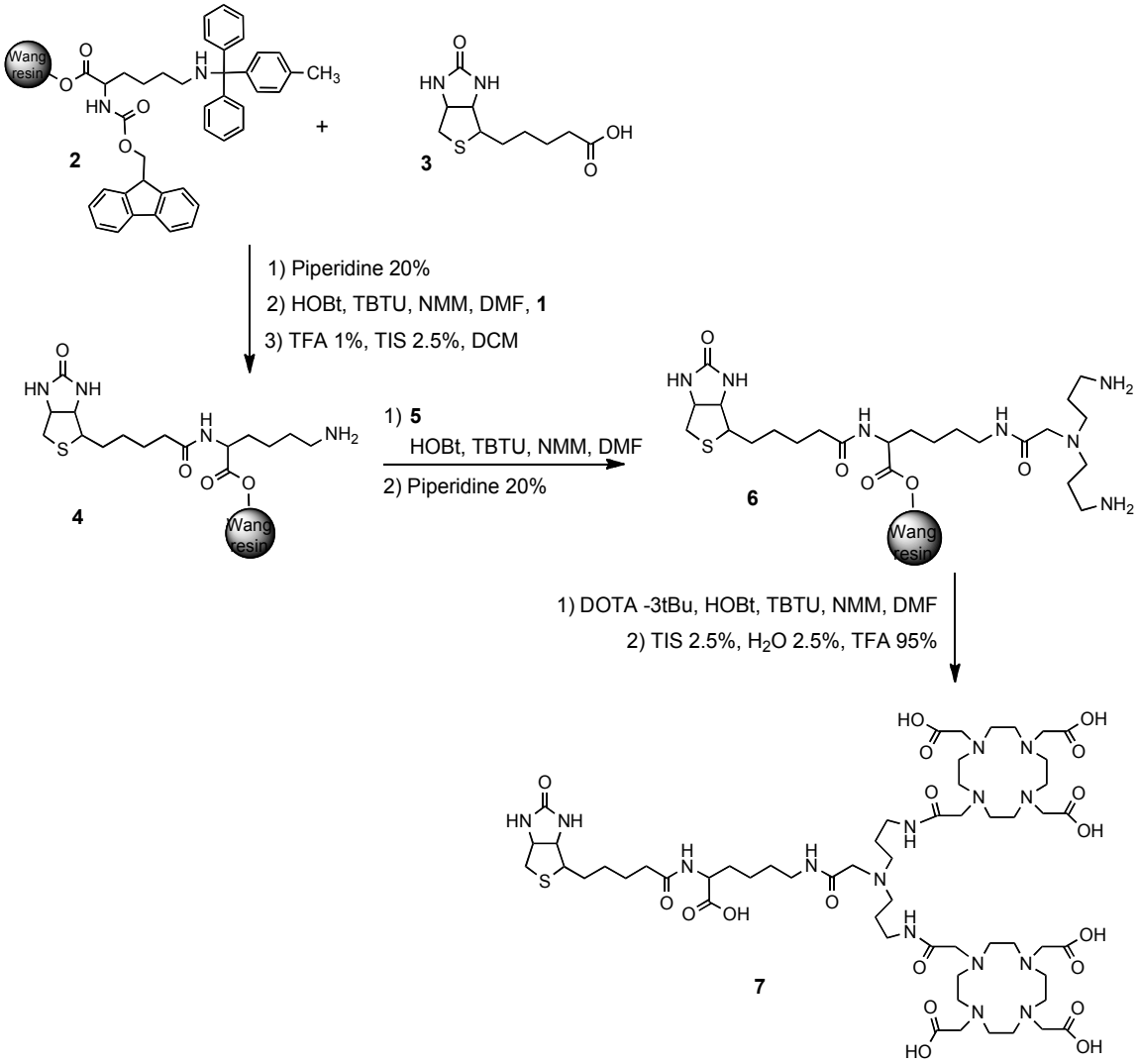

Scheme 2.2

[102] Bhorade, R.; Weissleder, R.; Nakakoshi, T.; Moore, A.; Tung, C.T. *Bioconjugate Chem.* **2000**, *11*, 301-305.

[103] Cheng, Z.; Chen, Y.; Miao, Y.; Owen, N.K.; Quinn, T.P.; Jurisson, S.S. *J. Med. Chem.* **2002**, *45*, 3048-3056.

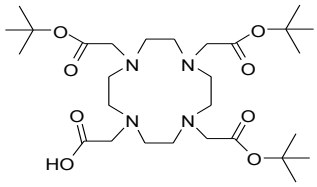

Figure 2.26 DOTA tris(*t*-butyl ester).

The tris-protected DOTA derivative appears more advantageous than the not protected one:

- it permits to overcame the mono-activation problem, by reason of only one of the carboxylic functions is able to react;
- it is soluble in the commonly solvents used in the SPPS (DMF).

The cleavage of the Fmoc protecting groups from **6** gave access to the free amino groups prone to conjugate with two mole equiv. of the commercially available DOTA-tris(*t*-butyl ester).

The reaction was performed using the same activating reagents as above described. Coupling reaction was controlled by the Kaiser test. The final compound, carrying two DOTA moieties, still protected as *t*-butyl esters, was then cleaved from the resin with a solution of TFA/H_2O/TIS (95:2.5:2.5). This TFA concentration was also able to hydrolyse (2 h) the ester functions at room temperature, affording the expected BisDOTA as the free carboxylic acid **7**. The crude product was purified by semipreparative RP-HPLC to give pure **7** in 35% yield. The structure was characterized by ESI-MS.

2.7.3 Synthesis of BisDOTA-Lys-(pAB)-C_3

In order to move further away from the Av pocket the bulk of the radio labelled DOTA moiety, we have designed a new derivative containing a rigid and planar spacer (Scheme 2.3). Therefore, the suitably protected *p*-amino benzoic acid was smoothly coupled with the biotinamido lysine anchored to the resin obtained following the synthetic procedure previously described (Scheme 2.2).

HOBt/TBTU/NMM method was used in the coupling reaction and only one coupling was necessary to obtain a negative Kaiser test.

After Fmoc deprotection, the spacer **5** was added giving the protected *bis*-amine **10** (Scheme 2.3).

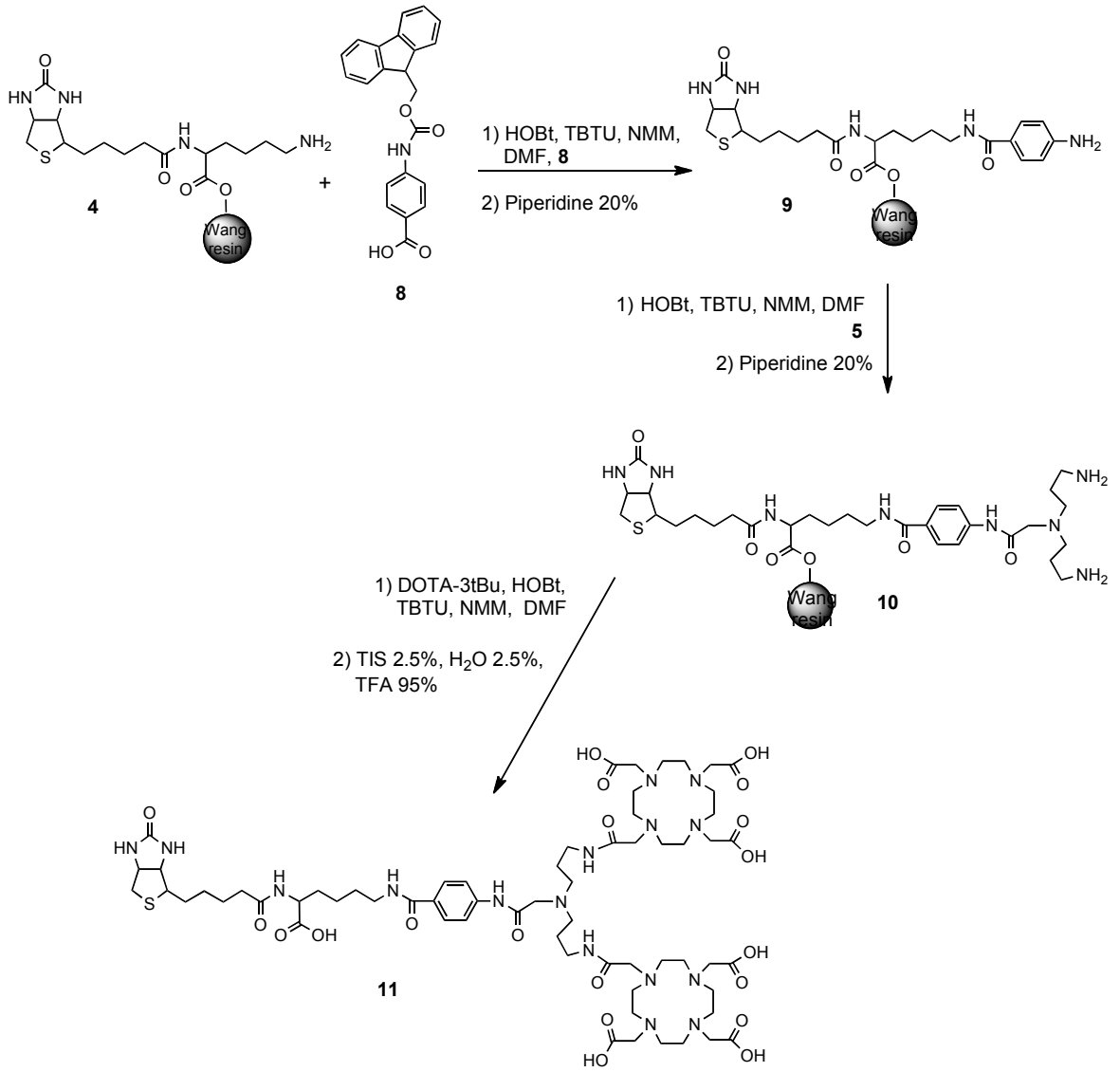

Scheme 2.3

In this coupling reaction the usual HOBt/TBTU/NMM method gave only a small quantity of the wanted derivative **9**, the remaining product being the starting reagent. This is probably due to the lower nucleophilicity of the NH_2 group bonded to aromatic ring.

HATU/NMM method was thus used in this case in order to overcome the coupling reaction difficulty. The Kaiser test does not yield useful results with the *p*-amino benzoic acid NH_2 group, for this reason the coupling reaction was controlled by subsequent micro

cleavages. Four couplings were necessary to observe the complete disappearance of starting reagent.

The conjugation with DOTA-tris(*t*-butyl ester) followed the same procedure as for BisDOTALys-C_3. Coupling reaction was controlled by the Kaiser test. Cleavage from the resin and removal of the *tert*-butyl protection was performed using a solution of TFA/H_2O/TIS (95:2.5:2.5). The crude product was purified by semipreparative RP-HPLC to give pure **11** in 20% yield. The final product was identified by ESI-MS and elemental analysis.

Thus the synthetic approach on solid phase resulted very efficient both in terms of yield and purification. The yields, calculated on the all reaction steps, are higher if compared to the BisDOTA derivatives synthesized in solution, avoiding the isolation and purification of intermediate products. However, DOTA tris(*t*-butyl) ester high cost represented, in this approach, the unique disadvantage.

2.8 Design and synthesis of new biotin derivatives

In this PhD thesis, the creation of new biotin derivatives was carried out through the synthesis of compounds mainly characterized by having two molecules of biotin.

These derivatives were called *BisBiotin*, and were designed and synthesized with the aim to increase the affinity between the radiopharmaceutical drug and avidin: since avidin has three pockets available for binding biotin, a compound with two biotin residues, should have twice probability to engage the site and this could affect not only the affinity towards the protein, but also minimize the amount of radiopharmaceutical dispersed in healthy tissue.

The compounds synthesized in this sense are divided into classes: BisBiotinaMonoDOTA (Figure 2.27 and Figure 2.28) and BisBiotinaBisDOTA (Figure 2.29), the second class includes two residues of biotin and two chelating groups, in order to redouble the amount of radiation conveyed by each molecule, and to increase the potency of the product.

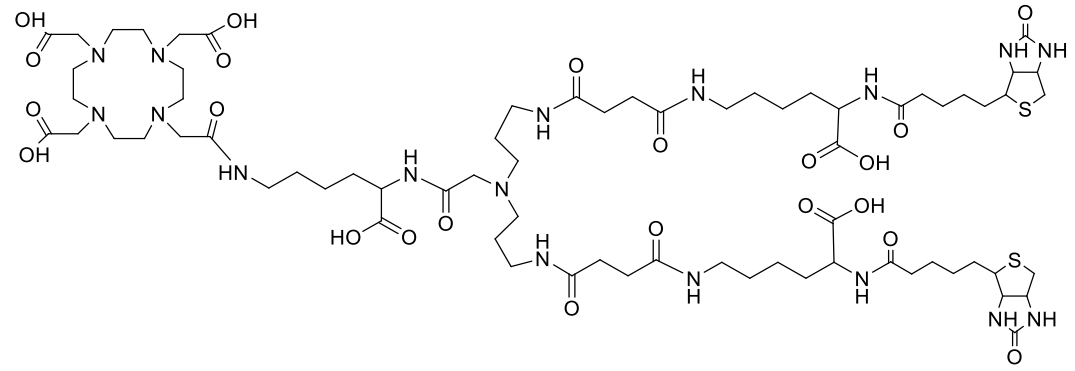

Figure 2.27 BisBiotinMonoDOTA

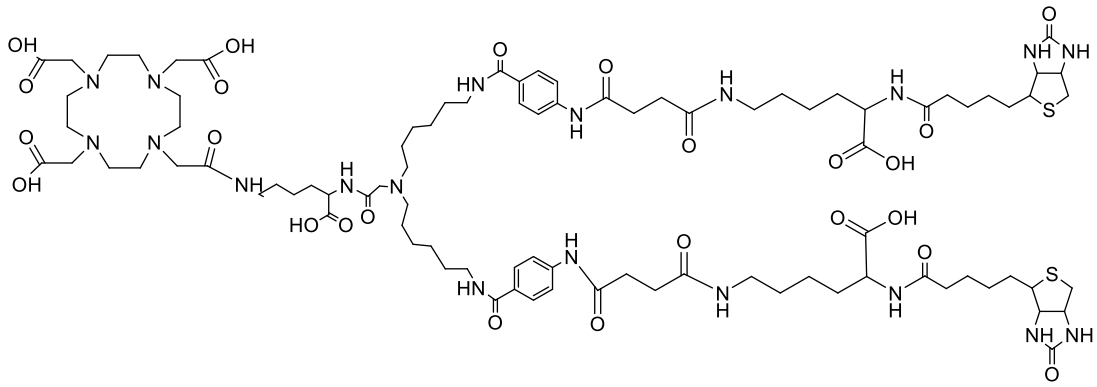

Figure 2.28 Bis BiotinMonoDOTA-(*p*AB)-C_6

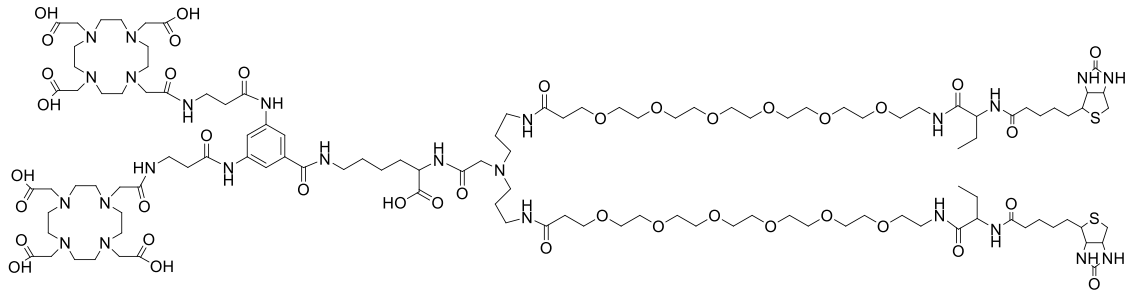

Figure 2.29 BisBiotinaBisDOTA-(PEG)-C_3

2.8.1 Synthesis of BisBiotinMonoDOTA-C_3

The synthesis of BisBiotinMonoDOTA-C_3 is made from Fmoc-Lys(MTT)-Wang resin, **2**, which has two orthogonal protections: the α-amino group is protected with Fmoc, that can be removed under basic conditions, whereas the protected ε-amino group (MTT) is deprotected under weakly acidic conditions. The first step planned for the reaction is the

coupling with the bifunctional spacer **5** on the α-amino group of Lys anchored to the Wang resin (Scheme 2.4).

Before carrying out this reaction, it is necessary to remove the Fmoc group, in weakly alkaline environment, followed by several washings to completely remove any residual solution of deprotection.

The amino groups are, therefore, free and reactive, so we can introduce a solution of the spacer *N,N*-Bis [3-(Fmoc-amino) propyl] glycine **5** (for simplicity called Spacer-C_3), properly activated. The Spacer-C_3 is in fact an amino acid, functionalized on the α-amino group in symmetrical way, it has two amine functions Fmoc-protected and the carboxyl groups is free and reactive.

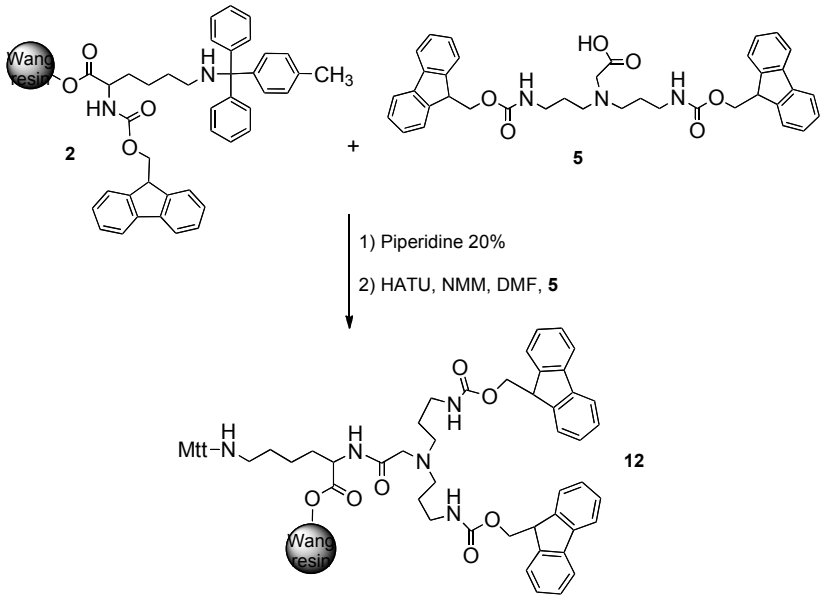

Scheme 2.4

After the obtainment of this first intermediate, **12**, we decided to extend the arms of the spacer. In fact at the ends of these arms two biotin residues were introduced so that to ensure the necessary distance between them to allow the correct disposition into two different avidin pockets.

The necessity to extend the arms of the molecule is accompanied by another requirement: the reagent used must have two carboxylic functions, one for the binding with the Spacer C_3, and the other to form an amide bond with the amine group of Lys side-chain. The compound identified for this purpose is succinic anhydride, **14**, an heterocyclic

molecule that, after the reaction, give rise to an amide bond and opens linearly, leaving a free carboxyl group.

The elongation of the chain (Scheme 2.5) involved the Fmoc deprotection of the two amino groups of the Spacer C_3 and then the reaction with succinic anhydride. The literature data shows that long time is required for this coupling and heating conditions not appropriate for this kind of products,[104,105] for this reason, we chosen to perform the reaction in a microwave reactor.

Under the mild reported conditions the reaction took place in a very short time (approx. 30 min.), without adding any activator and using anhydrous THF.

The choice of the solvent was due to the fact that THF has a relatively low dispersion factor, thus avoiding large increases of temperature after irradiation. For this reaction temperature remained between 40 and 65 °C.

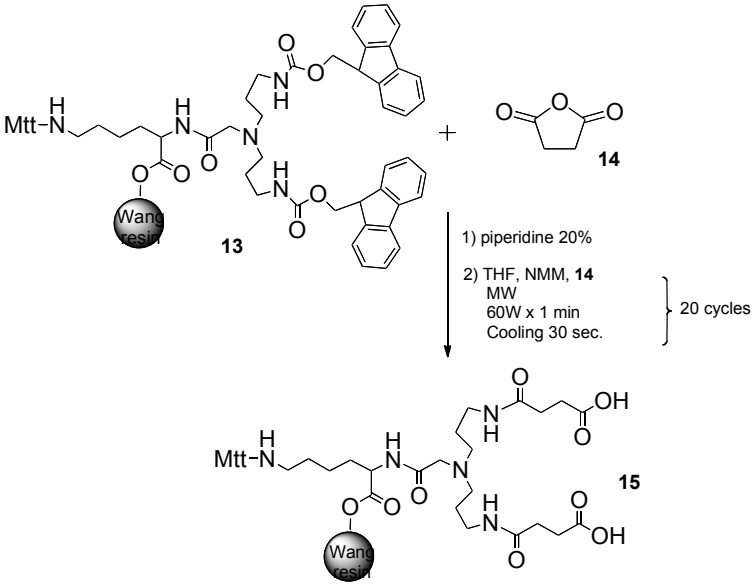

Scheme 2.5

The intermediate **15** is, in turn, a compound suitable to react with Fmoc-Lys(H)-OtBu, **17**, a building-block specially prepared in order to have the free ε-amino group, and the α-amino group protected with Fmoc while the and carboxy group was protected as tert-butyl ester. The preparation of the building block was necessary by the fact that this

[104] Kappel, J.C.; Barany, G. *Letters in Peptide Science* **2003**, *10*, 119-125.
[105] Jagesar, D.C.; Hartl, F.; Buma, W.J.; Brouwer, A.M. *Chem. Eur. J.* **2008**, *14*, 1935-1946.

product, important for the synthesis, is not a commercial one.[106] Masking the carboxyl group with tert-butyl ester we obtain an orthogonal protection, which is removed only during the final cleavage. The procedure for the synthesis of the protected Lysine is described in Experimental Section.

The function to be activated (i.e. the carboxyl group) is now on resin and therefore we introduced for the first the solution containing the activators and after this, the amino acid.

The coupling (Scheme 2.6) not needed to be preceded by deprotection and predisposed the molecule to the next step, namely the introduction of biotin.

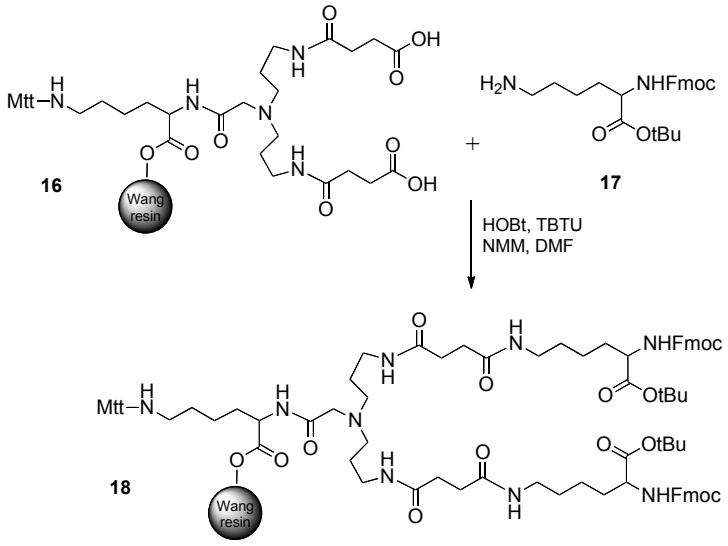

Scheme 2.6

Compound **18**, deprotected from Fmoc groups, was the suitable to react with biotin, properly activated: the resulting amide bond is surely resistant to the degradation by biotinidases, thanks by the steric hindrance of the carboxylic group on the Lys residue.[90]

The coupling (Scheme 2.7) completed the elongation of the of the spacer arms, so the next step is the removal of the MTT group from lysine anchored to the Wang resin.

[106] Kazuyoshi, T.; Akira, A.; Hiroko, N.; So-ichi, T.; Yoshihisa, M.; Hiroaki, T.; Yoshihiro, H. *Synthesis* **1994**, *10*, 1063-1066.

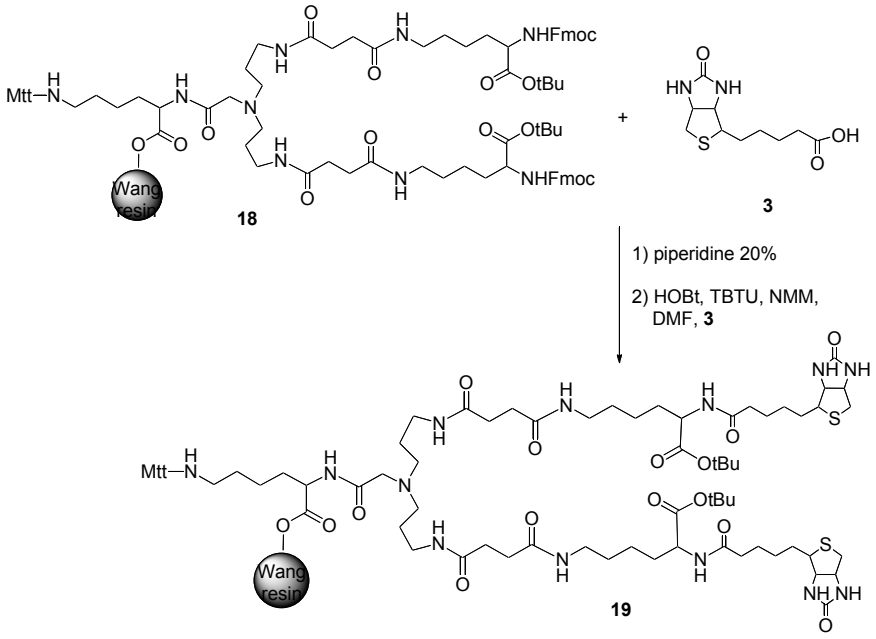

Scheme 2.7

The removal of the MTT protecting group, done in weakly acidic conditions, does not affected the permanent protective *tert*-butyl, which was removed within the total cleavage, in extremely acidic conditions.

The compound **19**, deprotected from methyltrityl group, is ready for the last reaction (Scheme 2.8) of this synthetic procedure, i.e. the coupling with the DOTAtris-*t*Bu, **20**, suitably activated. After the reaction, the whole molecule was prone to be obtained by the total cleavage in a strong acid, performed by long time reaction that allowed the complete removal of the permanent protections from the compound and the separation of the final product from the resin.

The presence of the TIS in solution ensured that the cleaved protecting groups should not be reactive again toward the molecule, the TIS acting as a scavenger for these ionic compounds.

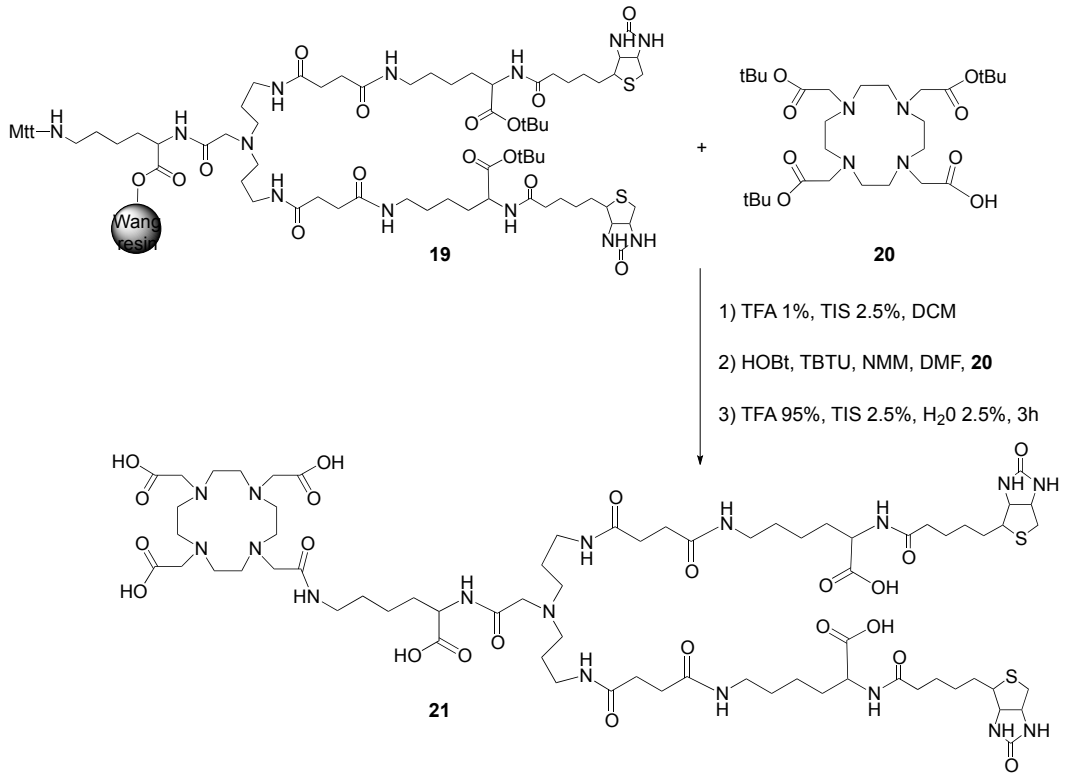

Scheme 2.8

2.8.2 Synthesis of BisBiotinMonoDOTA-(pAB)-C$_6$

The synthesis of the derivative BisBiotinaMonoDOTA-(*p*AB)-C_6 was carried out following the same synthetic route used for the previous compound, starting from Wang resin, **2**. The first step was the Fmoc deprotection, followed by the binding to the bifunctional spacer (Scheme 2.9).

In this second synthesis the compound *N,N*-Bis[6-(Fmoc-amino)hexyl]glycine, or Spacer C_6, **27**, was used as spacer; this is an higher homologue of C_3, being in fact an N-substituted Gly, carrying as substituents hydrocarbons with six carbon atoms.

The use of this spacer is useful in order to further extend the arms that hold biotin, with the aim to increase the chance that biotins will penetrate simultaneously in two different pockets of avidin. The spacer C_6 is not commercially available, and we were forced to prepare it as shown in Scheme 2.10.[107]

[107] Hujakka, H.; Ratilainen, J.; Korjamo, T.; Lankinen, H.; Kuusela, P.; Santa, H.; Laatikainen, R.; Narvanen, A. *Bioorg. Med. Chem.* **2001**, *9*, 1601-1607.

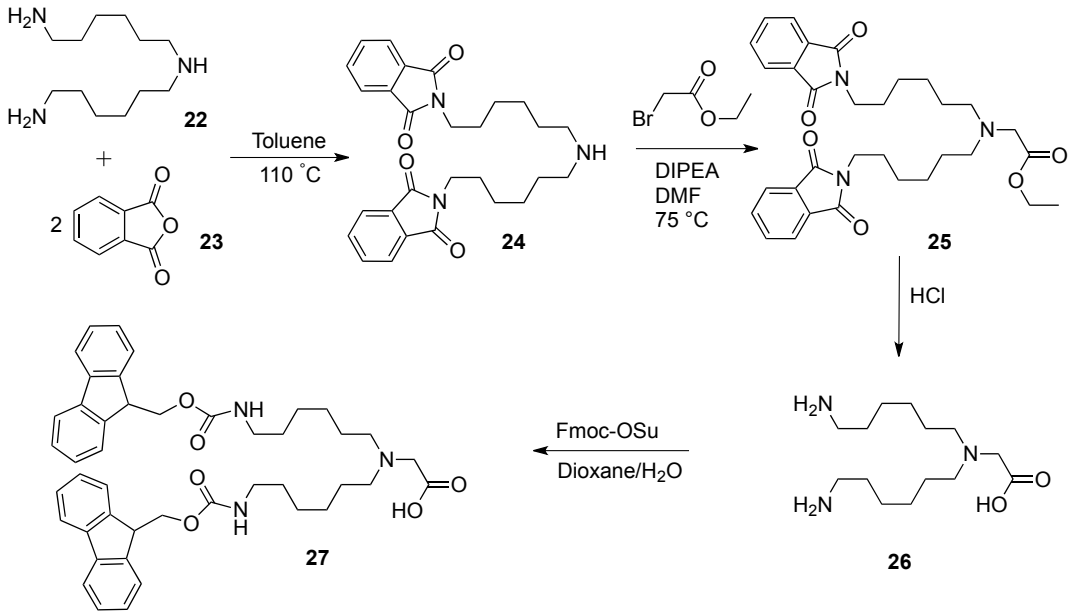

Scheme 2.9

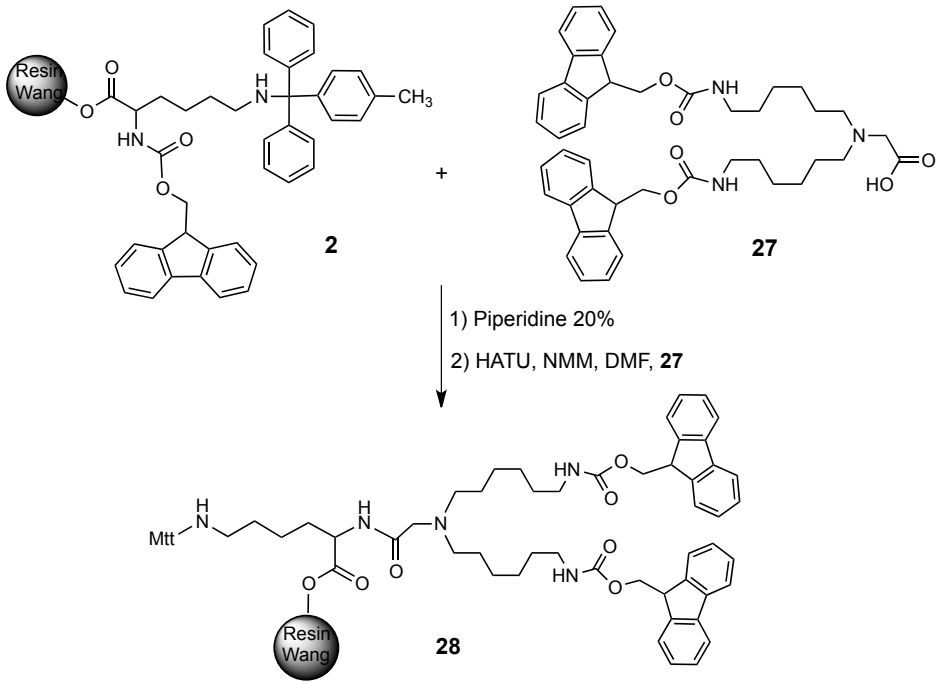

Scheme 2.10

The intermediate **28** after deprotection from Fmoc, has two free amino groups, ready to react with the carboxyl group of the compound **8**, Fmoc-*p*-aminobenzoic acid (Fmoc-PABA), properly activated (Scheme 2.11).

The introduction of this compound is not only important for the chain elongation, but also can provide a certain degree of rigidity to the two arms, so that they are sufficiently outstretched in physiological environment. The phenyl ring of PABA has precisely this purpose.

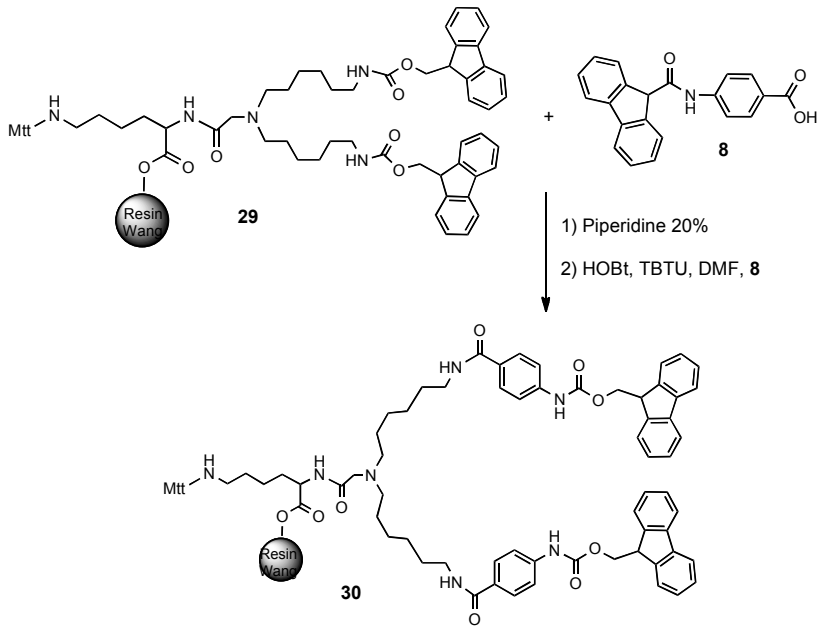

Scheme 2.11

The compound **30**, after removing of Fmoc groups, showed two free amino functions, that, as above reported, could react with the succinic anhydride, **14**: in this way we could obtain the two arms ending with two carboxyl groups, available at subsequent attack of Lys.

This step was been achieved, once again, (Scheme 2.12) with the aid of microwave: in this case the amino functions were in *para* position respect to the aromatic ring and thus were not prone to react rapidly because the EW effect of the *p*-CO group.

The MW radiations were useful, therefore, not only for the reduction of the reaction time, but also to lower the activation energy, which in these conditions did not require an activating group.

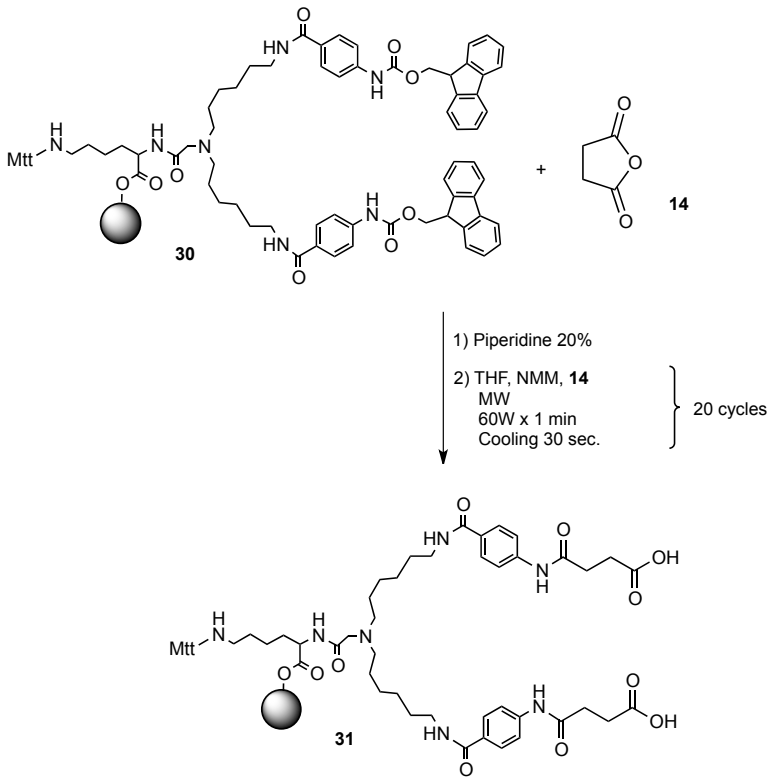

Scheme 2.12

During the process, because of the low reactivity of the two amino groups, we checked the reaction by a microcleavage in order to verify the formation of the amide bonds.

This was made on a small amount of resin and the crude compound was separated and analyzed by UPLC-MS in order to verify the presence of the intermediate **31**. The control provided an unexpected result: in addition to confirming the presence of compound **31**, we detected peaks corresponding to the cyclized compounds or on a single residue, or on both succinic residues were observed. (Figure 2.30 and Figure 2.31).

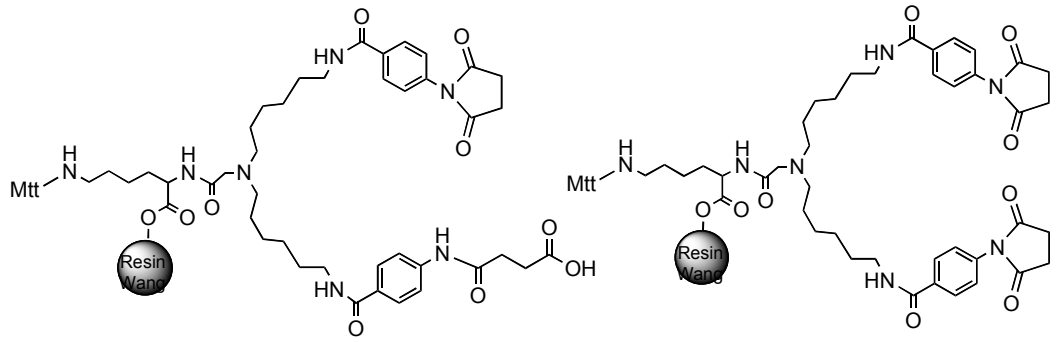

Figure 2.30 Cyclized form of **31**

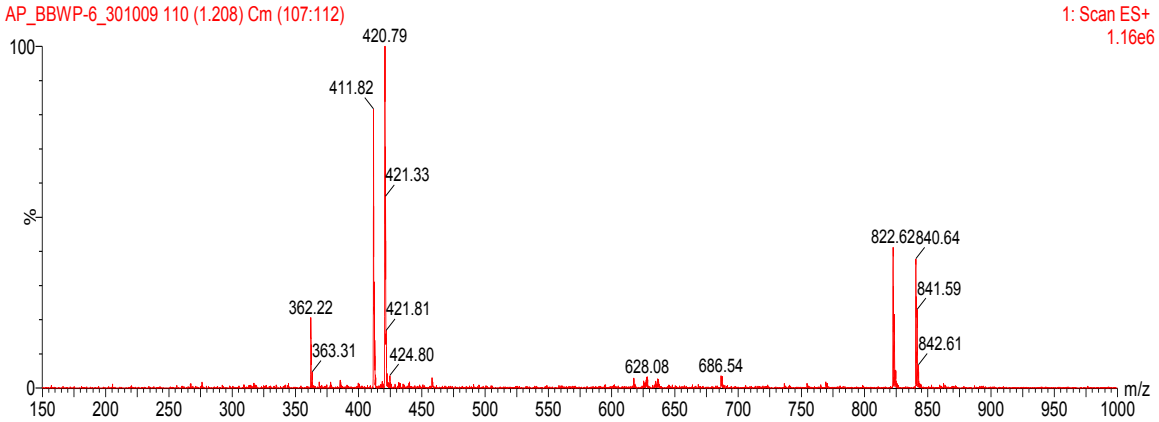

Figure 2.31 MS spectrum of the product **31**

The mass spectrum of the intermediate **31** showed a peak at *m/z* 840.64, corresponding to $[M+H]^+$ and a second peak at *m/z* 420.79, relating to $[M+2H]^{2+}$, it clearly denoted the presence of one mono succinimidic residue with mass of 18 units less: the peak at *m/z* 822.62, corresponding to $[M+H]^+$ and its double charged peak at *m/z* 411.82, relating to $[M+2H]^{2+}$ species.

The existence of an equilibrium (Scheme 2.13) between the acidic open form and the cyclic imide was confirmed by the study of Stieber and Waldmann.[108] The verification of the presence of succinimmides was made by addition of 1M NaOH in solution until alkaline pH values; the mass spectrum obtained (Figure 2.32) showed the instantaneous disappearance of peaks related to the cyclic derivatives.

[108] Stieber, F.; Waldmann, H. *Chem. Comm.*, **2002**, *16*, 1748-1749.

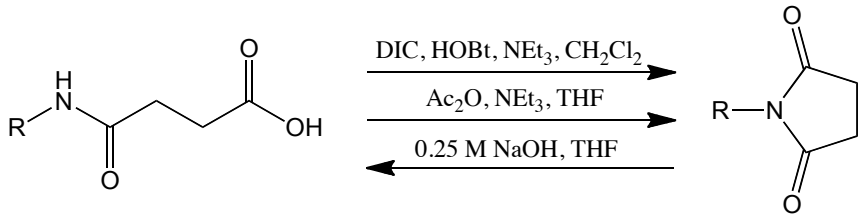

Scheme 2.13

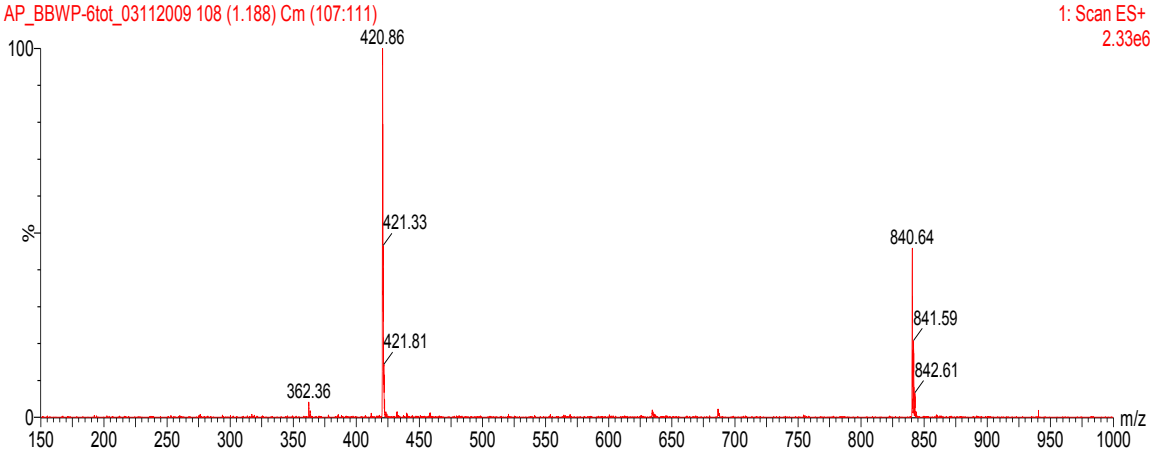

Figure 2.32 MS spectrum of **32** after alcalinization.

The presence of these analogues implied that part of the compound **31** was not really available for coupling with building-block **17**, thus causing a reduction in yield: in fact the reaction, despite the presence of NMM, did not occur in strong basic conditions, but between pH 7 and pH 8.

In order to maximize the yield of the synthetic process, the resin was treated with a strongly alkaline solution obtaining the shift of the equilibrium toward the product bounded with two succinic acid residues without the presence of terminal succinimmido residues.

Following this step, we proceeded with the coupling between the compound **31** and Fmoc-Lys(H)-O*t*Bu, **17**, in the presence of appropriate activator (Scheme 2.14).

The building-block was the same as in the previous synthesis, because we decided to maintain the same mechanism of resistance to degradative enzymes used in BisBiotinMonoDOTA-C_3, also for this molecule.

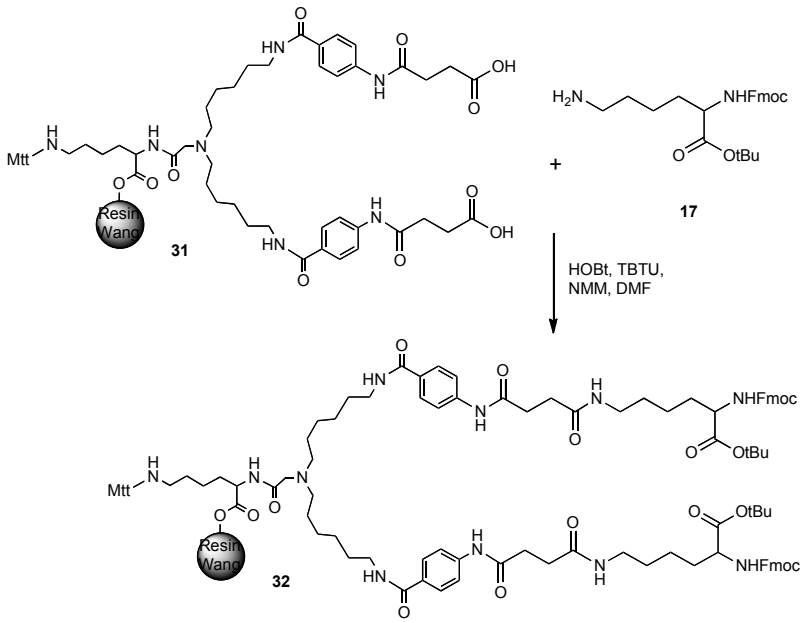

Scheme 2.14

The compound **32** was deprotected in alkaline medium to remove the Fmoc groups, so the molecule was then ready to react with biotin, **3** (Scheme 2.15). Once the coupling with biotin was performed, it was necessary to remove the MTT protecting group from the Lys anchored to the resin, and restore the reactivity of its ε-amino group in order to prepare the DOTA conjugation.

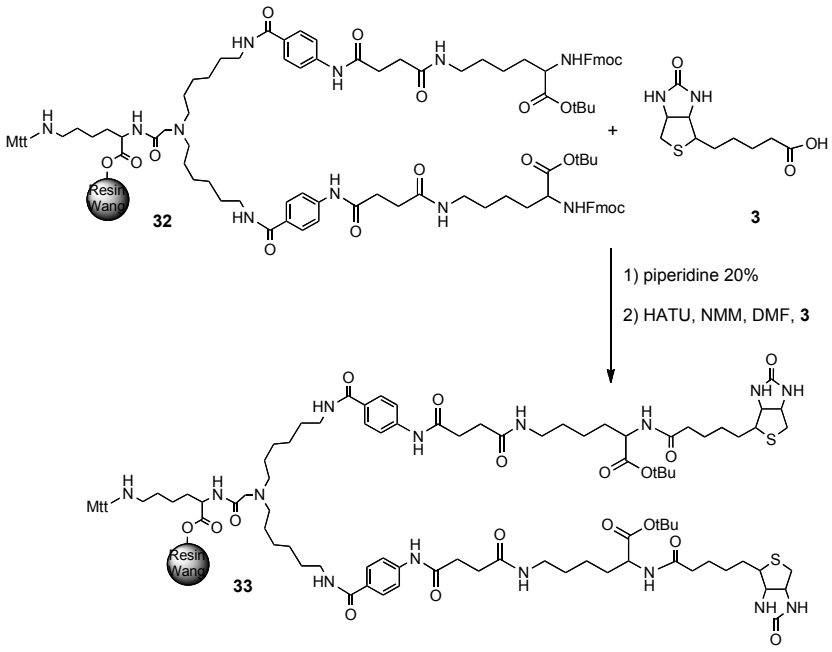

Scheme 2.15

The compound **33** in fact, once deprotected by MTT, contained the free NH_2 groups and was subjected to the last coupling (Scheme 2.16) with the DOTAtris-*t*Bu, **20**, suitably activated.

After the reaction with the chelating agent, we proceeded with the total cleavage: in this step was achieved the removal of all protections still bound to the molecule and the detachment of the crude compound from the insoluble matrix.

The resulting product, **34**, compared with **21**, has arms more rigid and longer, but essentially they have in common many elements of the structure. This molecule, in fact, was designed to be able to compare their biological characteristics with those of the derivative **21**, and understand the contribution determined by those modifications.

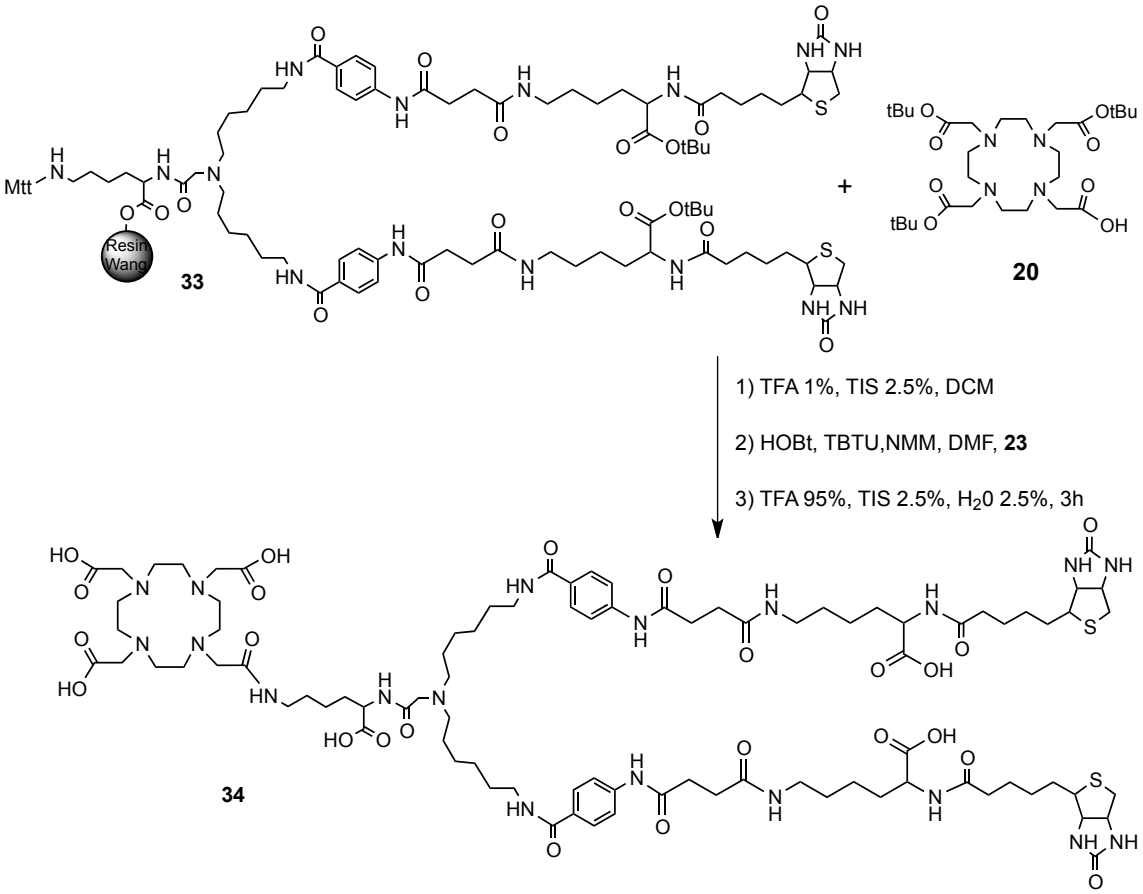

Scheme 2.16

2.8.3 Synthesis of BisBiotinBisDOTA-(PEG$_6$)-C$_3$

The compound BisBiotinBisDOTA-(PEG$_6$)-C$_3$ was synthesized, as in previous cases, from Fmoc-Lys(MTT)-Wang resin, **2**. The design of this derivative, however, provides some significant differences from the two previous products.

The first step of the synthesis was the Fmoc removal from the resin followed by coupling with the Spacer C$_3$ (Scheme 2.5), similarly to the synthesis of BisBiotinMonoDOTA-C$_3$, resulting in the intermediate **12**.

Subsequently, the compound **12** was, once again, deprotected from Fmoc groups coupled with 1-Fmoc-amino-3,6,9,12,15,18-esaossaenicosan-21-oic acid or Fmoc-NH-PEG$_6$-COOH, **35**, suitably activated (Scheme 2.17).

The latter reagent had the function to significantly stretch (and with a single synthetic step) the arms that hold the biotin and, most importantly, to keep unfolded the aliphatic chains in a very hydrophilic medium, as the physiological one.

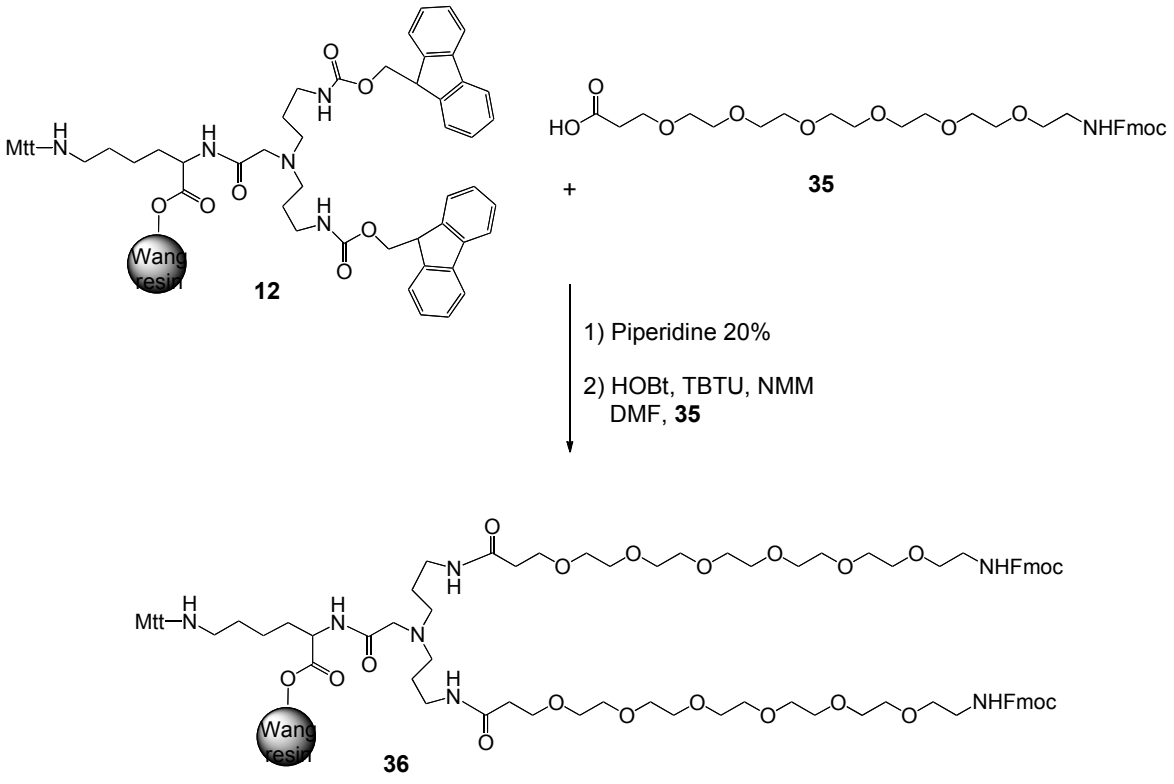

Scheme 2.17

The intermediate **36** was deprotected from Fmoc groups, with recovery of amine functions, and then reacted with Fmoc-α-aminobutyric acid, or Fmoc-L-Abu-OH, **37**, a non-natural amino acid (Scheme 2.18).

The choice of this reagent was not casual: in fact, previously experimental data confirmed that the amino acid side chain was able to protect the amide bond with biotin, making the molecule resistant to biotinidases.[109]

For the purpose of our thesis project, the introduction of this amino acid was used to assess whether its presence could change the avidin-biotin binding affinity in comparison when Lys used in compounds above described. In fact, while the carboxyl group of Lys was hydrophilic, Abu protected the amide bond with its side chain, which is an ethyl residue with hydrophobic properties. So we wanted to ascertain how this difference of hydrophilicity could affect the affinity of this molecule for the avidin.

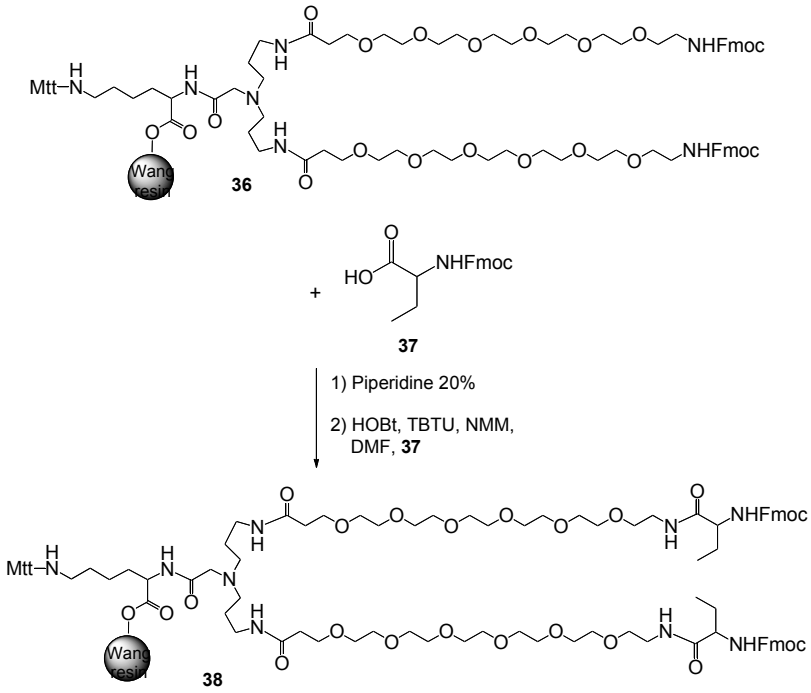

Scheme 2.18

The compound **38** was deprotected from Fmoc, with restoration of the reactivity of Abu amino groups. The chain formation was than completed through the coupling with biotin, **3** (Scheme 2.19).

[109] Wilbur S.D.; Hamlin D.K.; Chyan M.K. *Bioconjugate Chem*., **2006**, *17*, 1514-1522.

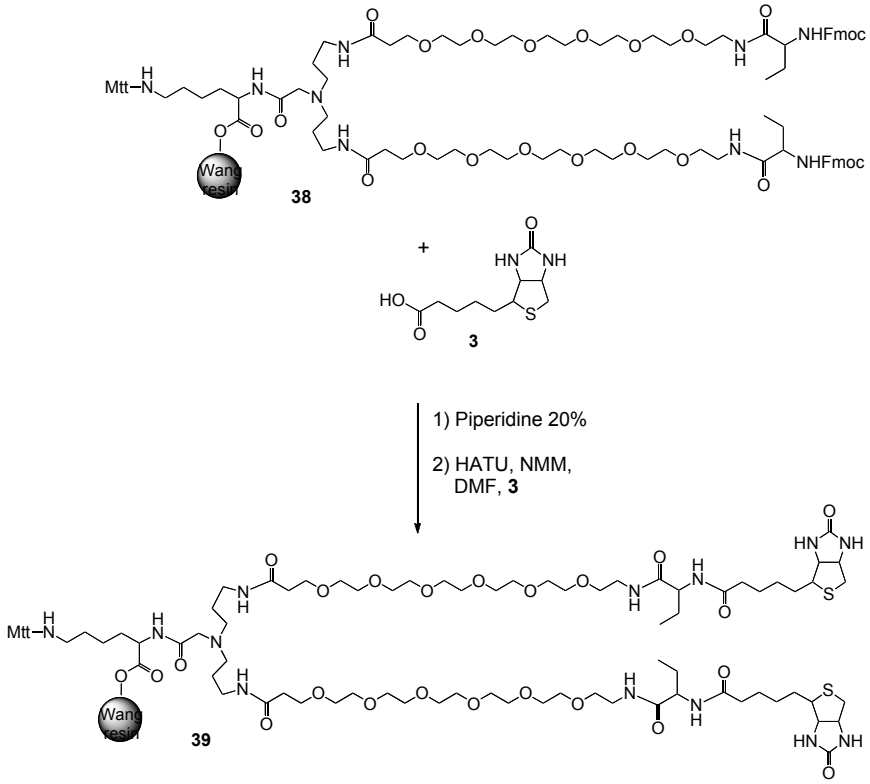

Scheme 2.19

The compound **39** thus obtained, was deprotected by MTT group: the ε-amino function of Lys, anchored to the Wang resin, was free and thus available for subsequent coupling with the bis-Fmoc-(3,5-diamino) benzoic acid, **40** (Scheme 2.20).

The aromatic compound was used to give rigidity to the structure of the molecule and, also, had the role of bi-functional spacer; after the Fmoc removal, in fact, there were two free amino functions on which we could build two symmetrical arms that retain two chelating groups. The design of this compound required, as its name suggests, the presence of two biotin residues, introduced with the aim to increase the affinity towards avidin, but also two DOTA groups in order to redouble the radiation dose delivered by each molecule of radiopharmaceutical.

The intermediate **41**, once deprotected from Fmoc, underwent the coupling with a non-natural aminoacid, the Fmoc-*β*Ala-OH, **42**, who, in the presence of the appropriate activator, gave the amide bond with the two amino groups on the aromatic ring (Scheme 2.21).

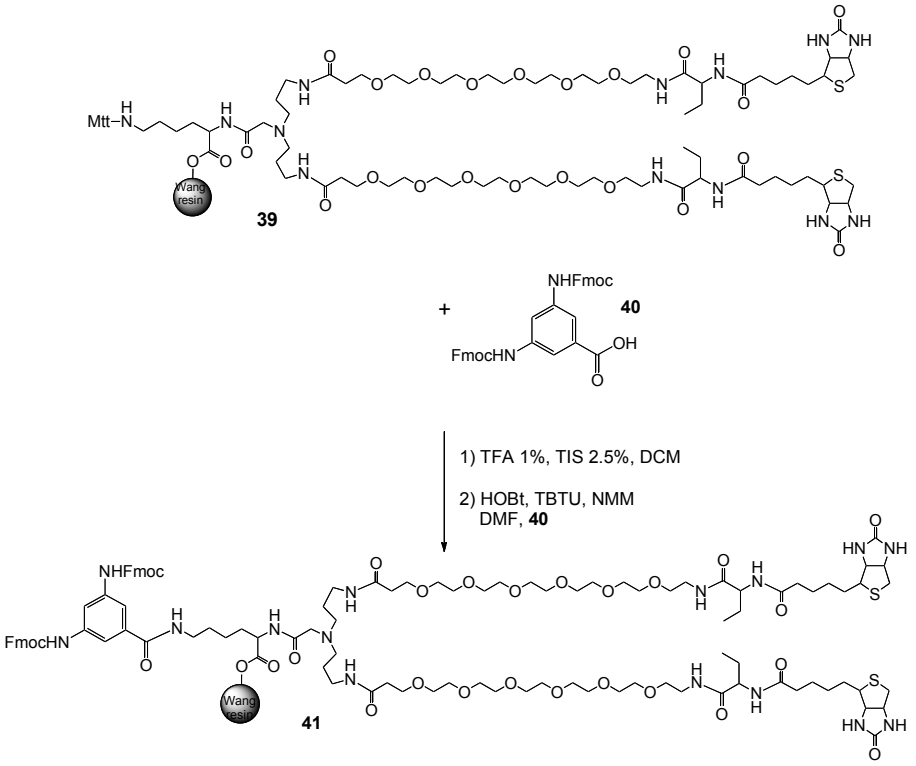

Scheme 2.20

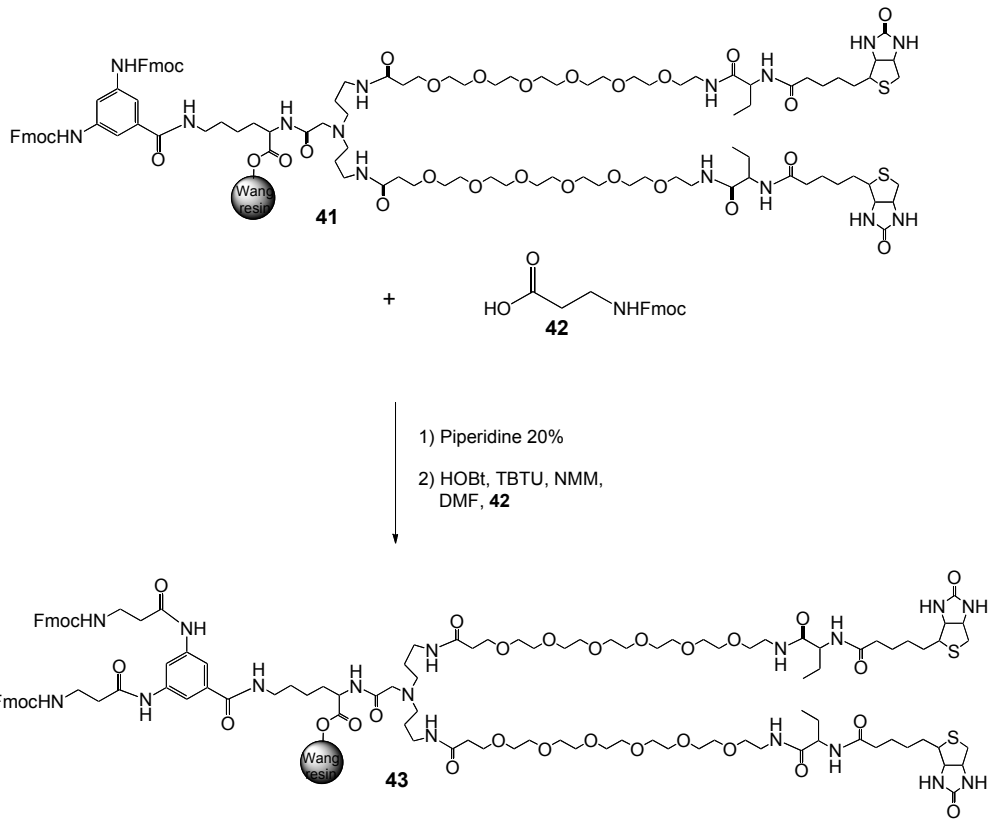

Scheme 2.21

The compound **43**, once deprotected from Fmoc groups, was ready to be coupled with activated DOTAtris-*t*Bu, **20** (Scheme 2.22).

The introduction of the aminoacid residue in the molecule has been principally designed to increase the distance between the DOTA and the diaminobenzoic acid, **40**: the intention was to avoid direct reaction of the chelating agents on the aromatic compound, in order to eliminate the possibility that the steric hindrance of DOTA could be of impediment for the coupling.

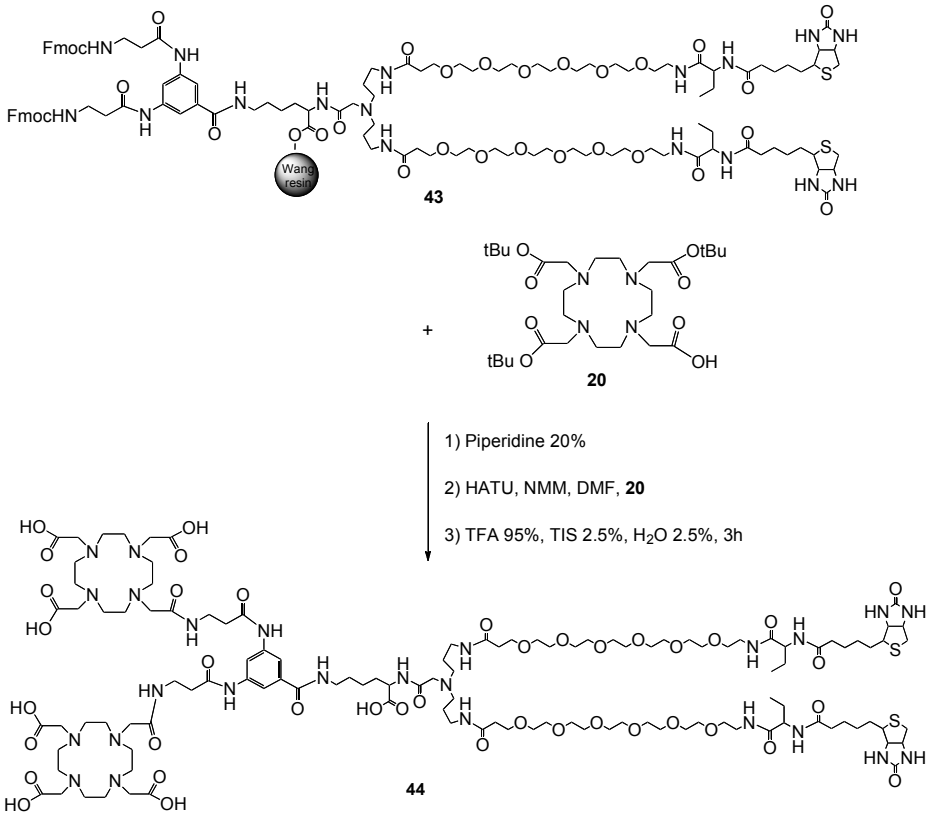

Scheme 2.22

This reaction completed the synthesis of the compound BisBiotinBisDOTA-(PEG)-C_3, **44**, who was so detached from the resin with the total cleavage.

In vitro studies on compounds **21**, **34** and **44** for having a preliminary idea of their future applicability, beyond the individual data, however, are extremely important to assess whether the changes has positively or negatively affected the pharmacokinetics of the derivative, in order to understand which way should be followed in the future. To make this type of assessment, a careful comparison of the results of *in vitro* tests of all BisBiotin compounds with those MonoDOTA and BisDOTA was therefore necessary.

2.8.4 BisBiotin-derivatives carrying the SCN group for tissues and cells biotinilation

Covalent attachment of Biotin-derivatives to cells and tissues could be used to solve several problems associated with cellular therapies. The surface of the cells or tissues could be modified with biotin-derivative-isothiocyanate (SCN), and the biotin could act as an antenna in order to carry the biomolecule selectively on a tissue previously avidinated.

These experiments, performed by our co-workers (unpublished data), were designed to define the feasibility of Biotin conjugation on the surface of live cells of different derivation as well as on islets of Langerhans. In preliminary experiments were utilized beta-TC3 and K562 cell lines as well as primary cell culture of bone marrow cells from GFP harvested transgenic mice (mice that ubiquitously express the Green Fluorescent Protein – GFP) and lather moved to dispersed human islets. The cells were incubated with biotin and co-incubated with native Avidin and Oxavidin-treated (an oxidized Avidin derivative) human islets. Cultures were monitored by fluorescence microscopy to assess the presence of cell-cell interactions, they appeared as bright green luminescence that, in case of Oxavidin,[110] were more intense than that of the native avidin (Figure 2.33).

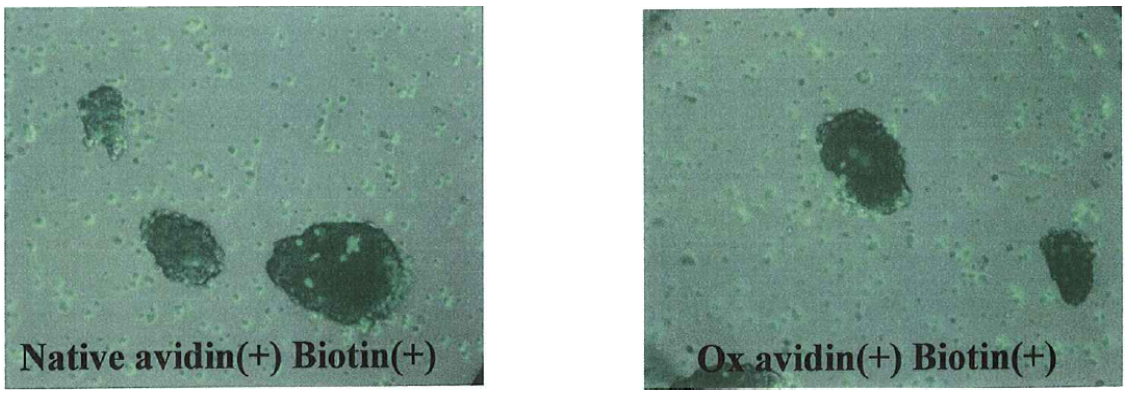

Figure 2.33 Fluorescence microscopy of biotinylated cells.

These interesting results led us to design and synthetize the BisBiotin-SCN compounds with the aim to improve the binding interactions through the presence of two arms containing two biotin residues. On the other hand, the presence of the isothiocyanate group could facilitate the docking of the modified biotin on the cell surface. In fact, the

[110] De Santis, R.; Leoni, B.; Rosi, A.; Albertoni, C.; Forni, G.; Cojoca, R.; Iezzi, M.; Musiani, P.; Paganelli, G.; Chinol, M.; Carminati, P. *Cancer Biother. Radiopharm.* **2010**, *25*, 143-148.

SCN group could react rapidly and in easier manner in physiological conditions than the carboxylic group of native biotin.

2.8.5 Synthesis of BisBiotin-(PEG$_6$)-Abu-SCN

The synthetic steps used for the obtainment of this compound were substantially the same for the last synthesis described. For this reason and for brevity are reported here only the general scheme but are adequately discussed the elements of novelty.

The synthetic route followed exactly what already reported in the Scheme 2.17, Scheme 2.18 and Scheme 2.19 until the product **39,** that was the new starting point, deprotected from MTT group, affording compound **39a** (Scheme 2.23).

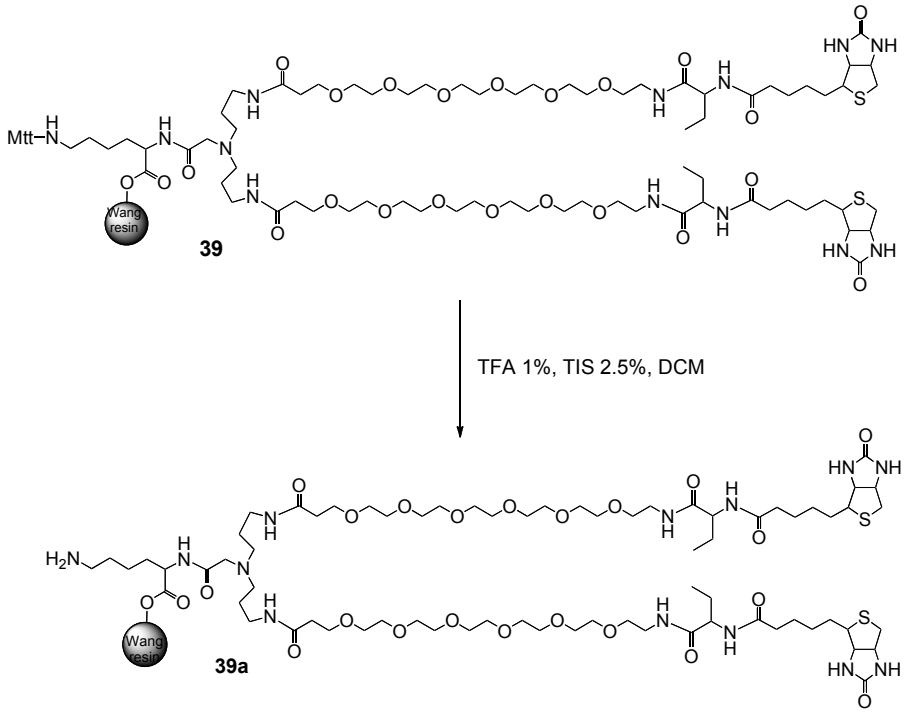

Scheme 2.23

In this way the original ε-amino group of Lys was restored and, using the procedure reported by Munch *et al.*,[111] easily and rapidly transformed in isothiocyanates using di-*tert*-butyl dicarbonate (Scheme 2.25). Although the traditional methods were efficient, we

[111] Munch, H.; Hansen, J.S.; Pittelkow, M.; Christensen, J.B.; Boas U. *Tetrahedron Letters* **2008**, *49*, 3117-3119.

preferred this synthesis of isothiocyanates which preceded cleanly without intermediate work-up, such as extraction or column chromatography, and which did not leave traces of by-products. These mild conditions were very useful in solid phase synthesis and the excess of reagents and by-products could be completely removed simply by filtrations and washes. For this kind of reaction, a desulfurylation reagent leaving only gases and volatile byproducts should fit this purpose. Di-*tert*-butyl dicarbonate (Boc_2O) seemed a good candidate for the desulfurylation of the corresponding dithiocarbamate as this reagent may evolve CO_2 and COS during the reaction, and residual carbon disulfide and tert-butanol together with the solvent should be removed easily by filtration. As the formation of dithiocarbamate in the case of most amines proceeds rapidly, the isothiocyanate can be synthesised directly from the amine in the presence of excess carbon disulfide.

In addition to Boc_2O, the authors suggest that a catalytic amount of DMAP (1–3 mol %) increased the reaction rate significantly, with visible evolution of gas from the reaction mixture. In the reaction pathway, the electrophilic Boc_2O reacts with the dithiocarbamate with evolution of CO_2 to form an unstable 'mixed dithiocarbamate/carbonate' adduct that rapidly decomposes to the isothiocyanate, COS and *tert*-butanol (Scheme 2.24). Triethylamine is necessary for the stabilisation and complete formation of the dithiocarbamate The reaction was carried out on the resin, stirring gently in THF at room temperature. The crude compound **45**, was recovered by cleavage from the solid support.

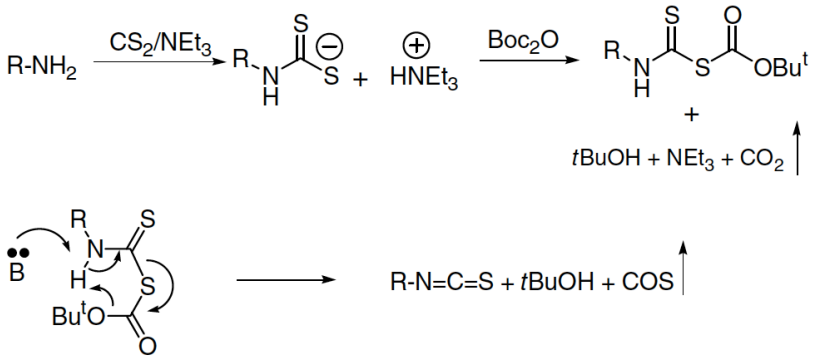

Scheme 2.24

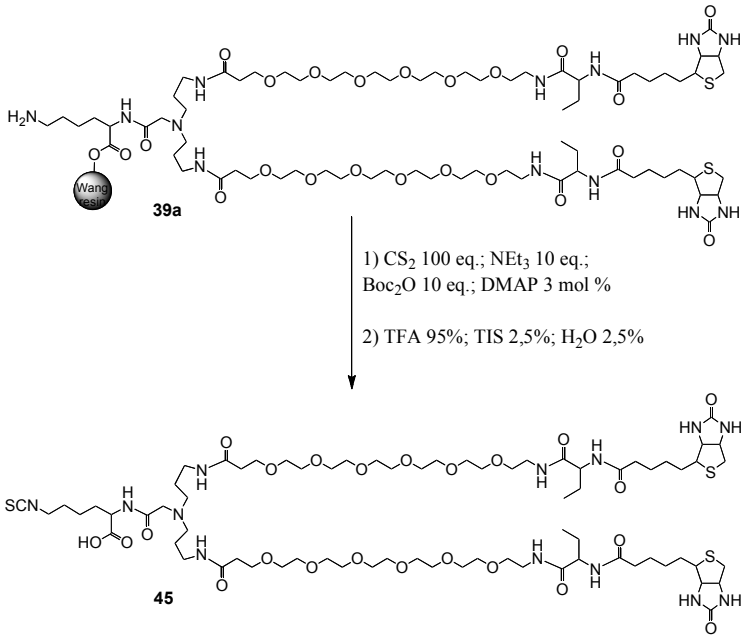

Scheme 2.25

2.8.6 Synthesis of BisBiotin-(PEG$_6$)-Asp-SCN

In order to assess the ability of different aminoacids to protect the molecule from the enzimatical action, we decided to insert one residue of Asp instead of Abu. The reaction was performed in the same way of the product **38** described in Scheme 2.18 but with the insertion of Fmoc-Asp-O*t*Bu, **46** instead of Fmoc-Abu-OH (Scheme 2.26).

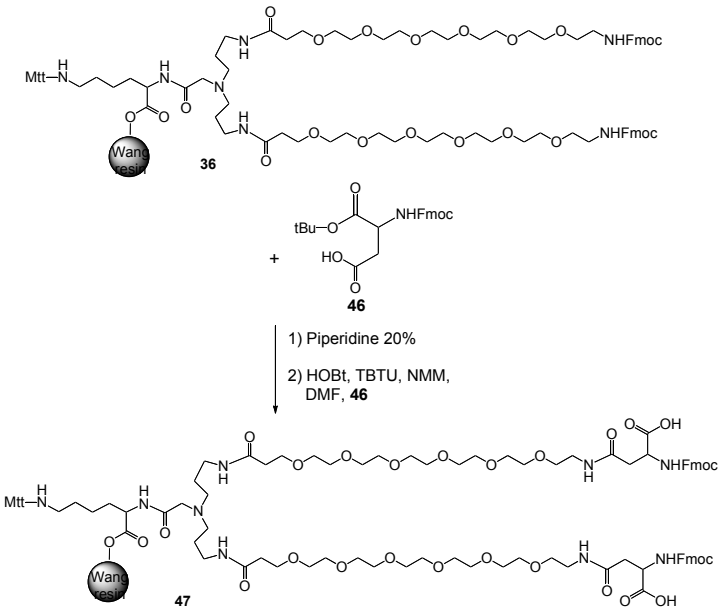

Scheme 2.26

Starting from this point the synthesis proceeded in accordance with the route previously described and, with the final cleavage, the crude compound **48** was released as showed in Scheme 2.27.

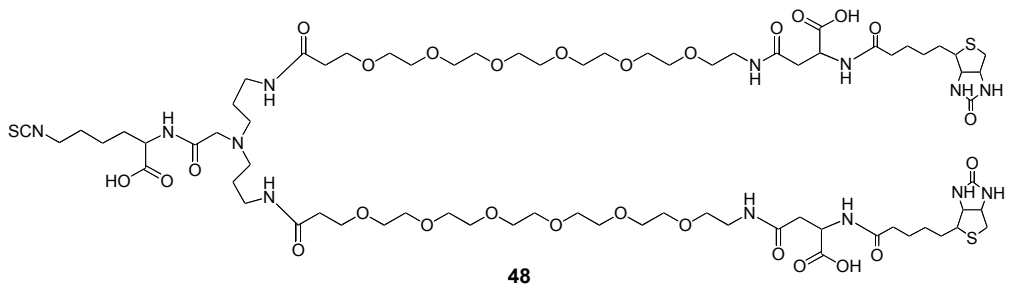

48

Scheme 2.27

2.8.7 Synthesis of BisBiotin-(PEG$_2$)-pAB-Abu-SCN

The last compound of this series was designed with the aim of merging the characteristics of hydrofilicity and flexibility of PEG with the structural rigidity carried by the *p*-amino benzoic acid. Moreover we decided to use the protection against biotinidases provided by the residue of Abu. This one is more hydrophobic than Asp, but the use of this molecule during the synthesis simplifies the final deprotection and avoids eventual unwanted hydrogen interactions between the carboxylic group of Asp side-chain and the oxygen atoms present in PEG. The first step of the synthesis was the deprotection of the Lys linked on resin, followed by coupling with the Spacer C_3 (Scheme 2.5), similarly to the synthesis of BisBiotinaMonoDOTA-C_3, resulting in the intermediate **12**. Subsequently, the compound **12** was deprotected from Fmoc groups and thus ready for coupling with Fmoc-8-amino-3,6-dioxaoctanoic acid (Fmoc-NH-PEG-COOH), **49**, suitably activated (Scheme 2.28).

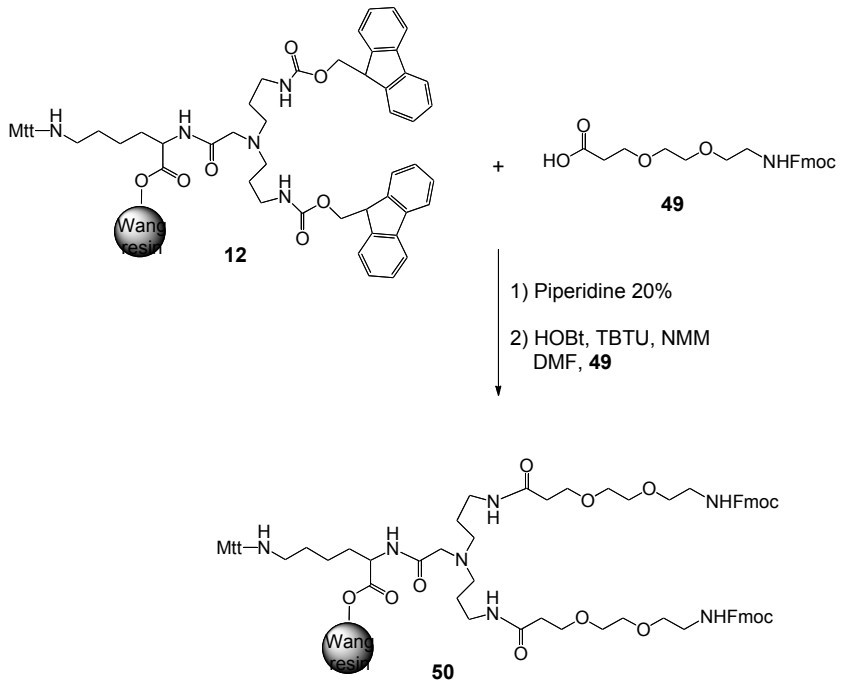

Scheme 2.28

The reaction started from the Fmoc removal of compound **50** and the subsequent coupling with Fmoc-*p*AB-OH, **8** (Scheme 2.29).

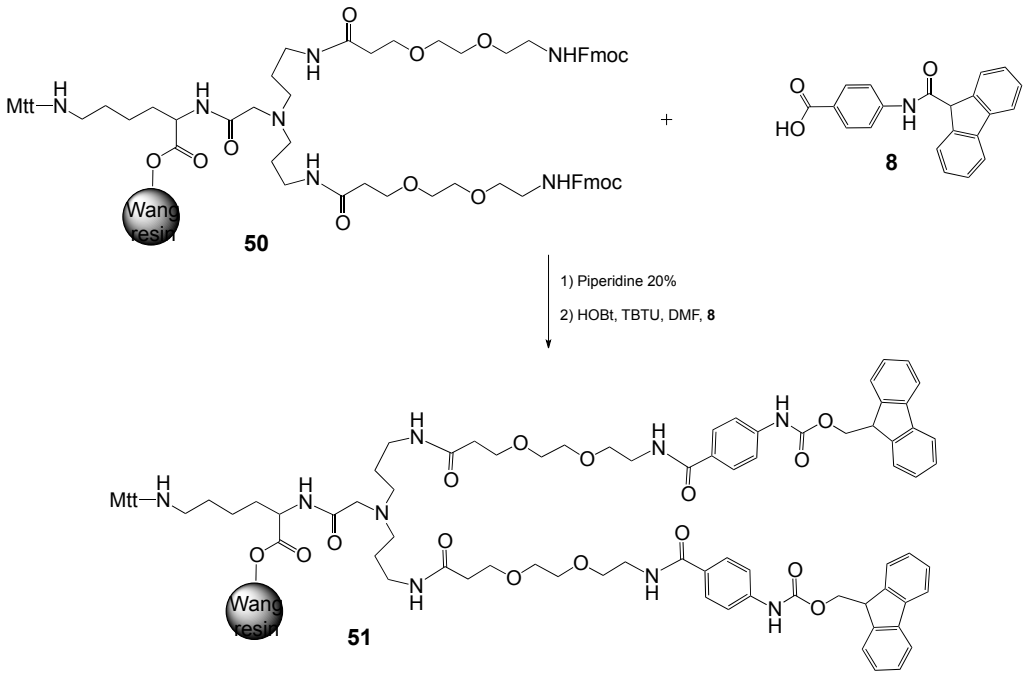

Scheme 2.29

The coupling with PEG, **49** was repeated once again, in order to obtain the desired length of the arms (Scheme 2.30).

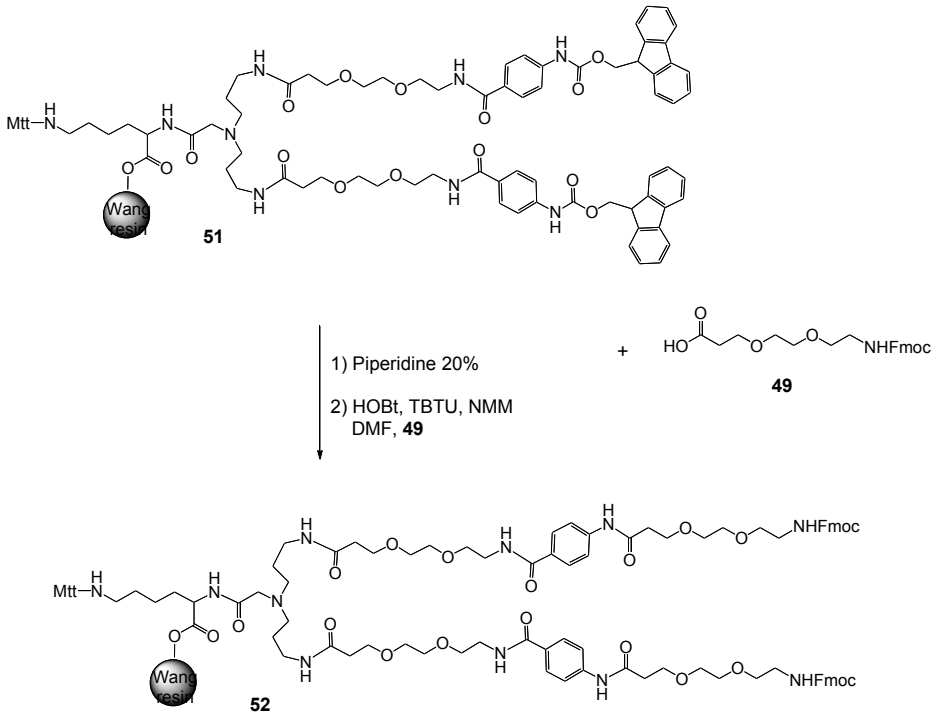

Scheme 2.30

The reaction was carried out as already described, by adding biotin on the growing structure **53**, the removal of the MTT group was achieved by TFA 1% in DCM with 2.5% TIS and the released amino group was coupled with Fmoc-*β*Ala-OH. After the Fmoc removal in piperidine, the amino group was transformed in isothiocyanate by reacting with CS_2, as showed in Scheme 2.31. The final crude product **55**, was recovered after cleavage from the resin in strongly acidic conditions.

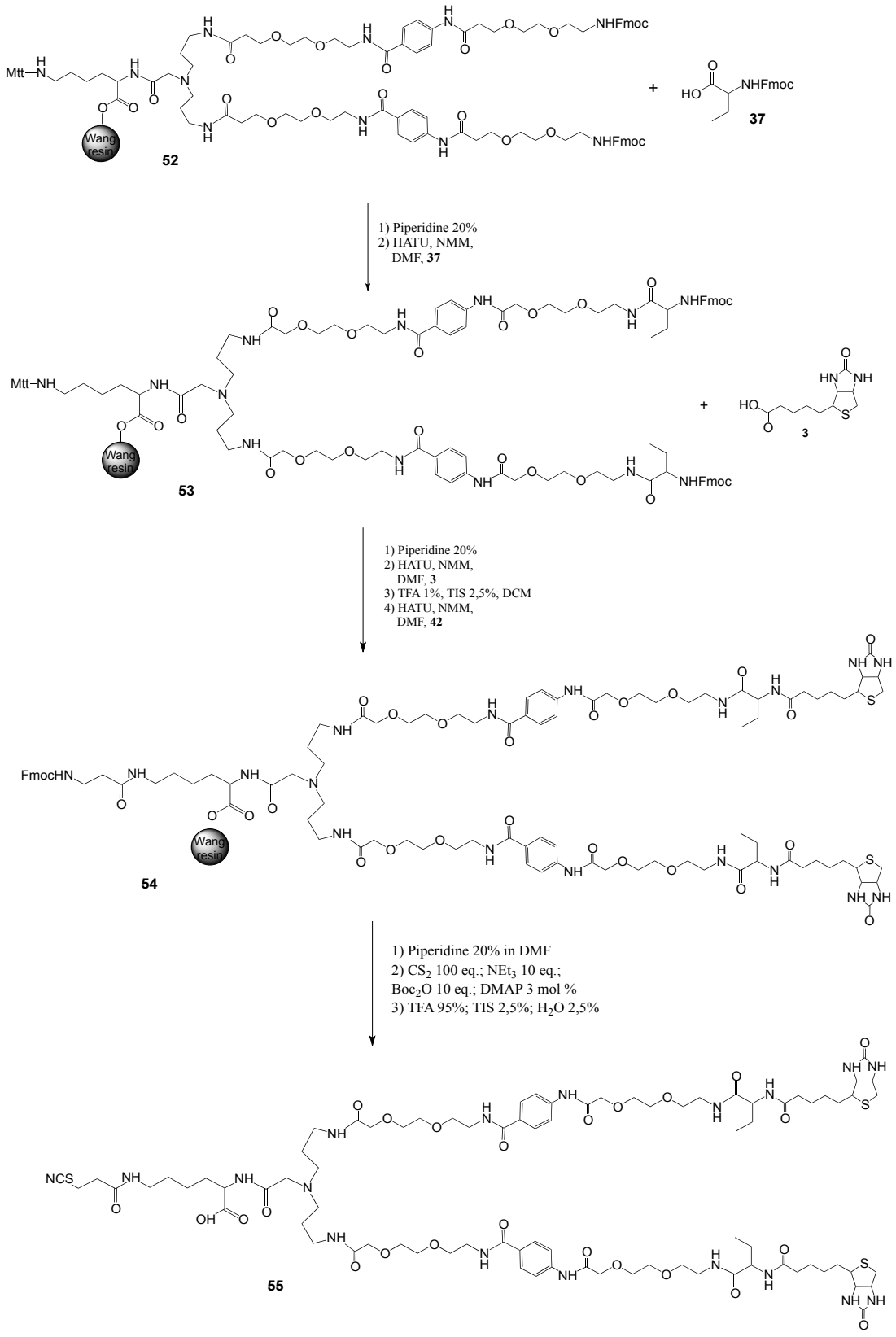
Mtt
Wang resin
52
NHFmoc
37
1) Piperidine 20%
2) HATU, NMM,
DMF, 37
53
3
1) Piperidine 20%
2) HATU, NMM,
DMF, 3
3) TFA 1%; TIS 2,5%; DCM
4) HATU, NMM,
DMF, 42
FmocHN
54
1) Piperidine 20% in DMF
2) CS2 100 eq.; NEt3 10 eq.;
Boc2O 10 eq.; DMAP 3 mol %
3) TFA 95%; TIS 2,5%; H2O 2,5%
NCS
OH
55

Scheme 2.31

2.9 Results and discussion

The *in vitro* experiments were essential to evaluate the potential role of these new biotin derivatives in the clinical settings. They are performed at European Institute of Oncology (Milan). Primarily, we estimated the radiochemical purity (RCP) of new molecules; then we checked the resistance of the molecule to the action of biotinidases and we attempted to verify whether the conjugation steps and the radiolabeling procedure altered the natural affinity of biotin for avidin.

2.9.1 Radiolabelling tests

Radiolabeling studies was carried adding to a solution of biotin derivative in H_2O MilliQ (2 mg/mL), sodium acetate buffer 1M (pH = 5) and then a solution of the radioisotope in the form of chloride (MCl_3, with M = ^{111}In, ^{90}Y, ^{177}Lu). The studies was carried out at a specific activity of 5.3 and 10.6 MBq/nmole, respectively double and quadruple compared with this used to label the MonoDOTA (**1**) derivative. For this latter compound a specific activity of 2.6 and 5.3 MBq/nmol were used. The mixture was incubated at 95 °C for 30 min.

The labelling yield, i.e. the percentage of the total radioactivity in the liked chemical form, was determined by Instant Thin Layer Chromatography (ITLC-SG). A molar excess of Av and DTPA in saline was added to an aliquot of the radiolabeled mixture. In this system, Av/biotin derivative complex remains at the starting point while free metal (bounded to DTPA) migrates with the solvent front. The strip was cut in two halves and counted in a β-counter (Figure 2.34).

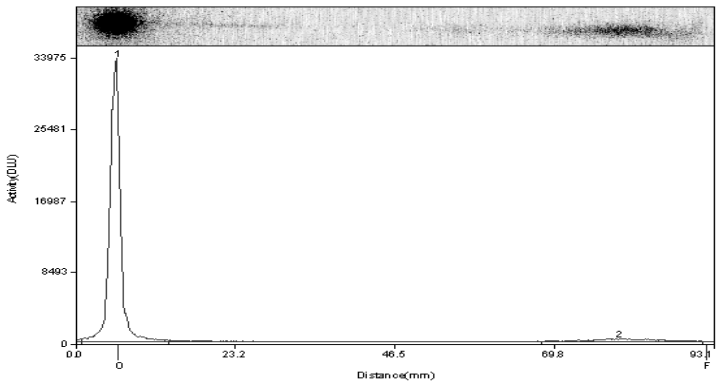

Figure 2.34 Radio-TLC profile for MonoDOTA (**1**).

RCP is then calculated according to the autoradiographic measures; for both radiometals used it was almost 99% or higher (Table 2.4) and the result is the same for tests where a specific activity of 5.3 MBq/nmol is used.[112]

For radiolabelling of BisDOTA compounds **7** and **11**, specific activities were used of 5.3 and 10.6 MBq/nmol of the compound under experimental conditions similar to those of MonoDOTA. Measured RCP was always above 99%.[93]

A further increase in specific activity (51.2, 212, 530 MBq/nmol) showed a decrease in RCP but still higher than 95%. The possibility of increasing considerably the specific activity maintaining high RCPs may represent a great advantage in the clinical application of the avidin-biotin system. A new-targeted locoregional therapy, based on avidin and ^{90}Y labeled MonoDOTA, has shown great potential in the treatment of breast cancer reducing the duration of radiotherapy.[22] In this approach, MonoDOTA has been labelled at a specific activity of 2.6 MBq/nmol. Using the herein described BisDOTA derivatives radiolabeled at high specific activity may lead to a higher uptake by the targeted tumor area administering lower ^{90}Y activity, thus reducing the radiation burden to nontarget organs.

Table 2.4 RCP of BisDOTA compounds related to MonoDOTA.

Modified Biotin	**^{90}Y**	**^{177}Lu**
MonoDOTA (2.6 MBq/nmol)	99.6%	99.6%
MonoDOTA (5.3 MBq/nmol)	99.5%	99.5%
BisDOTA-Lys-C_3 (5.3 MBq/nmol)	99.9%	99.7%
BisDOTA-Lys-C_3 (10.6 MBq/nmol)	99.1%	99.4%
BisDOTA-Lys-(*p*AB)-C_3 (5.3 MBq/nmol)	99.9%	99.6%
BisDOTA-Lys-(*p*AB)-C_3 (10.6 MBq/nmol)	99.3%	99.2%

[112] Urbano, N.; Papi, S.; Ginanneschi, M.; De Santis, R.; Pace, S.; Lindstedt, R.; Ferrari, L.; Choi, S.J.; Paganelli, G.; Chinol, M. *Eur. J. Nucl. Med. Mol. Imaging* **2007**, *34*, 68-76.

For BisBiotin compounds **21**, **34** and **44**, only preliminary data are available, the RCP was calculated on compounds radiolabelled with ^{111}In, always using the combined approach ITLC-SG and radio-TLC.

The behaviour of these compounds to radiolabeling test were different from the others, as showed in Table 2.5, BisBiotinMonoDOTA-C_3 (**21**) and BisBiotinBisDOTA-(PEG_6)-C_3 (**44**), showed high RCP at specific activity of 2.6 MBq/nmol, but it decreases at higher values of SA.

Somewhat unexpectedly, the BisBiotinaMonoDOTA-(*p*AB)-C_6 (**34**) reported a very low RCP; in practice the molecule seemed not to be able to chelate the radiometal.

The data in our possess are still too small to find a plausible reason for this radiolabel failure and the product tested was, anyway, of high chemical purity, so is reasonable to assume that the problem could be related to some variables of experimental nature.

Table 2.5 RCP of BisBiotin compounds.

BisBiotin Compounds	**^{111}I**
BisBiotinMonoDOTA-C_3 (2.6 MBq/nmol)	98.3%
BisBiotinMonoDOTA-C_3 (26 MBq/nmol)	84.2%
BisBiotinBisDOTA-(PEG_6)-C_3 (5.2 MBq/nmol)	99.6%
BisBiotinBisDOTA-(PEG_6)-C_3 (52 MBq/nmol)	60%
BisBiotinMonoDOTA-(*p*AB)-C_6 (2.6 MBq/nmol)	4%
BisBiotinMonoDOTA-(*p*AB)-C_6 (26 MBq/nmol)	0.5%

2.9.2 Stability studies

Stability studies *in vitro* were performed to verify the BisDOTA derivatives stability in human serum to esterases attack (in particular biotinidases). These results were obtained taking like benchmark their behaviour in saline. Testes stability were performed on the radiolabeled mixture in saline solution then adding an ascorbic acid solution (4 mg/mL in

sodium acetate buffer, pH = 5) as radical scavenger diluted 1:3 and finally in human serum.

In each case, the mixture was incubated at 37 °C for 24 and 48 h; the radiochemical purity was calculated using ITLC-SG as previously described.

The results showed that in both ascorbic acid (AA) and human serum (HS), the activity was almost completely associated to the labelled biotin derivatives up to 48 h, while they were degraded in saline solution.

These results are compared with those obtained for MonoDOTA compound (**1**). This one was threated in two different ways: aliquots from the labelling mixture were diluted with saline or human serum/saline 1:1 solution alternatively. After 2, 6, 12, 24, 36, and 48 h of incubation at 37 °C, two aliquots (10 μL) of both the mixtures were drawn: one was added to Av molar excess and the other was added to saline.

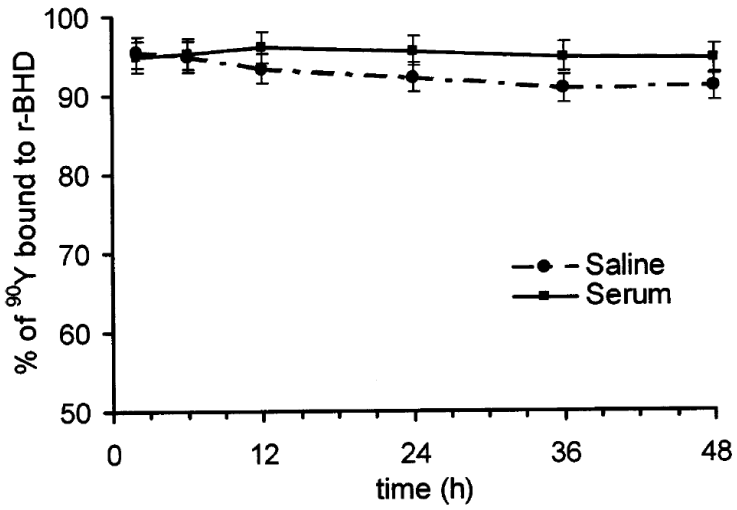

Figure 2.35 Stability of ^{90}Y-labeled MonoDOTA in saline and diluted human serum.

Stability studies showed that in both saline and diluted human serum the activity was almost completely associated to the labeled MonoDOTA molecule up to 48 h (Figure 2.35). Moreover, the activity dissociated from the ^{90}Y-labeled MonoDOTA conjugate was not attributable to the cleavage of the side chain by biotinidase. In fact, the amount of cleaved ^{90}Y-DOTA, was very low (about 3%) and did not increase from 2 to 48 h (in the serum free ^{90}Y was totally bound to serum protein, personal observation). The release of ^{90}Y in diluted human serum, observed after 48 h of incubation at 37 °C, is also very low

and in any case does not represent a major drawback toward the application of this compound in therapy trials. We can affirm that biotinidase was not able to break the MonoDOTA conjugate in a significant extent. For the BisDOTA compounds **7** and **11** we decided to perform the stability test in NMS, compared with results obtained for biocytin.

Biocytin is the natural substrate of the biotinidases, an hydrolytic enzyme family normally present in human and mouse sera, involved in the assimilation process of (+)-biotin from diet. Activity of biotinidases in freshly collected NMS was assessed by incubating commercial biocytin with NMS, at 37 °C, and verifying the presence of (+)-biotin as product of the reaction. As shown in Figure 2.36 (panels A and B, profiles 2 and 3), after 2 h of incubation, biocytin (retention time 12 min; $[M+H]^+$ = 373.5 Da) was effectively hydrolysed to produce a new species, at about t_R = 12.5 min, with a molecular weight $[M+H]^+$ = 245.1 Da, corresponding to (+)-biotin molecular weight (profile 3). Analysis of BisDOTA-Lys-(*p*AB)-C_3 (**11**) incubated with NMS for 2 h at 37 °C (profile 4) showed that no peak, with a retention time of about 12.5 min and corresponding to (+)-biotin, appeared, thus underlining the resistance of **11** to biotinidases activity. In strict agreement with these results, the peak of BisDOTA-Lys-(*p*AB)-C_3 was fully recovered after the incubation step. Similar results were obtained with BisDOTA-Lys-C_3 derivative (**7**) (data not shown).

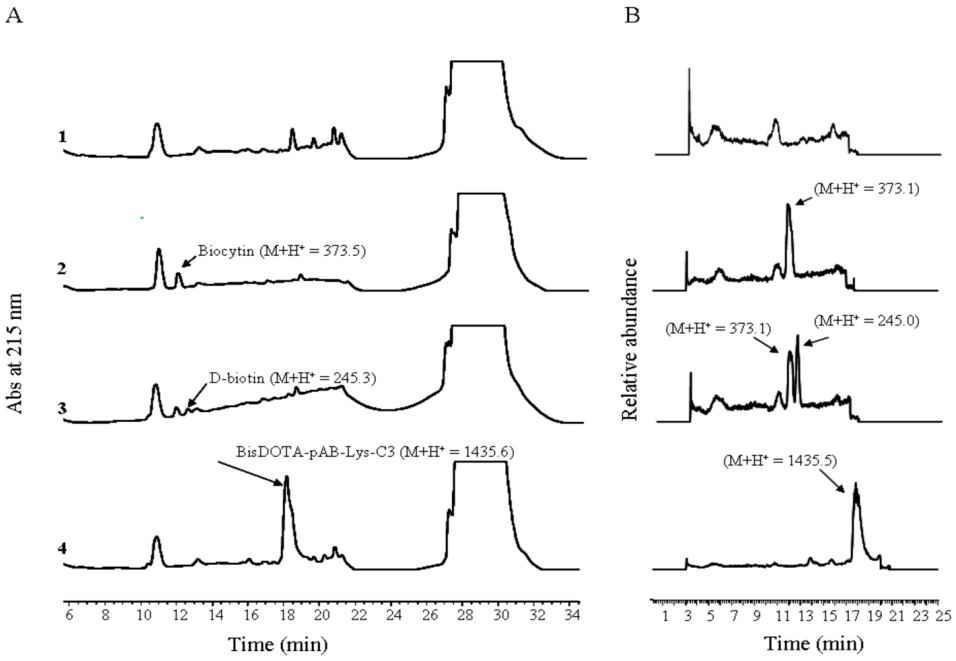

Figure 2.36 LC-MS analyses of BisDOTA derivatives resistance to biotinidase activity

2.9.3 Studies of binding to avidin

In vitro tests were realized in order to check whether the new biotin derivatives preserve the good affinity towards the Av or Sav.

The binding studies of the ^{90}Y-labeled MonoDOTA derivative (**1**), in the presence of a 1:2 Av/**1** molar ratio (which is two times the natural 1:4 molar ratio), showed that about 85% of ^{90}Y-labeled compound **1** was bound to Av, whereas at the natural 1:4 molar ratio only about 50% was bound (Figure 2.37). The average percentage of activity not specifically retained by the concentrator (about 4%) was subtracted from the counts found in the top part of the concentrator. Data at 2 and 24 h at 37 °C were similar, indicating that the binding occurs rapidly and is almost irreversible despite the linkage with the bulky DOTA molecule.

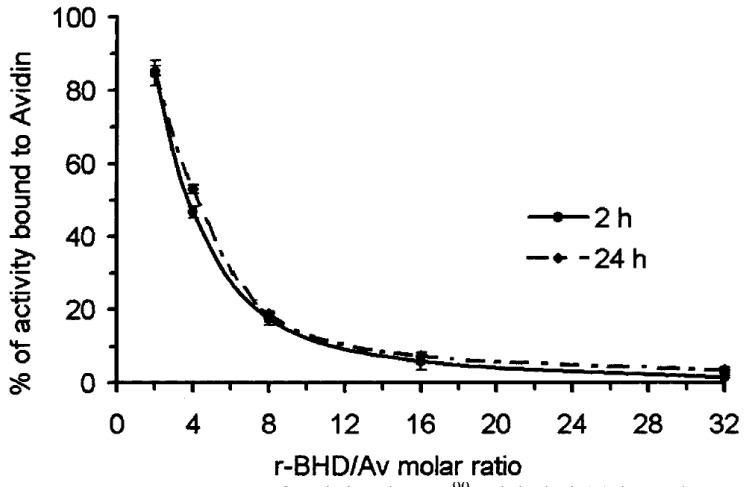

Figure 2.37 Percentage of activity due to ^{90}Y-labeled (**1**) bound to Av.

HABA (4'-hydroxyazobenzene-2-carboxylic acid) is a reagent that enables a quick estimation of the mole-to-mole ratio of biotin to protein. To quantify biotin label incorporation, a solution containing the biotin derivative is added to a mixture of HABA and avidin. Because of its higher affinity for avidin, biotin displaces the HABA from its interaction with avidin and the absorption at 500 nm decreases proportionately. By this method, an unknown amount of biotin in a solution can be evaluated in a single cuvette by measuring the absorbance of the HABA-avidin solution before and after addition of the biotin-containing sample. The change in absorbance relates to the amount of biotin in the sample. The typical protocol is the following: 900 μL of the avidin-HABA reagent in a 1

mL cuvette; measure the absorbance at 500 nm (A_{500} HABA/avidin); add 100 µL of biotinylated sample and mix. Measure of the absorbance at 500 nm (A_{500} HABA/avidin/biotin), the A_{500} should be stable.

$$\Delta A_{500} = (0.9 \times A_{500}\,H/A) - (A_{500}\,H/A/B)$$

For each biotin-derivative synthesized, a distribution curve showing biotin-avidin molar ratio *vs* ΔA_{500} was built (Figure 2.38).

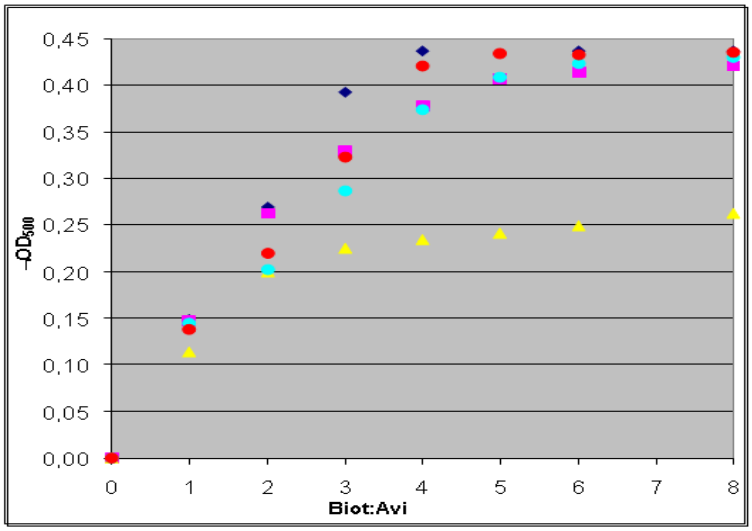

Figure 2.38 Inhibition of avidin/HABA complex by (+)-biotin (blue), BisDOTA-C_6 (yellow), BisDOTA-Lys-C_3 (cyan), BisDOTA-Lys-(*p*AB)-C_3 (red) and MonoDOTA (pink).

The avidin binding activity of BisDOTA derivatives was also determined by HABA assay in comparison with (+)-biotin. The assay utilizes the observation that HABA shows dramatic spectral changes when it binds to avidin. Free HABA has an absorption peak at 348 nm, while the HABA/avidin complex has strong absorption at 500 nm. Since the affinity between HABA and avidin is relatively weak ($K_d = 5.8 \times 10^{-6}$ M) compared to the affinity between (+)-biotin and avidin ($K_d = 1 \times 10^{-15}$ M), (+)-biotin can easily replace HABA from the HABA/avidin complex, resulting in a decrease of absorption at 500 nm. To estimate the apparent avidin binding affinity of biotin and biotin-derivatives, several competitive binding studies have been performed adding (+)-biotin and corresponding biotin-derivatives to the HABA/avidin sample and measuring any change in absorbance.

As shown in Figure 2.39, all BisDOTA compounds were able to inhibit the HABA/avidin complex in a dose dependent manner.

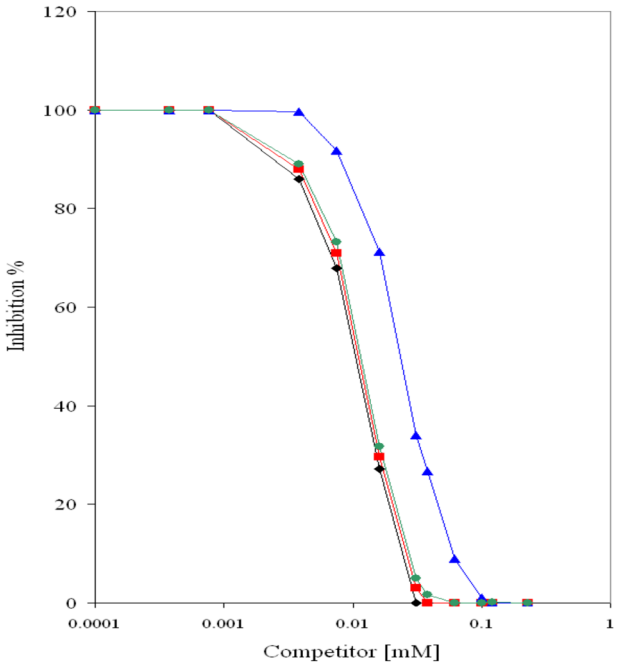

Figure 2.39 Inhibition of the HABA/avidin complex by (+)-biotin (◆, black line), BisDOTA-Lys-C_3 (■, red line), BisDOTA-Lys-(*p*AB)-C_3 (●, green line) and BisDOTA-C_3 (▲, blue line).

Nevertheless, due to the differences in their spacer arms, BisDOTA-Lys-C_3 (**7**) and BisDOTA-Lys-(*p*AB)-C_3 (**11**) are very similar to the native (+)-biotin. For sake of clarity, the relevant HABA displacement abilities are also compared in Table 2.6.

Table 2.6 Displacement of HABA from Avidin Complex.

Biotin derivatives	**HABA/Av inhibition %**
D-(+)-biotin	100%
MonoDOTA	87%
BisDOTA-C_3	66%
BisDOTA-C_6	64%
BisDOTA-Lys-C_3	95%
BisDOTA-Lys-(*p*AB)-C_3	97%

The melting curve of avidin/BisDOTA complex shows an inflection point at about 90 °C, which is higher than that of the avidin alone (about 80 °C) (Figure 2.40). Indeed, the melting curves of avidin/BisDOTA-Lys-C_3 and avidin/BisDOTA-Lys-(*p*AB)-C_3 complexes showed no valuable inflection point in the temperature range 25-95 °C, similarly to avidin/(+)-biotin complex.

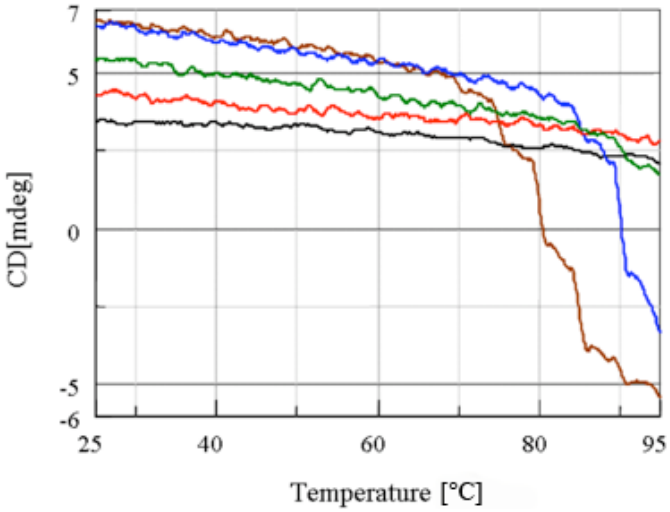

Figure 2.40 Melting curves of avidin (brown line); avidin/BisDOTA-C_3 complex (blue line); avidin/BisDOTA-Lys-C_3 complex (red line); Avidin/BisDOTA-Lys-(*p*AB)-C_3 complex (green line); avidin/(+)-biotin complex (black line).

The introduction of a spacer containing a carboxylate function in α to the biotinamide (BisDOTA-Lys-C_3, **7**), increased avidin affinity obtaining comparable values with MonoDOTA derivative.

The BisDOTA-Lys-C_3 modification with a more rigid and planar spacer (BisDOTA-Lys-(*p*AB)-C_3) carried an high increment in the binding affinity, indeed comparable with biotin.

The HABA affinity test was also useful for BisBiotin compounds **34** and **44**, providing data that can be compared with the previous results in order to assess the applicability of the products (Figure 2.41).

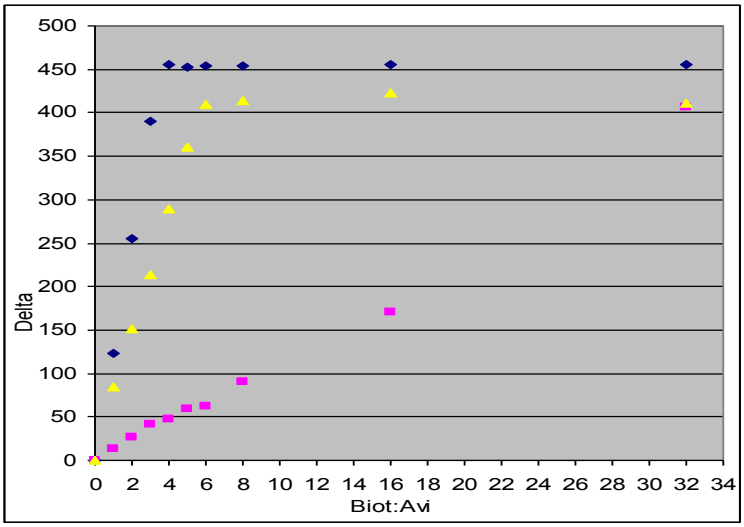

Figure 2.41 Inhibition of the avidin/HABA complex from biotina (blue), BisBiotinBisDOTA-(PEG$_6$)-C$_3$ (yellow) and BisBiotinMonoDOTA-(*p*AB)-C$_6$ (pink).

For BisBiotinMonoDOTA-C$_3$ (**21**) and BisBiotinBisDOTA-(PEG$_6$)-C$_3$ (**44**) data were similar: both compounds showed good affinity for avidin, but not so excellent as the BisDOTA compounds synthesized on solid phase.

In fact they showed an affinity slightly lower than MonoDOTA, but the affinity was, however, still of interesting level.

The BisBiotinMonoDOTA-(*p*AB)-C$_6$, in perfect harmony with the radiolabelling results, showed very little affinity for avidin. The data, once again, were not sufficient to make a weighted assessment regarding the poor performances of **34**, the low affinity of the similar BisDOTA could suggest a parallelism and indicate that the spacer C$_6$ is not suitable for these derivatives, but there aren't yet sufficient data to support this thesis.

In addition, the two compounds, presented differences in affinity for avidin, in fact the derivative **34** highlighted a very little affinity.

All of these results, positive or negative, are still essential to evaluate not only the products in question, but also the direction of research to be undertaken in future.

Chapter 3

CYCLOPEPTIDES AS CHELATING AGENTS

3.1 Introduction

Peptides are very efficient ligands for many metal ions. Their coordination capacity originates from presence of electron-donor functional groups in their side chains. Peptide complexes with first transition metals are under investigation because they mimic the metalloprotein binding sites.[113] Many natural peptides may contain a competitive donor atom in the side chain. The most important among them are the pyridine-like imidazole nitrogen of His (N^3) and the oxygen β-carboxylate of Asp. His or Asp residues are often critical for the biological activity of natural peptides and involving it in metal ion coordination may drastically change the biological activity of peptides.

The imidazole ring of His residues plays an important role in the biological function of the active sites in many enzyme systems and in the metal ion coordination points of several transport proteins. Furthermore, this residue is present in low molecular weight complexes that serve as delivery system of copper to tissue or that alters the growth rate or the state of differentiation of cultured cells and organism. This amino acid links metals ions, in particular Cu(II), in a strong way, by his imidazolic N^3 (N^π) which originates a high stably six-membered ring with the terminal amino group at pH > 4.[114,115] It is well known that three His residues constitute the ligands of zinc in carbonic anhydrase and that four His residues coordinate the copper in bovine superoxide dismutase.[116] On the other hand, the N-terminal region of the protein bovine serum albumin (BSA) containing the sequence Asp-Thr-His-Lys is known to provide a specific binding site for Cu(II) ions.[117] In

[113] Kozlowski, H.; Bal, W.; Dyba, M.; Kowalik-Jankowska, T. *Coord. Chem. Rev.* **1999**, *184*, 319-346.
[114] Casolaro, M.; Chelli, M.; Ginanneschi, M.; Laschi, F.; Muniz-Miranda, M.; Papini, A.M.; Sbrana, G.; *Spectrochim. Acta.* Part A, **1999**, *55A(7-8*), 1675-1689.
[115] Daniele, P.G.; Zerbinati, O.; Aruga, R.; Ostacoli, G. *J. Chem. Soc. Dalton Trans.* **1988**, 1115-1120.
[116] Tainer, J.A.; Getzoff, E.D.; Richardson, J.S.; Richardson, D.S. *Nature* **1983**, *306*, 284.
[117] Peters, T.Jr.; Blumenstock, F.A. *J. Biol. Chem*. **1967**, *242*, 1574.

1974 it was first reported that the tripeptide H-Gly-Gly-His-OH could mimic Cu(II) binding characteristic of serum albumin.[118] Recently, other linear peptides His-containing and mimicking the N-terminal Cu(II)-binding site of BSA have been synthesised and studied.[119] Subsequently, a study reported the interactions between divalent metal ions, such as Cu(II) and Zn(II) and short linear peptides containing His–Xaa–His. This motif in the peptide sequence is commonly used as a model for the copper(II) binding site of superoxide dismutase.[120] The multi-His sequences are also basic for the copper(II) binding motifs in other proteins like APP (amyloid precursor protein[121] or SPARC - secreted protein, acidic and rich in cysteine).[122] In the last decade, the neurodegenerative disorder called Creutzefeldt-Jacob disease, appeared onto the scene. The illness was due to the conversion of the normal cellular prion protein (PrP^{c}) into the pathological isoform PrP^{Sc}. Recently studies have shown PrPC is a copper(II) protein involved in copper metabolism in the brain. Studies with recombinant protein and peptides related to its sequence have shown that prion protein binds copper ions in its N-terminal region which contains a series of octapeptide repeats with the consensus sequence PHGGGWGQ.[123] These finds prompted the synthesis of numerous linear oligopeptides containing histidine in the effort to understand the behaviour of the normal and pathological octarepeat sequence.

There is great interest in the chemical characterisation of copper(II) complexes with oligopeptides. Indeed, a small but significant fraction of copper(II) in biological fluids appears to be associated with low molecular weight species; it is believed that this fraction is primarily responsible for the homeostasis of copper(II) and for its transfer among various storage and utilisation sites. Of particular significance is a recent study by Armstrong *et al.* where a detailed speciation of the various copper(II) species that are present in biological fluids is reported. Notably, in the blood stream, the low molecular weight copper(II) fraction is in equilibrium with macromolecular ligands such as serum albumin and serum transferrin.

---

[118] Lau, S.; Kruck, T.P.A.; Sarkar, B. *J. Biol. Chem.* **1974**, *249*, 5878-5884.
[119] Quagraine, E.K.; Kraatz, H.B.; Reid, R.S. *J. Inorg. Biochem*. **2001**, *85*, 23-32.
[120] Pogni, R.; Baratto, M.C.; Busi, E.; Basosi, R. *J. Inorg. Biochem.* **1999,** *73*, 157.
[121] Łuczkowski, M.; Wisniewska, K.; Łankiewicz, L.; Kozłowski, H. *J. Chem. Soc. Dalton Trans*. **2002**, 2266. Multhaup, G. *et al. Science* **1996,** *271*, 1406.
[122] Remelli, M.; Łuczkowski, M.; Bonna, A.M.; Mackiewicz, Z.; Conato, C.; Kozłowski, H. *New J. Chem*. **2003**, *27*, 245–250.
[123] Kramer, M.L.; Kratzin, H.D.; Schmidt, B.; Romer, A.; Windl, O.; Liemann, S.; Hornemann, S.; Kretzschmar, H. *J. Biol. Chem*. **2001**, *276*, 16711.

Starting from the study of a series of linear tetrapeptides[124] and cyclotetrapeptides[125] containing the histidine residue, synthesized in the "Laboratory of Peptides & Proteins Chemistry & Biology" of the University of Florence, the role of His and Gly residues coordination abilities towards copper(II) ions was been addressed. Particular emphasis is given to the consequences of the specific position of a unique histidine residue within a model, N-terminal protected, tetrapeptide sequence. For this aim we have synthesized the N-acetylated linear tetrapeptides with a single His, N and COOH protected oligopeptides with two His, but *in primis* we have investigated a series of cyclotetrapeptides containing two His.

Cyclotetrapeptides are constrained cyclic peptides whose synthesis is considered a difficult task. A methodology based on head-to-tail on-resin cyclization by anchoring the His side-chain was used. The combination of this strategy with an orthogonal three-dimensional protection scheme such as the Fmoc/*t*Bu/OAl results in a powerful head-to-tail cyclization methodology. The use of a three-dimensional protection scheme allows the orthogonal deprotection of the C- and N-termini for the subsequent head-to-tail on-resin cyclization. The solid-phase cyclization, compared to the solution one, takes advantage from the pseudodilution phenomenon to avoid cyclooligomerization that is critical in the synthesis of cyclotetrapeptides, where the ring closure is not favoured over the intermolecular cyclization, due to the intrinsic rigidity induced by the π-character of the peptide bond. The proposed synthetic approach presents the great advantage of obtaining cyclic scaffolds still bound to the resin, with functionalities ready for further modifications. The optimization of all the parameters and the comprehension of their role can be considered a starting point for the synthesis of libraries of constrained cyclopeptides.

This work has the aim to find a suitable alternative to the traditional chelating agents (DOTA and TETA) for use in radioimmunoterapies, and more specifically for the obtainment of a chelating agent designed *ad hoc* for each radiometal used and moreover for an efficient chelation of $^{64}Cu/^{67}Cu$ used in PET and SPECT.

[124] Matera-Witkiewicza, A.; Brasun, J.; Swiatek-Kozłowska, J.; Pratesi, A.; Ginanneschi, M.; Messori L. *J. Inorg. Biochem.* **2009**, *103*, 678–688.

[125] Brasun, J.; Matera-Witkiewicz, A.; Ołdziej, S.; Pratesi, A.; Ginanneschi, M.; Messori, L. *J. Inorg. Biochem.* **2009**, *103*, 813–817.

3.1.1 Radiometals for imaging of disease

Single-photon emission computed tomography (SPECT) and positron emission tomography (PET) were the first molecular imaging modalities used clinically. SPECT requires the use of a contrast agent labeled with a γ-emitting radionuclide, which should have an ideal γ energy of 100-250 keV. These γ rays are recorded by the detectors of a dedicated γ camera or SPECT instrument and after signal processing can be converted into an image identifying the localization of the radiotracer. PET requires the injected radiopharmaceutical to be labelled with a positron-emitting radionuclide. As the radionuclide decays, it ejects a positron from its nucleus, which travels a short distance before being annihilated with an electron to release two 511 keV γ rays 180° apart that are detected by the PET scanner. After sufficient acquisition time, the data are reconstructed using computer-based algorithms to yield images of the radiotracer's location within the organism. Compared with SPECT, PET has greater advantages with respect to sensitivity and resolution and has been gaining in clinical popularity, with the number of PET-based studies expected to reach 3.2 million by 2010.[126] While SPECT and PET technologies have been around for decades, their use remained limited because of the limited availability of relevant isotopes, which had to be produced in nuclear reactors or particle accelerators. However, the introduction of the small biomedical cyclotron, the self-contained radionuclide generator, and the dedicated small animal or clinical SPECT and PET scanners to hospitals and research facilities has increased the demand for SPECT and PET isotopes.

Traditional PET isotopes such as ^{18}F, ^{15}O, ^{13}N, and ^{11}C have been developed for incorporation into small molecules, but due to their often lengthy radiosyntheses, short half-lives, and rapid clearance, only early time points were available for imaging, leaving the investigation of biological processes, which occur over the duration of hours or days, difficult to explore. With the continuing development of biological targeting agents such as proteins, peptides, antibodies and nanoparticles, which demonstrate a range of biological half-lives, a need arose to produce new radionuclides with half-lives complementary to their biological properties. As a result, the production and radiochemistry of radiometals such as Zr, Y, In, Ga, and Cu have been investigated as radionuclide labels for

[126] Society of Nuclear Medicine. http://interactive.snm.org/index.cfm?, 2009.

biomolecules since they have the potential to combine their favorable decay characteristics with the biological characteristics of the targeting molecule to become a useful radiopharmaceutical (Table 3.1 and Table 3.2).[127]

In case that copper is used with a chelating agent, is important to investigate its coordination chemistry. While +1 and +3 oxidation states are both accessible for copper in the presence of suitable donors, $3d^9$ Cu(II) remains the predominant state for radiocopper chemistry in protic media.

Table 3.1 γ- and β-Emitting radiometals.

Isotope	$t_{1/2}$ (h)	production methods	decay mode	E_γ (keV)	E_β (keV)
^{67}Cu	62.01	accelerator ^{67}Zn(n,p)	β^- (100%)	91, 93, 185	577, 484, 395
^{67}Ga	78.26	cyclotron	EC (100%)	91, 93, 185, 296, 388	
^{90}Y	64.06	^{90}Sr/^{90}Y generator	β^- (72%)		2288
^{111}In	67.9	cyclotron, ^{111}Cd(p,n)^{111}n	EC (100%)	245, 172	

Table 3.2 Positron-emitting radiometals.

isotope	$t_{1/2}$ (h)	methods of production	decay mode	E_{β^+} (keV)
^{60}Cu	0.4	cyclotron, ^{60}Ni(p,n)^{60}Cu	β^+ (93%) EC (7%)	3920, 3000 2000
^{61}Cu	3.3	cyclotron, ^{61}Ni(p,n)^{61}Cu	β^+ (62%) EC (38%)	1220, 1150 940, 560
^{62}Cu	0.16	^{62}Zn/^{62}Cu generator	β^+ (98%) EC (2%)	2910
^{64}Cu	12.7	cyclotron, ^{64}Ni(p,n)^{64}Cu	β^+ 19(%) EC (41%) β^- (40%)	656
^{66}Ga	9.5	cyclotron, ^{63}Cu(α,nγ)^{66}Ga	β^+ (56%) EC (44%)	4150, 935
^{68}Ga	1.1	^{68}Ge/^{68}Ga generator	β^+ (90%) EC (10%)	1880, 770
^{86}Y	14.7	cyclotron, ^{86}Sr(p,n)^{86}Y	β^+ (33%) EC (66%)	2335, 2019 1603, 1248 1043
^{89}Zr	78.5	^{89}Y(p,n)^{89}Zr	β^+ (22.7%) EC (77%)	897 909, 1675, 1713, 1744

The aqueous cupric ion was long believed to have a tetragonally distorted hexa-aqua structure until a 2001 report suggested only five-coordination.[128] Its water-exchange rate has been found to be very rapid compared with most common first-row transition metal cations and as a result it has relatively facile substitution chemistry despite having some crystal-field stabilization. This is usually ascribed to the Jahn-Teller distortion that elongates one or more of its coordinated ligands. Classified as a cation of borderline

[127] Welch, M.J.; Redvanly, C.S., Eds.; *Handbook of Radiopharma-ceuticals: Radiochemistry and Applications*; John Wiley & Sons Inc.: Hoboken, NJ, **2003**.

[128] Pasquarello, A.; Petri, I.; Salmon, P.S.; Parisel, O.; Car, R.; Toth, E.; Powell, D.H.; Fischer, H.E.; Helm, L.; Merbach, A.E. *Science* **2001**, *291*, 856.

hardness, the high affinity of Cu(II) for borderline nitrogen donors is well established. With a relatively small ionic radius of between 57 and 73 pm for coordination numbers 4-6, it is particularly suitable for the formation of five membered chelate rings; indeed the chelate effect is epitomized in its ethylenediamine family of complexes.[129] The popular use of polyazamacrocycles, especially cyclen and cyclam, for strong binding of Cu(II) is a consequence of the added advantage of the macrocyclic effect,[130] as borne out by their extensive coordination literature.[131,132] The importance of *in vivo* redox activation of metallodrugs incorporating Pt(IV), Ru(III), and Co(III) has received increasing attention. The role of bioreduction in copper radiopharmaceutical efficacy has been intensively studied in their thiosemicarbazone complexes.[133] Convincing evidence for the formation and selective retention/decomplexation of Cu(I)-intermediates from Cu(II) precursors in hypoxic tissues has been presented.[134] Whether Cu(II)/Cu(I) bioreduction is also a viable pathway for irreversible *in vivo* radiocopper loss from other chelator complexes and their bioconjugates is an intriguing possibility. There is some compelling evidence for the deteriorated *in vivo* performance of related Cu(II) complexes differing only in their reduction propensities. Specifically, the "long arm" dicarboxyethyl pendant-armed Cu(II) complex of cross- bridged cyclam has an E_{red} almost 400 mV higher (or more positive) than that its carboxymethyl-armed analogue.[135] The former has been found to exhibit significantly inferior bioclearance behavior despite very similar coordination geometry and acid-inertness. The plasticity of the Cu(II) coordination geometry can be gleaned from a literature survey of 89 of its complexes with cyclen and cyclam derivatives. Coordination numbers (CN) ranging from 4 to 6 were found with geometries approximating square planar, square pyramidal, trigonal bipyramidal, and octahedral. Tetradentate chelators are usually designed to cater to Cu(II)'s strong affinity for ligands favouring a square-planar geometry. Common donor sets include two amino or imino nitrogens combined with two

[129] Mukherjee, R. Copper. In *Comprehensive Coordination Chemistry II: Transition Metal Groups 7 and 8*; Constable, E.C., Dilworth, J., Eds.; Elsevier Limited: San Diego, CA, **2004**; Vol. 6, p 747.
[130] Cabbiness, D.K.; Margerum, D.W. *J. Am. Chem. Soc.* **1969**, *91*, 6540.
[131] Bencini, A.; Bianchi, A.; Paoletti, P.; Paoli, P. *Coord. Chem. Rev.* **1992**, *120*, 51.
[132] Delgado, R.; Felix, V.; Lima, L.M. P.; Price, D.W. *Dalton Trans.* **2007**, *26*, 2734.
[133] Holland, J.P.; Barnard, P.J.; Collison, D.; Dilworth, J.R.; Edge, R.; Green, J.C.; McInnes, E.J.L. *Chem. Eur. J.* **2008**, *14*, 5890.
[134] Holland, J.P.; Giansiracusa, J.H.; Bell, S.G.; Wong, L.L.; Dilworth, J.R. *Phys. Med. Biol.* **2009**, *54*, 2103.
[135] Heroux, K.J.; Woodin, K.S.; Tranchemontagne, D.J.; Widger, P.C.B.; Southwick, E.; Wong, E.H.; Weisman, G.R.; Tomellini, S.A.; Wadas, T.J.; Anderson, C.J.; Kassel, S.; Golen, J.A.; Rheingold, A.L. *Dalton Trans.* **2007**, *21*, 2150.

charge neutralizing anionic amido, oxo, or thiolato sites. These include numerous Schiff base or amino acid derived chelators. As a result, hexadentate chelators have become the most investigated in radiocopper chemistry (Figure 3.1). Popular scaffolds include tetraazamacrocycles, derived from cyclic tetrapeptides.

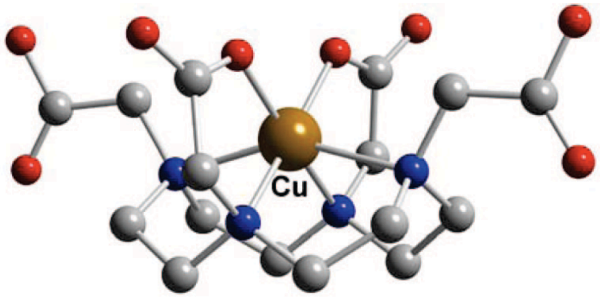

Figure 3.1 Cu(II)/DOTA.

3.2 Synthesis of cyclen scaffolds from cyclotetrapeptides

The development of new coordinating ligands is of straightforward actuality for the study and the synthesis of diagnostic and therapeutic drugs, which can mimic the binding site of metalloproteins. Tetraazamacrocyclic compounds, as 1,4,8,11-tetraazacyclotetradecane (cyclam) and 1,4,7,10-tetraazacyclododecane (cyclen) derivatives (Figure 3.2) have found wide application in medicinal chemistry.[136] In particular, cyclen derivatives have recovered considerable interest in the development of MRI contrast agents[137] and as radionuclides vehicles.[138]

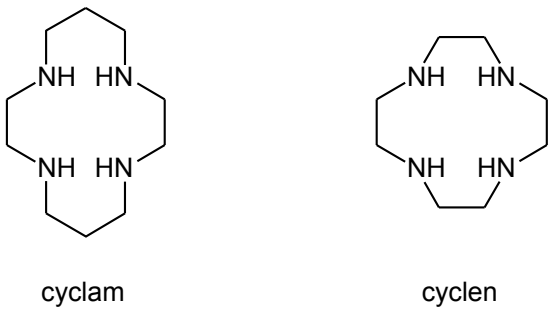

Figure 3.2 Cyclam and Cyclen.

[136] Bradshaw, J.S.; Krakowiak, K.E.; Izatt, R.M. In "*Aza-Crown Macrocycles: The Chemistry of Hetericyclic Compounds*", Wiley&Sons, New York, **1993**, pp. *16-21*, *83-85*, 157-165.
[137] Caravan, P.; Ellison, J.J.; McMurray, T.J.; Lauffer, R.B. *Chem. Rev.* **1999**, *99*, 2293-2352.
[138] Burgess J. *Chem. Soc. Rev.* **1996**, 85-92.

Cyclen is the key intermediate for the preparation of more complex compounds,[139] such as bis-tetraazamacrocycles, polyazamacrocycles and *N*-alkylated cyclens. Different condensation strategies for the synthesis of cyclens have been described, but the traditional approach reported by Richman and Atkins,[140] with its variants, where the condensation reaction involves a tris-*N*-tosyl diethylenetriamine and an *N*-tosyl diethanolamine ditosylate, remains the most convenient. In order to avoid tosylate chemistry, different protections of the aza-compounds were considered either envisaging condensation of tricyclic intermediates,[141] or tetracyclic precursors.[142]

A convenient retro-synthetic pathway to tetraazamacrocycles can be envisaged considering cyclen and cyclam derivatives as pseudopeptides. In fact, reduction of the amide bond of head-to-tail cyclotetrapeptides, containing four α-amino acids, can lead to cyclen derivatives, while cyclams can be obtained by cyclotetrapeptides containing α and β-amino acids in alternate positions.[143] Moreover, the cyclen core derived from cyclotetrapeptides is a possible scaffold for metal complexation with increased chelating properties, thanks to the side-chains of suitable amino acids to be introduced in the precursor peptide sequence.

Syntheses leading to cyclen derivatives mono-substituted at position 2 were described;[144] only one compound, tetraethyl substituted at positions 2, 5, 8, and 10, was reported.[145]

In PeptLab was investigated the synthesis of an enantiomerically pure cyclen derivative disubstituted at positions 2 and 8 obtained by reduction of cyclo(His-Gly-His-Gly), using a solid-phase strategy.

[139] Bender, J.A.; Meanwell, N.A.; Wang, T. *Tetrahedron* **2002**, *58*, 3111-3128.
[140] Richman, J.E.; Atkins, T.J. *J. Am. Chem. Soc.* **1974**, *96*, 2268-2270; Atkins, T.J.; Richman, J.E.; Oettle, W.F. *Org. Synth.* **1978**, *58*, 86-98.
[141] Jazwinski, J.; Kolinski, R. *Tetrahedron Lett.* **1981**, *22*, 1711-1714.
[142] Weisman, G.R.; Reed, D.P. *J. Org. Chem.* **1996**, *61*, 5186-5187; Hervé, G.; Bernard, H.; Toupet, L.; Handel, H. *Eur. J. Org. Chem.* **2000**, 33-35; Athey, P.S.; Kiefer, G.E. *J. Org. Chem.* **2002**, *67*, 4081-4085.
[143] Achmatowicz, M.; Jurczak, J. *Tetrahedron: Asymmetry* **2001**, *12*, 111-119.
[144] Garrity, M.L.; Brown, G.M.; Elbert, J.E.; Sachleben, R.A. *Tetrahedron Lett.* **1993**, *34*, 5531-5534.
[145] Tsuboyama, K.; Higashi, I.; Yanagita, M. *Tetrahedron Lett.* **1970**, *11*, 1367-1370.

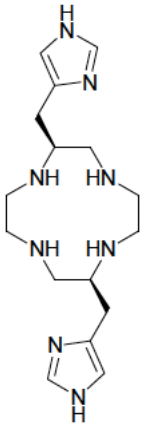

Figure 3.3 2,8-bis-(1*H*-imidazol-4-ylmethyl)-1,4,7,10-tetraazacyclododecane

Reduction of the amide bonds of cyclo[His-Gly-His(trityl-resin)-Gly] was undertaken by an on-resin procedure, by treatment with a solution of $BH_3 \cdot THF$.[146]

The new scaffold cyclen analogue 2,8-bis-(1*H*-imidazol-4-ylmethyl)-1,4,7,10-tetraazacyclododecane (Figure 3.3), containing two imidazole groups (coming from the His residues present in the skeleton of the starting material), possesses increased chelating properties, respect to the usual tetraazamacrocycles, which can be used as coordinating systems in metalloproteins characterization.

Anyway the method applied showed very low yields of completely reduced compounds, with formation of by-products containing only one, two or three reduced peptide bonds. Tentative reduction with $LiAlH_4$ in THF gave same results.

Because of this problem we decided to study the coordination properties of the various cyclic peptides without reduction of the amidic bonds.

3.3 14-membered tetraza cyclic tetrapeptide

A small but still significant fraction of copper(II) ions in biological fluids appears to be associated with low molecular weight species; it is believed that this fraction is primarily responsible for the homeostasis of copper(II) and for its transfer among various storage and utilization sites.

[146] Alcaro, M.C.; Orfei, M.; Chelli, M.; Ginanneschi, M.; Papini, A.M. *Tetrahedron Lett.* **2003**, *44,* 5217-5219.

Peptides form a special group of substances capable of effective copper(II) binding; among them, cyclopeptides deserve a special attention. Cyclopeptides play a variety of roles in living organisms; indeed they may act as hormones, toxins, antibiotics, molecules with enzymatic functions or as carrier molecules.[147,148,149] The most known is valinomicin, cyclopeptide is able of binding the alkali metal ions and transporting them through the biological membranes.

The previous studies on the binding abilities of cyclopeptides towards Cu(II) ions[150,151,152,153] showed that His-containing cyclopeptides are able to bind copper(II) tightly through imidazole as well as amide nitrogens. The pH and the peptide ring size have a great impact on the kind of the coordinated nitrogens. The acidic pH favors the formation of complexes with imidazole nitrogens coordinated to the metal ion while in the basic conditions the binding of the amide nitrogens is highly preferred. The ring size is significant for the coordination mode. The study on the cyclopeptides with twelve membered rings have shown that the ring is too small for the formation of the complex with the [4 × N^-] binding mode. Insertion of one more carbon atom into the peptide cycle causes that the oxidation of the copper is observed.[152] For the peptides with greater than 13-membered rings the formation of the complex with the [4 × N^-] binding mode is preferred.

The cyclopeptides with four amide nitrogens may be somehow related to the corresponding tetraazamacrocycles,[154,155] commonly endowed with very high binding constants for Cu(II), of potential use in ^{64}Cu-based radiotherapeutic strategies.[156]

---

[147] Ovchinnikov, Y.A.; Ivanov, V.T. *Tetrahedron* **1975**, *31*, 2177–2209.
[148] Kemmer, H.; Tripier, D.; Jouvenal, K.; Scriba, D.; Zanotti, G.; Maione, A.M.; Ziegler, K. *Biochem. Pharmacol.* **1997**, *54,* 481–490.
[149] Odier, F.; Vey, A.; Bureau, J.P. *Biol. Cell* **1992**, *74,* 267–271.
[150] Brasun, J.; Gabbiani, C.; Ginanneschi, M.; Messori, L.; Orfei, M.; Swiatek-Kozlowska, J. *J. Inorg. Biochem.* **2004**, *98*, 2016–2021.
[151] Brasun, J.; Matera, A.; Ołdziej, S.; Swiatek-Kozłowska, J.; Messori, L.; Gabbiani, C.; Orfei, M.; Ginanneschi, M. *J. Inorg. Biochem.* **2007**, *101,* 452–460.
[152] Pratesi, A.; Zanello, P.; Giorgi, G., Messori, L.; Laschi, F.; Casini, A.; Corsini, M.; Gabbiani, C.; Orfei, M.; Rosani, C.; Ginanneschi, M. *Inorg. Chem.* **2007**, *46,* 10038–10040.
[153] Schapp, J.; Haas, K.; Sünkel, K.; Beck, W. *Eur. J. Inorg. Chem.* **2003**, 3745–3751.
[154] Motekaitis, R.J.; Rogers, B.E.; Reichert, D.E.; Martell, A.E.; Welch, M.J. *Inorg. Chem.* **1996**, *35,* 3821–3827.
[155] Martell, A.E.; Smith, R.M. Critical Stability Constants, vol. 62, Plenum Press, New York, **1989** (Suppl.).
[156] Ferreira, C.L.; Yapp, D.T.; Lamsa, E.; Gleave, M.; Bensimon, C.; Jurek, P.; Kiefer, G.E. *Nucl. Med. Biol.* **2008**, *35*, 875–882.

The cyclic peptide that is investigated here, *c*(β[3]homoLys-DHis-*β*Ala-His) (DK14 hereafter), is a structural analog of *c*(Lys-DHis-Gly-His), but bears two additional carbons thus consisting of 14 members peptide cycle (Figure 3.4). In principle, the greater ring size might confer a higher flexibility to this ligand than shown by 12-member cyclopeptides. Also, we thought that a the detailed comparison of the behaviour of the here reported copper(II) complexes with those formed by *c*(Lys-DHis-Gly-His) might provide further insight into the structural and thermodynamic properties of copper(II) cyclopeptide systems.

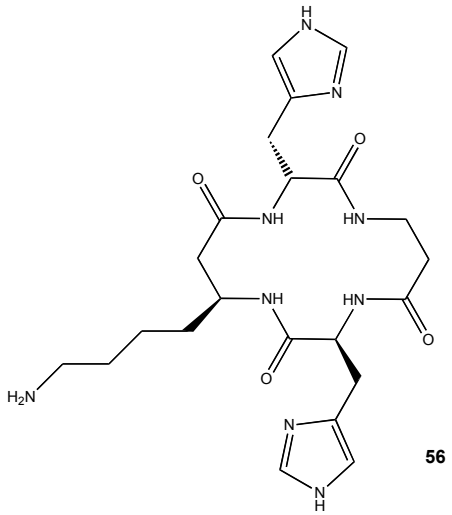

Figure 3.4 *c*(β3homoLys-DHis-*β*Ala-His) (DK14)

The protonation constants for the studied peptide are given in Table 3.3. The *c*(β[3]homoLys-DHis-*β*Ala-His) (**56**) (DK14) is characterized by three protonation constants which can be assigned to the two histidine and one lysine residues. The protonation constants for the ligand with the 14-atoms cycle are slightly higher than those earlier obtained for its analog with the twelve-member ring (DK12) (Table 3.3).

The coordination of copper(II) starts around pH 4.5 through the formation of the CuH_2L species (Figure 3.5). The presence of the maximum absorption at 703nm (Table 3.4) suggests copper(II) coordination of 1N type. The value of log K* = -2.47 (log K* = log β_{CuH2L} - logβ_{H3L})[157] supports binding of the nitrogen from a first imidazole ring.

[157] Kozłowski, H.; Kowalik-Jankowska, T.; Jezowska-Bojczuk, M.; *Coord. Chem. Rev.* **2005**, *249,* 2323–2334.

When pH increases, dissociation of the next proton takes place from the second imidazole ring leading to formation of the CuHL species. However, the concentration of this species is too low for any satisfactory spectroscopic characterization. Nevertheless, the value of log K = 6.45 (Table 3.3) for proton dissociation from the 2-nd His is almost the same as for free ligand ($logK_{Im2}$ = 6.63).

Table 3.3 Potentiometric data for Cu(II) complexes with **56** and **58**.

	***c*(β^{3}homoLysDHis*β*AlaHis)**	**c(LysDHisGlyHis)**
HL	9.99±0.01	9.51
H_2L	16.62±0.02	16.05
H_3L	22.38±0.01	21.45
$logK_{(NH2)}$	9.99	9.51
$logK_{(Im)}$	6.63	6.54
$logK_{(Im)}$	5.76	5.40
	log*β*	
CuH_2L	19.91±0.06	-
CuHL	13.46±0.10	14.76
$CuH_{-1}L$	1.22±0.02	3.49
$CuH_{-2}L$	-6.86±0.03	-5.54
$CuH_{-3}L$	-15.57±0.03	-
$CuH_{-4}L$	-26.16±0.03	-26.22
$log\beta_{CuH2L}$-$log\beta_{CuHL}$	6.45	-
$log\beta_{CuHL}$-$log\beta_{CuH-1L}$	12.24	11.27
$log\beta_{CuH-1L}$-$log\beta_{CuH-2L}$	8.08	9.03
$log\beta_{CuH-2L}$-$log\beta_{CuH-3L}$	8.71	-
$log\beta_{CuH-3L}$- $log\beta_{CuH-4L}$	10.59	-
$log\beta_{CuH-2L}$-$log\beta_{CuH-4L}$	-	20.68

This finding suggests that the presence of the copper(II) ion in the complex has no impact on dissociation of the proton from 2nd His residue and that binding of a second nitrogen to the metal does not take place.

With a further pH increase, the cooperative dissociation of two protons is observed and the $CuH_{-1}L$ species is formed. The spectroscopic data (Table 3.4) are suggestive of 3N type copper(II) coordination. Analysis of CD data (Table 3.4, Figure 3.6) suggests that nitrogen from the imidazole ring as well as two amide nitrogens are bound to the metal ion. This type of coordination dominates at physiological pH (Figure 3.5).

The proposed $CuH_{-1}L$ structure obtained from theoretical calculations is shown in Figure 3.7. Thus, DK14 similarly to DK12 predominantly forms a complex with a characteristic [N_{Im}, 2 × N^-] binding mode at physiological pH (Figure 3.5).

Table 3.4 Spectroscopic data for Cu(II) complexes with **56** and **58**.

	***c*(β[3]homoLysDHis*β*AlaHis)**						**c(LysDHisGlyHis)**					
Comp.	**UV-Vis**		**CD**		**EPR**		**UV-Vis**		**CD**		**EPR**	
	λ	**ε**	**λ**	**Δε**	**A_{II}**	**g**	**λ**	**ε**	**λ**	**Δε**	**A_{II}**	**g**
			-	-								
CuH_2L	703	34			136	2.359	-	-	-	-	-	-
CuHL	-	-	-	-			681.5	46	665 337[b]	0.04 -0.05	-	-
$CuH_{-1}L$	681 495 341	71 90 sh	520 467,50 414,5 sh 363,5 sh 317,50 291,5 sh 257,50	0,27 -0,26 0,12 sh 0,30 sh 0,09 0,24 sh 0,78	191	2.244	596 325	124 sh	645[d] 553[d] 488[d] 355[b]	0.12 -0.06 0.07 -0.35	171	2.210
$CuH_{-2}L$	495 440	119 Sh	-	-	-	-	587.5 326	211 722	647[d] 562[d] 489[d] 355[b]	0.07 -0.05 0.12 -0.34	174	2.215
$CuH_{-3}L$	495 443	86 91	517,20 463,60 414,20 sh 327 291,60 280,80 261,20 240	0,88 -0,58 0,08 sh -0,05 0,35 0,26 0,95 -1,19	216	2.151	-	-	-	-	-	-
$CuH_{-4}L$	495 446	100 105	517,20 463,60 414,4 sh 325 sh 291 261,20	1,04 -0,73 0,07 sh -0,14 sh 0,44 1,23	216	2.151	580 326	205 730	587[d] 492[d] 348	-0.05 0.2 -0.21	174	2.220

I = 0.1 M KNO_3, 25 °C. The ligand concentration was 1 × 10^{-3} M. Ligand to metal ratio 1.5:1.

In Figure 3.7 the structure of the $CuH_{-1}L$ species obtained from theoretical calculations is shown. Central metal ion is coordinated by two deprotonated amide nitrogen atoms and nitrogen from imidazole moiety. Three calculated Cu–N distances are almost equal (1.96 Å). All of these four atoms (central ion and three nitrogen atoms) are located in one plane. The deviation from the planarity, calculated as deviation of sum of three N–Cu–N angles minus 360 degrees is only about 7 degrees. Planar geometry of the coordination sphere is suggested by spectroscopic measurements (Table 3.4, Figure 3.5).

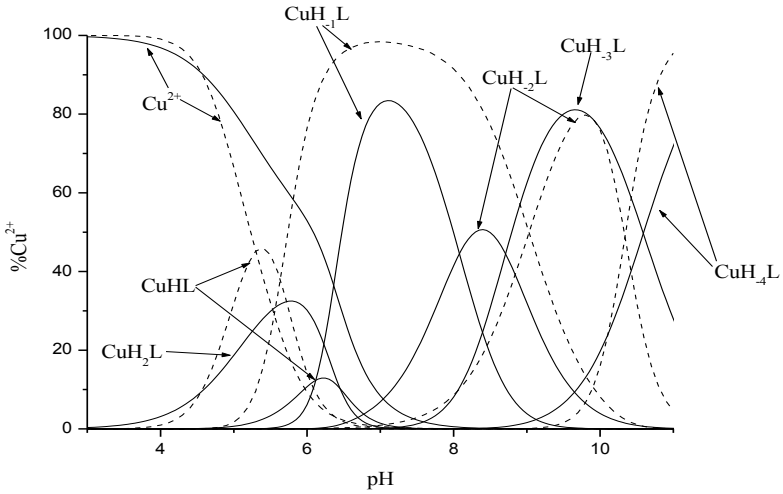

Figure 3.5 Species distribution curves for DK14-Cu^{2+} (solid line) and DK12-Cu^{2+} (dashed line) complexes at 25 °C and I = 0.1 M KNO_3. The ligand concentration was 1×10^{-3} M. Ligand to metal ratio 1.5:1.

The fourth coordination position is completely exposed to solvent and is probably occupied by water molecule. Additionally, we can observe that one of the carbonyl oxygen atoms from the peptide is located perpendicular to the coordination plane defined by the central copper(II) ion and the three nitrogen atoms and forms an additional coordination bond with metal ion (the Cu–O distance is 2.1 Å).

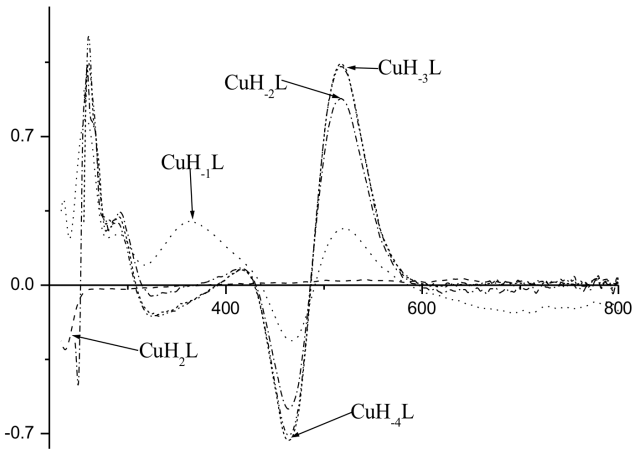

Figure 3.6 The CD spectra for the Cu(II)-DK14 system.

Above pH 8 two additional protons are dissociate and the $CuH_{-2}L$ and $CuH_{-3}L$ species are formed. The log K = 8.08 for the first complex and log K = 8.71 for second one suggest proton dissociation from the two remaining amide nitrogens and subsequent formation of the 4 N complex with four amide nitrogens bounded to the metal ion. The spectroscopic parameters show the square planar symmetry of the formed species. The strong blue shift in the absorption spectra of the species mentioned above (Table 3.4) suggests the very strong influence of four nitrogens in the equatorial plane on the copper ion. This result and the major EPR parameters confirm copper(II) coordination by four nitrogen atoms (N4 equatorial donor set) at the highest pH values.

In the CD spectrum (Figure 3.6) the charge transfer contribution around the 290 nm seems also to support an increasing contribution from the Cu–N transitions starting from $CuH_{-1}L$ species. Notably, large CD perturbation is observed in concomitance with the transition from $CuH_{-1}L$ (Figure 3.7) to the $CuH_{-2}L$ species, while this latter show similar CD behaviour to the $CuH_{-3}L$ and $CuH_{-4}L$ species.

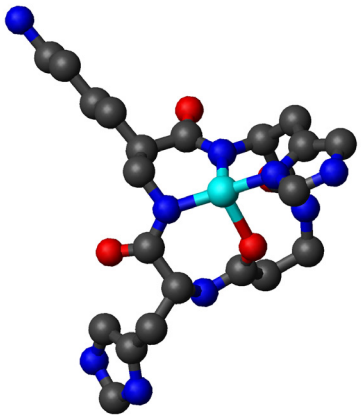

Figure 3.7 The proposed structure of the $CuH_{-1}L$ species. The copper(II) ion is shown in cyan, oxygen, carbon and nitrogen atoms are shown in red, black and blue respectively.

In Figure 3.8 the proposed structure of the $CuH_{-3}L$ complex obtained from theoretical calculations is shown. The central metal ion is completely separated from solvent by six nitrogens. Two of these come from the two histidine side-chains, while the other four are deprotonated amide nitrogens forming an octahedral arrangement. The whole coordination sphere of the central copper(II) ion is thus very symmetrical. Four

deprotonated amides form a very regular square planar system. All Cu–N distances are equal to 1.98 Å and the N–Cu–N angles are equal to 85 or 95 degrees, which suggests very small deviation from ideal coplanar location of the ligands and the central ion. This type of coordination is confirmed by spectroscopic studies (Table 3.4). Both imidazole rings are located perpendicular to the plane defined by the central ion and the four deprotonated amide nitrogens; both Cu–N_{im} distances are in this case equal to 2.35 Å. Stereochemistry of the ligand clearly shows that the complex presented here is the only case where two imidazole rings are bound to the same metal ion. At low pH, only complexes with one imidazole ring bound to the copper(II) center are observed, because imidazole rings of two histidine residues are located from the opposite sides of the cyclopeptide ring.

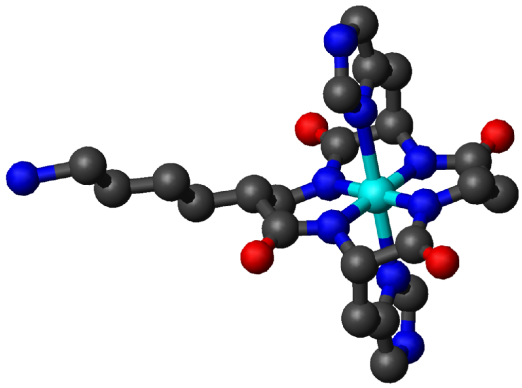

Figure 3.8 The proposed structure of $CuH_{-3}L$ complex obtained from theoretical calculations. The copper(II) ion is shown in cyan, oxygen, carbon and nitrogen atoms are shown in red, black and blue respectively.

The theoretical calculations thus point out that the $CuH_{-3}L$ species is characterized by a [2 × N_{Im}, 4 × N^-] binding mode (Figure 3.8). The some support for the proposed $CuH_{-3}L$ structure can be find in the CD data.

The CD features that are observed around 290 nm should be assigned to amide to copper(II) charge transfers.[158,159] In turn, features assignable to His to Cu(II) CT should fall in the 330–350 nm range. Notably we can see a well-shaped positive band in that range at low pH; then this band changes its sign (becomes negative) and then shows a clear increase at high pH values. Possibly this band is indicative of apical coordination of at least one

[158] Kowalik-Jankowska, T.; Biega, Ł.; Kuczer, M.; Konopinska, D. *J. Inorg. Biochem.* **2009**, *103,* 135–142.
[159] Gralka, E.; Valensin, D.; Porciatti, E.; Gajda, C.; Geggelli, E.; Valensin, G.; Kamysz, W.; Nadolny, R.; Guerrini, R.; Bacco, D.; Remelli, M.; Kozłowski, H. *Dalton Trans.* **2008**, 5207–5219.

imidazole. The presence of such band in the CD spectra might be stressed as indicative of imidazole coordination but we have to avoid excessive speculation.

The last formed species is the $CuH_{-4}L$ complex. LogK = 10.56 for $CuH_{-4}L$ formation and the same spectroscopic characteristics (Table 3.4) suggest proton dissociation from the Lys residue.

The comparison of the copper(II) coordinating abilities of *c*(β^3homoLys-DHis-*β*Ala-His) with those of its 12 member cyclic analog, *c*(Lys-DHis-Gly-His) (Figure 3.5), shows that DK12 coordinates Cu(II) more effectively than its β-analog. The smaller ring size makes formation of the complex with [N_{Im}, 2 × N^-] binding mode easier and the formed complex is thus more stable (Figure 3.5). However, the insertion of two additional atoms in the peptide ring allows copper(II) coordination by four amide nitrogens from the cyclopeptide starting from pH 8.

3.4 13-membered tetraza cyclic tetrapeptide

3.4.1 Introduction to copper complexation in biological systems

Among the metallic oligoelements necessary to the human organism, the copper, even if it is not the most abundant one, is still among the most active in the biochemical pattern, especially for the correct working of the high number of the cellular redox reactions. Cu(II) ion is the most tightly bound metal ion in the chelating centers, which accounts for the fact that the copper present in living cells is almost entirely complexed with proteins or peptides. Copper ions lies at the active center of a versatile group of redox catalysts like cytochrome-c oxidase, galactose oxidase or superoxide dismutase (SOD). Copper(II) is stored in the brain cells in the human prion protein (PrP) where is bonded to four repeats of eight-residue sequence PHGGGWGQ where the Cu(II), at neutral pH values, is bonded to one imidazole and two amide nitrogens. The necessary amount of copper(II) ion assumed by the diet is in the range of 1.5-3.0 mg *pro die*. A correct homeostasis of copper and of the other transition metals, so called oligo-elements, is fundamental for the correct physico-chemical equilibrium of the organism. The control of toxicity of copper is based on mechanisms like redox enzymes function, extra- and intra-cellular chelation and a fine tuning of transmembrane transport. Hence the correct plasma

transport of copper is fundamental for the homeostasis of this metal and is ensured by various proteins among them ceruloplasmin and serum albumin play an important role. Noteworthy, a significant fraction of Cu(II) is bonded to low molecular peptide species which act as carriers in the biological fluids.[160] It is know that at the physiological pH values Cu(II) is tightly bonded to the imidazole side chain of the histidine residues, that is able to coordinate copper ions since acidic pH. Peptide bonds also are also deprotonated at pH 7 in Cu(II) coordination, often in collaboration with the N_{im} atom. Notably, cyclopeptides of suitable size, containing histidine residues, are generally able to coordinate Cu(II) stronger than the corresponding linear oligopeptides. That is true when cyclotetrapeptides with the -His-Xaa-His- motif are involved in the coordination.[151] Cyclopeptides are growing in importance as their action like hormones, antibiotics, enzymes or carrier molecules is lightened. Moreover, the metals complexation of these molecules shows great interest as mimics of the sites of coordination in the macromolecular ligands like proteins. This prompted us some time ago to undertake the study of the speciation of the complexes of Cu(II) ion with several oligopeptides, linear but especially cyclopeptides, containing histidine residues.[114,124,161,162,163,164,165]

The coordination with Cu(II) ion was studied by the best useful spectroscopic methods, in a large range of pH values, detecting the principal donor sets and determining, with the aid of the potentiometric slopes, the structure of the most abundant species. Recently, a new 13 membered cyclotetrapeptide was prepared (Scheme 3.1), containing L- and D-His residues *c*(Lys-DHis-*β*Ala-His) (DK13) (**58**) and Cu(II) was added. Surprisingly, the investigation methods used (optical spectroscopy, NMR, MS and electrochemistry) all strongly suggested that at alkaline pH only a *stable* species of Cu(III) was present, being formed through the action of dioxygen on the original reduced Cu(II).[152]

---

[160] Jones, P.W.; Taylor, D.M.; Williams, D.R. *J. Inorg. Biochem.* **2000**, *81*, 1-10.
[161] Chelli, M.; Ginanneschi, M.; Laschi, F.; Muniz-Miranda, M.; Papini, A.M.; Sbrana, G. *Spectrochim. Acta, Part A,* **1999**, *55A*, 1675-1689.
[162] Sabatino, G.; Chelli, M.; Mazzucco, S.; Ginanneschi, M.; Papini, A.M. *Tetrahedron Lett.* **1999**, *40*, 809-812.
[163] Orfei, M.; Alcaro, M.C.; Marcon, G.; Chelli, M.; Ginanneschi, M.; Kozlowski, H.; Brasun, J.; Messori, L. *J. Inorg. Biochem*. **2003**, *97,* 299-307.
[164] Alcaro, M. C.; Sabatino, G.; Uziel, J.; Chelli, M.; Ginanneschi, M.; Rovero, P.; Papini, A.M. *J. Pept. Science*, **2004**, *10,* 218-228.
[165] Brasun, J.; Gabbiani, C.; Ginanneschi, M.; Messori, L.; Orfei, M.; Swiatek-Kozlowka, J. *J. Inorg. Biochem*. **2004**, *98*, 2016-2021.

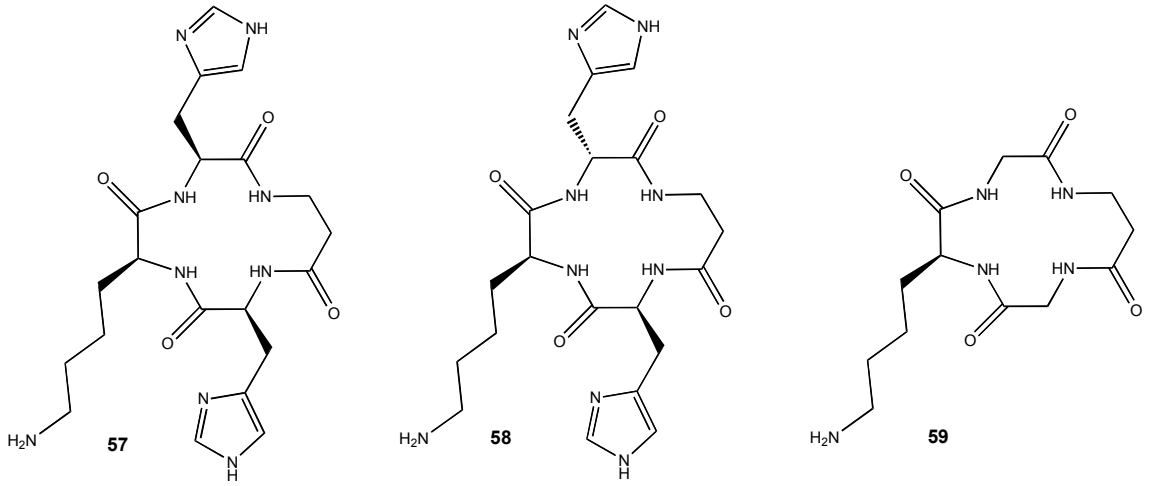

Cyclo(Lys-His-βAla-His) (LK13) Cyclo(Lys-DHis-βAla-His) (DK13) Cyclo(Gly-βAla-Gly-Lys) (GK13)

Scheme 3.1 The three cyclopeptides studied.

3.4.2 Preliminary study on Cu(III)/DK13 complex

The ligand *c*(Lys-DHis-*β*Ala-His) (DK13, **58**) (Scheme 3.1) manifested a very peculiar and unexpected reactivity towards copper(II) ions. Indeed, addition of a stoichiometric amount of copper(II) sulphate to a DK13 solution, adjusted at pH 8 by NaOH, resulted into the progressive development of a very intense and unexpected orange colour. The colour intensity was even higher at pH 12. The process was thus investigated by UV-Vis spectroscopy. Typical spectrophotometric profiles for DK13/copper(II) samples at various pH values are shown in Figure 3.9.

At pH 12.2 two main bands are detected at about 250 and 330 nm (ε ≅ 9840 and ε ≅ 5580, respectively) while a very weak absorption around 500 nm indicates the persistence of a residual amount of the copper(II) species. We quickly realised that the development of the above characteristic spectral pattern is critically dependent on the presence of atmospheric oxygen: as a matter of fact, the bands at 250 and 330 nm did not appear when working under strict anaerobic conditions. We also observed that this process is pH dependent, being stressed by the highest pH values. When recording the spectrum of the same sample after 24 h (r.t., pH = 12.2) the two main absorption maxima looked substantially conserved, with a small decrease in intensity, implying a substantial stability for the obtained species.

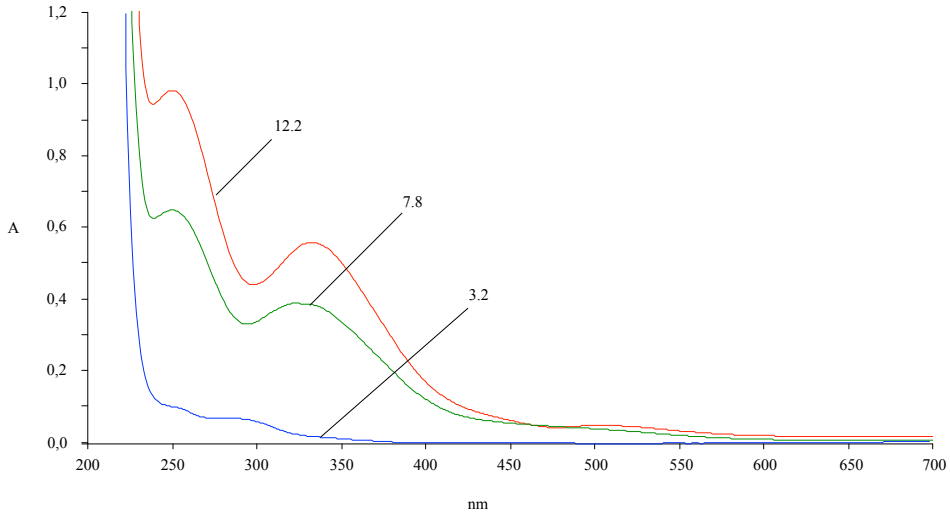

Figure 3.9 UV-vis spectrum of the system DK13/copper(II) at increasing pH values. The UV maxima corresponding to the copper(III) formation are shown (DK13, 0.15 × 10^{-3} M; $CuSO_4$, 0.1 × 10^{-3} M). pH values are specified on the profiles.

On the basis of previous literature we hypothesized that the above spectrophotometric behaviour might be ascribed to the progressive oxidation of copper(II) to copper(III), induced by atmospheric oxygen and favoured by copper coordination to four deprotonated amide nitrogen donors, within a roughly square planar chromophore.[166] Indeed, square planar d^8 copper(III) centers are known to exhibit very intense LMCT bands in the UV region,[167] as it is the case here. ^{1}H-NMR spectra, recorded on the orange solution, showed four relatively narrow signals of the imidazole protons. Also, the entire protons pattern suffered of a very modest line broadening at variance with previously reported cases. This behaviour is indicative of a possible extensive copper(II)-to-copper(III) oxidation. The spectrum of the same sample recorded after 1 h did not reveal any new signals again implying a substantial stability of the existing copper(III) species. The orange solution was further analysed by electrospray (ESI) mass spectrometry (MS). The ESI-MS measurements were carried out in methanolic equimolar (5×10^{-4} M) DK13-copper solutions at different pH values (Figure 3.10). It is noteworthy that, independently from the pH of the solution, only monoprotonated species are detected, while highly charged ions are not formed.

[166] Burke, S.K.; Xu, Y.; and Margerum, D.W. *Inorg. Chem*. **2003**, *42*, 5807-5817 and references therein.
[167] McDonald, M.R.; Fredericks, F.C.; Margerum, D.W. *Inorg. Chem.* **1997**, *36*, 3119-3125.

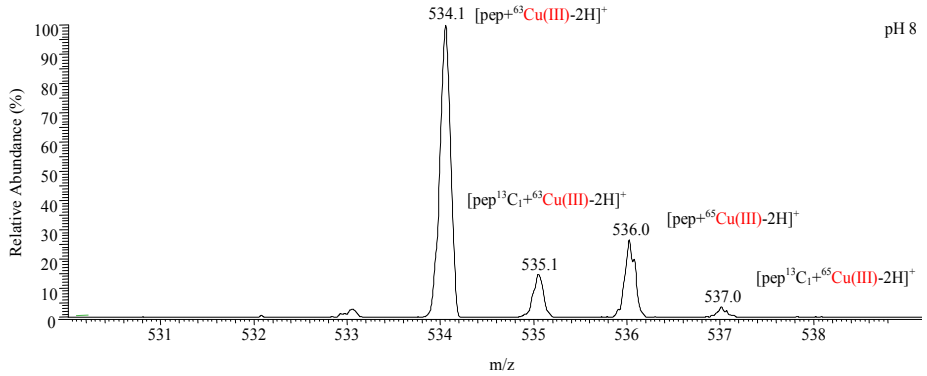

Figure 3.10 ESI-MS spectra of a 1:1 DK13-Cu(II) solution at pH 8.

Under basic conditions, the most abundant ions in the 530-540 *m/z* region are at *m/z* 534 (Figure 3.10). These species differ 1 u from the expected ions at *m/z* 535 due to the $[L\text{-}Cu(II)–H]^+$ species. This shift suggests that the measured positive species has a proton less than expected, thus clearly indicating an almost quantitative oxidation of Cu(II) to Cu(III). Tandem mass spectrometry has been used to obtain information about copper coordination in the complexes. The most abundant decomposition produced by the species $[L\text{-}Cu(III)\text{-}2H]^+$ is due to the elimination of an ammonia molecule (Figure 3.11). Ions at *m/z* 309 are attributable to consecutive eliminations of Ala and His from $[L\text{-}Cu(III)\text{-}NH_3\text{-}2H]^+$. Abundant ions attributable to elimination of one or more aminoacidic residues are not detectable. This suggests strong interactions of the metal with DK13.

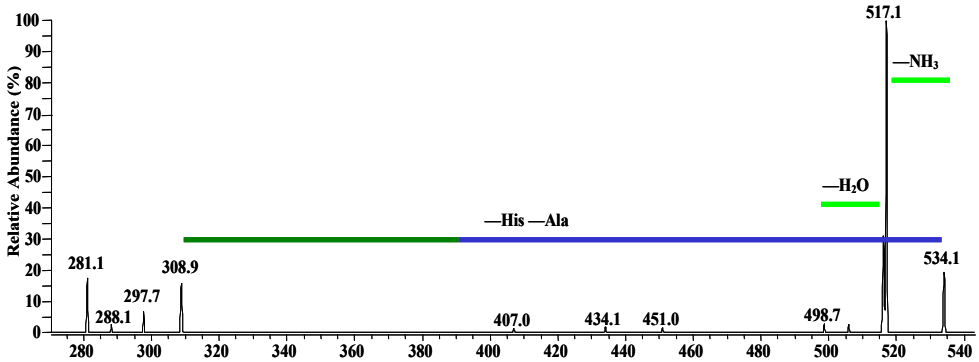

Figure 3.11 ESI-MS/MS spectra of the species $[L\text{-}Cu(III)\text{-}2H]^+$ (*m/z* 534).

The physicochemical results reported so far point out quite unambiguously that the formed orange product is truly a copper(III) species resulting from progressive aerobic oxidation of copper(II) to copper(III). The process is spontaneous under normal aerobic

conditions suggesting that the DK13 ligand strongly stabilizes the oxidation state +3 of copper. Since the oxidation process is highly favoured by strong alkaline conditions, it is well conceivable that the observed stabilisation arises from coordination of four deprotonated amide groups to copper, generating a [Cu(III)($H_{-4}L$)] species.

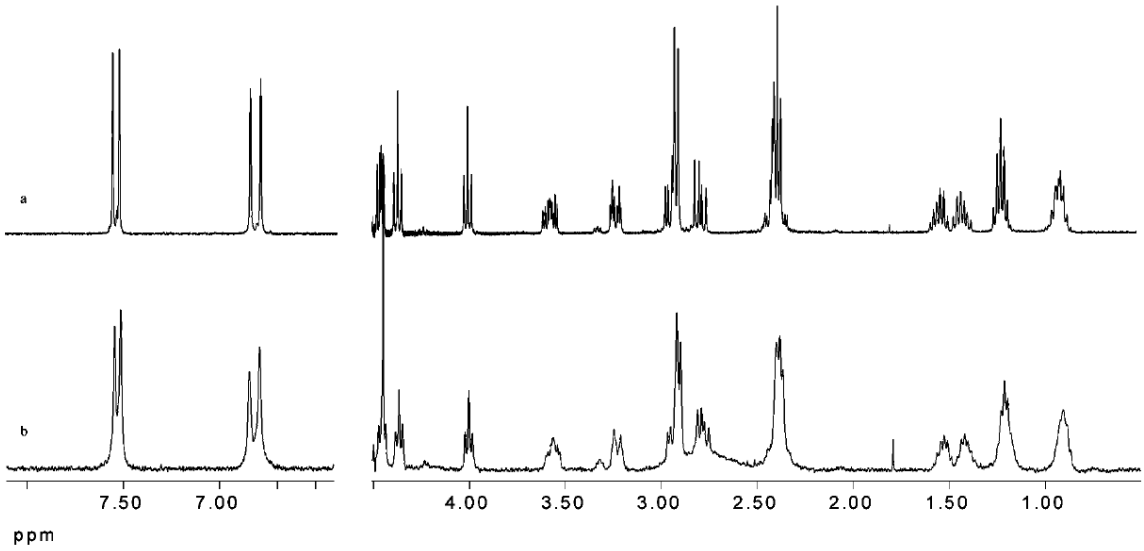

Figure 3.12 ^{1}H-NMR spectrum (D_2O, pH 12.5): (a) DK13 ligand; (b) DK13/$CuSO_4$ 3:1 (DK13, 6.0×10^{-3} M). Spectra were recorded on a Varian 400 MHz Mercury Plus at room temperature.

Notably, ^{1}H-NMR spectra, recorded on the orange solution, showed four narrow signals of the imidazole protons. The entire proton pattern, collected at low ligand-to-copper(II) ratio, did not suffer from significant line broadening at variance with previously reported cases (Figure 3.12). This behaviour is suggestive of nearly quantitative oxidation of paramagnetic copper(II) to diamagnetic copper(III).

The ^{1}H-NMR spectrum of the same sample taken after 1 h did not reveal any significant change, implying a substantial stability of the copper(III) species.

To further define such a stabilisation, electrochemical and spectroelectrochemical measurements were carried out. A freshly prepared mixture of DK13 and $CuSO_4$ in diluted NaOH solution (pH 12) under nitrogen atmosphere affords a substantially colourless solution that does not exhibit any response in cyclic voltammetry. This means that the strong coordination of the Cu(II) ion to the DK13 ligand shifts the Cu(II) reduction beyond the cathodic window of the alkaline solution. In fact, a $CuSO_4$ solution at pH 6.5

undergoes the Cu(II)/Cu(I)/Cu(0) sequence at +0.15 V and at +0.01 V, respectively, and exhibits in the reverse scan the anodic stripping of electrodeposed copper metal at +0.24 V (V, *vs*. NHE). Upon standing at air, the DK13-$CuSO_4$ solution progressively turns orange affording, after 24 hours, the voltammetric profiles shown in Figure 3.13. A poorly resolved reduction process in cyclic voltammetry (asterisked peak-system), but sufficiently well defined in differential pulse voltammetry appears (E°' = +0.04 V, *vs*. NHE) which apparently features partial chemical reversibility. Since no anodic stripping is present in the reverse scan, it seems reasonable to attribute the actual cathodic process to the copper(III)/copper(II) transition.

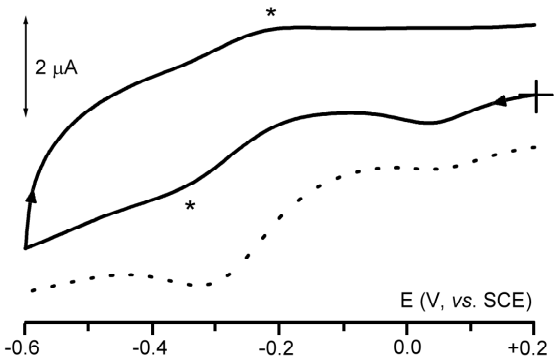

Figure 3.13 Cyclic (—) and differential pulse (•••) voltammograms recorded at a glassy carbon electrode in NaOH solution (pH 12) containing $CuSO_4$ ($0.6x10^{-3}$ M) and DK13 ($0.7x10^{-3}$ M). Scan rates: (—) 0.05 Vs^{-1}; (•••) 0.02 Vs^{-1}.

A similar, poorly resolved, cyclic voltammetric pattern was earlier found for the *c*(β-Ala-Gly-*β*Ala-Gly)/CuIII complex, which was prepared by anodic oxidation of the related copper(II) complex.[168]

For a better definition of the extent of chemical reversibility of the CuIII/CuII reduction in our system, we recorded the spectroelectrochemical trend of DK13/copper(III) at pH 12 upon stepwise reduction (Figure 3.14), followed by stepwise reoxidation. Notably, the two main bands (λmax 245 and 324 nm, respectively) progressively decrease, but upon step-by-step reoxidation (*E*w +0.2 V), the original spectrum is restored. This characteristic behaviour as well as the presence of a well-defined isosbestic point at 220 nm testifies to the chemical reversibility of the CuIII/CuII interconversion.

[168] Rybka, J.S.; Margerum, D.W. *Inorg. Chem*. **1981**, *20*, 1453-1458.

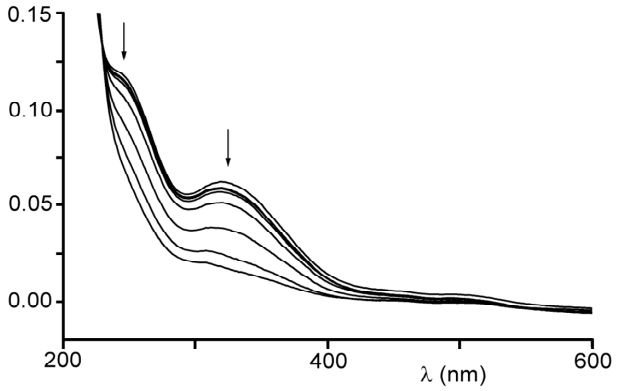

Figure 3.14 UV-Vis spectral trend recorded in a OTTLE cell upon progressive reduction.

This means that the apparent partial chemical reversibility detected in cyclic voltammetry most likely arises from electrode surface phenomena. Previous studies reported that the CuII/Gly_4 solutions are autoxidized by dioxygen uptake at pH 7-10 through the formation of an autocatalytic $[Cu(III)(H_{-3}Gly_4)]^-$ complex.[169] In any case, a copper(III)-coordinated species could only be obtained by chemical or electrochemical oxidation. At variance, the present DK13/copper(II) system is nearly quantitatively oxidized to copper(III) by atmospheric oxygen at room temperature. Because this oxidation process is highly favoured by strong alkaline conditions, it is well conceivable that the stabilization observed arises from copper coordination to four deprotonated amide nitrogen atoms, thus generating a $[Cu(III)(H_{-4}L)]^-$ species. Margerum et al. stated for their peptide ligands that N^- ions from the deprotonated peptide backbone are the strongest σ donors in copper/peptide complexes and can stabilize a copper(III) species. We can assume that copper(III) ions may accommodate the ligand's cavity, thus affording a square-planar complex. Notably, the stabilization effects brought about by our ligand are far higher than those reported by Margerum et al. for the related 14-membered peptide *c*(β-Ala-Gly-*β*Ala-Gly). As a matter of fact, the formal electrode potential of the DK13/copper(III,II) system is lower (by about 0.4 V) than that reported for *c*(β-Ala-Gly-*β*Ala-Gly) at alkaline pH, probably reflecting the thermodynamic stabilization triggered by the higher planarity imposed by the present 13-membered macrocycle. To better understand the role of the His side chains in the overall reaction, we prepared the new ligand *c*(Lys-Gly-*β*Ala-Gly) (GK13, **59**), where the two histidines are replaced by two glycines. Upon the addition of an

[169] Kurtz, J.L.; Burce, G.L.; Margerum, D.W. *Inorg. Chem*. **1978**, *17*, 2454-2460.

equimolar amount of $CuSO_4$ at pH 12, a light-blue precipitate soon formed. Ultraperformance liquid chromatography MS (UPLC-MS) inspection of the remaining aqueous solution did not reveal the presence of the GK13 ligand. Thus, in view of the highly different behavior shown by GK13 in comparison to DK13, we can say that the presence of the histidine ligands is crucial to ensure complete occurrence of the copper(II) to copper(III) oxidation reaction and solubilisation of the resulting copper(III) species.

3.5 Study on Cu(III)/DK13 complex using synchrotron radiation

In order to define the three dimensional structure of this unexpected Cu(III)/Cyclopeptide complex X-Ray Absorption Spectroscopy (XAS) data have been collected at the ID26 beamline of the European Synchrotron Radiation Facility (ESRF) storage ring (Grenoble, F) in collaboration with Dr. Gabriele Giuli from the University of Camerino. Cu K-edge XANES (X-ray Absorption Near Edge Structure) and EXAFS (Extended X-ray Absorption Fine Structure) step scan spectra were acquired in fluorescence mode with ring current ranging from 90 to 60 mA. Radiation was monochromatised by means of a double-crystal Si (311) monochromator to achieve high-energy resolution at the Cu K-edge. Beam size at the sample was 250 × 1000 μm. Cu K-edge XANES and EXAFS spectra were acquired in fluorescence mode monitoring the emitted fluorescence signal with a high-purity multi-element Ge detector. XAS data were collected in quick-scan mode by simultaneously scanning the monochromator angle and the undulator gap with a typical energy step of 0.2 eV and counting about 160 ms per point. In order to reduce radiation induced damage of the peptide samples, spectra have been collected at 10 K in a He cryostat, and the intensity of the incident radiation at the sample has been adjusted by means of Al filters. Preliminary time scans allowed to ascertain that the samples suffered no damage within 1300 seconds exposure to the X-ray beam. For each sample 1000 seconds long spectra have been acquired at different sample positions in order not to alter the sample. Average of 10 to 60 scans, depending on sample Cu concentration, allowed to obtain a good signal to noise ratio for all the samples.

Experimental XANES spectra were corrected by background subtraction with a linear function and then normalised for atomic absorption on the average absorption coefficient of the spectral region from 9030 to 9210 eV. Energy was calibrated against a standard of Cu metal (8979 eV). The threshold energy was taken as the first maximum of the first derivative of the spectra, whereas peak positions were obtained by calculating the second derivative of the spectra. Pre-edge peak analysis was carried out following the same procedure found in Wilke et al.[170] The pre-edge peak was fitted by a sum of pseudo-Voigt function, and the integrated intensities along with centroid energies were compared with those of the standards analysed here and others from the literature in order to extract information on Cu oxidation state and coordination number in the samples studied.

EXAFS data reduction and analysis was done by means of the GNXAS package (Filipponi & Di Cicco, 2000).[171] This program extracts χ(k) signal from the raw spectrum without performing Fourier filtering and thus avoiding possible biases deriving from incorrect background subtraction. The theoretical amplitudes and phase shifts are calculated *ab initio* according to the Muffin-Tin approximation. The Hedin-Lundquist complex potential[172] was used for the exchange-correlation potential of the excited state. The amplitude reduction factor (S_0^2) has been fixed to 0.85.

3.5.1 Theoretical XANES calculations

XAS calculations are carried out starting from the Fermi's golden rule to obtain the photoabsorption cross section within the dipole approximation. One important step is to calculate the final state of the photoelectron transition moment, which describes the physical process of scattering the electron photoemitted by the central atom by outer atoms. This is done in the framework of MS theory[173] using a MT approximation for the shape of the potential of the cluster of atoms included. The cluster size and the l_{max} value (i.e. the maximum l value of the spherical harmonic expansion of the scattering path operators) were chosen on the basis of a convergence criterion; MT radii were chosen on

[170] Wilke, M.; Farges, F.; Petit, P.E.; Brown, G.E.; Martin, F. *American Mineralogist* **2001**, *86*, 714-730.
[171] Filipponi, A.; Di Cicco, A. "GNXAS: a software package for advanced EXAFS multiple-scattering calculations and data-analysis", *TASK Quarterly* **2000**, *4*, 575-669.
[172] Hedin, L.; Lundquist, B.I. *J. Phys. C* **1971**, *4*, 2064-2083.
[173] Natoli, C.R.; Benfatto, M.; Della Longa, S.; Hatada, K. *J. Synchrotron Radiat.* **2003**, *10*, 26-42.

the basis of the Norman criterion,[174] including an overlap between MT spheres that is optimized by fitting the *ovlp* parameter (only one parameters for the entire set of MT radii). The choice of MT radii fixes the constant MT potential V_0 and the charge densities within each MT sphere. Different values of *ovlp*, within reasonable values (between 1% and 10%), change the goodness of the fit but without relevant effects in the structural parameters determination.

V_{0imp} is the value of the Muffin-Tin potential (V_0) when it is refined to best fit the XANES spectra of copper compounds. The potential generator of MXAN (program VGEN) calculates this parameter automatically, however refining V_{0imp} provides an improvement both in c2 and thus in the accuracy of structural results. The value of (10 ± 2) eV was found to be optimal for the system under study.

The real part of the exchange term was calculated using the Hedin-Lundqvist energy-dependent potential,[172] while all of the inelastic losses were taken into account by a phenomenological method previously described in detail.[175] According to this method, inelastic processes are taken into account by a convolution with a broadening function, with a width Γ given by $\Gamma = \Gamma_c + \Gamma(E)$. The constant part Γ_c includes contributions from the core-hole lifetime (1.5 eV, lorentzian convolution) and the experimental resolution (0.6-0.8 eV, gaussian convolution), while the energy dependent term Γ(E) (lorentzian convolution) represents the inelastic processes. Γ(E) is zero below an onset energy E_s, and begins to increase from a value A_s following the universal functional form related to the mean free path in a solid.[176] This method introduces three nonstructural parameters that are derived during the fit on the basis of a Monte Carlo search at each step of computation.

A constant experimental error of 0.012 normalized units (i.e. units for which the absorption jump is equal to 1) was chosen. Starting model structure used for the calculations has been built according to DFT calculations. Preliminary calculations of theoretical spectra have been performed using Hedin-Lundquist real potential, calculating Muffin-Tin radii according to the Norman criterion, and allowing 10% sphere overlap. The minimization of the c^2 function was performed in the space of structural parameters**,** i.e. the first (4 nitrogens) and second (8 carbons) coordination shell.

[174] Norman, J.G. *Mol. Phys.* **1974**, *81*, 1191-1198.
[175] Benfatto, M.; Della Longa, S.; Natoli, C.R. *J. Synchrotron Radiat.* **2003**, *10*, 51-57.
[176] Müller, J.E.; Jepsen, O.; Wilkins, J.W. *Solid State Commun*. **1984**, *42*, 4331-4343.

3.5.2 XANES Pre-edge analysis

In Figure 3.15 are shown the XANES spectra of representative Cu model compounds with known oxidation state and the peptides under study. As the metal K-edge structures vary according to number, type and geometric arrangements of ligands, as well as the metal oxidation state, comparison of the peptide spectra with those of model compounds can allow to get information on the oxidation state and structural surrounding of the studied metal (i.e. Cu). It is apparent a general shift to higher energy of the absorption threshold of the model compound spectra with increasing Cu oxidation state from Cu(I) to Cu(III). Also a peak labeled A in the edge region shifts to higher energy with increasing Cu oxidation state. Moreover, a peak in the pre-edge region (peak P) is absent in the Cu(I) model compounds whereas is present in Cu(II) and Cu(III) compounds. This peak, often referred as pre-edge peak, is related to a 1s to 3d electronic transition in the photoabsorbing atom (in this case Cu) and is a direct probe of the unfilled d orbital population.

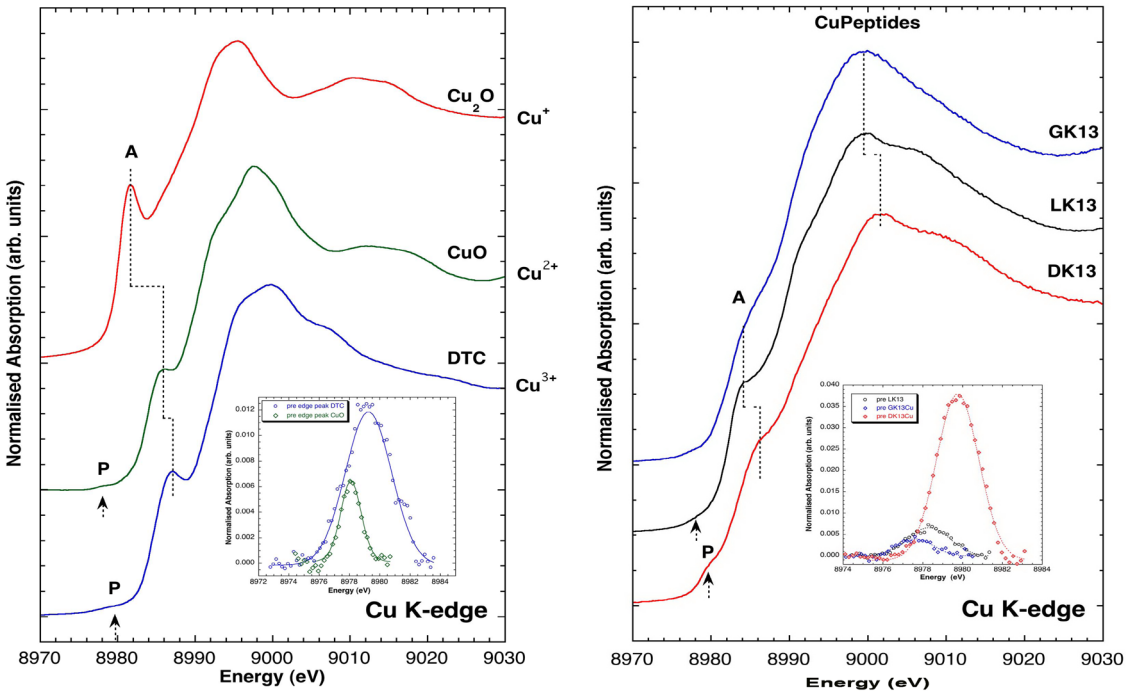

Figure 3.15 XANES spectra of Cu model compounds with known oxidation state (left panel) and the peptides under study (right panel).

The observed variations of edge positions and pre-edge peak position and intensities have been already observed in a number of systems of both organic and inorganic nature.[177,178,179,180] However, the quantitative interpretation of XANES spectra is sometimes rendered difficult because of the high complexity of multiple scattering paths invilved and because of the huge number of parameters affecting the shape of the XANES region. In this respect, the pre-edge peak can be a useful indication of the metal oxidation state.[181]

The background subtracted pre-edge peak is shown in the inset of Figure 3.15 for both the model compounds (left panel) and peptides (right panel). The energy position of this peak can be a precise indication of the Cu oxidation state: while it is absent in Cu(I) compounds, it is present at ca. 8978 eV for most Cu(II) model compounds. Its shift to higher energy and increase in integrated intensity in the case of Cu(III) compounds. The Cu(III) model compound shown here ($Na_5[Cu\{TeO_4(OH)_2\}_2]\cdot 16H_2O$ - ditelluratocuprate DTC - Figure 3.16) display a pre-edge peak centroid at 8979.3 ± 0.3 eV with an integrated intensity of 0.044.

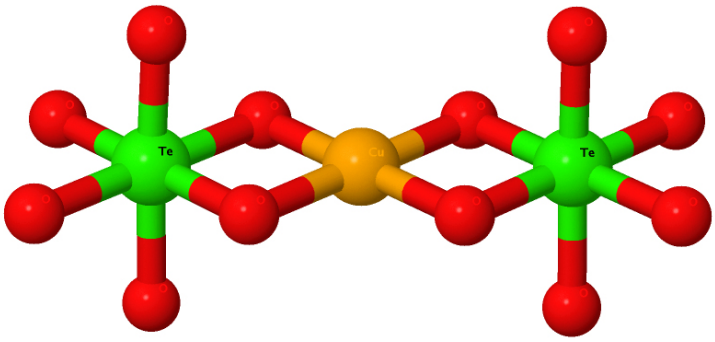

Figure 3.16 Ditelluratocuprate(III)

[177] Kau L.S.; Spira-Solomon D.J.; Penner-Hahn J.E.; Hodgson K.O.; Solomon E.I. *J. Am. Chem. Soc.* **1987**, *109*, 6433-6442.
[178] DuBois, J.L.; Mukherjee, P.; Stack, T.D.P.; Hedman, B.E.; Solomon, I.; Hodgson, K.O. *J. Am. Chem. Soc.* **2000**, *122*, 5775-5787.
[179] Farges, F.; Siewert, R.; Ponader, C.W.; Brown, G.E.; Pichavant, M.; Behrens, H. *Can. Mineral.* **2006**, *44*, 755-773.
[180] Chillemi, G.; Barone, V.; D'Angelo, P.; Mancini, G.; Persson, I.; Sanna, N. *J. Phys. Chem. B* **2005**, *109*, 9186-9193.
[181] Brown, G.E.; Farges, F.; Calas, G. *Rev. Mineral. Geochem*. **1995**, *32*, 317-410.

Comparison of peptide pre-edge peak data with those of model compounds can probe Cu oxidation state in the studied peptide samples. Accurate analysis of pre-edge peak data of the peptide samples allowed to ascertain the presence of Cu(III) in the DK13 sample and Cu(II) in the GK13. In particular, while the pre-edge peak of the GK13 sample is perfectly compatible with those of divalent Cu model compounds analysed here and reported in the literature, the pre-edge peak of DK13 spectrum display an energy (8979.8 eV) compatible to that of the DTC shown here (and with other data from the literature[178]) but has an higher integrated intensity (0.095) than the DTC, possibly due to a less centrosymmetric geometrical environment around Cu than in the DTC. The pre-edge peak of LK13 sample is compatible with the presence of Cu(II) with minor contribution from Cu(II).

3.5.3 EXAFS analysis

In Figure 3.17a are shown the experimental (open symbols), theoretical (solid lines) and residual EXAFS signals of the Cu(III) (DK13) and Cu(II) (GK13) peptide samples. The theoretical signals have been calculated starting from a simplified model structure reproducing the 13-element ring and neglecting the imidazole side chains contributions. The signals have a low intensity and are almost completely dumped in the high-energy region. The Fourier transforms of the EXAFS signals confirm that there are no important contributions from distances farther than 4 Å.

The theoretical contributions to the EXAFS signals from each shell of the model structure are shown in Figure 3.17b for two peptides: the most important contributions comes from the 4 N atoms bonded to Cu and from the 6 nearest C atoms. The EXAFS derived Cu-N distances are sensibly shorter in the DK13 sample relative to GK13 (1.78 ± 0.02 Å and 1.91 ± 0.02 Å respectively). The shorter distance (1.78 Å for DK13) is consistent with other Cu(III)-N distances found in the literature[178] and is thus a further confirmation of the presence of trivalent copper in this peptide. On the other hand, the Cu-N distance found for GK13 (1.91 Å) compares well with known values for divalent copper.[178]

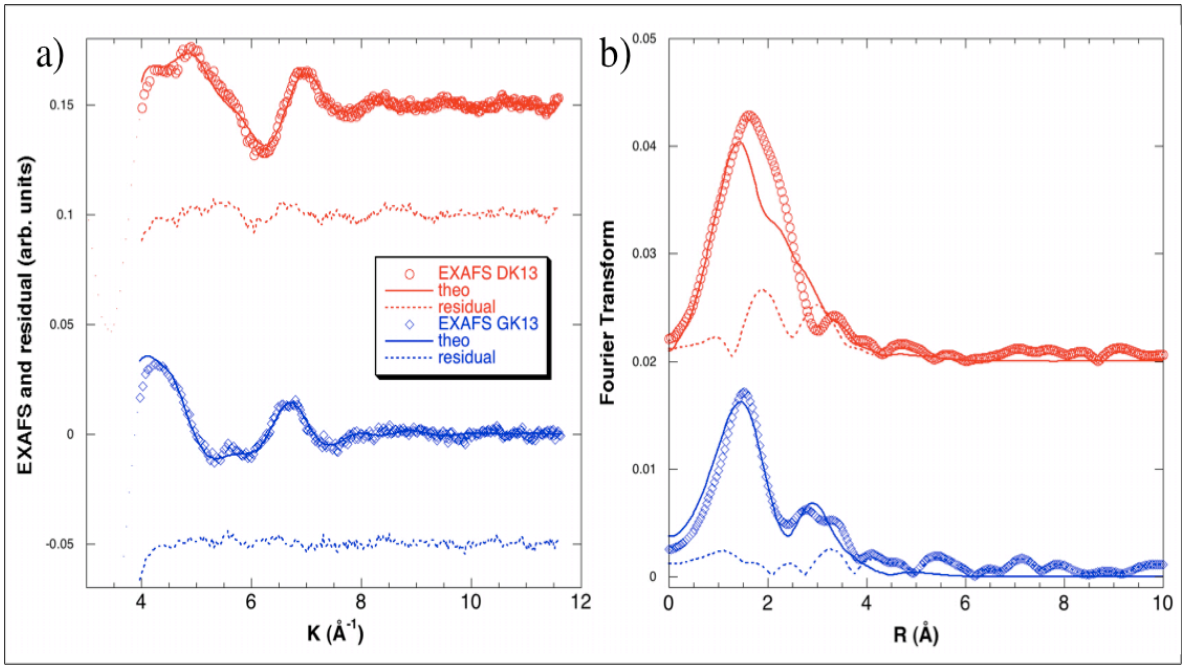

Figure 3.17 Cu K-edge EXAFS signals (a) and Fourier Transforms (b) of Cu(III) and Cu(II) peptide samples.

3.5.4 XANES analysis

Theoretical XANES spectra of DK13 and GK13 are shown in Figure 3.18. Their changes going from GK13 to DK13 are satisfactorily reproduced in the one-electron, multiple scattering scheme adopted by the MXAN program. In particular the observed blue-shift of the spectrum going from the cuprous to cuprate compound correspond to a decrease of the average first shell distance. In this figure the experimental spectra have been shifted by ca. 8985 eV to lower energy in order to match the theoretical spectra. The fits include the first and second shell average distances. The results of the MXAN fits are in quite agreement with the EXAFS analysis. The Cu-N average distance is (1.80 ± 0.04) Å for DK13 and (1.91 ± 0.02) Å for GK13, and the average second shell Cu-C distance is (2.84 ± 0.08) Å and (2.94 ± 0.02) Å, respectively.

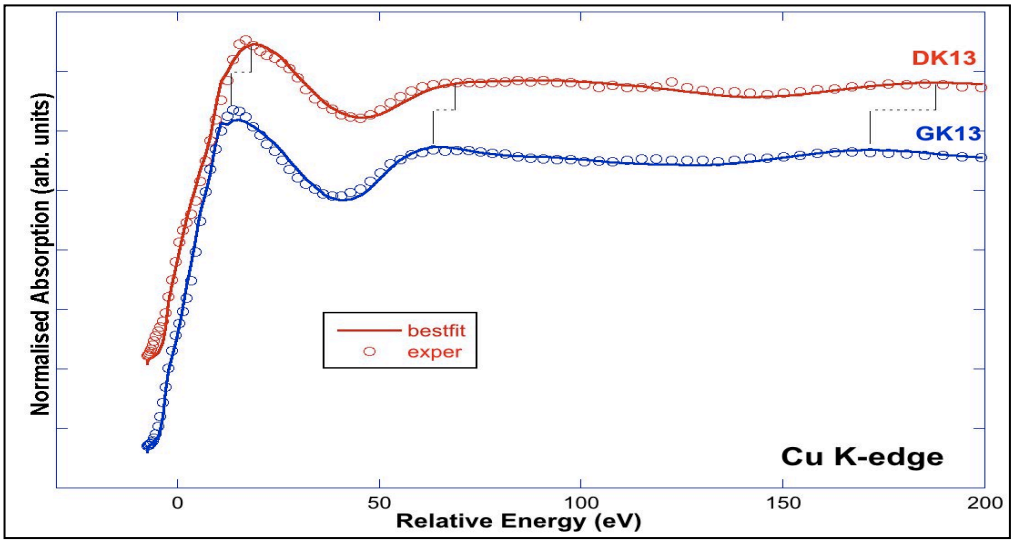

Figure 3.18 Experimental XANES curves for DK13 (in red) and GK13 (in blue), compared with those obtained after the structural refinements (solid lines).

3.5.5 Conclusions

Comparison of XANES pre-edge peak features with those of Cu model compounds allowed to determine the Cu oxidation state in the three peptides: Cu is purely divalent in GK13 purely trivalent in DK13 and present as both Cu(II) and Cu(III) in LK13. Also edge energies and the <Cu-N> distances derived independently by GNXAS (1.79 Å and 1.90 Å in the EXAFS range) and MXAN (1.80 Å and 1.91 Å in the XANES range) for DK13 and GK13 respectively, are consistent with the XANES determined Cu oxidation states.

Preliminary theoretical XANES spectra (data not shown) calculated using the MXAN code in a different way (i.e. by fixing the optimized distances and releasing angular parameters) suggest that the CuN_4 unit is not perfectly planar but form a distorted pyramid. The Cu(III) is bonded to the four peptide nitrogens, giving rise a *quasi*-planar square structure. In fact the deviation from the planar coordination is very small (the angle N-Cu-N of two opposite nitrogens is about 170°) and the pyramidal structure is near to be flat.

The lack of a similar structure of Cu(III) in the other compounds studied, although having the same size of the peptide cycle, may be explained by the lack of the imidazole side chains, that are no present in compound **59** (Figure 3.19) and are of the same chirality in compound **57**. The mechanism by which the histidine residues act in forming the

suitable cradle for Cu(III) forming by dioxygen is not clarified at this stage. A pH dependent study in aqueous solution will be necessary for revealing the chaperon mechanism of the D- and L-histidine in compound **58** (Figure 3.20).

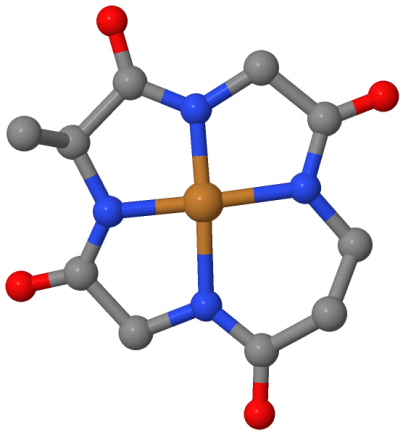

Figure 3.19 Proposed planar three-dimensional structure for Cu(II)/GK13; the angle N-Cu-N with the two opposite nitrogens is about 180°.

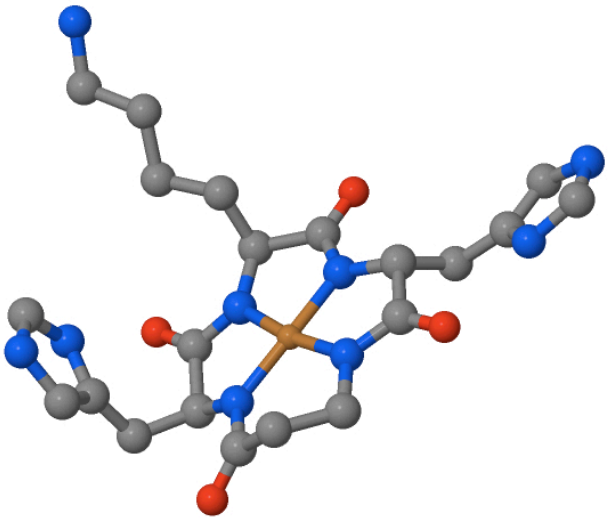

Figure 3.20 Proposed three-dimensional structure for Cu(III)/DK13; the angle N-Cu-N with the two opposite nitrogens is about 170°.

Chapter 4

TrxR AS A TARGET FOR ANTICANCER DRUGS

4.1 Introduction

4.1.1 Gold compounds, new attractive metallodrugs for cancer treatment

The serendipitous discovery of the anticancer properties of cisplatin and its platinum(II) analogues and their wide clinical success in current cancer treatments promoted a great deal of interest in the area of metal-based antitumor agents.[182,183] The outstanding anticancer effects observed for platinum(II) compounds suggested that other metal-based compounds might be similarly useful as antitumor drugs while, hopefully, displaying different patterns of anticancer activities and selectivities. Among the several classes of metal compounds that have been taken into consideration as potential anticancer agents starting from the 80's (e.g. ruthenium, palladium, titanium, copper, tin, and so on), a few investigations have focused on a variety of gold compounds in the oxidation states either +3 or +1.[184,185] Notably, gold(I) compounds were quickly considered as possible antiproliferative agents soon after the discovery of cisplatin, as some of them were already in the clinics for the treatment of rheumatoid arthritis; in turn, gold(III) compounds looked pairwise very attractive for cancer treatment as the gold(III) centers are known to originate square planar complexes that are isoelectronic and isostructural to those of platinum(II) and might exhibit similar biological actions.

A conspicuous number of gold(I) and gold(III) compounds were thus assayed, during the 80's, either in vitro or in vivo, as antitumor agents but the results obtained at that time were rather disappointing.[184,185] Indeed, gold(I) compounds turned out to be fairly active *in*

[182] Bruijnincx, P.C.; Sadler, P.J. *Curr. Opin. Chem. Biol.* **2008**, *12,* 197.
[183] Zhang, C.X.; Lippard, S.J. *Curr. Opin. Chem. Biol.* **2003**, *7,* 481.
[184] Messori, L.; Marcon, G. in: Sigel, A.; Sigel H. (Eds.), Metal Ions in Biological Systems, vol. 42, Marcel Dekker Inc., New York, **2004**.
[185] Gabbiani, C.; Casini, A.; Messori, L. *Gold Bull.* **2007**, *40,* 73.

vitro but practically ineffective *in vivo*, most likely as a consequence of extensive binding to serum proteins and inactivation; conversely, gold(III) compounds, although highly cytotoxic *in vitro*, manifested, on the average, a poor chemical stability and, also, a rather pronounced systemic toxicity in animal models that heavily limited their further investigation or application. Studies on gold compounds as experimental anticancer agents were therefore rapidly stopped and almost completely abandoned for many years.

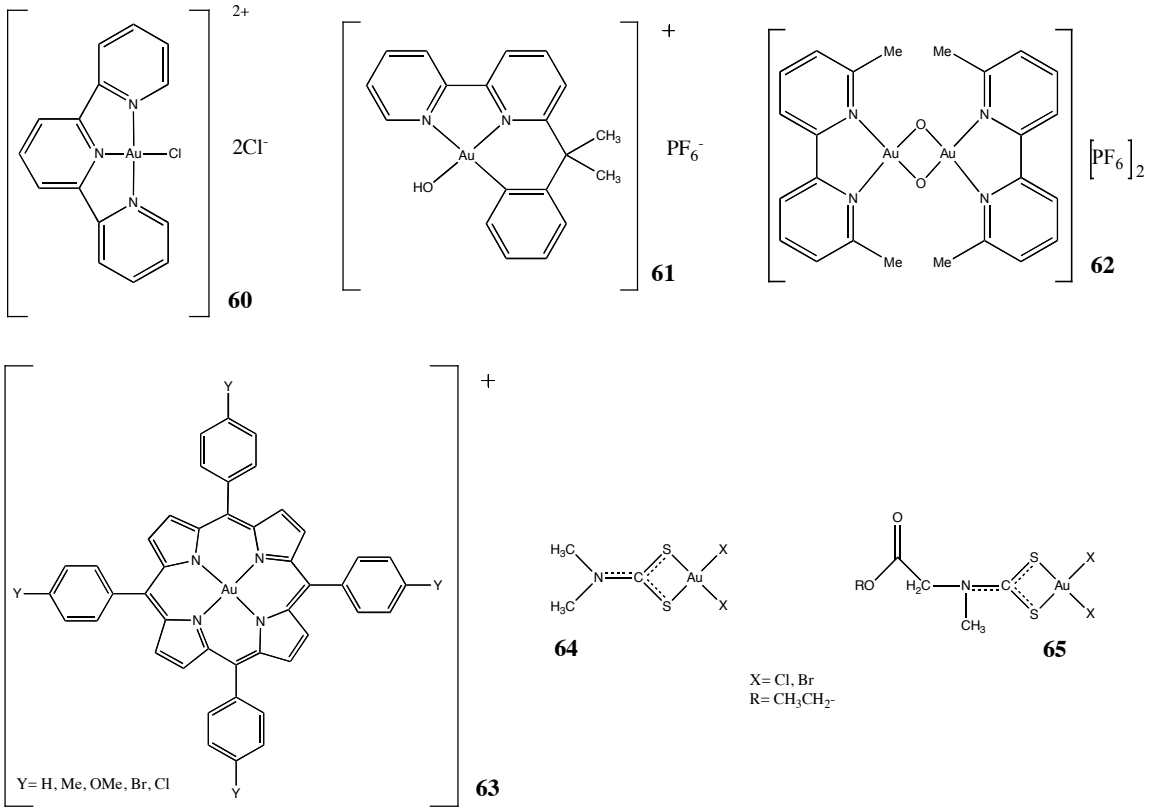

Scheme 4.1 Schematic drawing of $[Au(terpy)Cl]Cl_2$ (**60**), $[Au(bipy^c\text{-}H)(OH)][PF_6]$ (**61**), meso-tetraarylporphyrins complexes (**62**), $Au(py^{dmb}\text{-}H)(AcO)_2]$ (**63**) (where py^{dmb} = 2-(1,1-dimethylbenzyl)-pyridine)) and of the gold(III) dithiocarbamate complexes containing N,N-dimethyldithiocarbamate (**64**) and ethylsarcosinedithiocarbamate (**65**) ligands.

Only around the mid 1990s, new classes of gold(III) compounds were synthesized and characterised that showed improved stability profiles and turned out to be more appropriate for pharmacological application; most of those novel compounds were assayed

on simple *in vitro* or *in vivo* biological models of cancer, with quite promising results.[186] The new gold compounds studied, depicted in Scheme 4.1, comprise classical gold(III) compounds with polydentate ligands (e.g. AuTerpy) (**60**),[187] a few organogold(III) compounds (e.g. DAMP and Aubipyc) (**61**),[188] various gold(III) porphyrins (**63**), two major gold(III) dithiocarbamates (**64**, **65**),[189] a series of dinuclear gold(III) compounds (e.g. AuOXO6) (**62**).[190] Pairwise, various gold(I) compounds, with innovative chemical and biological features, were prepared and characterised, in the same years, by Berners-Price and coworkers.[191]

On the average, all these novel gold compounds turned out to be highly cytotoxic *in vitro* against representative human tumor cell lines, with IC_{50} values often falling in the low micromolar or even nanomolar range. For a few of them an appreciable activity *in vivo* was also established although the reported *in vivo* data were rather fragmentary and preliminary. Mechanistic studies showed that the majority of these novel cytotoxic gold compounds induce evident signs of apoptosis in treated human tumor cells but their actual modes of action were not univocally identified. However, as gold compounds manifested, on the whole, a far lower affinity for DNA than platinum(II) compounds, it was hypothesized that apoptotic cell death should be the result of DNA-independent processes. Accordingly, the new cytotoxic gold compounds were often found to overcome resistance to cisplatin confirming the occurrence of a substantially different mode of action. Pairwise, at variance with classical platinum(II) compounds, only very modest effects on the cell cycle were highlighted. These observations led researchers to postulate the existence of preferential protein targets for gold compounds.

Interestingly, all the mechanistic studies and hypotheses formulated about the action of this metal compounds, suggest that mitochondria represent the most likely site for the

[186] Bindoli, A.; Rigobello, M.P.; Scutari, G.; Gabbiani, C.; Casini, A.; Messori, L. *Coord. Chem. Rev.* **2009**, *253*, 1692–1707.

[187] Messori, L.; Abbate, F.; Marcon, G.; Orioli, P.; Fontani, M.; Mini, E.; Mazzei, T.; Carotti, S.; O'Connell, T.; Zanello, P. *J. Med. Chem.* **2000**, *43,* 3541.

[188] Marcon, G.; Carotti, S.; Coronnello, M.; Messori, L.; Mini, E.; Orioli, P.; Mazzei, T.; Cinellu, M.A.; Minghetti, G. *J. Med. Chem.* **2002**, *45,* 1672.

[189] Ronconi, L.; Marzano, C.; Zanello, P.; Corsini, M.; Miolo, G.; Maccà, C.; Trevisan, A.; Fregona, D. *J. Med. Chem.* **2006**, *49,* 1648.

[190] Gabbiani, C.; Casini, A.; Messori, L.; Guerri, A.; Cinellu, M.A.; Minghetti, G.; Corsini M.; Rosani, C.; Zanello, P. *Inorg. Chem.* **2008**, *47,* 2368.

[191] Humphreys, A.S.; Filipovska, A.; Berners-Price, S.J.; Koutsantonis, G.A.; Skelton, B.W.; White, A.H. *Dalton Trans.* **2007**, *21,* 4943.

biological action of gold compounds; in other words, gold-based cytotoxic drugs should be primarily considered as selective antimitochondrial drugs. There is indeed much recent evidence suggesting that mitochondria play a critical role in the regulation of apoptosis (programmed cell death), making them an attractive target for the design of new anticancer drugs. This issue is of particular interest as mitochondria are critically involved in the regulation of the intracellular redox state. In addition, mitochondria contain a specific thioredoxin reductase, a selenzoenzyme that seems to be an optimal target for gold compounds. Strong inhibition of mitochondrial thioredoxin reductase (TrxR) would eventually lead to altered mitochondrial functions and to initiation of the apoptotic process.

4.1.2 Inhibitors of thioredoxin reductases

A few observations revealed that cancer cells often overexpress both thioredoxin and thioredoxin reductase[192] implying that the thioredoxin system may have a crucial role in tumor onset and progression. Accordingly, both thioredoxin and thioredoxin reductase might be considered as suitable targets for the development of new anticancer agents (Figure 4.1).[193] The view that thioredoxin reductase constitutes an effective druggable cancer target has received significant experimental support and validation. Indeed, Yoo *et al.*,[194] by transfecting lung cancer cells with siRNA specifically directed against TrxR1, found that these cells largely reverse their tumor morphology and growth properties returning similar to normal cells. Moreover, some established antitumor agents used in clinic several years ago were retrospectively found to act as potent inhibitors of thioredoxin reductase as it will be shown in this section.

It follows that targeting thioredoxin reductase may be an appropriate strategy in modern cancer drug research. Interestingly, TrxR contains a very accessible selenocysteine on its flexible C-terminal arm; thus the several electrophilic compounds that are capable of modifying – selectively and irreversibly – this active site residue might be well considered as potential enzyme inhibitors and candidate anticancer agents.

[192] Nakamura, H.; Masutani, Y.; Tagaya, A.; Yamauchi, T.; Inamoto, Y.; Nanbu, S.; Fuji, K.; Ozawa, J. *Cancer* **1992**, *69,* 2091.
[193] Urig, S.; Becker, K. *Semin. Cancer Biol.* **2006**, *16,* 452.
[194] Yoo, M.-H.; Xu, X.-M.; Carlson, B.A.; Gladyshev, V.N.; Hatfield, D.L. *J. Biol. Chem.* **2006**, *281,* 13005.

It is now well established that thioredoxin reductases can be easily and efficiently inhibited by a large array of compounds ranging from natural products to synthetic organic compounds (dinitrohalobenzenes, quinines, etc.), from simple metal ions (Ca, Zn, Mn, Cd, Tl) to structurally elaborated metal coordination compounds (Au, Pt, Ru, Gd). Several inhibitors of thioredoxin reductase, either of natural origin or synthetic, have been developed during the last decade and are of potential interest as anticancer agents.

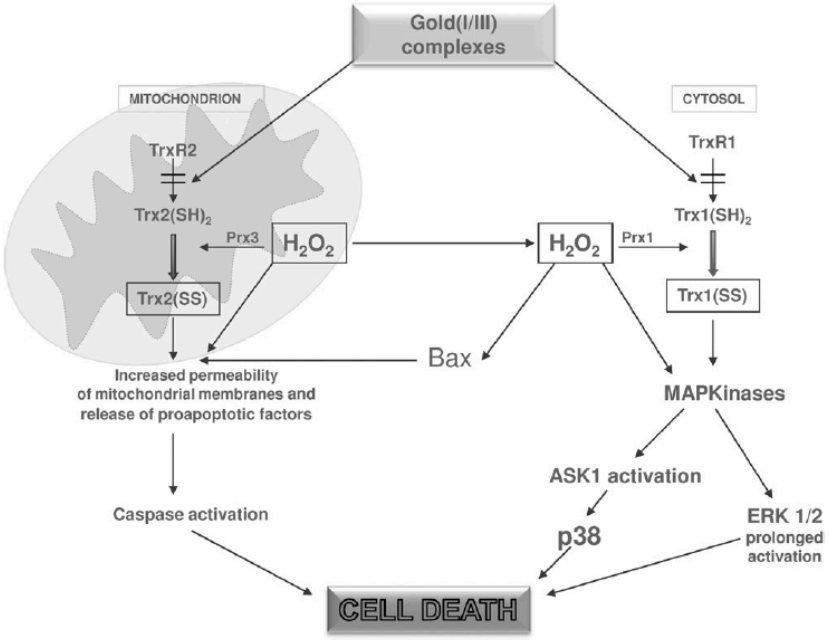

Figure 4.1 Mechanism of action of cell death induction by gold(I/III) compounds.

The role of TrxR inhibitors with reference to cancer therapy was recently reviewed by Urig and Becker;[193] a list of representative thioredoxin reductase inhibitors with their respective IC_{50} values is reported in Table 4.1.

It is apparent that most of the above compounds will directly target the active site selenolate as this chemical group is characterised by an appreciably high reactivity. In the case of a few organic compounds, e.g. carmustine and curcumin, that are known to be efficient alkylating agents, inactivation of the selenolate group via alkylation has been proposed and documented. However, for other bulkier organic TrxR inhibitors such as quinoids, anthracyclines and naphthoquinones, a direct interaction at the FAD binding site is also conceivable.

Table 4.1 TrxR inhibitors (MGD, Motexafin gadolinium).

Substance class	TrxR inhibition potency; in vitro data
Nitrosoureas	IC_{50} ~ 50 μM for BCNU
Platinum(II) complexes	IC_{50} ~ 15 μM for cisplatin
Phosphole complexes	IC_{50} ~ 2 nM for Pt-phosphole
Organocalchogenides	IC_{50} ~ 0.26 μM for diorganyl telluride
Polyphenol flavonoids	IC_{50} ~ 3.6 μM for curcumin
Texaphyrins (MGD)	IC_{50} ~ 6 μM for MGD
Quinoid compounds	IC_{50} ~ 6.3 μM for 9,10-phenantrene quinone
Naphtoquinones spirochetal derivatives	IC_{50} ~ 0.35 μM for palmarumycin

Inorganic compounds will preferentially target the active site selenolate function. Thus, arsenic and organochalcogenides are believed to form direct As-Se and Te-Se bonds.[195] Finally, as mentioned above, metal complexes of platinum and ruthenium were shown to be good inhibitors of thioredoxin reductase. Cisplatin (cis-diamminedichloroplatinum(II)) was able to irreversibly inhibit thioredoxin reductase activity suggesting a covalent interaction with the thiol/selenol active site.[196] A similar effect on TrxR was also observed with other platinum complexes such as terpyridine platinum(II).[197] After the successful utilization of platinum complexes in cancer chemotherapy other metal complexes were considered and, in particular, ruthenium complexes were shown to present antitumor activity mainly against metastatic cancer.[198] Interestingly, several ruthenium(III) complexes were shown to markedly inhibit, although at different levels, the cytosolic isoform of thioredoxin reductase, while they are scarcely effective towards the mitochondrial isoform.[199] This effect is similar to that of calcium ions that potently inhibit TrxR1, but are weak inhibitors of the mitochondrial isoform, indicating that the redox signalling stimulated by these complexes occurs primarily in the cytosolic compartment. The numerous studies appeared so far concerning the interactions

[195] Engman, L.; Al-Maharik, N.; McNaughton, M.; Birmingham, A.; Powis, G. *Bioorg. Med. Chem.* **2003**, *11,* 5091.
[196] Arnér, E.S.J.; Nakamura, H.; Sasada, T.; Yodoi, J.; Holmgren, A.; Spyrou, G. *Free Radic. Biol. Med.* **2001**, *31*, 1170.
[197] Becker, K.; Herold-Mende, C.; Park, J.J.; Lowe, G.; Schirmer, R.H. *J. Med. Chem.* **2001**, *44,* 2784.
[198] Clarke, M.J. *Coord. Chem. Rev.* **2003**, *236,* 209.
[199] Rigobello, M.P.; Vianello, F.; Folda, A.; Roman, C.; Scutari, G.; Bindoli, A. *Biochem. Biophys. Res. Commun.* **2006**, *343,* 873.

of gold compounds with thioredoxin reductase will be considered in detail in the next paragraph.

4.2 Gold compounds as TrxR inhibitors: previous results

Since the very first studies on the protein chemistry of thioredoxin reductases and the discovery of an essential selenocysteine residue in its active site, it was soon apparent that gold compounds (in particular gold(I) compounds) might behave as potent enzyme inhibitors. This hypothesis was initially grounded on the simple chemical consideration that gold compounds, especially those in the oxidation state +1, are "soft Lewis acids" and "thiol reactive species" with the ability to target, potently and selectively, thiol and selenol groups of proteins.

Although the effects of numerous gold compounds on thioredoxin reductase activity were widely investigated during the last decade and potent enzyme inhibition highlighted in several cases, the actual mechanisms of interaction of gold compounds with this enzyme have been poorly explored at the molecular level. It was just assumed that the "soft", catalytically relevant, selenolate group should constitute the common anchoring site for gold-based inhibitors; this assumption was grounded on the concept that "soft" gold ions, especially in the oxidation state +1, are able to form strong bonds with "soft" Lewis donors. Notably, important although indirect, support to this hypothesis was recently provided by Deponte *et al*.[200] who reported that gold phospholes inhibit native thioredoxin reductase orders of magnitude stronger than a mutant where the C-terminal selenol group is replaced by a cysteine.

This substantial lack of molecular information prompted us to analyse in more detail the interactions taking place between gold compounds and thioredoxin reductase with the aid of a few specific biophysical and biochemical tools. In particular, we have exploited advanced mass spectrometry methods to explore the reactions of representative gold compounds with thioredoxin reductase. Some remarkable results emerging from our studies will be briefly described below.

[200] Deponte, M.; Urig, S.; Arscott, L.D.; Fritz-Wolf, K.; Réau, R.; Herold-Mende, C.; Koncarevic, S.; Meyer, M.; Davioud-Charvet, E.; Ballou, D.P.; Williams Jr., C.H.; Becker, K. *J. Biol. Chem.* **2005**, *280,* 20628.

Today's mass spectrometry methods may allow a direct monitoring of the TrxR enzyme in spite of its relatively large size (~110 kDa for the homodimeric protein). A series of MALDI (Matrix-Assisted Laser Desorption Ionization) TOF (Time-of-Flight) spectra were thus recorded on TrxR1 samples, pre-reduced with NADPH, either alone or incubated with a stoichiometric excess of various gold complexes, for 1 h at 37 °C; a similar approach had been previously adopted by Deponte *et al.*, when studying the reaction of gold phospholes with human glutathione reductase.[200] Representative MALDI spectra for TrxR1 and for its auranofin adduct are shown in Figure 4.2. Interestingly, treatment of TrxR1 with gold compounds results into significant mass increases, whose extent clearly depends on the applied gold-to-protein molar ratios. For example, in the case of the auranofin-treated sample, the main peak is located at ~56,600 Da, while the peak of untreated TrxR1 falls at ~55,500Da, suggesting protein binding of ~4 $AuPEt_3^+$ fragments. These observations provide direct evidence for extensive protein metallation and point out that a certain number of sites, beyond Sec, are available for gold binding on the protein surface, most likely Cys, Met and His residues. A similar situation, i.e. the presence of multiple gold binding sites on the protein surface, was recently hypothesized for the reaction of human serum albumin with antiarthritic gold(I) compounds and cytotoxic gold(III) compounds.[201]

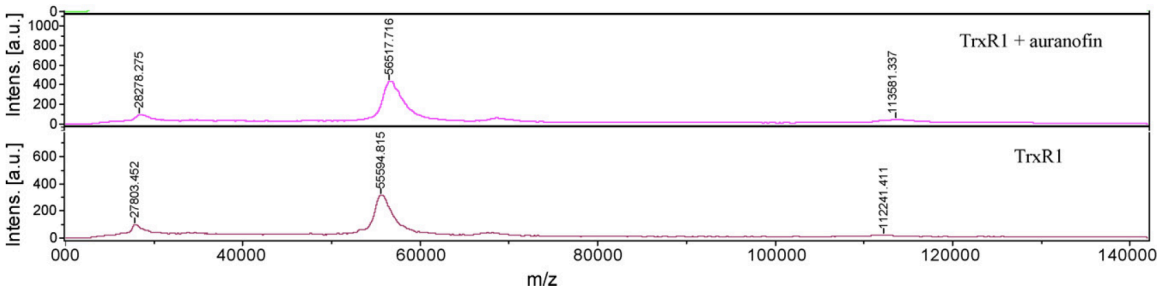

Figure 4.2 MALDI MS spectra of intact rat TrxR1, pre-reduced with NADPH, alone or after 1 h incubation with *Auranofin*, at 10:1 gold to protein molar ratio, and removal of unbound gold.

[201] Marcon, G.; Messori, L.; Orioli, P.; Cinellu, M.A.; Minghetti, G. *Eur. J. Biochem.* **2003**, *270,* 4655.

4.3 Reactions of gold compounds with the C-terminal motif of thioredoxin reductase

4.3.1 Rationale of the study

Thioredoxin reductases are important and widespread proteins playing a crucial role in the intracellular redox metabolism. Indeed, thioredoxin reductases (TrxRs) (EC 1.8.1.9) are the only known enzymes capable of reducing thioredoxin (Trx), a key molecule - together with glutathione- in governing the intracellular redox balance.[202,203] Thioredoxin reductase, comprised of two identical 316-residue subunits, catalyzes the reduction of thioredoxin using NADPH as a source of electrons (Figure 4.3). Notably, the mammalian enzyme contains a functionally relevant selenol group at its C-terminal extension.[204]

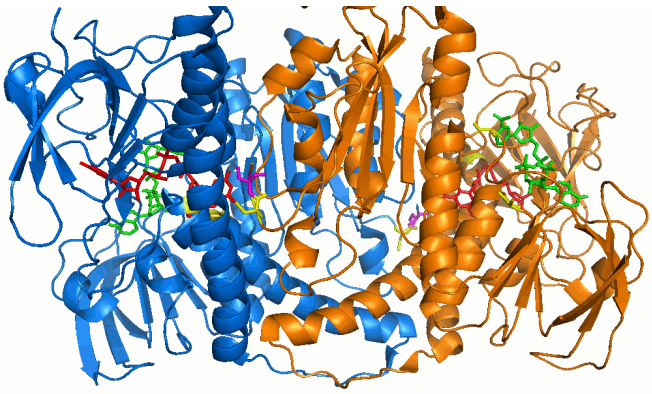

Figure 4.3 Ribbon representation of the dimer of human TrxR (Sec→Cys) (PDB entry 2J3N). The two subunits are shown in blue or orange colors, respectively. Cys58/Cys63, Cys58'/Cys63', Cys497 and Cys 497' are shown in yellow, Cys498 and Cys498' in magenta. Bound FAD (red) and $NADP^+$ (green) are shown as ball-and-stick models.

Recent studies pointed out that thioredoxin reductase might constitute an effective biomolecular target for a variety of anticancer inorganic drugs. For instance, TrxR was claimed to represent the major target for the arsenic based drug *Trisenox*, recently

[202] Arnér, E.S.J. *Biochim Biophys Acta.* **2009**, *6*, 495-526.
[203] Arnér, E.S.J.; Holmgren, A. *Eur. J. Biochem.* **2000**, *267*, 6102–6109.
[204] Fritz-Wolf, K.; Urig, S.; Becker, K. *J. Mol. Biol.* **2007**, *370*, 116-127.

approved by FDA for the treatment of promyelocytic leukemia.[205] In addition, gold(I) compounds, like the antiarthritic drug *Auranofin* (**67**), were shown to act as potent and selective thioredoxin reductase inhibitors.[206] Potency and selectivity were tentatively associated to the pronounced "*soft*" character of the gold(I) center and to its high affinity for selenium. Very likely, gold(I) might block TrxR active site selenocysteine.[206] Recently, the reaction of *Auranofin* (**67**) with the C-terminal peptide of TrxR was reproduced theoretically by DFT analysis and preferential gold coordination to selenol over the adjacent thiol strongly supported.[207] Consistently, Millet *et al*.[208] showed that an engineered mutant of TrxR, bearing a cysteine residue in the place of selenocysteine, is far less sensitive to inhibition by metallodrugs than the native protein. Moreover, a few gold(III) compounds were reported to be effective inhibitors of TrxR; in this latter case enzyme inhibition could arise either by oxidation of key enzyme residues or by gold coordination to *C*-terminal active site.[186] In any case, no conclusive and direct evidence has been gained so far that gold compounds specifically target the selenol group of thioredoxin reductase.

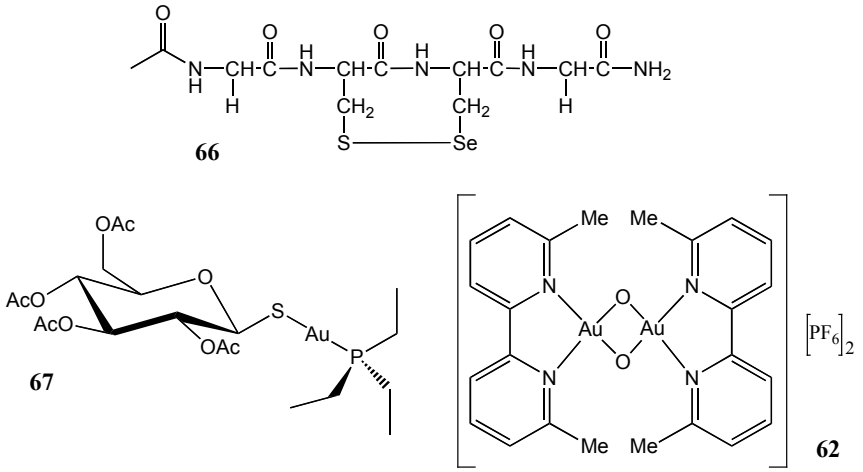

Scheme 4.2 The tetrapeptide (**66**); *Auranofin* (**67**) and AuOXO6 (**62**).

These arguments led us, in collaboration with Prof. Luigi Messori, to design and synthetize a short peptide with the sequence Ac-Gly-[Cys-Sec]-Gly-NH_2 (**66**); the

[205] Lu, J.; Chew, E.H.; Holmgren, A. *Proc. Natl. Acad. Sci. U S A* **2007**, *104*, 12288-12293.
[206] Omata, Y.; Folan, M.; Shaw, M.; Messer, R.L.; Lockwood, P.E.; Hobbs, D.; Bouillaguet, S.; Sano, H.; Lewis, J.B.; Wataha, J.C. *Toxicol. In Vitro* **2006**, *20*, 882-890.
[207] Howell, J.A.S. *J. Organomet. Chem.* **2009**, *694*, 868–873.
[208] Millet, R.; Urig, S.; Jacob, J.; Amtmann, E.; Moulinoux, J.P.; Gromer, S.; Becker, K.; Davioud-Charvet, E. *J. Med. Chem.* **2005**, *48*, 7024-7039.

sequence of this tetrapetide exactly matches that of TrxR C-terminus. The reactivity of **66** toward *Auranofin* (**67**) and two representative gold(III) compounds *i.e.* the dinuclear *AuOXO6* complex (**62**) and sodium tetra-chloroaurate ($NaAuCl_4$) was tested by MS analysis.[209] The peptide **66**, and compounds **67** and **62** are schematically represented in Scheme 4.2.

4.3.2 Chemical synthesis of TrxR fragment

The synthesis of the peptide was not trivial. Selenocysteine was prepared starting from Selenocystine, in accordance with Moroder[210] and Hondal,[211] Fmoc-Sec(Mob)-OH was obtained with a bidimensional orthogonal protection scheme suitable for solid phase peptide synthesis. The peptide Ac-Gly-[Cys-Sec]-Gly-NH_2 (**66**) was synthesized starting from Rink Amide MBHA resin. All the reactions were performed on a semi automatic synthesizer (MultiSyn Tech - Germany) following the standard SPPS method and using the orthogonal Fmoc/Trt/*t*-Bu protection scheme. The linear peptide-resin was acetylated on the -NH_2 terminal group with a solution of acetic anhydride and NMM.

Formation of S-Se bridge was obtained by changing the original method for Mob removal,[212] while detaching the peptide from the resin (Scheme 4.3) using TFA 93%, TIS 2.5%, Tioanisole 2.5% and H_2O 2.5%, a cleavage cocktail with 1.0 equivalent of 2,2′-Dithiobis(5-nitropyridine) (DTNP) *per* selenium. On the ground of literature data, the rationale for this reaction is that the highly acidic solution of DTNP in TFA activates DTNP by protonation of the pyridine nitrogen atom. This creates a very good electron sink and enhances the electrophilicity of the disulfide bond of DTNP. The highly nucleophilic selenium atom attacks the DTNP to form a Sec(5-Npys) residue.

Since there is a nearby Cys(Mob) residue, the sulphur atom of this aminoacid can attack the reactive selenilsulfide bond, with concomitant loss of the Mob group and the formation of cyclic peptide **66** (Scheme 4.3).

[209] Pratesi, A.; Gabbiani, C.; Ginanneschi, M.; Messori, L. *Chem. Commun.* **2010**, *46*, 7001–7003.
[210] Besse, D.; Moroder, L. *J. Pept. Sci.*, **1997**, *3*, 442-453.
[211] Hondal, R.J.; Nilsson, B.L.; Raines, R.T. *J. Am. Chem. Soc.* **2001**, *123*, 5140-5141; Hondal, R.J.; Raines, R.T. *Methods Enzymol.* **2002**, *347*, 70-83.
[212] Harris, K.; Flemer Jr, S.; Hondal, R.J. *J. Pept. Sci.* **2007**, *13*, 81-93.

The crude peptide was prepurified by solid phase extraction (SPE) with a RP-8 LiChroprep silica. The purification of the peptide was performed by semipreparative RP-HPLC.

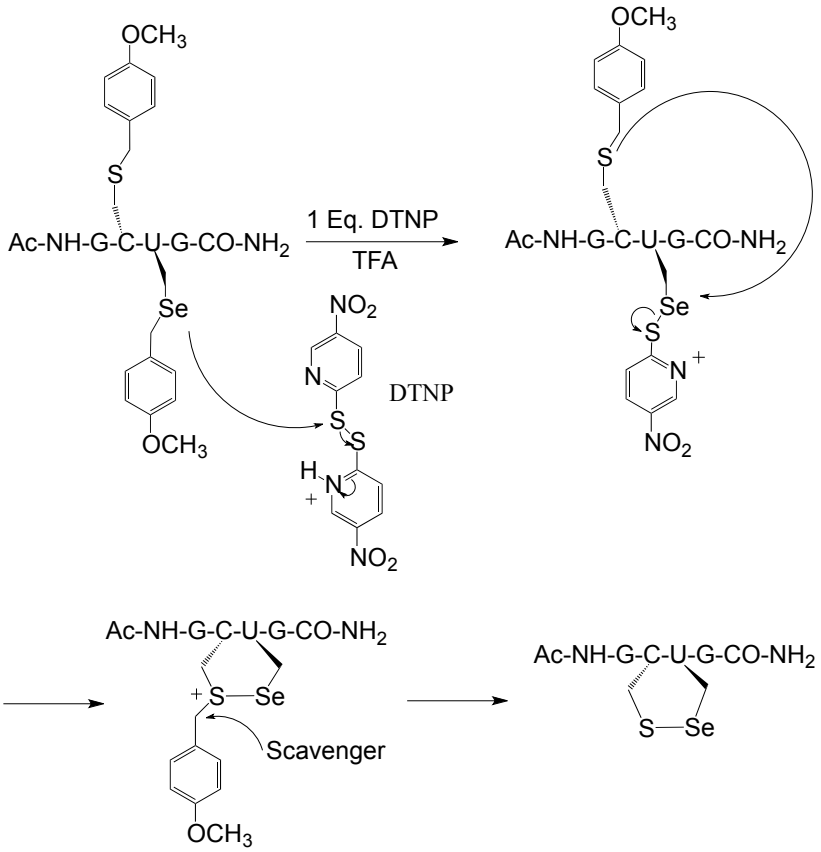

Scheme 4.3 Supposed mechanism of DTNP mediated S-Se bond formation.

4.3.3 MS analysis of TrxR-gold compounds

The peptide **66** was reduced by adding 5.0 equivalents of DTT and then reacted with 1.1 equivalents of the various gold drugs for 30 min at room temperature. The reaction products were analysed through ESI mass spectrometry, in the positive ion mode. ESI-MS spectra were recorded by direct injection at a 5 μl/min flow rate in a LCQ Advantage ion trap (Thermo, San Jose, California), equipped with a conventional ESI source. The specific conditions used for these experiments were as follows: the spray voltage was 4.5 kV, the capillary voltage was 1.5 V and the capillary temperature was kept at 270 °C. Sheath gas was set at 35 (arbitrary units) whereas auxiliary gas was kept at 0 (arbitrary units). The MS/MS was acquired on peak 742.00 *m/z* with an isolation width ±1.0 *m/z*, source

fragmentation collision energy set at 15 V and 30% of Normalized Collision Energy. All ESI spectra were elaborated using Xcalibur software (Thermo).

Notably, no reaction takes place in the absence of reducing agents. At variance, when the peptide was pre-reduced with DTT and treated with the various gold drugs a number of new peaks of greater molecular mass appeared that could be assigned to well defined metal-peptide species. A representative ESI-MS spectrum of the reaction with *Auranofin* (**67**) is shown in Figure 4.4. The main product shows a signal at *m/z* 741.84, peak (**A**), whose molecular mass exactly matches the tetrapeptide with a bound $AuPEt_3^+$ group. Another intense peak is detected at *m/z* 1055.86 (**B**) corresponding to the tetrapeptide bearing two $AuPEt_3^+$ groups. Both peaks show the characteristic isotopic pattern of selenium, as reported in Figure 4.5.

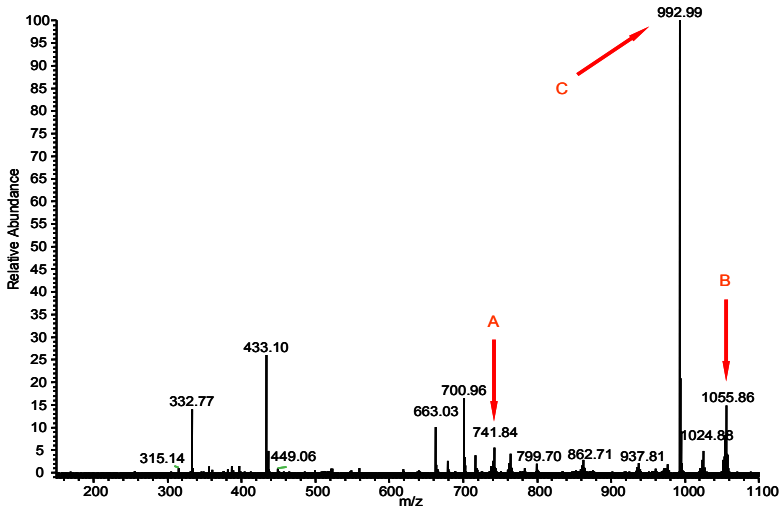

Figure 4.4 Mass spectra of the reduced peptide (**66**) with *Auranofin* (**67**).

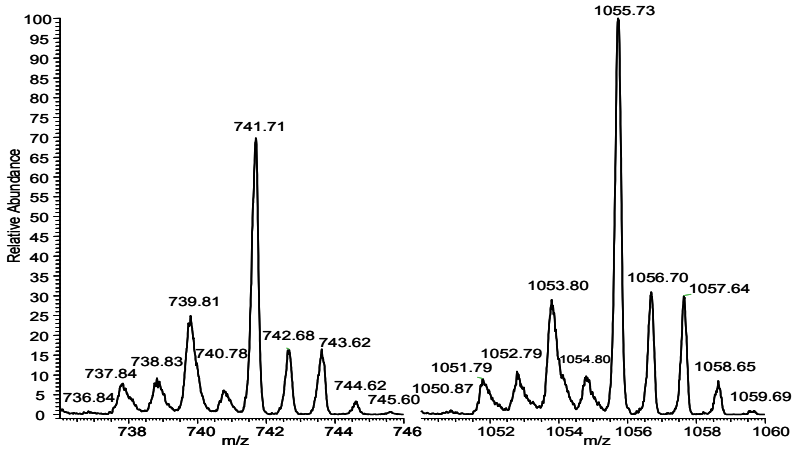

Figure 4.5 Isotopic pattern for mono- and di-Au(I) peptide complexes, single ion monitoring experiment.

At variance, peak (**C**) just corresponds to a peculiar rearrangement of *Auranofin* (**67**), previosuly described.[213]

The reported ESI-MS results are in nice agreement with expectations. *Auranofin* (**67**) binds the peptide tightly; apparently, enzyme binding takes place through replacement of the thiosugar moiety while the phosphine ligand is kept. It can be proposed that gold binding preferentially occurs at the level of the selenocysteine, in fact the MS/MS spectrum (Figure 4.6) for peak (**A**) in Figure 4.4, just shows a signal at *m/z* 536.40 corresponding to the loss of the fragment [Ac-Gly-Cys-] with no evidence of bound gold atoms. However, the binding of two $AuPEt_3^+$ fragments to Ac-Gly-Cys-Sec-Gly-NH_2 was also observed (Scheme 4.4, compounds **68, 69**). Instead, any evidence was obtained for one gold center bridging the adjacent selenocysteine and cysteine residues nor for peptide binding of bare gold(I) ions.

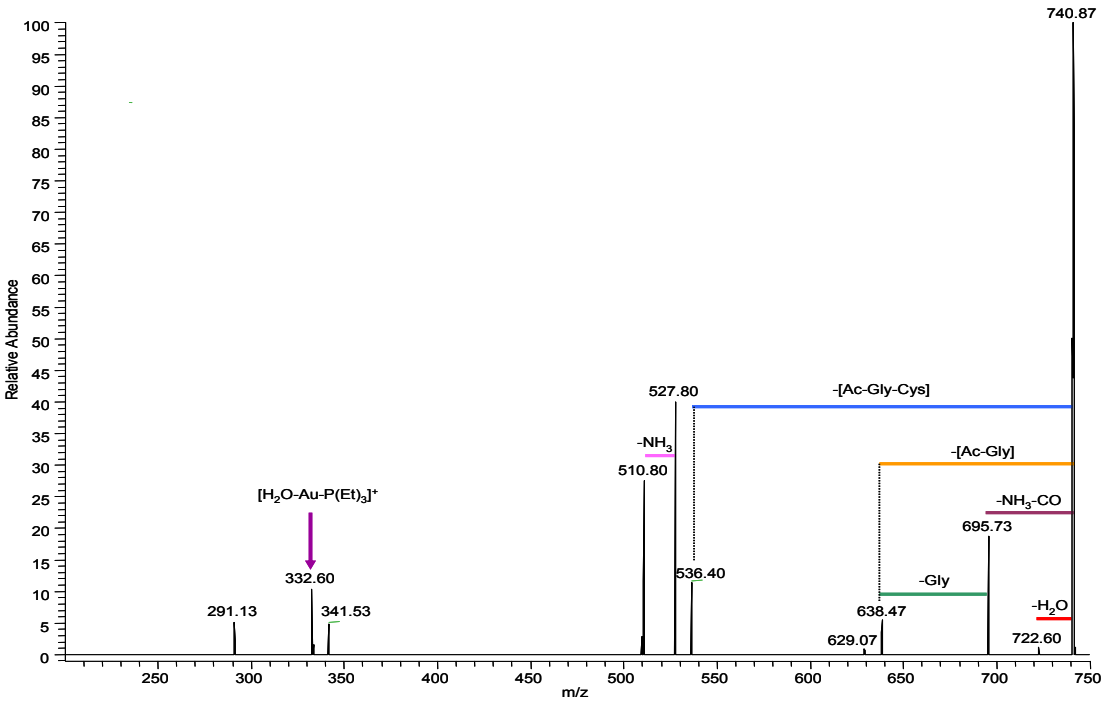

Figure 4.6 MS/MS spectra for the mono-Au(I) peptide complex.

[213] Shoeib, T.; Atkinson, D.W.; Sharp, B.L. *Inorganica Chimica Acta* **2010**, *363,* 184-192.

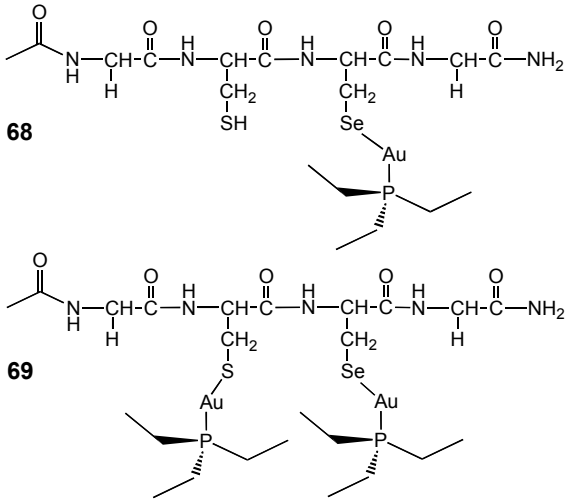

Scheme 4.4 *Auranofin* complexes revealed in ESI-MS spectra

Afterward, the reactions of Ac-Gly-Cys-Sec-Gly-NH_2 with the above mentioned gold(III) compounds, namely **62** and $NaAuCl_4$, were investigated. The resulting ESI-MS profiles are shown in Figure 4.7. Interestingly, treatment of the tetrapetide with these two gold(III) compounds invariantly afforded quantitative transformation of the original species into two main adducts of greater molecular mass. Notably, the *same* products were obtained in the two cases ruling out that any gold(III) ligands are eventually incorporated in the final species. Both adducts contain selenium as witnessed by their isotopic patterns.

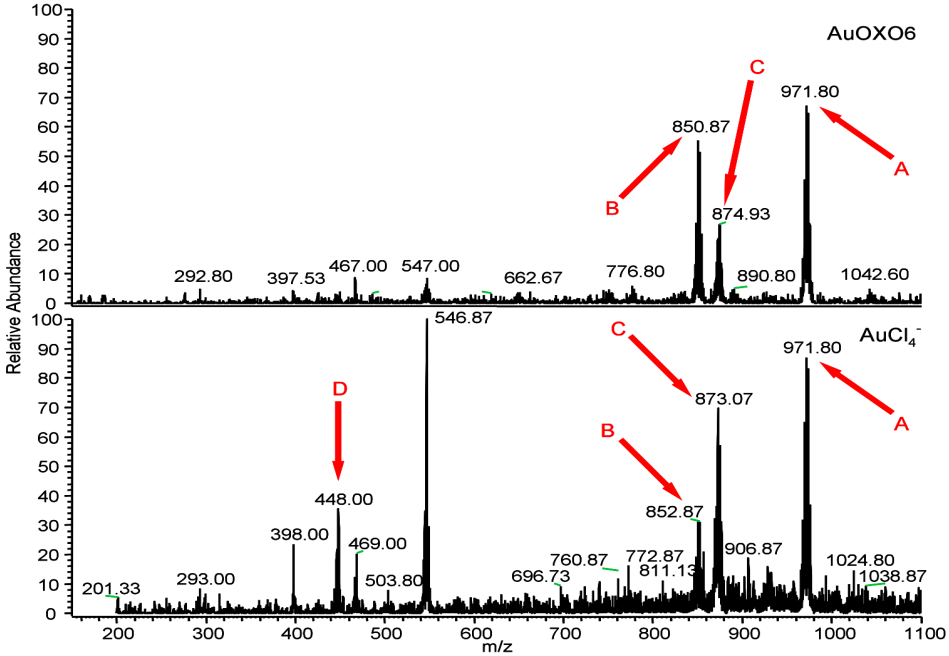

Figure 4.7 ESI-MS spectra with the two gold(III) compounds.

Analysis of the spectra led us to propose that peak (**A**) located at 971.80 *m/z* corresponds to the tetrapeptide bearing two bare Au^+ ions. Linear coordination is probably completed by a macrochelate DTT molecule as tentatively depicted in Scheme 4.5, (structure **70**). The parent peak (**B**) and its Na^+ form (**C**), reported in Figure 4.7, are due to association of two molecules of the tetrapeptide through formation of a S-S (not Se-Se) bond (structure **71**).

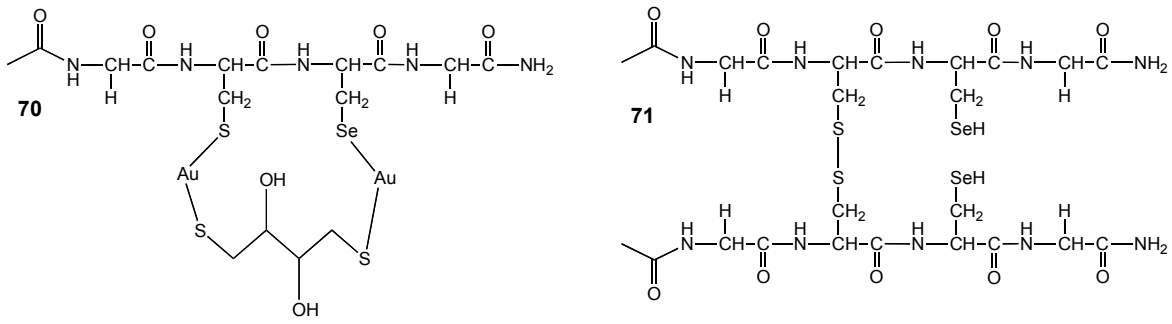

Scheme 4.5 Adducts formed during the complexation with AuOXO6 and $NaAuCl_4$.

Excess of DTT in solution is known to cause oxidation of SH to S-S.[214] This reaction occurs because the redox potential of the selenol group is far higher than that of the thiol group. Peak (**D**) at *m/z* 448.00 was assigned to the free peptide in its oxidised state ($[M+Na]^+$). Remarkably, selenol or thiol oxidation by gold(III) to the respective selenenic or sulfenic species may be ruled out as the characteristic peaks of the oxidised tetrapeptide incorporating one or more oxygen atoms were not detected at all.

4.3.4 Conclusions

The synthetic tetrapeptide Ac-Gly-[Cys-Sec]-Gly-NH_2 is a suitable model for the C-terminal site of the selenoenzyme TrxR. We have shown here that Ac-Gly-Cys-Sec-Gly-NH_2, in its reduced form, reacts eagerly with a few gold compounds, either gold(I) or gold(III). Such reactions are likely to reproduce closely the interactions taking place between the selenoenzyme and its gold-based inhibitors. Notably, the reaction with *Auranofin* (**67**) leads to predominant formation of a gold(I)-selenolate complex through

[214] Li, Y.; Rothwarf, D.M.; Scheraga, H.A. *J. Am. Chem. Soc.* **1998**, *120,* 2668-2669.

replacement of the thiosugar ligand (while the triethyl phosphine ligand is retained). On the other hand, reactions of Ac-Gly-Cys-Sec-Gly-NH_2 with two distinct gold(III) compounds -AuOXO6 and $AuCl_4^-$- afforded the *same* products. The main product was identified as a DTT/$Au(I)_2$/tetrapeptide species implying that gold(III) reduction has taken place. At variance, any evidence was obtained for extensive oxidation of the selenol/thiol groups by gold(III) to the respective selenenic/sulfenic species. Detailed information is thus inferred on the likely mechanisms of interaction of gold drugs with the enzyme. Apparently, in both cases, gold(I) coordination to the active site selenol group seems to be the crucial event leading to strong enzyme inhibition. Notably, these findings are roughly consistent with recently published ESI-MS results for the reaction of *Auranofin* (**67**) with cysteine and selenocysteine[213] though showing a few significant differences. In any case, we believe that the Ac-Gly-[Cys-Sec]-Gly-NH_2, tetrapeptide, characterised by the presence of adjacent thiol and selenol groups, is a far better model for the "real" enzyme.

Chapter 5

EXPERIMENTAL METHODS

5.1 Radiolabeling

5.1.1 Radiolabeling of MonoDOTA

$^{90}YCl_3$ in hydrochloric acid (0.04 M) was purchased from AEA Technology (Harwell, UK). Radiolabeling was carried out at a specific activity of 37 MBq ^{90}Y/10 μg of MonoDOTA (**1**), buffering with 1 M ammonium acetate pH 7.0. After being heated for 25 min at 85 °C, the mixture was diluted to 1 mL with saline. The labeling yield was determined by Instant Thin Layer Chromatography (ITLC SG, Gelman Science, Ann Arbor, MI) in saline, adding a molar excess of Av and EDTA to an aliquot of the radiolabeled mixture. In this system, Av/biotin derivative complex remains at the starting point while free ^{90}Y (bound to EDTA) migrates with the solvent front. The strip was cut in two halves and counted in a β-counter (Tri-Carb 2900TR Liquid Scintillation Analyzer, Packard).

5.1.2 Radiolabeling of BisDOTA and BisBiotin

Radiolabeling general procedure was performed using the three derivatives BisDOTA-Lys-C_3 (**7**), and BisDOTA-Lys-(pAB)-C_3 (**11**), BisBiotinMonoDOTA-C_3 (**21**), BisBiotinMonoDOTA-(*p*AB)-C_6 (**34**) and BisBiotinBisDOTA-(PEG_6)-C_3 (**44**) at a concentration of 3 mg/mL in saline. Equal volumes of 1.0 M sodium acetate buffer (pH 5.0) and of the radionuclide chloride solution were used. In each experiment, biotin solution was added to the buffer and transferred into the radionuclide supplier vial. The mixture was then mixed and heated at 95 °C for 30 min. RCP was assayed in triplicate for each radiolabeled sample by ITLC. An aliquot (usually 0.05 mL) of the radiolabeling solution was mixed with 0.2 mL of an avidin-DTPA solution (0.4 mM Av and 2.5 mM

DTPA, final pH 6.0) and kept at room temperature for 5 min. Subsequently, an amount of 5 μL of the radioactive mixture was spotted on a silica gel ITLC paper strip and then developed in saline solution. In this chromatographic system, Av-radio-biotin complex remains at the origin whereas free radiometal, bound to DTPA, migrates to the solvent front. The radiochromatographic profile was determined by an autoradiographic system using high performance storage phosphor screen and RCP consequently calculated. Labelling yields greater than 97% were routinely achieved.

5.1.3 High specific activity (SA) radiolabeling

To determine the achievable SA (expressed as MBq/nmol), the derivatives **7**, **11**, **21**, **34** and **44** were radiolabeled with ^{90}Y at the following increasing of SA: 2.6, 5.2, 10.6, 51.2, 212, 530 MBq/nmol. RCP was determined in each sample as previously described.

5.2 Studies of binding

5.2.1 Studies of Binding on MonoDOTA

Different molar ratios of ^{90}Y-labeled MonoDOTA (**1**) toward Av were studied. The same amount of radiolabeled MonoDOTA (1 μg) was reacted with decreasing amounts of Av (Mw 66 kDa), to obtain 1:2, 1:4, 1:8, 1:16, and 1:32 Av/**1** molar ratios. The mixtures were incubated at 37 °C and analysed at 2 and 24 h using Centricon YM-10 concentrators (Millipore, Bedford, MA, 10kDa Mw cutoff). Aliquots from the top and bottom parts of the Centricon were counted in the β-counter as previously described (see above). To evaluate the activity aspecifically bound to the Centricon, an ^{90}Y-labeled MonoDOTA aliquot was centrifuged without adding Av. All runs were performed in duplicate.

5.2.2 Studies of Binding on BisDOTA and BisBiotin

HABA Assay. Preliminary experiments were performed by varying the concentration of HABA (from 3 mM to 0.3 μM) and avidin (15.1, 7.6, and 3.8 μM) to calculate their optimal concentrations in the competitive binding studies. In the final experiments, carried out in 1 mL sample cuvettes, various concentrations of competitors

[(+)-biotin and BisDOTA or BisBiotin derivatives] were added to the HABA/Av complex, obtained by mixing avidin and HABA to a final concentration of 7.6 and 0.25 μM, respectively. Changes in absorbance were measured at 500 nm. All experiments were in triplicate, and the % inhibition was calculated as {[(absorbance with competitor) - (absorbance without HABA)/(Av complex)]/[(absorbance without competitor) - (absorbance without HABA)/(Av complex)]}×100.

CD Assay on Avidin/BisDOTA and BisBiotin Complexes Stability. Each spectrum (195-260 nm) was obtained from averaging three scans and subtracting the contribution from the buffer solution. Other experimental settings were as follows: 20 nm min scan speed, 2.0 nm bandwidth, 0.2 nm resolution, 50 mdeg sensitivity, and 4 s response. Melting curves of wild type avidin, with or without 4 eq. of (+)-biotin and its BisDOTA derivatives, were recorded by following the decrease of dichroic signal at 225 nm, keeping the temperature in the range 25-95 °C. Instrument settings were as follows: bandwidth 1 nm, response 0.5 s, data pitch 1 °C, temperature slope 10 °C/min. At every temperature increment of 5 °C, a far-UV CD spectrum was collected, assay utilizes the observation that HABA shows dramatic spectral changes when it binds to avidin. Free HABA has an absorption peak at 348 nm, while the HABA/avidin complex has strong absorption at 500 nm. Since the affinity between HABA and avidin is relatively weak (K_d = 5.8 10^{-6} M) compared to the affinity between (+)-biotin and avidin (K_d = 1 10^{-15} M), (+)-biotin can easily replace HABA from the HABA/avidin complex, resulting in a decrease of absorption at 500 nm. To estimate the apparent avidin binding affinity of biotin and BisDOTA derivatives, several competitive binding studies have been performed adding (+)-biotin and corresponding BisDOTA derivatives to the HABA/avidin sample and measuring any change in absorbance.

5.3 Stability studies

5.3.1 Stability Studies on MonoDOTA

Aliquots from the labelling mixture were diluted with saline or human serum/saline 1:1 solution alternatively. After 2, 6, 12, 24, 36, and 48 h of incubation at 37 °C, two aliquots (10 μL) of both the mixtures were drawn: one was added to Av molar excess and the other was added to saline. The samples were centrifuged in Centricon YM-10 and subsequently washed with 3 × 200 μL saline. The presence of ^{90}Y-labeled MonoDOTA/Av complex, free ^{90}Y ion, and biotinidase-cleaved ^{90}Y-DOTA, potentially generated during incubation, was determined by the activity counts of the top and bottom parts of the Centricon with and without Av excess.

5.3.2 Stability studies on BisDOTA and BisBiotin

Serum Stability. Normal mouse serum, freshly collected just before each experiment, was used as the source of biotinidase activity. Each experiment was carried out by mixing 50 μL of NMS with 10-25 μL of samples (BisDOTA derivatives or Biocytin). The volume was adjusted to 500 μL with reaction buffer (100 mM sodium acetate, pH 5.5), and each sample was incubated at 37 °C in water bath up to 2 h. To stop the reaction, an amount of 50 μL of each sample was diluted 10-fold with 0.08% TFA (v/v) in water, either before and after incubation, and 40 μL of this solution was applied to the HPLC columns. The chromatographic separations were carried out at a flow rate of 0.2 mL/min and by applying a gradient from 2% to 60% of B in 20 min. Main settings of ESI source were the following: spray voltage, 4.2 kV; capillary temperature, 300 °C; capillary voltage, 6 V.

5.4 Materials and methods

DOTA was purchased from Macrocyclics (Richardson, Texas, USA), Fmoc-Lys(MTT)-Wang resin (100-200 mesh) was from Novabiochem AG (Laufelfingen, Switzerland), 6Cl-HOBt was from Luxembourg (Israel), HATU was from PerSeptive Biosystem, TBTU was from Chem Impex International. Peptide-synthesis grade DMF was

from Scharlau (Barcelona, Spain). HPLC-grade MeCN was purchased from Carlo Erba (Italy). Dry solvents were distilled immediately before use: THF over sodium/benzophenone. All other chemicals were commercial compounds and were used as received.

^{1}H-NMR spectra were recorded on a Varian Gemini 200 MHz spectrometer or Varian Inova 400 MHz. Chemical shifts (δ) are reported in ppm downfield from tetramethylsilane. The elemental analyses were performed on a Perkin Elmer 240 C Elemental Analyzer.

Thin layer chromatographies (TLC) were carried out on SiO_2 (Merck; 60 Å F254) and spots located with: UV light (254 and 366 nm), methanolic ninhydrin, Fluram (Fluka; fluorescamine, 4-phenyl-spyro[furan-2(3H),1'-isobenzofuran]-3,3'-dione) in acetone, Cl_2/O-tolidine [O-tolidine (75 mg), AcOH (3 mL), and KI (21 mg) in water (47 mL)].

Semi-preparative purification via HPLC were performed by a Supelco C_{18} 180Å (250 × 10 mm, 5μm, metals < 10 ppm) column at 28 °C using a Beckman Gold Noveau instrument (detector diode array). Analytical HPLC were performed using a Phenomenex Jupiter column 5μ C_{18} 300Å (250 × 4.6 mm). The solvent systems used were: A (0.1% TFA in H_2O) and B (0.1 % TFA in CH_3CN). The flow rates were 1 mL/min for analytical HPLC and 4 mL/min for semi-preparative HPLC, with the indicated linear gradients. Electrospray ionization mass spectra (ESI-MS) were acquired on a LCQ-Advantage ESI ion trap spectrometer (ThermoFinnigan) for positive and negative ions detection.

LC-ESI MS analyses were performed on a Phenomenex Aqua C_{18} column (5 μm, 250 × 4.6 mm) (flow rate: 1000 μL/min), on a ThermoFinnigan Surveyor HPLC system coupled to the ESI-MS, using the solvent systems reported above.

LC was performed in automatic with a Biotage Isolera One.

The peptide syntheses were performed using a semi-automatic synthesizer from MultiSyn Tech (German) and the microwave-assisted steps were carried out with a CEM Explorer microwave reactor.

All the *in vitro* were experiments were performed at the Division of Nuclear Medicine of the European Institute of Oncology (Milano, Italy).

5.5 Chemical synthesis

5.5.1 Fmoc-Lys(H)-OtBu

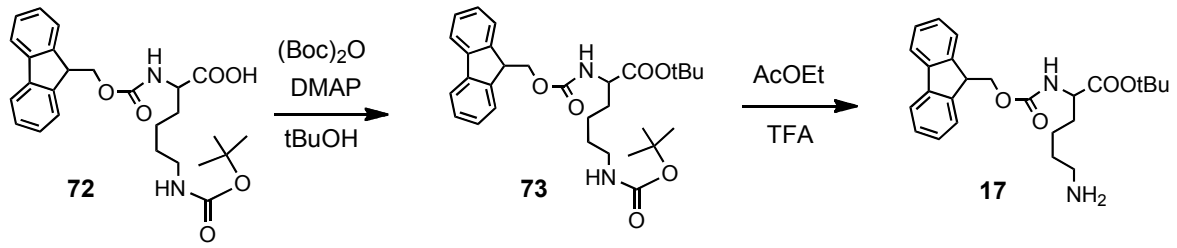

Scheme 5.1 Synthesis of **17**

2.0 g of Fmoc-L-Lys(Boc)-OH (**72**) were added with 2.33 g of di-terbuthyl dicarbonate, Boc_2O, and 156.5 mg of 4-dimethylaminopiridine, DMAP, in 30 ml of anhydrous *ter*-buthanol. The reaction was stirred for 30 min at 35°C and for 15 h at room temperature. At the end of the reaction the product, **73**, was checked by TLC (AcOEt/exane 2:1), $R_f = 0.75$.

The solvent was removed under vacuum and the solid residue was dissolved 30 ml of ethyl acetate and 5 ml of water; the organic layer was washed with a saturated solution of $NaHCO_3$ (20 ml for 3 times), and with water (20 ml for 3 times). The organic phase was dried with anhydrous Na_2SO_4, the solvent was removed under vacuum and the crude product was purified by direct-phase LC on silica gel using AcOEt/exane 30:70.

1.70 g of the purified product **73** were dissolved in 56 ml of solution containing 28% of TFA in AcOEt. The solution was stirred at 45 °C for 1 h. After, another 10 ml of TFA were added. The reaction was stirred for 2h and at the end, TFA was removed under nitrogen flow. The crude compound **17**, was solubilized in 10 ml of CH_3CN/H_2O 2:3 and purified by solid phase extraction on reverse-phase C_{18} silica gel, obtaining the pure compound Fmoc-Lys(H)-O*t*Bu, **17** (311 mg, 57% yield). ESI-MS: calculated *m/z* 425.5 $[M+H]^+$; found 425.5.

5.5.2 SPPS synthesis: general procedures

The products were synthesized using classical SPPS method. The coupling was checked by the Kaiser test. The products were synthesized on Fmoc-Lys(MTT)-Wang resin (50 mg, 0.03 mmol or 500 mg, 0.3 mmol as specified for each compound) using the semiautomatic synthesizer. Before the synthesis the resin was swelled for 20 min in DMF.

Step 1: Fmoc deprotection was performed by 20% piperidine in DMF (2 × n mL) for 10 min. The resin was twice washed with DMF, one time with DCM and twice with DMF.

Step 2: coupling reactions.

Method 1: TBTU/HOBt/NMM method with formation of active esters. The coupling reaction was performed by using the reagent (2.5 eq), HOBt (2.5 eq), TBTU (2.5 eq) and NMM (5 eq) in DMF, under vortex mixing for 45 min. The resin was then washed with DMF (3 × n mL) and DCM (2 × n mL). Coupling reactions were controlled by the Kaiser test.

Method 2: HATU/NMM method; the coupling reaction was performed by using the reagent (2.5 eq), HATU (2.5 eq), and NMM (5 eq) in DMF, under vortex mixing for 45 min. The resin was then washed with DMF (3 × n mL) and DCM (2 × n mL).

Step 3: removal of MTT protecting group was performed by a solution containing 2% TFA, 2.5% TIS and 95.5% DCM. (20 × n mL) for 3 min. Initially the solution became fluorescent yellow, indicating the presence of MTT. Washing was continued until the solution became colourless again.

Step 4: cleavage the resin and removal of the *tert*-butyl protection was performed with 2.5% TIS, 2.5% H_2O and 95% TFA for 3 h. The resin was filtered off and the solution was concentrated by flushing with N_2. The peptide was precipitated from cold Et_2O, centrifuged and lyophilized. The purification of the crude products was performed by semipreparative reverse-phase HPLC. Eluents: A (0.1% TFA in H_2O) and B (0.1% TFA in CH_3CN). Characterization of the products was performed by using ESI-MS and LC-ESI-MS.

The volume of solvents, n, used in washes was calculated with the general principle: 1 mL for 100 mg of resin.

5.5.3 BisDOTA-Lys-C_3

2,2',2''-(10-(15-carboxy-2,9,17-trioxo-21-(2-oxohexahydro-1H-thieno[3,4-d]imidazol-4-yl)-7-(3-(2-(4,7,10-tris(carboxymethyl)-1,4,7,10-tetraazacyclododecan-1-yl)acetamido)propyl)-3,7,10,16-tetraazahenicosyl)-1,4,7,10-tetraazacyclododecane-1,4,7-triyl)triacetic acid

Compound (4)

After Fmoc deprotection (step 1), the biotin residue was introduced according to the TBTU/HOBt/NMM method (step 2, method 1): biotin (13.18 mg, 0.054 mmol), HOBt (7.3 mg, 0.054 mmol), TBTU (17.3 mg, 0.054 mmol) and NMM (9 μL, 0.081 mmol) in DMF (0.5 mL). Coupling reaction was controlled by the Kaiser test. MTT deprotection was performed following step 3. HPLC (5 to 30% of B in 20 min): t_R = 9.6 min; ESI-MS: *m/z* calcd $[M+H]^+$ 373.2, found 373.3.

Compound (6)

Spacer C_3 conjugation to the lysine side chain was performed using step 2, method 1: spacer C_3, **5** (41.6 mg, 0.054 mmol), HOBt (7.3 mg, 0.054 mmol), TBTU (17.3 mg, 0.054 mmol) and NMM (9 μL, 0.081 mmol) in DMF (0.5 mL). We were used three couplings to obtain a negative Kaiser test. HPLC (10 to 90% of B in 20 min): t_R = 17.7 min; ESI-MS: *m/z* calcd $[M+H]^+$ 988.46, found 988.72.

BisDOTA-Lys-C_3 (7)

After Fmoc deprotection (step 1), for the DOTA conjugation (step 2, method 1) was used: DOTA-tris(*tert*-butyl) ester (**20**) (61.8 mg, 0.108 mmol), HOBt (14.6 mg, 0.108 mmol), TBTU (34.6 mg, 0.108 mmol) and NMM (18 μL, 0.162 mmol) in DMF (0.5 mL). Coupling reaction was controlled by the Kaiser test. Cleavage from the resin and removal of the *tert*-butyl protection was performed using step 4. The crude product was purified by semipreparative RP-HPLC to give pure **7** (13 mg, 35% yield). HPLC (5 to 30% of B in 20 min): t_R = 11.1 min; ESI MS: *m/z* calcd $[M+H]^+$, 1316.68, found 1316.5. Elemental analysis. Found: C, 38.38; H, 5.42; N, 10.02%. Calculated: $C_{56}H_{97}N_{15}O_{19}S{\cdot}6H_2O{\cdot}6TFA$: C, 38.73; H, 5.50; N, 9.96%.

5.5.4 BisDOTA-Lys-(pAB)-C_3

Compound (9)

4-Aminobenzoic acid with primary amino-group Fmoc-protected **8** was conjugated to the lysine side chain using step 2, method 1: *p*AB acid **8** (19.4 mg, 0.054 mmol), HOBt (7.3 mg, 0.054 mmol), TBTU (17.3 mg, 0.054 mmol) and NMM (9 μL, 0.081 mmol) in DMF (0.5 mL). One coupling was necessary to obtain a negative Kaiser test. HPLC (10 to 90% of B in 20 min): t_R = 16.3 min; ESI MS: *m/z* calcd $[M+H]^+$, 714.29, found 714.8.

Compound (10)

After Fmoc deprotection (step 1), the spacer C_3 **5** residue was introduced according to the HATU/NMM method (step 2, method 2): spacer C_3 **5** (52 mg, 0.067 mmol), HATU (25.67 mg, 0.067 mmol), and NMM (15 μL, 0.135 mmol) in DMF (0.5 mL). Coupling reaction was controlled by Kaiser test. Four couplings were necessary. HPLC (10 to 90% of B in 20 min): t_R = 17.8 min; ESI-MS: *m/z* calcd $[M+H]^+$, 1107.49, found 1107.3.

BisDOTA-Lys-(pAB)-C_3 (11)

Coupling was carried out with a mixture of DOTA-tris(*tert*-butyl) ester (**20**) (61.8 mg, 0.108 mmol), HOBt (14.6 mg, 0.108 mmol), TBTU (34.6 mg, 0.108 mmol) and NMM (18 μL, 0.162 mmol) in DMF (0.5 mL). Coupling reaction was controlled by the Kaiser test. Cleavage from the resin and removal of the *tert*-butyl protection was performed using step 4. The crude product was purified by semipreparative RP-HPLC to give pure **11** (8 mg, 20%). HPLC (5 to 30% of B in 20 min): t_R = 12.967 min; ESI-MS: *m/z* calcd $[M+H]^+$, 1435.72, found 1436.6. Elemental analysis. Found: C, 37.70; H, 4.49; N, 10.92%. Calculated: $C_{63}H_{102}N_{16}O_{20}S \cdot 10H_2O \cdot 7TFA$: C, 38.31; H, 5.39; N, 9.28%.

5.5.5 BisBiotinMonoDOTA-C_3

16-(2-(1-carboxy-5-(2-(4,7,10-tris(carboxymethyl)-1,4,7,10-tetraazacyclododecan-1-yl)acetamido)pentylamino)-2-oxoethyl)-8,11,21,24-tetraoxo-2,30-bis(5-(2-oxohexahydro-1H-thieno[3,4-d]imidazol-4-yl)pentanamido)-7,12,16,20,25-pentaazahentriacontane-1,31-dioic acid

Compound (12)

After Fmoc deprotection from Fmoc-Lys(MTT)-Wang resin, (**2**) (500 mg, 0.3 mmol) (step 1), the spacer C_3 conjugation to the lysine side chain was performed using step 2, method 2: spacer C_3, **5** (2.5 eq, 577 mg), HATU (2.5 eq, 285 mg) and NMM (5 eq, 166 µL). in DMF. HPLC (10 to 90% of B in 20 min): t_R = 17.7 min; ESI-MS: *m/z* calcd $[M+H]^+$ 988.46, found 988.72.

Compound (15)

Fmoc group removal was performed by treating the resin **13** with 20% piperidine in DMF (step 1). The succinic anhydride (**14**) (20 eq, 600 mg) and NMM (40 eq, 1.33 mL) were introduced, with the resin in anhydrous THF, in a microwave reactor. Program: 20 cycles (60 Watt for 1 min and cooling for 30 sec), Tmax = 65°C.

Compound (18)

Fmoc-Lys-O*t*Bu (**17**) was introduced by activation of the carboxyl function on resin **15**. HOBt (2.5 eq, 115 mg), TBTU (2.5 eq, 241 mg) and NMM (4.5 eq, 149 µL) in DMF were added on the resin and vortexed for 1 min. *Building-block*, **17** (2.5 eq, 318 mg) in DMF was then added an vortexed for 1 h. Coupling reaction was controlled by the Kaiser test and micro cleavage. Two couplings were necessary.

Compound (19)

Biotin residue was introduced according to the TBTU/HOBt/NMM method (step 2, method 1): biotin (**3**) (4 eq, 293 mg), HOBt (4 eq, 184 mg), TBTU (4 eq, 385 mg) e NMM (8 eq, 265 µL) in DMF.

BisBiotinMonoDOTA-C$_3$ (21)

MTT deprotection was performed following step 3. Coupling was carried out with a mixture of DOTA-tris(*tert*-butyl) ester (**20**) (2 eq, 344 mg), HOBt (2 eq, 92 mg), TBTU (2 eq, 193 mg) and NMM (3 eq, 100 μL) in DMF. Coupling reaction was controlled by the Kaiser test. Cleavage from the resin and removal of the *tert*-butyl protection was performed using step 4. The crude product was purified by semipreparative RP-HPLC to give pure **21** (90 mg, 19%). HPLC (10 to 90% of B in 15 min): t_R = 6.94 min; ESI-MS: *m/z* calcd $[M+H]^+$, 1612.80, found 1612.62. Elemental analysis. Found: C, 38.54; H, 5.32; N, 10.11%. Calculated $C_{70}H_{117}N_{17}O_{22}S_2 \cdot 9H_2O \cdot 7TFA$, C, 39.21; H, 5.56; N, 9.25%.

5.5.6 Spacer-C$_6$

2,2'-(iminodi-6,1-hexanediyl)bis-1H-isoindole-1,3(2H)-dione (24)

N-(6-aminohexyl)-1,6-hexanediamine (**22**) (2.00 g, 9.28 mmol) was dissolved in warm toluene (10 mL) in a Dean-Stark. A solution of phthalic anhydride (**23**) (recrystallized from $CHCl_3$) (2.83 g, 19.1 mmol) in warm toluene (20 mL) was added. The reaction mixture was monitored by TLC analysis (MeOH/$CHCl_3$ 1:10) and heated to reflux for 8 h. The precipitated phthalic acid was filtered off and the filtrate concentrated under reduced pressure to give **24** (4.2 g, 95 %) as an orange-brown oil which was used in the next step without further purification. ^{1}H-NMR (200 MHz, $CDCl_3$): δ (ppm) 7.81-7.77 (m, 4H), 7.68-7.64 (m, 4H), 3.62 (t, 4H), 2.57 (t, 4H), 2.20 (s, 1H), 1.75-1.55 (m, 4H), 1.5-1.4 (m, 8H), 1.35-1.2 (m, 4H); ESI-MS: *m/z* calcd $[M+H]^+$ 476.3, found 476.5.

N,N-bis[6-(1,3-dihydro-1,3-dioxo-2H-isoindole-2-yl)hexyl]glycine ethyl ester (25)

DIPEA (275 μL, 1.57 mmol) was added to a warm solution of **24** (350 mg, 0.73 mmol) in DMF (5 mL) and the reaction mixture was heated at 75-80 °C. Ethyl brome acetate (105 μL, 0.95 mmol) in DMF (1 mL) was added dropwise during 1 h. The solution was stirred and monitored by TLC (MeOH/CH_2Cl_2 1:20). After 16 h the solvent was evaporated under reduced pressure. The orange-brown oil was purified by FCC (silica gel 60, 40-63 μm; eluent: AcOEt/petroleum ether 1:1) affording pure **25** as an yellow-orange oil (150 mg, 44 %). RP-HPLC (30 to 80% of B in 20 min), t_R = 15.6 min; ^{1}H-NMR (200

MHz, $CDCl_3$): δ (ppm) 7.81-7.75 (m, 4H), 7.70-7.64 (m, 4H), 4.10 (q, 2H), 3.62 (t, 4H), 3.24 (s, 2H), 2.49 (t, 4H), 1.66-1.56 (m, 4H), 1.44-1.26 (m, 15H); ESI-MS: *m/z* calcd $[M+H]^+$ 562.3, found 562.4.

N,N-bis(6-aminohexyl)glycine (26)

Compound **25** was dissolved in HCl (6 M, 10 mL); the reaction mixture was heated to reflux for 3 days and monitored by TLC (AcOEt/ petroleum ether 1:1). HCl (12 M, 4 mL) was added and the solution was refluxed for 19 h, and then allowed to cool at room temperature. The phthalic acid produced was filtered off and the aqueous phase lyophilized to give quantitatively **26**. RP-HPLC (20 to 60% of B in 20 min): t_R = 6.47 min; ^{1}H-NMR (200 MHz, DMSO-d_6): δ (ppm) 10.22 (br s, 1H), 8.18 (br s, 4H), 4.06 (s, 2H), 3.13-3.08 (m, 4H), 2.8-2.55 (m, 4H), 1.58-1.55 (m, 8H), 1.4-1.15 (m, 8H); ESI-MS: *m/z* calcd $[M+H]^+$ 274.3, found 274.3.

N,N-bis[[[6-(9H-fluoren-9-ylmethoxy)carbonyl]amino]hexyl]glycine (27)

Compound **26** (394 mg, 1.03 mmol) was dissolved in dioxane (9.5 mL) and H_2O (2.5 mL) and Fmoc-Succinimide ester (729.6 mg, 2.16 mmol) in dioxane was added. The resulting mixture was stirred at room temperature and the pH adjusted to 8 with 2 M NaOH. The reaction was monitored by TLC analysis ($CHCl_3$/MeOH 3:1) and stirred for 1 h. The mixture was treated with H_2O and 3 M HCl and the suspension extracted with $CHCl_3$ (3 × 20 ml). The combined organic layers were dried (Na_2SO_4), filtered and concentrated. The crude product was purified by FCC (silica gel 60, 40-63 μm; eluent: $CHCl_3$/MeOH 3:1) to provide compound **27** (248 mg, 34% yield). RP-HPLC (30 to 100% of B in 20 min): t_R = 17.92 min; ^{1}H-NMR (200 MHz, $CDCl_3$): δ (ppm) 7.71 (d, 4H), 7.56 (d, 4H), 7.38-7.22 (m, 8H), 4.33-4.29 (m, 2H), 4.16 (d, 4H), 3.60-3.44 (m, 2H), 3.3-2.95 (m, 8H), 1.72-1.20 (m, 16H); ESI-MS: *m/z* calcd $[M+H]^+$ 718.4, found 718.4.

5.5.7 BisBiotinMonoDOTA-(pAB)-C_6

2,2',2''-(10-(13-carboxy-9-(6-(4-(4-(5-carboxy-5-(5-(2-oxohexahydro-1H-thieno[3,4-d]imidazol-4-yl)pentanamido)pentylamino)-4-oxobutanamido)benzamido)hexyl)-1-(4-(4-(5-carboxy-5-(5-(2-oxohexahydro-1H-thieno[3,4-d]imidazol-4-yl)pentanamido)pentylamino)-4-oxobutanamido)phenyl)-1,11,19-trioxo-2,9,12,18-tetraazaicosan-20-yl)-1,4,7,10-tetraazacyclododecane-1,4,7-triyl)triacetic acid

Compound (28)

The Fmoc-Lys(MTT)-Wang resin (**2**) (500 mg, 0.3 mmol) was swelled for 20 min in DMF and deprotected from Fmoc (step 1). The spacer C_6 conjugation to the lysine side chain was performed using step 2, method 2: spacer C_6, **27** (2 eq, 430 mg), HATU (2 eq, 228 mg) and NMM (4 eq, 133 μL) in DMF. Reaction time: 1 h. HPLC (10 to 90% of B in 20 min): t_R = 11.21 min; ESI-MS: *m/z* calcd $[M+H]^+$ 402.59, found 402.50.

Compound (30)

The product **28** was deprotected from Fmoc (step 1). 4-Aminobenzoic acid with primary amino-group Fmoc-protected **8** was conjugated to the lysine side chain using step 2, method 1: *p*AB acid **8** (4 eq, 432 mg), HOBt (4 eq, 184 mg), TBTU (4 eq, 385 mg) and NMM (8 eq, 266 μL) in DMF. Reaction time: 45 min. The coupling was checked by Kaiser test and microcleavage. HPLC (10 to 50% of B in 20 min): t_R = 6.65 min; ESI-MS: *m/z* calcd $[M+H]^+$, 640.83, found 640.64.

Compound (31)

Fmoc group removal was performed by treating the resin **30** with 20% piperidine in DMF (step 1). The succinic anhydride (**14**) (20 eq, 600 mg) and NMM (40 eq, 1.33 mL) were introduced, with the resin in anhydrous THF, in a microwave reactor. Program: 20 cycles (60 Watt for 1 min and cooling for 30 sec), Tmax = 65 °C.

The coupling was controlled with Kaiser test and microcleavage. HPLC (10 to 70% of B in 20 min): t_R = 7.12 min; ESI-MS: *m/z* calcd $[M+H]^+$, 840.44, found 840.50.

Compound (32)

The intermediate **31** was vortexed for 30 sec with THF containing 10% of 0.25 M NaOH in aqueous solution. Then, the compound **31**, was activated on resin by adding HOBt (3 eq, 138 mg), TBTU (3 eq, 289 mg) and NMM (5 eq, 166 μL) in DMF and vortexing for 1 min. Subsequently, *building-block* **17** (3 eq, 382 mg) in DMF was added to the mixture. Reaction time 1 h. HPLC-MS (10 to 90% of B in 20 min): t_R = 5.78 min; *m/z* calcd $[M+H]^+$ 1098.29, found 1098.08.

Compound (33)

Compound **32** was deprotected from Fmoc (step 1) and Biotin was introduced according to the TBTU/HOBt/NMM method (step 2, method 2): biotin (**3**) (2.5 eq, 183 mg), HATU (2.5 eq, 285 mg) and NMM (4 eq, 133 μL) in DMF. Coupling reaction was controlled by the Kaiser test and microcleavage. Compound **33** was characterized by HPLC-MS (10 to 90% of B in 20 min): t_R = 6.37 min; *m/z* calcd $[M+H]^+$ 1549.91, found 1549.86.

BisBiotinMonoDOTA-(pAB)-C_6 (34)

MTT deprotection was performed following step 3. Coupling was carried out with a mixture of DOTA-tris(*tert*-butyl) ester (**20**) (2.5 eq, 430 mg), HOBt (2.5 eq, 115 mg), TBTU (2.5 eq, 241 mg) and NMM (5 eq, 166 μL) in DMF. Coupling reaction was controlled by the Kaiser test. Cleavage from the resin and removal of the *tert*-butyl protection was performed using step 4. The crude product was purified by semipreparative RP-HPLC to give pure **34** (85 mg, 18%). HPLC (35 to 45% of B in 20 min): t_R = 7.56 min; ESI-MS: *m/z* calcd $[M+H]^+$, 1936.31, found 1935.87; $[M+2H]^{2+}$, 968.27. Elemental analysis. Found: C, 43.34; H, 5.12; N, 10.11%. Calculated $C_{90}H_{139}N_{19}O_{24}S_2 \cdot 10H_2O \cdot 6TFA$: C, 43.76; H, 5.94; N, 9.51%.

5.5.8 BisBiotinBisDOTA-(PEG$_6$)-C$_3$

The procedure for the first intermediate was already described for compound **12**.

Compound (36)

Fmoc group removal was performed by treating the resin **12** with 20% piperidine in DMF (step 1). The coupling was performed following method 2, with 1-Fmoc-amino-3,6,9,12,15,18-esaossaenicosan-21-oic acid (Fmoc-NH-PEG$_6$-COOH, **35**) (4 eq, 553 mg), HOBt (4 eq, 147 mg), TBTU (4 eq, 308 mg) and NMM (6 eq, 159 μL) in DMF and the mixture was vortexed for 1h. Coupling reaction was controlled by the Kaiser test and microcleavage. Compound **36** was analyzed by HPLC-MS (10 to 90% of B in 20 min): t_R = 12.43 min; *m/z* calcd $[M+H]^+$ 989.21, found 989.38.

Compound (38)

The product **36** was deprotected from Fmoc (step 1). Fmoc-α-aminobutyric acid, (Fmoc-L-Abu-OH, **37**) was conjugated to the terminal PEG amino group using step 2, method 1: Fmoc-L-Abu-OH (**37**) (5 eq, 391 mg), HOBt (5 eq, 184 mg), TBTU (5 eq, 385 mg) and NMM (8 eq, 212 μL) in DMF. Reaction time: 45 min. The coupling was checked by Kaiser test and microcleavage. Two couplings were necessary to obtain a negative Kaiser test. HPLC (10 to 90% of B in 20 min): t_R = 8.87 min; ESI MS: *m/z* calcd $[M+H]^+$, 1159.42, found 1159.12.

Compound (39)

Compound **38** was deprotected from Fmoc (step 1) and Biotin was introduced according to the HATU/NMM method (step 2, method 2): biotin **3** (3 eq, 176 mg), HATU (3 eq, 274 mg) and NMM (5 eq, 133 μL) in DMF. Coupling reaction was controlled by the Kaiser test and microcleavage. Compound **39** was analysed by HPLC-MS (10 to 90% of B in 20 min): t_R = 7.53 min; *m/z* calcd $[M+H]^+$ 1612.01, found 1612.45.

Compound (41)

MTT deprotection of **39** was performed following step 3. Bis-Fmoc-3,5-diaminobenzioc acid (**40**) (2.5 eq, 358 mg) was introduced (step 2, method 1) with HOBt (2.5 eq, 92 mg), TBTU (2.5 eq, 193 mg) and NMM (5 eq, 133 μL) in DMF. Reaction time: 45 min. Two couplings were necessary in order to obtain a negative Kaiser test. HPLC-MS (10 to 90% of B in 20 min): t_R = 9.21 min; *m/z* calcd $[M+H]^+$ 1746.15, found 1746.63.

Compound (43)

The intermediate **41** was deprotected from Fmoc, using the step 1. Fmoc-*β*Ala-OH, (**42**) (5 eq, 374 mg) was introduced, in accordance with the method 1, by using HOBt (5 eq, 184 mg), TBTU (5 eq, 385 mg) and NMM (8 eq, 212 μL) in DMF. Reaction time: 45 min. only one coupling was necessary in order to obtain a negative Kaiser test. HPLC-MS (10 to 90% of B in 20 min): t_R = 11.54 min; *m/z* calcd $[M+2H]^{2+}$ 1166.89, found 1167.04.

BisBiotinBisDOTA-(PEG$_6$)-C$_3$ (44)

Fmoc deprotection was performed following step 3. Coupling was carried out with a mixture of DOTA-tris(*tert*-butyl) ester (**20**) (5 eq, 688 mg), HATU (5 eq, 457 mg) e NMM (8 eq, 212 μL) in DMF (method 2). Coupling reaction was controlled by the Kaiser test. Cleavage from the resin and removal of the *tert*-butyl protection was performed using step 4. The crude product was purified by semipreparative RP-HPLC to give pure **44** (94 mg, 20%). HPLC (20 to 40% of B in 20 min): t_R = 15.79 min; ESI-MS: *m/z* calcd $[M+2H]^{2+}$, 1331.05, found 1330.52. Elemental analysis. Found: C, 42.01; H, 6.34; N, 9.02%. Calculated: $C_{117}H_{199}N_{25}O_{40}S_2 \cdot 8H_2O \cdot 8TFA$: C, 42.98; H, 6.05; N, 9.42%.

5.5.9 BisBiotin-(PEG$_6$)-Abu-SCN (45)

34-ethyl-6-(28-ethyl-5,27,30-trioxo-34-(2-oxohexahydro-1H-thieno[3,4-d]imidazol-4-yl)-8,11,14,17,20,23-hexaoxa-4,26,29-triazatetratriacontyl)-2-(4-isothiocyanatobutyl)-4,11,33,36-tetraoxo-40-(2-oxohexahydro-1H-thieno[3,4-d]imidazol-4-yl)-14,17,20,23,26,29-hexaoxa-3,6,10,32,35-pentaazatetracontan-1-oic acid

The starting point was the compound **39**, and the synthetic procedures were the same described for compounds **36**, **38** and **39**.

The MTT protecting group was removed from **39** by using the step 3, and the compound **39a** was obtained. The amino group was transformed in isothiocyanate by adding to the resin **39a** (150 mg, 0.09 mmol) CS_2 (100 eq, 543 μL) and triethyl amine (10 eq, 125 μL). The mixture was stirred for 15 min at r.t. After this time, a solution of di-tert-buthyl dicarbonate (10 eq, 196 mg) and dimethyl amino pyridine (3 mol%, 0.33 mg) was added and the reaction was cooled in an ice bath for 10 min and then reacted for other 30 min at r.t. The solution was filtered off and the resin was washed three times with DMF and two times with DCM. Cleavage from the resin was performed using step 4. The crude product was purified by semipreparative RP-HPLC to give pure **45** (10.8 mg, 8% overall yield). HPLC (20 to 40% of B in 20 min): t_R = 12.91 min; ESI-MS: *m/z* calcd $[M+H]^+$, 1653.07, found 1652.72. Elemental analysis. Found: C, 41.56; H, 6.98; N, 7.02%. Calculated: $C_{73}H_{129}N_{13}O_{23}S_3 \cdot 9H_2O \cdot 5TFA$: C, 41.79; H, 6.42; N, 7.63%.

5.5.10 BisBiotin-(PEG$_6$)-Asp-SCN

31-(2-((1-carboxy-5-isothiocyanatopentyl)amino)-2-oxoethyl)-4,26,36,58-tetraoxo-2-(5-((3aS,4S,6aR)-2-oxohexahydro-1H-thieno[3,4-d]imidazol-4-yl)pentanamido)-60-(5-(2-oxohexahydro-1H-thieno[3,4-d]imidazol-4-yl)pentanamido)-8,11,14,17,20,23,39,42,45,48,51,54-dodecaoxa-5,27,31,35,57-pentaazahenhexacontane-1,61-dioic acid

Compound (47)

The starting point was the compound **36** (300 mg, 0.18 mmol). The Fmoc removal was achieved following the step 1. Fmoc-Asp-O*t*Bu (**46**) was conjugated to the terminal

PEG amino group using step 2, method 1: Fmoc-Asp-O*t*Bu (**46**) (5 eq, 370 mg), HOBt (5 eq, 138 mg), TBTU (5 eq, 289 mg) and NMM (8 eq, 160 μL) in DMF. Reaction time: 45 min. The coupling was checked by Kaiser test and microcleavage. Two couplings were necessary to obtain a negative Kaiser test. HPLC (10 to 50% of B in 20 min): t_R = 12.34 min; ESI-MS: *m/z* calcd $[M+H]^+$, 1218.39, found 1218.56.

Compound (47a)

Compound **47** was deprotected from Fmoc (step 1) and Biotin was introduced according to the HATU/NMM method (step 2, method 2): biotin (**3**) (3 eq, 132 mg), HATU (3 eq, 206 mg) and NMM (5 eq, 99.5 μL) in DMF. Coupling reaction was controlled by the Kaiser test and microcleavage. Compound **47a** was analysed by HPLC-MS (10 to 90% of B in 20 min): t_R = 6.65 min; *m/z* calcd $[M+H]^+$ 1670.98, found 1670.50.

BisBiotin-(PEG$_6$)-Abu-SCN (48)

The MTT protecting group was removed from **47a** (250 mg, 0.15 mmol) by using the step 3. The amino group was transformed in isothiocyanate by adding to the resin CS_2 (100 eq, 904 μL) and triethyl amine (10 eq, 209 μL). The mixture was stirred for 15 min at r.t. After this time, a solution of di-tert-buthyl dicarbonate (10 eq, 327 mg) and dimethyl amino pyridine (3 mol%, 0.55 mg) was added and the reaction was cooled in an ice bath for 10 min and then reacted for other 30 min at r.t. The solution was filtered off and the resin was washed three times with DMF and two times with DCM. Cleavage from the resin was performed using step 4. The crude product was purified by semipreparative RP-HPLC to give pure **45** (35 mg, 14% overall yield). HPLC (20 to 40% of B in 20 min): t_R = 11.00 min; ESI-MS: *m/z* calcd $[M+H]^+$, 1713.04, found 1712.42. Elemental analysis. Found: C, 40.21; H, 6.64; N, 7.74%. Calculated: $C_{73}H_{125}N_{13}O_{27}S_3 \cdot 9H_2O \cdot 5TFA$: C, 40.77; H, 6.10; N, 7.45%.

5.5.11 BisBiotin-(PEG$_2$)-pAB-Abu-SCN

16-(1,11-dioxo-1-(4-(3-(2-(2-(5-(2-oxohexahydro-1H-thieno[3,4-d]imidazol-4-yl)pentanamido)ethoxy)ethoxy)propanamido)phenyl)-5,8-dioxa-2,12-diazapentadecan-15-yl)-1,11,18-trioxo-1-(4-(3-(2-(2-(5-(2-oxohexahydro-1H-thieno[3,4-d]imidazol-4-yl)pentanamido)ethoxy)ethoxy)propanamido)phenyl)-20-(4-((3-thiocyanatopropyl)amino)butyl)-5,8-dioxa-2,12,16,19-tetraazahenicosan-21-oic acid

Compound (50)

The on resin compound **12** (350 mg, 0.189 mmol) was swelled for 20 min in DMF and deprotected from Fmoc (step 1). Fmoc-8-amino-3,6-dioxaoctanoic acid (Fmoc-NH-PEG-COOH, **49**) was conjugated using step 2, method 2: Fmoc-NH-PEG-COOH (**49**) (4 eq, 291.3 mg), HATU (4 eq, 287.5 mg) and NMM (8 eq, 167 μL) in DMF. Reaction time: 40 min. The coupling was checked by Kaiser test and microcleavage. HPLC (05 to 50% of B in 20 min): t_R = 9.55 min; ESI-MS: *m/z* calcd $[M+H]^+$, 608.74, found 608.51.

Compound (51)

The product **50** was deprotected from Fmoc (step 1). 4-Aminobenzoic acid with primary amino-group Fmoc-protected **8** was conjugated to the PEG amino group using step 2, method 2: Fmoc-*p*AB-OH (**8**) (5 eq, 339.6 mg), HATU (5 eq, 359.3 mg) and NMM (10 eq, 208.9 μL) in DMF. Reaction time: 45 min. The coupling was checked by Kaiser test and microcleavage. HPLC (10 to 90% of B in 20 min): t_R = 17.70 min; ESI-MS: *m/z* calcd $[M+H]^+$ 846.98, found 846.38.

Compound (52)

The compound **51** was deprotected from Fmoc (step 1). Fmoc-8-amino-3,6-dioxaoctanoic acid (Fmoc-NH-PEG-COOH, **49**) was conjugated using step 2, method 2: Fmoc-NH-PEG-COOH (**49**) (4 eq, 291.3 mg), HATU (4 eq, 287.5 mg) and NMM (8 eq, 167 μL) in DMF. Reaction time: 45 min. The coupling was checked by Kaiser test and microcleavage. HPLC (10 to 90% of B in 20 min): t_R = 9.21 min; ESI-MS: *m/z* calcd $[M+H]^+$ 1136.29, found 1136.43.

Compound (53)

Compound **52** was deprotected from Fmoc (step 1) and Fmoc-Abu-OH was introduced according to the HATU/NMM method (step 2, method 2): Fmoc-Abu-OH (**37**) (5 eq, 307.5 mg), HATU (5 eq, 359.3 mg) and NMM (10 eq, 208.9 μL) in DMF. Reaction time: 45 min. Coupling reaction was controlled by the Kaiser test and microcleavage. Compound **47a** was analysed by HPLC-MS (10 to 90% of B in 20 min): t_R = 11.49 min; *m/z* calcd $[M+H]^+$ 1307.50, found 1307.21.

Compound (54)

Compound **53** was deprotected from Fmoc (step 1) and Biotin was introduced according to the HATU/NMM method (step 2, method 2): biotin (**3**) (3 eq, 138.5 mg), HATU (3 eq, 215.6 mg) and NMM (6 eq, 125.4 μL) in DMF. Coupling reaction was controlled by the Kaiser test and microcleavage. The reaction intermediate **53a** was analysed by HPLC-MS (10 to 90% of B in 20 min): t_R= 12.26 min; *m/z* calcd $[M+H]^+$ 1759.09, found 1758.61.

The intermediate **53a** was deprotected from MTT, using the step 3. Fmoc-*β*Ala-OH, (**42**) (2.5 eq, 147.10 mg) was introduced, in accordance with the method 2, by using HATU (2.5 eq, 179.8 mg) and NMM (5 eq, 212 μL) in DMF. Reaction time: 45 min. Coupling reaction was controlled by the Kaiser test and microcleavage. The compound **54** was analysed by HPLC-MS (10 to 90% of B in 20 min): t_R = 12.24 min; *m/z* calcd $[M+H]^+$ 1830.17, found 1829.64.

BisBiotin-(PEG$_2$)-pAB-Abu-SCN (55)

The Fmoc protecting group was removed from **54** by using the step 1. The amino group was transformed in isothiocyanate by adding to the resin CS_2 (100 eq, 1.2 mL) and triethyl amine (10 eq, 263 μL). The mixture was stirred for 15 min at r.t. After this time, a solution of di-tert-buthyl dicarbonate (10 eq, 413 mg) and dimethyl amino pyridine (3 mol%, 0.66 mg) was added and the reaction was cooled in an ice bath for 10 min and then reacted for other 30 min at r.t. The solution was filtered off and the resin was washed three times with DMF and two times with DCM. Cleavage from the resin was performed using step 4. The crude product was purified by semipreparative RP-HPLC to give pure **55** (42

mg, 11% overall yield). HPLC (20 to 60% of B in 20 min): t_R = 13.85 min; ESI-MS: *m/z* calcd $[M+H]^+$ 1872.23, found 1871.63. Elemental analysis. Found: C, 40.89; H, 5.31; N, 8.59%. Calculated: $C_{84}H_{130}N_{18}O_{24}S_3 \cdot 10H_2O \cdot 6TFA$: C, 42.13; H, 5.75; N, 9.21%.

5.5.12 Fmoc-His(trityl-resin)-OAl

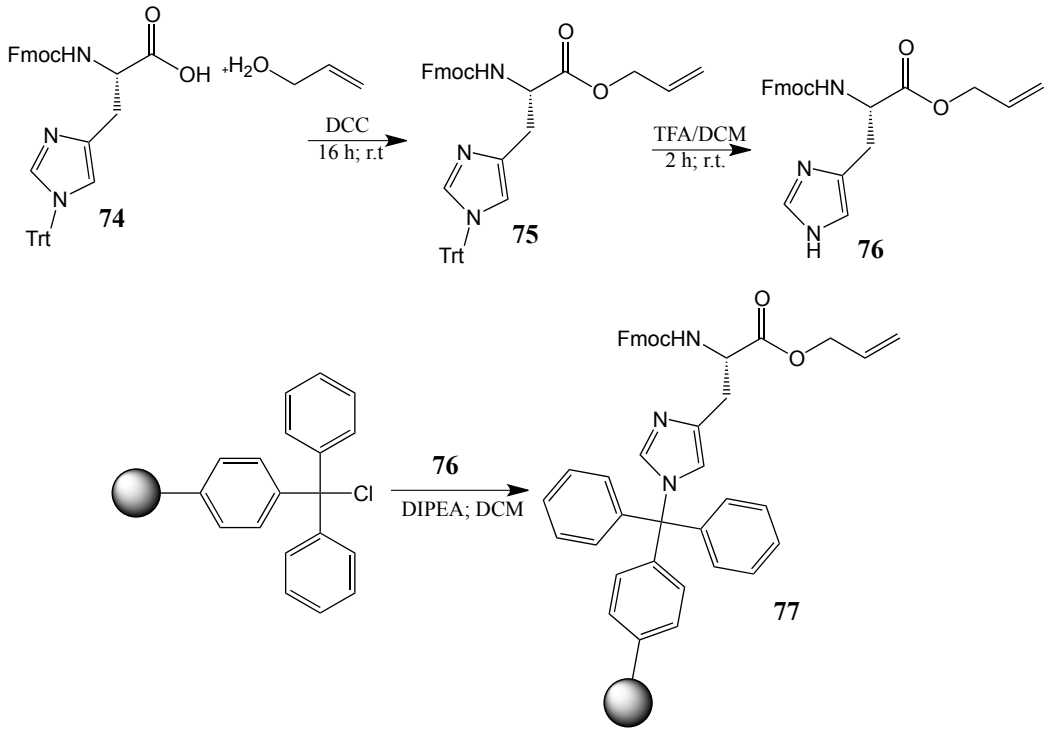

Scheme 5.2 Synthesis of Fmoc-L-His(Trityl-Resin)-OAl (**77**).

Compound (75)

A solution of DCC (400 mg, 1.94 mmol) in allyl alcohol (1.0 ml, 14.7 mmol) was slowly added at 0 °C to a stirred suspension of Fmoc-His(Trt)-OH (**74**) (1.0 g, 1.6 mmol) in dry DCM (20 mL). The mixture was stirred at room temperature for 16 h, and the reaction monitored by TLC (DCM/MeOH 10:1; R_f = 0.90). The white precipitate was filtered off and the excess of DCC was eliminated with AcOH (0.5 mL). The filtered solution was concentrated to dryness, and the residue recrystallized from EtOAc/hexane (780 mg, 74% yield). ^{1}H-NMR ($CDCl_3$, 200 MHz), δ (ppm): 2.86–3.16 (2 H, m, β-H_2), 4.20 (1 H, t, Fmoc 9-H), 4.3–4.7 (3 H, α-H and Fmoc 10-H_2), 4.65 (2 H, d, allyl O-CH_2),

5.20–5.34 (2 H, CH_2=CH), 5.8–6.0 (2 H, NH and CH_2=CH), 7.32 (4 H, m, Fmoc 2-H, 3-H, 6-H and 7-H), 7.57 (2 H, d, Fmoc 1-H and 8-H), 7.73 (2 H, d, Fmoc 4-H and 5-H).

Compound (76)

The product **75** was treated with TFA (7 mL) in 20 ml of DCM at 0 °C and stirred for 2 h, monitoring deprotection by TLC (DCM/MeOH 10:1; R_f = 0.35). The solution was evaporated to dryness and at the residue was added water (2 mL) and lyophilized. The crude oil was treated with Et_2O to obtain a white powder (450 mg, 93% yield). ^{1}H-NMR ($CDCl_3$, 200 MHz), δ (ppm): 3.49-3.09 (2 H, m, β-H_2), 4.26 (2 H, m, Fmoc CH_2), 4.50 (1 H, His α-H), 4.58 (2 H, m, All 1-H_2), 5.29 (2 H, m, All 3-H), 5.79 (1 H, All 2-H), 6.34 (1 H, d, His NH), 6.97 (1 H, s, His 5-H), 7.71-7.19 (8 H, d, Fmoc Ar), 7.71 (2 H, m, Fmoc CH_2).

Fmoc-His(trityl-resin)-OAl (77)

The chloro-trityl resin (2.57 g, 1.35 mmol/g) was dried under vacuum and then swollen with dry DCM. A solution of Fmoc-His-OAl (**76**) (0.868 g, 0.41 mmol) and DIPEA (1.54 mL, 8.34 mmol) in dry DCM (20 mL) was added to the resin. After 2 h, the resin was washed with DMF (3 times × 2 min) and DCM (2 times × 2 min), and then endcapped with DCM/MeOH/DIPEA (17:2:1) (2 times × 2 min). After washing with DCM (2 times × 2 min), DMF (2 times × 2 min) and DCM (2 times × 2 min), the resin was dried under vacuum and the resin loading was determined from the Fmoc release, monitored by UV absorbance.

5.5.13 c(β^{3}homoLys-DHis-βAla-His), DK14 (56)

(3R,7S,10S)-3,10-bis((1H-imidazol-4-yl)methyl)-7-(4-aminobutyl)-1,4,8,11-tetraazacyclotetradecane-2,5,9,12-tetraone

The tetracyclopeptide **56** was synthesized starting from Fmoc-His(trityl-resin)-OAl (**77**) (500 mg, 0.46 mmol/g), on semi automatic synthesizer (MultiSyn Tech – Germany) and following the SPPS method by using the orthogonal Fmoc/Trt/allyl protection scheme. Deprotection of amino acids were performed by 20% piperidine in DMF. The amino acids

residues (*β*-Ala; DHis and β^3homoLy*s*, respectively) were introduced according to the TBTU/HOBt/NMM method with formation of active esters. The coupling reactions were performed by using excess of the amino acids, HOBt and TBTU (4 eq.) and of NMM (8 eq.) in DMF, under vortex mixing for 40 min. After each coupling, the resin was washed with DMF and DCM. Coupling reactions were controlled by the Kaiser test.

The obtained peptide-resin was dried under vacuum and swollen in dry DCM under Ar. The resin was shaken for 5 min with a solution of $PhSiH_3$ (24 eq) in dry DCM under Ar, and then a solution of $Pd(PPh_3)_4$ (0.25 eq.) in dry DCM was added for the allyl group cleavage (total volume of DCM should be 5 mL). After 40 min the resin was washed with dry DCM. The treatment with $PhSiH_3$/$Pd(PPh_3)_4$ was repeated once again. The resin was washed with DCM, with a solution of 0.5% sodium diethyldithiocarbamate in DMF, DMF and DCM. The Fmoc group on the β^3homoLys terminus was then removed with 20% piperidine in DMF and washed with DMF, DCM and DMF. The on-resin linear peptide was vortexed at r.t. for 2 h with a solution of the coupling reagents, TBTU (1 eq.) and base DIPEA (2 eq.), in DMF. After the cyclization, the resin was washed with DMF, and DCM. The reaction was checked by the Kaiser test. Peptide cleavage from the resin and deprotection from the trityl groups were carried out during 2.5 h with TFA/H_2O/TIS (95:2.5:2.5). The resin was washed with TFA and the filtrate was partially evaporated. The crude product was precipitated with cold diethyl ether, collected by centrifugation, dissolved in H_2O and lyophilized. After cleavage and lyophilization, the peptide **56** was pre-purified by solid phase extraction (SPE) and purified with RP-HPLC (0% to 20% of B in 30 min) affording the product **56** (14 mg, HPLC purity >98%, cyclization yield >90%, 16% overall yield). HPLC (03 to 15% of B in 10 min): t_R = 5.61 min; ESI-MS: *m/z* calcd $[M+H]^+$ 419.2, found 419.6. Elemental analysis. Found: C, 40.19; H, 4.14; N, 15.08%. Calculated: $C_{22}H_{33}N_9O_4 \cdot 1H_2O \cdot 3TFA$: C, 39.67; H, 4.52; N, 14.87%.

5.5.14 Fmoc-Lys(trityl-resin)-OAl

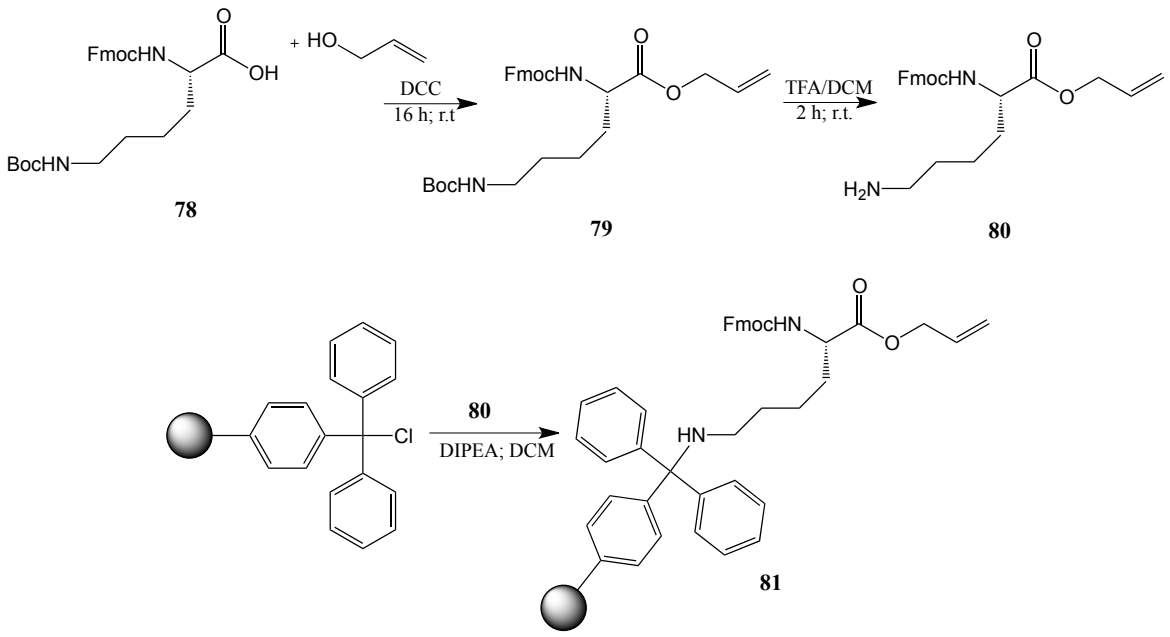

Scheme 5.3 Synthesis of Fmoc-L-Lys(Trityl-Resin)-OAl (**81**).

Compound (79)

Product **79** was prepared starting from Fmoc-Lys(Boc)-OH (**78**) (2.01 g, 4.29 mmol), following the same steps and ratios described for **75**. The reaction was monitored by TLC (DCM/MeOH 10:1; R_f = 0.8), and the product (1.9 g, 87% yield) analysed by ^{1}H-NMR ($CDCl_3$, 200 MHz), δ (ppm): 1.18-1.94 (15 H, m, 3×CH_2 e *t*Bu), 3.18-2.85 (2 H, m, CH_2NH), 4.40-4.0 (4 H, m, α-CH, 9-H Fmoc, CH_2 Fmoc), 4.62-4.43 (2 H, m, allyl O-CH_2), 5.14–5.30 (2 H, m, CH=CH_2), 5.94-5.70 (1 H, m, CH_2=CH), 6.70 (1 H, s br, α-NH), 7.30 (4 H, m, Fmoc 2-H, 3-H, 6-H e 7-H), 7.59 (2 H, d, *J* = 7.4, Fmoc 1-H e 8-H), 7.69 (2 H, d, *J* = 7.4, Fmoc 4-H e 5-H).

Compound (80)

Product **80** was obtained by Boc removal from product **79**, following the same steps and ratios described for **76**. The complete Boc removal was monitored by TLC (DCM/MeOH 10:1; R_f = 0.59), and the final product (1.506 g, 96% yield) analysed by ^{1}H-NMR ($CDCl_3$, 200 MHz), δ (ppm): 1.18-1.94 (6 H, m, 3×CH_2), 3.14-2.81 (2 H, m, CH_2NH), 4.40-4.0 (4 H, m, α-CH, 9-H Fmoc, CH_2 Fmoc), 4.62-4.43 (2 H, m, allyl O-

CH_2), 5.14-5.30 (2 H, m, CH=CH_2), 5.94-5.70 (1 H, m, CH_2=CH), 6.70 (1 H, s br, 1α-NH), 7.30 (4 H, m, Fmoc 2-H, 3-H, 6-H e 7-H), 7.59 (2 H, d, *J* =7.4, Fmoc 1-H e 8- H), 7.69 (2 H, d, *J* =7.4, Fmoc 4-H e 5-H).

Fmoc-Lys(trityl-resin)-OAl (81)

The building-block was prepared as described for **77**, and the resin loading was determined from the Fmoc release, monitored by UV absorbance.

5.5.15 c(Lys-LHis-βAla-His) (LK13) (57)

(3S,6S,9S)-3,9-bis((1H-imidazol-4-yl)methyl)-6-(4-aminobutyl)-1,4,7,10-tetraazacyclotridecane-2,5,8,11-tetraone

Compound **57** was prepared following the same procedure for compound **56**. Amino acids residues (*β*-Ala; LHis and Lys, respectively) were introduced according to the TBTU/HOBt/NMM method with formation of active esters. The coupling reactions were performed by using excess of the amino acids, HOBt and TBTU (4 eq.) and of NMM (8 eq.) in DMF, under vortex mixing for 40 min. After deprotection and cyclization the crude **57** was pre-purified by solid phase extraction (SPE) and semi-preparative RP-HPLC (0% to 20% of B in 30 min.). Analytical HPLC (03% to 20% of B in 5 min.; flow 600 μL/min) t_R = 1.47 min; (65 mg, 16% overall yield) ESI-MS: *m/z* calcd $[M+H]^+$, 474.53, found 474.42. Elemental analysis. Found: C, 39.09; H, 4.46; N, 15.21%. Calculated: $C_{21}H_{31}N_9O_4 \cdot 1H_2O \cdot 3TFA$: C, 38.90; H, 4.35; N, 15.12%.

5.5.16 c(Lys-DHis-βAla-His) (DK13) (58)

(3R,6S,9S)-3,9-bis((1H-imidazol-4-yl)methyl)-6-(4-aminobutyl)-1,4,7,10-tetraazacyclotridecane-2,5,8,11-tetraone

Compound **58** was prepared following the same procedure for compound **56**. Amino acids residues (*β*-Ala; DHis and Lys, respectively) were introduced according to the TBTU/HOBt/NMM method with formation of active esters. The coupling reactions were

performed by using excess of the amino acids, HOBt and TBTU (4 eq.) and of NMM (8 eq.) in DMF, under vortex mixing for 40 min. After deprotection and cyclization the crude **58** was pre-purified by solid phase extraction (SPE) and semi-preparative RP-HPLC (0% to 20% of B in 30 min.). Analytical HPLC (03% to 20% of B in 5 min.; flow 600 μL/min) t_R = 1.17 min; (60 mg, 15% overall yield) ESI-MS: *m/z* calcd $[M+H]^+$, 474.53, found 474.41. Elemental analysis. Found: C, 39.11; H, 4.39; N, 15.46%. Calculated: $C_{21}H_{31}N_9O_4 \cdot 1H_2O \cdot 3TFA$: C, 38.90; H, 4.35; N, 15.12%.

5.5.17 c(Gly-βAla-Gly-Lys) (GK13) (59)

(S)-6-(4-aminobutyl)-1,4,7,10-tetraazacyclotridecane-2,5,8,11-tetraone

Compound **59** was prepared following the same procedure for compound **56** but, in this case, the starting material was Fmoc-Lys(Trityl-Resin)-OAl (**81**). Amino acids residues (Gly; *β*-Ala and Gly, respectively) were introduced according to the TBTU/HOBt/NMM method with formation of active esters. The coupling reactions were performed by using excess of the amino acids, HOBt and TBTU (4 eq.) and of NMM (8 eq.) in DMF, under vortex mixing for 40 min. After deprotection and cyclization the crude **59** was pre-purified by solid phase extraction (SPE) and semi-preparative RP-HPLC (0% to 20% of B in 30 min.). Analytical HPLC (03% to 20% of B in 5 min.; flow 600 μL/min) t_R = 1.09 min; (58 mg, 14% overall yield) ESI-MS: *m/z* calcd $[M+H]^+$, 314.35, found 314.40. Elemental analysis. Found: C, 39.95; H, 5.31; N, 15.02%. Calculated: $C_{13}H_{23}N_5O_4 \cdot H_2O \cdot TFA$: C, 40.45; H, 5.88; N, 15.72%.

5.5.18 Synthesis of Copper/Cyclopeptide complexes

The purified cyclopeptide (obtained as trifluoroacetate salt) DK13·3TFA (**58**) (815.22 g/mol; 18.7 mg) was dissolved in 0.5 mL of water (MilliQ grade). In order to avoid the presence of free copper(II), the complex was prepared with DK13/Cu ratio of 1:0,8 respectively, so 2.94 mg of anhydrous $CuSO_4$ were added to the solution and the pH was adjusted to 12,0 with diluted NaOH. The resulting solution was lyophilized and the solid obtained stored under argon. The same methods and quantities were used also for

LK13·3TFA (**57**) (815.22 g/mol; 18.7 mg). Instead, for GK13·1TFA (**59**) (427.17 g/mol; 18.7 mg) were used 1.54 mg of anhydrous $CuSO_4$ in order to maintain the same cyclopeptide/Copper ratio.

The preparation of the sample for the measurements was done in to a glove box under argon atmosphere, because of the presence of small particle of solid NaOH in the sample; it was very hygroscopic and deliquescent. The solid sample was then milled in a mortar and applied in a thin layer between two Kapton films.

5.5.19 Synthesis of Sodium Ditelluratocuprate(III)

The synthesis of the internal standard compound Ditelluratocuprate(III) $Na_5[Cu\{TeO_4(OH)_2\}_2]\cdot 16H_2O$ (DTC) was performed in accordance with the method reported by Sen Gupta *et al.*

Copper sulphate (0.78 g) was added to a mixture of telluric acid (1.43 g), potassium persulfate (2.11 g), and potassium hydroxide (4.0 g) in water (40 mL). The mixture was heated until the solution was an intense red. The boiling was continued for another 30 min to ensure the complete removal of persulfate. The ditelluratecuprate(III) was crystallized by the solution, cooled at r.t. and 10 mL of saturated $NaNO_3$ solution were added. Almost immediately deep red crystals started appearing and crystallisation is complete (ca. 12 h) when the supernatant liquid is colourless. The crystals were filtered and washed several times with demineralised water and dried under vacuum.

The final product was characterized by X-Ray structure analysis, and the results are in complete agreements with those reported in literature.

5.5.20 Ac-Gly-[Cys-Sec]-Gly-NH_2 (66)

7-(2-acetamidoacetamido)-N-(2-amino-2-oxoethyl)-6-oxo-1,2,5-thiaselenazocane-4-carboxamide

Selenocysteine was prepared starting from Selenocystine, in accordance with Moroder and Hondal (for the references see chapter 4.3.2), Fmoc-Sec(Mob)-OH was obtained with a bidimensional orthogonal protection scheme suitable for solid phase peptide synthesis. The

peptide Ac-Gly-[Cys-Sec]-Gly-NH_2 (**66**) was synthesized starting from Rink Amide MBHA resin (500 mg; 0,4 mmol/g). All the reactions were performed on a semi automatic synthesizer (MultiSyn Tech - Germany) following the standard SPPS method and using the orthogonal Fmoc/Trt/*t*-Bu protection scheme.

The resin was swelled in DMF for 20 minutes and the removal of the Fmoc amino acids protecting group was performed by 20% piperidine in DMF. The amino acids Fmoc-Gly-OH, Fmoc-Sec(Mob)-OH, Fmoc-Cys(Mob)-OH; according to the reported sequence, were introduced following the TBTU/HOBt/NMM method with formation of active esters. The coupling reactions were performed by using an excess of the amino acids, of the activating agents HOBt and TBTU (2.5 eq.) and of NMM (5 eq.) in DMF, vortexing for 40 min at room temperature. After each coupling, the resin was washed with DMF and DCM. Coupling reactions efficiency was controlled by the Kaiser test.

The linear peptide was deprotected with 20% piperidine in DMF and the -NH_2 terminal group was acetylated with a solution of acetic anhydride (20 eq.) and NMM (20 eq.). The resin-containing mixture was then swollen at room temperature for 30 min. The reaction was repeated once again with fresh solutions. After deprotection, the resin was washed with DMF, DCM and dried under vacuum.

Formation of S-Se bridge was obtained by changing the original method for Mob removal, while detaching the peptide from the resin was achieved by using TFA 93%, TIS 2.5%, Tioanisole 2.5% and H_2O 2.5%, a cleavage cocktail with 1.0 equivalent of 2,2′-Dithiobis(5-nitropyridine) (DTNP) *per* selenium.

The crude peptide **66** was purified by solid phase extraction (SPE) and by semi-preparative RP-HPLC (20% to 60% of B in 20 min). Analytical HPLC (20% to 60% of B in 20 min.; flow 1000 μL/min) t_R = 11.85 min; ESI-MS: *m/z* calcd $[M+H]^+$, 425.33, found 425.95.

5.6 Abbreviations

^{1}H-NMR, Proton Nuclear Magnetic Resonance Spectroscopy; Ag, antigen; Av, avidin; *t*-Bu, *tert*-butyl; Cyclam, 1,4,8,11-tetraazacyclotetradecane; Cyclen, 1,4,7,10-tetraazacyclododecane; DCC, *N,N'*-dicyclohexylcarbodiimide; DCM, dichloromethane; DCI, diisopropylcarbodimide; DCU, *N,N'*-dicyclohexylurea; DMF, *N,N*-dimethylformamide; EDT, 1,2-ethanedithiol; EtOAc, ethyl acetate; DMSO, dimethylsulfoxide; Fmoc, 9H-fluoren-9-ylmethyloxycarbonyl; MeCN, acetonitrile; MeOH, methanol; DOTA, 1,4,7,10-tetraazacyclododecane-1,4,7,10-tetraacetic acid; EDC, 1-(3-dimethylaminopropyl)-3-ethylcarbodiimide hydrochloride; ELISA, Enzyme-Linked Immunosorbent Assay; ESI-MS, electron spray-ionization mass spectrometry; FCC, Flash Column Chromatography; Fmoc, 9-fluorenylmethyloxycarbonyl; GHG, glioma high grade; HATU, 1-[bis(dimethylamino)methylene]-1H-1,2,3-triazole(4,5-b)pyridinium 3-oxide hexafluorophosphate; HCTU, 1-[bis(dimethylamino)methylene]-5-chloro-1H-benzotriazolium 3-oxide hexafluorophosphate; HOAt, 1-hydroxy-7-azabenzotriazole; HOBt, 1-hydroxybenzotriazole; HOSu hydroxysuccinimide; HPLC, high performance liquid chromatography; HSA, human serum albumin; Ig, immunoglobuline; i.v., intravenous; ITLC-SG, silica gel instant layer chromatography; LC-MS liquid chromatography-mass spectrometry; MoAb, monoclonal antibody; MTT, methyltrityl; NMM, *N*-methylmorpholine; NMP, 1-methyl-2-pyrrolidinone; RCP, radiochemical purity; R_f, retention factor; RIT, radioimmunotherapy; RP-CC, reverse phase column chromatography; RP-HPLC, reverse phase high-performance liquid chromatography; t_R, retention time; Sav, streptavidin; SPE, solid phase extraction; SPECT, single photon emission computed tomography; SPPS, solid-phase peptide synthesis; sulfo-NHS, N-hydroxysulfosuccinimide sodium salt monosodium 1-hydroxy-2,5-dioxo-3-pyrrolidinesulfonate; TBTU, 1-[bis(dimethylamino)methylene]-1H-benzotriazolium 3-oxide tetrafluoroborate; TFA, trifluoroacetic acid; TETA, 1,4,8,11-tetraazacyclotetradecane-1,4,8,11-tetraacetic acid; TIS, triisopropylsilane; TLC, thin layer chromatography; UPLC, ultra performance liquid chromatography.